Metal oxide modified tubular ceramic membrane for the separation of oil-in-water emulsion.

AISUENI, F.A.

2024

Metal Oxide Modified Tubular Ceramic Membrane for the Separation of Oil-In-Water Emulsion

Florence Anem Aisueni

PhD

2024

METAL OXIDE MODIFIED TUBULAR CERAMIC MEMBRANE FOR THE SEPARATION OF OIL-IN-WATER EMULSION

FLORENCE ANEM AISUENI

A thesis submitted in partial fulfilment of the requirements of Robert Gordon University for the degree of Doctor of Philosophy

March 2024

ABSTRACT

Lower concentration of Oil-in-water (O/W) emulsion (< 250 mg/l) and smaller oil droplet size (< 20 μm) has been a challenge in the industry to separate with conventional methods which include adsorption, electrocoagulation, flocculation, bioremediation, centrifugation, membrane, etc. This is mostly due to the oil droplet size falling in the emulsified range or nano range that is easily stabilised with surfactant present in the O/W. Membrane technology has been recently most researched for the separation of O/W emulsion. This springs from the massive potential of its usage for future water purification and effluent treatment with environmentally friendly, high permeate rate, high percentage (%) oil rejection, and low-cost separation processes.

This study, therefore, focuses on modifying microporous asymmetric Aluminium Oxide (Al_2O_3) tubular ceramic membrane with metal oxides nanoparticles for surface wettability to improve hydrophilicity and increase O/W emulsion separation efficiency.

A novelty material – Magnesium Oxide (MgO) nanoparticles modified tubular ceramic membrane was investigated and discovered to have a high hydrophilicity and O/W emulsion separation efficiency in this study. This investigation which includes modification of MgO nanoparticles on commercial Al_2O_3 tubular ceramic membrane using deep coating method of membrane modification was also applied to other naturally hydrophilic nanoparticle compounds (Manganese Oxide (MnO_2) & Chromium Oxide (Cr_2O_3)) where MgO nanoparticle emerged the most hydrophilic on tubular ceramic membrane measured using contact angle measurement.

The MgO-modified tubular ceramic membrane was characterized to determine morphology, elemental composition, hydrophilicity, porosity, and pore size and compared with unmodified Al_2O_3 tubular ceramic membrane using various analytical instruments and methods.

A novelty method of testing MgO-modified tubular ceramic membrane for the separation of lower concentration (< 500 mg/l) of synthesize O/W emulsion was investigated and achieved using in-house rig set up. The MgO-modified tubular ceramic membrane test for O/W emulsion included test parameters for

percentage oil rejection, flux, and flux recovery ratio. Where results from these tests were compared to results from unmodified Al_2O_3 tubular ceramic membrane.

The MgO-modified membrane displayed a higher %oil rejection efficiency of 98%, leaving behind an O/W emulsion concentration of 11.63 mg/l from the 500 mg/l initial O/W emulsion concentration. Meanwhile, an Al_2O_3 unmodified ceramic membrane shows 69% of oil rejection, leaving behind 156.25 mg/l from 500 mg/l O/W emulsion. This generated over 30% difference in % oil rejection between Al_2O_3 unmodified and MgO-modified ceramic membranes. This MgO-modified ceramic membrane % oil rejection concentration of only 11.63 mg/l falls within the OSPAR regulatory limit. Compared to Al_2O_3 unmodified ceramic membrane, the MgO-modified tubular ceramic membrane demonstrated a lesser performance in terms of permeate flux with a higher flux decline due to quick concentration polarization and smaller pores sizes during O/W emulsion cross-filtration analysis.

With this result, an MgO-modified ceramic membrane can be an alternative to other metal oxide ceramic membranes to improve separation efficiency >90%. The success of this MgO-modified ceramic membrane can tackle the lower oil concentrations (250 mg/l) and oil droplet size (< 20 um) challenges that arise from unmodified ceramic membranes and conventional methods of O/W emulsion separation.

Keywords: Ceramic membrane, MgO-modified, Al_2O_3 Unmodified, O/W emulsion, Separation, Characterization, Flux, % Oil rejection, Flux recovery ratio, metal oxides, nanoparticles.

DEDICATION

This work is dedicated to God Almighty, who has guided me all through every step of this journey, and to my Dear husband, Philip, for effortlessly supporting and comforting me through the entire process.

DECLARATION

I hereby declare that the material presented in this report is my own work, and where this is not the case, the source material has been duly acknowledged.

ACKNOWLEDGEMENT

Sincere gratitude to my husband, Philip Aisueni, for his enduring dedicated support from the inception of the proposal, processes to completion; thank you for encouraging me and believing in the process. I appreciate my children enduring and sharing their mummy time with my academic pursuits. To my first principal supervisor, Late Professor Edward Gobina, I cannot emphasise enough how you have been a pillar to the successful completion of this PhD process. Thank you for believing in me and for your acceptance. I also appreciate Dr Somasundar Kannnan for taking me on to completion of this study as my new principal supervisor. I want to acknowledge Professor Radhakrishna Prabhu for being the best co-supervisor and for immensely imparting your knowledge, patience, and corrections towards completing this research. Thank you both for your expert guidance. I wholeheartedly appreciate all my lab colleagues, Dr Ofasa Abunumah, Evans Ogoun, Muktar Ramalan, Idris Hashim, and my dear friend Chioma Onoshakpor for their help and support. Thank you all for being there for me, even beyond the academic sphere. Many thanks to the technical support and administration team of the School of Engineering and the School of Pharmacy and Life Sciences for guidance through health and safety and for always being available as and when needed for support. Last but not least, special thanks to my parents, Late Paul Igbara and Charity Paul-Igbara and my siblings for first telling me that I can do this. I look forward to more accomplishments in the future.

Table of Contents

List of Figures

List of Tables

Publications & Conferences Attended

2024

AISUENI, F., PRABHU, R., Kannan, S., and OGOUN, E. 2024. MgO-Modified Ceramic Membrane For Lower Concentration Oil-In-Water Emulsion Separation. Submitted Article to M

2022

AISUENI, F., RAMALAN, M., ABUNUMAH, O., OGUNLUDE, P., ORAKWE, I., OGOUN, E., GIWA, A., SHEHU, H. and GOBINA, E. 2022. Gas diffusion, transport characteristics and modelling in porous membrane systems with application for polymer electrolyte membrane fuel cells. In Proceedings of the 2nd International congress on scientific advances 2022 (ICONSAD'22), 21-24 December 2022, [virtual conference]. Turkey: ICONSAD [online], pages 144-157. Available from: https://en.iconsad.org/_files/ugd/1dd905_c45aeddf416d497e93113f00f465739b.pdf

AISUENI, F., ABUNUMAH, O., HASHIM, I., RAMALAN, M., OGOUN, E., PRABHU, R., GIWA, A. and GOBINA, E. 2022. Effect of pore size and porosity on contact angle of ceramic membrane for oil-in-water emulsion separation. In Techconnect briefs 2022: papers from 2022 TechConnect world innovation conference and expo, 13-15 June 2022, Washington, USA. Danville: TechConnect [online], pages 59-62. Available from: https://briefs.techconnect.org/wp-content/volumes/TCB2022/pdf/174.pdf

AISUENI, F., GOBINA, E., HASHIM, I. and OGOUN, E. 2022. Characterization and hydrodynamic evaluation of the relationship between permeability and microstructure parameters ceramic membranes for the separation of oil-in-water emulsion. International journal of engineering, science and technology [online], 4(1), pages 14-20. Available from: https://doi.org/10.46328/ijonest.69

2021

AISUENI, F. and GOBINA, E. 2021. Effect of hydrodynamic and microstructural parameters on ceramic membrane for oil-in-water separation. In Proceedings of 2021 International congress of Scientific Advances (ICONSAD'21), 22-25 December 2021, [virtual conference]. Turkey: ICONSAD [online], pages 1022. Available from: https://tinyurl.com/2p8uy2rh

AISUENI, F., HASHIM, I., OGOUN, E. and GOBINA, E. 2021. Comparative evaluation of oil-in-water emulsion separation with aluminium oxide and zinc oxide nanoparticles ceramic membrane. Presented to 2021 TUBA (Turkish Academy of Science) World conference on energy science and technology (TUBA WCEST-2021), 8-12 August 2021, [virtual conference]. https://rgu-repository.worktribe.com/output/1411484

AISUENI, F.A., OGUON, E., HASHIM, I. and GOBINA, E. 2021. Characterization and evaluation of nanoparticles ceramic membrane for the separation of oil-in-water emulsion. In Proceedings of the ICANM 2021: 8th International conference and exhibition on advanced and nanomaterials 2021 (ICANM 2021), 9-11 August 2021, [virtual conference]. Ontario: ICANM, pages 17-26.https://rgu-repository.worktribe.com/output/1427924

LIST OF ACRONYMS

SEM – Scanning Electron Microscope
O/W - Oil-in-water
OSPAR – Oslo Paris
Al2O3 - Aluminium Oxide
EDXA – Energy Dispersive X-ray Analysis
UV- Ultraviolet
MgCl2 - Magnesium Chloride
MgO – Magnesium Oxide
MF – Microfiltration
NF- Nanofiltration
UF- Ultrafiltration
PAHs – Polycyclic Aromatic Hydrocarbons
NSO- Nitrogen Sulphur Oxygen
AOPs – Advanced Oxidation Process
ASP – activated Sludge Process
HOW – Heavy Oil Wastewater
PTFE – polytetrafluoroethylene
PVDF – polyvinylidene fluoride
PE – Polyethylene
PP – Polypropylene
RO- Reverse Osmosis
CVD – Chemical Vapour Deposition
ZrO2 - Zirconia dioxide
ZnO – Zinc Oxide
TiO2 – Titanium dioxide
SiO2 – Silicon dioxide
VP – Variable Pressure
BSD – Backscatter Detector
FPS – Frame per second
MnO2 – Mangane dioxide
Cr2O3 – Chromium Oxide
CrCl3 – Chromium Chloride
MnCl2 – Mangane Chloride
BET - Brunauer, Emmett and Teller
BJH - Barret, Joyner and Halenda

LIST OF SYMBOLS

Micrometre - µm
Milligram per litre – mg/L
Nanometre – nm
Litre per meter square time height – L/m2.h
Litre per metre square times height time bar - L/m2.h.bar
Percentage - %
Microlitre - µL
2 pi radius times height - 2πrh
Centimetre –cm
Centimetre square –cm2
Meters square - m2
Litre per hour – L/H
Flux recovery ratio – R
Pure water flux after cross-filtration – Jw'
Pure water flux – Jw
Ceramic membrane area – A
Ceramic membrane height – h
Time – t
Permeate flux – Qp
Porosity - Ɛ
Wet weight – Ww
Dry weight – Wd
Volume of membrane – V
Density of water – dw
Contact angle - [0]
Grams – g

Chapter One

1.0 Introduction

Water is a naturally occurring resource chemically consisting of an oxygen and two hydrogen atoms connected via covalent bond. It is in abundance such that 71% of the earth constitute water and the sources of water are divided into two: surface and ground water. Surface waters are waters above the ground levels which includes, rivers, lakes, reservoir, creeks, streams, and the like. Ground waters includes waters beneath land surfaces gathered in a place like aquifers and wells (Giri and Qiu 2016). Water is especially useful due to the composition and abundance to all living organisms. It is used directly for drinking, bathing, cooking etc. and indirectly in various industrial sectors like agriculture, industry, recreation, and habitat. Based on this wide usage, water quality must be maintained by evaluating the usage of water in different activities using physical, chemical, and biological parameters (Dulic et al. 2010).

Maintaining this water quality has become a challenge especially with the high quantity of indirect usage of water from rapid growth and development of industrial activities rising from oil and gas, food processing, metallurgical, petrochemical, and pharmaceutical industries all over the world (Shi et al. 2019a). Spotlight on oil pollutants generated from these industrial activities constitute oily wastewater produced daily and discharged into water bodies or soil. Typically, the concentrations of oil and grease mixed with water produced daily from these industrial activities into the environment ranges from about 100-1000 mg/l if not more ((Rashad et al. 2021). If left untreated before discharge into environment may continually cause environmental pollution. Due to lack of fresh water and environmental degradation it is now imperative to treat oily wastewater prior to discharge into the environment.

Oily wastewater also known as produced water was voluminously generated primarily from industry petroleum activities because of oil exploration (Abdalla et al. 2019). Oil-in-water (O/W) emulsion is also present as a stable form of oily wastewater defined as oily drops in water within the diameter range of 20 μm and below (Shi et al. 2019b). Separation technology is faced with the challenge of separating emulsified O/W. This is due to the droplet size falling between the range of tens of nanos and micrometres (Deng et al. 2019). Hence, this has posed a threat to the usage of traditional or conventional separation methods

which includes sedimentation, centrifugation, electrocoagulation, and vacuum evaporation (Khan et al. 2019) (Chen, H. et al. 2015) (Wang, D. et al. 2020). Gravity alone is not enough to separate the oil phase from water phase in O/W emulsion even though there exist an interphase between the phases ((Chang et al. 2014a). This might be due to the interfacial reactions between both phases that might have produced emulsion compounds or dissolved oil in the water phase. This becomes a long-time environmental pollution challenge with increase in production of O/W emulsion & grease and proliferation of petroleum activities around the globe.

1.1 Background of the Study

An average concentration of 80% O/W emulsion is generated and released into the environment from the oil and gas sector alone ((Zolfaghari et al. 2016) that can cause serious ecological concerns owing to the hazardous components present in the emulsion. This has led to regulatory bodies of some countries to set limits for oil and grease discharge into the environment. The recent discharge limits set by regulatory bodies should be mentioned to enable a comparative evaluation of the treatment methods with the limit. Several regulatory bodies have always stated their limit for O/W emulsion discharge (Igunnu and Chen 2014). During the Oslo Paris (OSPAR) convention held in 1999, it was agreed that the O/W maximum discharge be reduced to 30 ppm (Zolfaghari et al. 2016). The United State Environmental Protection Agency (USEPA) placed the discharge of oil and grease into the environment at 40 ppm. Republic of China benchmarked the monthly average oil and grease discharge at 10 ppm. As the years went by, an increase in environmental concern has resulted in more stringent discharge limits. Many countries have adopted the "zero discharge" of oil and grease into the environment (Igunnu and Chen 2014). In 2000, the EU Water Framework Directive embrace the "zero discharge" in view of protecting the aquatic environment (Kristensen et al. 2018). The Oil Pollution and Prevention Control (OPPC) Regulations 2005 for "permitted concentration and Quantity of Oil discharge which is in line with OSPAR Recommendation 2001/1 states 30 mg/l monthly average is the limit for any individual offshore installation to discharge oily produced water into the sea (Acheampong and Kemp 2022). Based on these limits, most oil and gas industries across the world are progressing towards the application of the zero

discharge of O/W into the environment (Tong and Elimelech 2016) and as such, seeking several technologies for the effective treatment or separation of O/W emulsions.

To tackle this concern, a selection of O/W emulsion separation techniques and innovative materials have been researched and stated in literature. Various kinds of mechanical devices which includes skimmers (Wang, J., Wang and Geng 2018), in industry have been used to separate O/W emulsions, but they all need the usage of energy and high pressure to function. In addition, foams (Nguyen et al. 2012) and sponges (Calcagnile et al. 2012) have been used in emergency of oil spill to absorb oil. However, the disadvantage is in low capacity as it simultaneously absorbed oil and water, which becomes a challenge during separation due to time consumption making it unfit for recycling or reuse. This results in the burning or burying of the material which leads to secondary pollution (Gupta et al. 2017).

Several promising methods have been reported so far by researchers for the separation of oil from O/W emulsions before discharge into the environment, which have their advantages and disadvantages, so materials that can meet the challenging requirements of real-world applications are still in the process of development. Hence, there is a need for the advancement of a recyclable, cost-effective, environmentally friendly, simple, and efficient method that can separate large volumes of O/W emulsions with high flux and oil rejection rates.

(Gupta et al. 2017) reported and a continuation from this present research have also reported an increase in articles depicting O/W emulsion separation before discharge into the environment as seen in Figure 1. This increase is because of several methods researched and reported for the separation of O/W emulsions. Some of these methods are adsorption, electrocoagulation, flocculation, bioremediation, centrifugation, membrane etc (Shi et al. 2019a).

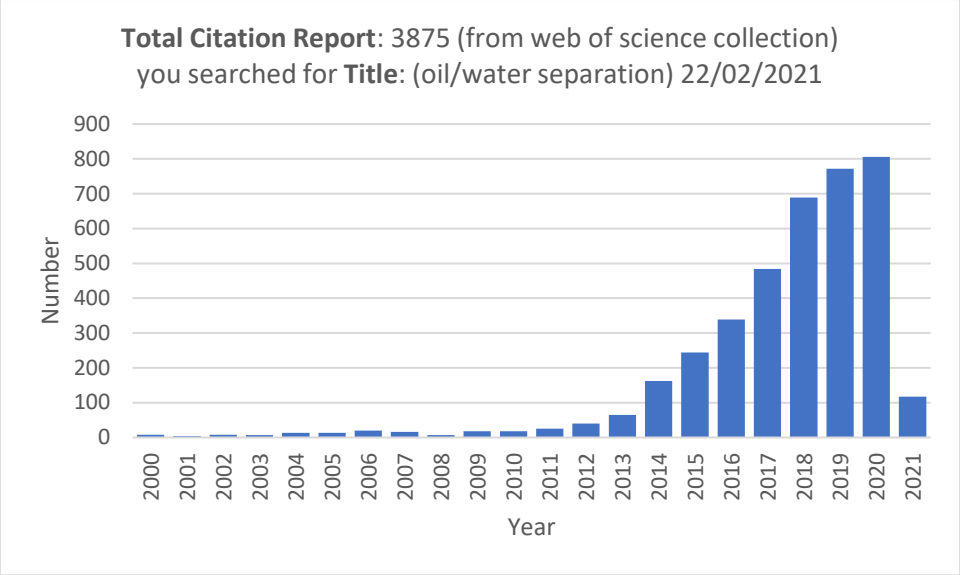

Figure 1: Number of articles of oil/water separation indexed in web of science by the title of "oil/water separation"

These traditional methods are insufficient in the treatment of O/W emulsions due to the small size of oil droplets (<20 μm) as well as lower concentrations of oil in water because below 250mg/l separation is usually not possible ((Shi et al. 2019a). The common method used for the treatment of O/W emulsion involves the destruction of the emulsion state with the addition of chemical reagents ((Chang et al. 2014b). This in turn form a sludge that will become a pollutant to the environment since this cannot easily be separated or recycled.

Nevertheless, membrane technology has been recently most researched for the separation of O/W emulsion. This springs from the almost endless possibilities of its usage for future water purification and effluent treatment with environmentally friendly high permeate rate, and low-cost separation processes ((Suresh and Katara 2021; Chang et al. 2014c). Ceramic membrane separation specifically may have been widely used because of its merit features which includes an excellent combination of longer shelf life, better self-cleaning properties, mechanical, chemical, and thermal strength, survival in organic solvent, low cost, compact design, removal of secondary separation and superior separation factor (Suresh and Pugazhenthi 2016). Membrane technology has been developed and seen as an efficient way to respond to the issues of separation of low concentrations and small droplet size of O/W emulsion. This has been achieved by the development and design of membranes with different pore sizes and surface wettability, thereby attaining precise separation

technologies through sieving by size in nano, ultra or micro scale and surface charge sieving (Deng et al. 2019). Despite this attainment, membrane fouling sometimes poses a challenge during separation that may arise due to oil concentration polarization, pore blocking, oily layer over membrane surface or adsorption creating a decrease in separation efficiency or flux in membrane technology (Lu, C., Bao and Huang 2021; Maddela and Torres 2021). To tackle this fouling problem, extensive research has focused on the modification of membrane surface characteristics to increase hydrophilicity or hydrophobicity depending on the aim of research.

1.2 Scope of this Work

This study places focus on the laboratory experimental approach of preparing, characterizing, testing, and comparing Al_2O_3 tubular ceramic membrane and modified ceramic membrane with nanoparticles metal oxide for the separation of synthetic O/W emulsion that are below 500 mg/l. This scope is generated from the challenge that arises from conventional separation methods not being able to separate O/W emulsion with tiny droplet size below 20 µm or lower concentrations below 250 mg/l. In this case the membrane preparation involves the dispersive deposition of Magnesium oxide nanoparticles on the surface and into the tiny micropores of the Al_2O_3 unmodified ceramic membrane and then evaluate the flux and separation efficiency and reusability of the tubular ceramic membrane in comparison to the unmodified ceramic membrane to meet regulatory limits. This research elaborates on the use of ceramic membrane technology to provide a recyclable, cost -effective, environmentally friendly, simple, and efficient method that can separate O/W emulsions with high flux and oil rejection. This research also suggests a ceramic membrane technology that can separate O/W emulsion to meet the stringent requirement acceptable limits of regulatory bodies stated above which is 30 mg/l daily discharge.

1.3 Aim and Objectives

The aim of this research is to modify, characterize, test, and compare the use of metal oxide nanoparticle modified ceramic membrane with Al_2O_3 unmodified tubular ceramic membrane for the separation of lower concentrations (<500 mg/l) and smaller oil droplets (<20 µm) of synthetic O/W emulsion to meet up stringent regulatory limits (30 mg/l).

1.3.1 Objectives

This research seeks to:

1. Design, fabricate, and install the rig (separator) for separation of O/W emulsion.
2. Evaluate and identify specific nanoparticles or materials for modifying the surface and pores of Al_2O_3 tubular ceramic membrane.
3. Determine an appropriate method for modification, modification process and characterization of modified ceramic membrane using existing literature procedures and equipment.
4. Prepare O/W emulsion with selected oil and surfactants and characterize and measure O/W emulsion droplet size using existing literature measurement equipment/procedure.
5. Determine flux, recovery ratio and % oil rejection after O/W emulsion permeation; and quantitatively analyse the permeate from unmodified and modified tubular ceramic membrane.

1.4 Contribution to Knowledge

Membrane technology has recently been the most researched for separating O/W emulsion. This springs from the almost endless possibilities of its usage for future water purification and effluent treatment, environmentally friendly high permeate rate, and low-cost separation processes (Suresh and Katara 2021; Chang et al. 2014b). Ceramic membrane separation specifically may have been widely used because of its merit features which include an excellent combination of longer shelf life, better self-cleaning properties, mechanical, chemical, and thermal strength, survival in an organic solvent, low-cost, compact design, removal of secondary separation and superior separation factor (Suresh and Pugazhenthi 2016). However, most ceramic membranes are insufficient in separation efficiency >90%. Most times pose, a challenge during separation that may arise due to oil concentration polarisation, pore blocking, oily layer over membrane surface or adsorption, creating a decrease in separation efficiency (Lu, C., Bao and Huang 2021; Maddela and Torres 2021). Hence, modifying ceramic membranes for active surface wettability or pore size can be more hydrophilic or oleophilic and aid separation efficiency. This has been achieved by developing and designing membranes with different pore sizes and surface wettability, thereby attaining precise separation technologies through sieving by size in nano, ultra or micro-scale and surface charge sieving (Deng et al. 2019). Some metal oxides such as Fe_2O_3, TiO_2, CuO, CeO_2, and MnO_2 have previously been used to deposit on the surface of ceramic membranes to improve hydrophilicity and influence separation efficiency (Lu, D., Zhang et al. 2016).

Although $MgAl_2O_4$ has been fabricated from scratch with aluminium dross waste to prepare a microporous ceramic membrane (Abd Aziz et al. 2019), studies showing tubular Al_2O_3 ceramic membrane modified with nanoparticles magnesium oxide (MgO) for the separation of O/W emulsion separation have not been reported in the literature. This study, therefore, focuses on modifying microporous asymmetric Al_2O_3 tubular ceramic membrane with MgO nanoparticles for surface wettability to improve hydrophilicity and increase O/W emulsion separation efficiency compared to the unmodified ceramic membrane. The separation results of this MgO-modified ceramic membrane are compared to the Al_2O_3 unmodified ceramic membrane. The parameters to determine the separation efficiency of this MgO-modified ceramic membrane include

characterisation parameters such as – morphology, porosity, and hydrophilicity; and cross-filtration parameters such as – permeate flux, % oil rejection and flux recovery ratio. This MgO-modified ceramic membrane can be an alternative to other metal oxide ceramic membranes to improve separation efficiency >90%. The success of this MgO-modified ceramic membrane can tackle the lower oil concentrations (250 mg/l) and oil droplet size (<20 μm) challenges that arise from unmodified ceramic membranes and conventional methods of O/W separation.

Hence, this technology of MgO-modified ceramic membrane used in compact rig set up reactors can be used industrially in offshore, onshore, manufacturing plants etc. for the separation of oily wastewater before discharge into the environment or reinjection into the system. The separator tanks offshore and onshore for example can serve as feed tanks for the reactor containing MgO-modified ceramic membrane. Recommendations have been provided in this report for future work towards making the MgO-modified ceramic membrane a reality in the industry.

1.5 Thesis Outline

This research report is made up of 7 chapters alongside references and appendices. This sub-section outlines a summary of each chapter below.

Chapter 1: presents a detailed introduction of the research work conducted which mostly includes the background and scope of the study, outline of the aim and objectives of the research, and a summary of the methodology applied. Publications and conferences attended are also presented in this chapter inclusive of the outline of the research work based on each chapter.

Chapter 2: this chapter presents detailed information on literature review for O/W emulsion, conventional methods used for treatment of O/W emulsion, membrane technology, common metal oxides used for membrane modifications, membrane reactor concepts, factors affecting the use of ceramic membrane industrialization, and characterization instruments.

Chapter 3: This chapter presents an introduction of the methodology used in this research. The chapter also explains the methodology for synthesis of O/W emulsion, preparation and testing of three different metal oxides for hydrophilicity using contact angle measurement, MgO modification of ceramic membrane process, and finally characterization of unmodified and modified ceramic membrane. This chapter also elaborates on the reactor design beginning with the patency and components of the reactor, followed by the ceramic membrane support design and finally the metal oxide (MgO) modified ceramic membrane process design. This chapter presents in detail the crossflow filtration method used for the separation of O/W emulsion. It starts with the equipment and apparatus used and the health and safety measures applied. The chapter explains the experimental procedure involves in flux, flux recovery ratio, and percentage oil rejection.

Chapter 4: This chapter presents an elaborate report and discussion of the synthesis of O/W emulsion, characterization of unmodified and modified ceramic membrane which involves contact angle measurement, porosity, morphology, and pore size. The flux, flux recovery ratio, and percentage oil rejection of modified and unmodified ceramic membrane are also reported and discussed in this chapter.

Chapter 5: this chapter presents the conclusion of the entire research with the aim in mind, and the recommendation for future work.

Chapter 6: consist of the list all the references used in this study.

Chapter 7: this chapter presents appendices of the equipment, chemicals and materials involved in the experimental procedure, health and safety measures applied. Some other results and calculations are also listed in this section.

Chapter Two

2.0 Literature review

This chapter is a broad chapter that encompasses eight sub sections. It starts with how O/W emulsion is produced, and the steps involved in the synthetic production of O/W emulsion. The chapter further explains the conventional methods that has been used for the treatment and separation of O/W emulsion. Subsequently, this section elaborates on the use of membrane technology so far for the separation of O/W emulsion. Furthermore, it elucidates common metal oxides that have successfully been used for surface wettability of ceramic membranes. The chapter also explains membrane reactors and how it functions in the separation of O/W emulsions. Then the chapter goes ahead to expatiate factors affecting the use of ceramic membrane for O/W emulsion separation in industrial levels. The principles, instrumentation and applications of all analytical instruments used in this research was explained in this chapter. Finally, the chapter wraps up with the anticipated contribution to knowledge of this research work.

2.1 O/W Emulsion

O/W emulsion are being generated from industrial companies who create this as a waste during the transformation of raw materials to products that are used daily by the entire world. These industrial companies such as metal/steel petrochemical, food, textile, and mining industries produce enormous volumes of O/W emulsion from wastewater generated every day. For instance, 140000 litres of oil contaminated water are produced every day from mining operations (Saha and Bauddh 2021). However, these industries play a significant role in the civilization and development of humans (Zhao et al. 2017). With this obvious fact, shutting down these sectors due to environmental pollution is unlikely. Hence, industries in these sectors need advanced technological means to meet the regulatory limits of the wastewater generated from their activities.

Industrial activities like oil and gas extraction, food industry, petroleum refining, metal manufacturing etc., generate oily wastewater in large volumes daily (Križan Milić et al. 2013). There are classifications involved in the oily wastewater based on size of oil present. Oil droplet sizes in oily wastewater

>100 μm are classified as free oil, and those between 100-10 μm are classified as dispersed oil, the oil droplet size <10 μm are classified as emulsified oil which form the O/W emulsion and are also known as dissolved oil (Lu, D., Zhang et al. 2016). These emulsified and dissolved oils have been reported to be the most challenging to efficiently remove or separate from water. Based on chemical structure, the organic components present in O/W emulsion can be divided into four sections which includes the asphaltenes, aliphatic, aromatics and the nitrogen sulphur oxygen (NSO) compounds. For example, oily wastewater can consist of several organics like xylene, alkanes, benzene, phenols, naphthalene, cycloalkanes, benzofluorene, chrysene and other polycyclic aromatic hydrocarbons (PAHs). The most organic present up to 75% in the wastewaters are usually aliphatic and aromatics PAHs (Behroozi and Ataabadi 2020). The whole idea is to remove or separate oil droplets from water.

Usually, an emulsifier like a surfactant is introduced in the formulation with oil and water to form O/W emulsion. This surfactant addition reduces the interfacial differences or tension between oil and water phases in the mixture (Kong and Li 1999). Based on the emulsified and dissolved oil in water which are difficult to remove, most country environmental guidelines have set regulatory limits for the release of maximum oil and grease concentrations in effluents to be less than 10-15 mg/l, increasing the criticality of efficient separation or treatment of O/W emulsion (Engineering et al. 1992).

For instance, there is the Heavy oil wastewater (HOW) which consist of oil droplets, suspended solids, and dissolved salts (Zeng et al. 2007). Less than 10 μm oil droplet size which forms O/W emulsions stabilized with surfactants, are most challenging when it comes to separation and cannot be efficiently removed by conventional methods such as skimming, flotation, cyclone, centrifugation etc (Tian, Liao and Wang 2020). The effectiveness of ceramic membrane processes in the microfiltration (MF) and ultrafiltration scales, addresses the challenge of micrometre size O/W emulsions separation. Though it is accompanied with a fouling demerit that plagues microfiltration ceramic membranes over a period of separation reported by (Suresh and Pugazhenthi 2016) and will be discussed in the research.

2.1.1 Problems resulting from O/W Emulsions in the Environment

Daily production of large oily wastewater from industrial activities must be adequately treated or separated before discharge into the environment due to environmental and human health requirements. These wastewaters are to be treated because of the constituents present in the oily wastewater that form the components of the wastewater which becomes harmful to health and environment at large. These components are made up of polycyclic aromatic hydrocarbons (PAHs). The following disasters can be generated from direct discharge of untreated oily wastewater into the environment (Yu, Han and He 2017) :- influencing and pollution of drinking water, ground water and aquatic resources; threat to human life and health; pollution of the environment; negative effect on cultivated plants; destruction and pollution of land; changing of structures and food chain present in aquatic community; accumulation of oily droplets in the environment. All these can lead to the decrease or lack of freshwater in the environment. Apart from the toxicity present in oily wastewater, these components can also increase the risks of cancers in humans and cause growth decline in both plants and animals (Liu, W. et al. 2020; Kundu and Mishra 2019; Huang, S., Ras and Tian 2018). Hence the purification of oily wastewater is necessary especially to meet up the stringent regulatory limits set by environmental guidelines of various countries.

2.1.2 Preparation of synthetic Oil-in-water Emulsion

The preparation of synthetic O/W emulsion involves several steps to achieve a fine uniform droplet size oil below the range of 10 μm that will be suitable for ceramic membrane O/W separation analysis. Some major steps include deciding the right oil for mixture, deciding the right surfactant or blend to use for bridging the interfacial tension between oil and water phases, the mixing speed and tool, ranging from shear, food blender, magnetic stirrer, or ultrasonic bath etc. Next steps may involve characterizing the prepared synthetic O/W emulsion for pH, Viscosity, oil droplet sizes, pour point etc. Table 1 below summarises a detailed literature review of different steps or procedures used by various researchers for the preparation of synthetic O/W emulsion.

Table 1: Literature Review of different parameters for the preparation of synthetic O/W emulsion

Oil Type	Surfactant	Oil Conc. mg/l	Mixing tool	Mixing speed (RPM)	Mixing time (Min.)	Mixing temp (0^0C)	Average droplet size (nm)	Author
Crude oil	-	100-1000	Food blender	500	1	20	386.8	(Gohari et al. 2015)
Crude oil	R-100	-	Food blender	-	0.5	20	3000	(Fang et al. 2013)
Hydraulic oil	Span 80 and tween 80	-	Food blender	mediate	2	-	6000	(Chang et al. 2014c)
Machine oil	Sodium dodecyl sulfate	250	Ultra sonic & magnetic stirrer	-	720	-	-	(Chen, T., Duan and Fang 2016)
Crude oil	-	250, 500 & 1000	Mechanical agitator	14000	8	-	-	(de Melo et al. 2022)
Olive oil	Tween 80	250, 500 & 1000	Mechanical shear	18000	2	-	-	(Rashad et al. 2021)
Crude oil	Sodium dodecyl sulfate	100	Mechanical agitator	18000	20	-	-	(Lesak et al. 2022)

2.2 State-of-the-art methods used for O/W Emulsion Separation

Over the years several conventional methods were used to treat O/W emulsion. The methods include physical, chemical, and biological treatments like floatation, coagulation, biological treatment, adsorption, Hydroclones and skimming.

2.2.1 Adsorption

Organic compounds present is O/W emulsion tends to adhere to porous absorbent media of carbon surfaces. This porous absorbent media separates the organic compound from oily wastewater or O/W emulsion. Most surface modifications material used in adsorption procedures are activated carbon, organoclay, copolymers, zeolite, and resins. Adsorption occurs when organic molecules in O/W emulsion bind to the surface of an absorbent (a solid). This binding of organic molecules leaves the O/W emulsion less oily. However, the

performance of absorbers can be restricted by several factors which include temperature and pH, suspended oil, and dissolved organic chemicals (Fakhru'l-Razi et al. 2009). Numerous studies have reported the use of absorbers for the treatment of wastewater. (Santos et al. 2020) the preparation of activated carbon from the seed and pods of Moringa oleifera for the treatment of produced water. (Younker and Walsh 2014) reported the use of organoclay adsorption method for the bench scale removal of organic present in produced water. Khader (Khader et al. 2022) proposed the use of two absorbent i.e., activated carbon and zeolite for the removal of organic pollutants present in produced water with batch adsorption technique. The most challenging demerits with adsorption method of O/W emulsion treatment is that particles that are suspended tend to plug the media thereby reducing separation efficiency. Another major drawback is the chemical waste generated from the absorbents becomes difficult to dispose of (Fakhru'l-Razi et al. 2009).

2.2.2 Hydrocyclones

Another physical treatment or separation method for O/W emulsion is the use of hydroclones that separates oil droplets present in oily wastewater. In hydroclones methodology, a centrifugal force is, and flow pattern produced with the use of fluid pressure, that can separate oil droplets from a liquid medium. The mechanism used is ensuring the oil droplet size has a higher density than the fluid medium to achieve separation (Amakiri et al. 2022). The hydrocyclone tool is comprised of a conical body housing a cylindrical chamber that leads to a cone apex at the exit of the chamber. From Figure 2 below, the oil droplets flow towards the overflow exit, while the separated water flows towards the underflow exit. Hydroclones has been known to separate and reduce oil concentration from 2000 ppm to 100 ppm and it is a good physical oil separation method for oil droplet size of 50 µm and above (Bennett and Williams 2004). It has been reported that the use of hydroclones method for treatment or separation of O/W emulsions with droplet size below 5 µm decreases separation efficiency of this method. The merit with this separation technique is the lack of chemical usage in the entire process, minimal maintenance cost and the low energy usage (Stewart and Arnold 2011).

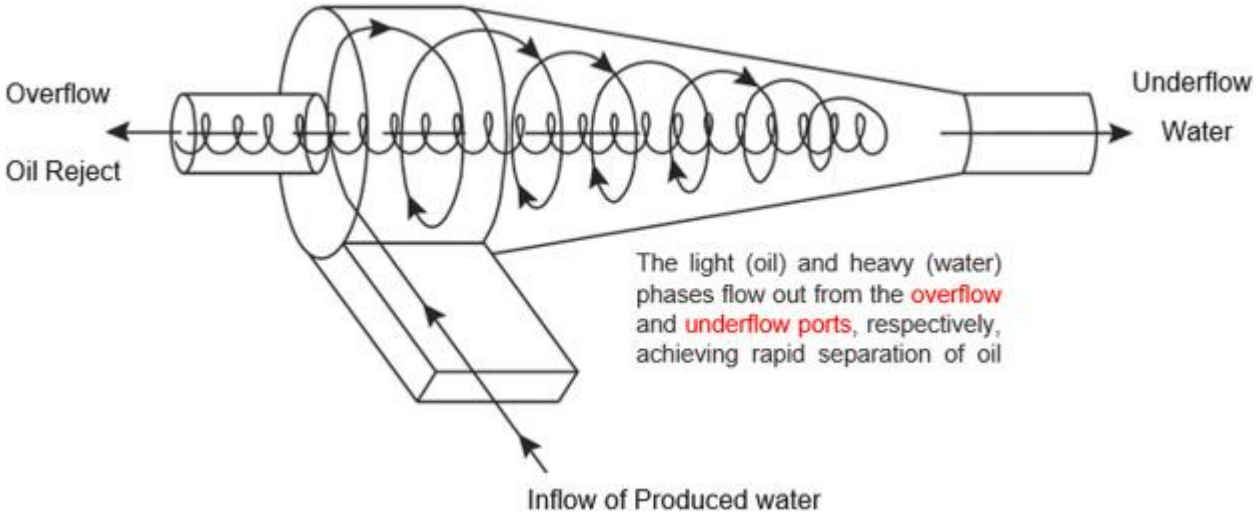

Figure 2: Hydroclones O/W emulsion separation mechanism *(Amakiri et al. 2022)*.

2.2.3 Floatation

It is a Physico-chemical method of treatment. According to (Ishak et al. 2017), the process of separating small particles of various materials by treatment with chemicals in the water which results in some of these particles adhering to air bubbles and rising to the surface for removal while others remain in water is referred to as flotation. Figure 3 below according to (Syarifah Nazirah et al. 2017), shows a usual gas (dissolved) flotation system.

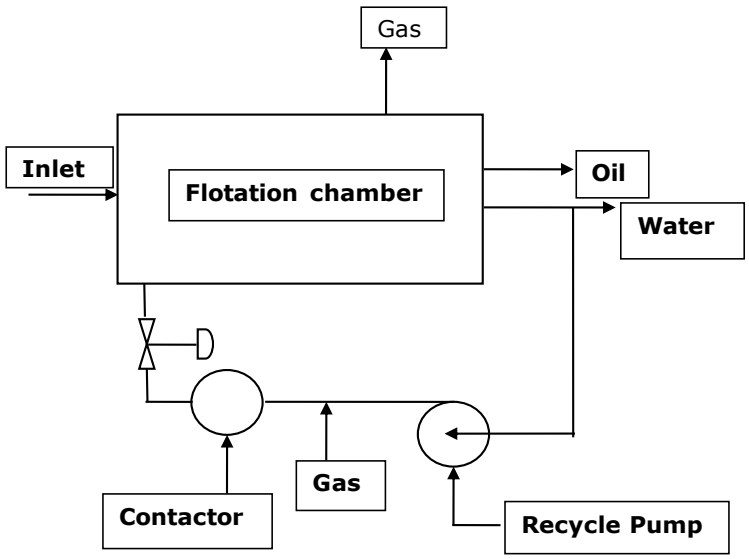

Figure 3: Gas dissolved flotation system *(Syarifah Nazirah et al. 2017)*

The major advantage about flotation is that it helps with the removal of small particles, as well as particles of low density more completely and in a shorter time. Its retention time is shorter. However, for O/W emulsion, it becomes difficult because of the size of the bubbles and the several factors that are sensitive to the process. Several factors can affect the efficacy. The factors include the pH, pressure, and feed rate. (Ran et al. 2013), clearly explains that for the performance of the floatation process to be improved, characteristics of the floatable particles and the process parameters need to be determined properly. This has resulted in the method being more stressful, time consuming and several use of apparatuses which always increases the cost.

2.2.4 Coagulation and Flocculation

It is another chemical method of treatment of O/W emulsion. Suspended particles like oil droplets in O/W emulsion can be removed with coagulation by the addition of chemical agents also known as coagulant such as ferric chloride, polymers, aluminium sulphate, or ferric sulphate. This method makes use of coagulants which scatters the colloids by defusing the forces that makes them stay separate. Lowering of the zeta potential of the colloids to lesser value where they can no longer stick together is the mechanism used in coagulation (Amakiri et al. 2022). The method is usually accompanied by flocculation which causes the fine particles to merge and infuse into larger particles to reduce the cloudiness of the fluid. The process involves two stages, which are the rapid mixing coagulant in the produced water and the flocculation for merging of the small particles into a well-defined floc because of a calm agitation. This method has a straightforward operation, a straightforward design, and makes use of low energy. It is also very adaptable and can be used at various stages of O/W emulsion ((Teh, Wu and Juan 2014). The coagulants used include aluminium sulphate and poly aluminium chloride. As seen in Figure 4, the success of this process is determined by the selected coagulant, the dosage of this coagulant, the treatment technique to be applied and the composition/ characteristics of the emulsion.

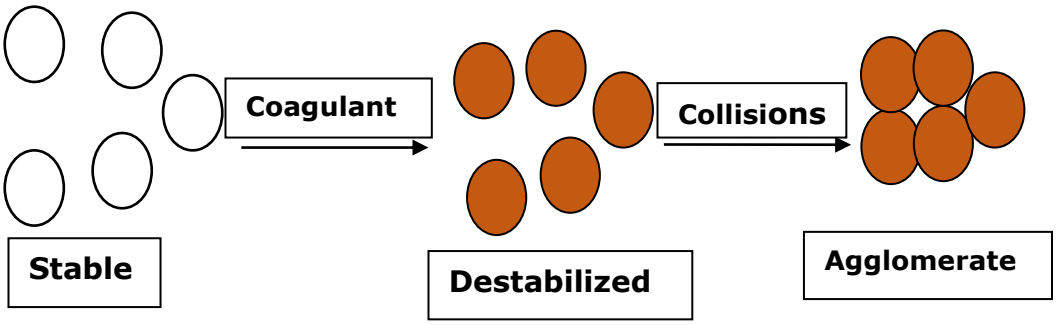

Figure 4: The process of coagulation. *(Syarifah Nazirah et al. 2017)*

Dosage plays a key role in the efficacy of this method, because overdosing the coagulant could lead to the restabilising of the particles. The chemical coagulant could as well pose a threat to health if not properly monitored. Coagulant utilization was employed by (Sun et al. 2017) to treat oily wastewater and it was discovered that the coagulant affected the filtration flux. It found that the filtration flux improved because of the coalescence between the droplets taken together and the consequent size of the emulsion. However, the flux decrement was found to be as result of the excess dosage of the coagulant.

2.2.5 Advanced Oxidation Processes (AOP)

Produced water is composed of oil and grease, mono and polycyclic aromatic hydrocarbons, phenols, benzenes, and naphthalene all of which forms multiple organic compounds that can be degraded at once with AOPs (Advanced Oxidation Processes). AOP transforms pollutants into hydrophilic, degradable, or biodegradable short chain compounds via the use of highly reactive species such as hydroxyl radicals in advanced oxidation techniques (Mendonça et al. 2017; Comninellis et al. 2008). Furthermore, advanced oxidation processes using nanotechnology will offer a better separation efficiency in lower O/W emulsion.

This method is an eco-friendly method for separation of O/W emulsion (Ameta and Ameta 2018).

An example of the chemical reactions characterising AOP is the reaction given by (Comninellis et al. 2008) where discharge of water above 1.23 V potential vs standard hydrogen electrode (SHE) under standard conditions. The anode active sites (M) produced adsorbed hydroxyl radicals $(M(*OH)_{ads}$ that participates in the mineralisation of organic pollutants (R) in aqueous solutions:

$$R_{(aq)} + (n/2)M(*OH)_{ads} \rightarrow (n/2)\,M + mineralisation$$

$$products + (n/2)H^{+} + (n/2)\,e^{-}$$

Equation 1: AOP chemical reaction

Where n represents the total number of electrons involved in the oxidation reactions of the organic pollutants.

Hence focus should be placed on AOPs as an advancement instead of the conventional methods. AOPs can be used for pre or post treatment of O/W emulsion for either highly concentrated or lesser concentrations with even lower or higher oil droplet sizes. A major merit of AOP is the absence of any secondary waste radicals as AOPs radical reacts directly with pollutant to degrade and convert to simpler eco-friendly compounds (Nicholas 2019). The demerit associated with this AOP method is the choice of design for a particular pollutant and the cost from electrical energy consumption needed to degrade a pollutant and the unit of water volume required.

2.2.6 Biological treatments

The use of microbial metabolism so that the colloidal organic pollutants in the emulsion are converted into harmless substances is referred to as biological treatment. O/W emulsion have been overcome using anaerobic and facultative digestion. According to (Sadhukhan et al. 2016), it involves four fundamental phenomena, which are hydrolysis, fermentation, acetogenesis and methanogenesis. This process is very energy consuming. An example of a biological treatment for O/W emulsion is Activated Sludge Process (ASP).

2.2.6.1 Activated Sludge Process

Well oxygenated mixture of wastewater and bacteria along with other microorganisms in a sludge are stirred up continuously. This is known as the activated sludge process for biological treatment of O/W emulsion. This involves the process of mixing microorganisms with oily wastewater allowing proper oxygenation. After aeration stage of the procedure, the flocculants are allowed to settle at the bottom of a secondary tank; the effluent from the process is released for discharge. The sludge is recycled back into the initial tank for a repeat process. (Magalhães, E. R. et al. 2021) used activated sludge process for the treatment of produced water and a 91% yield of separation of oil and grease was achieved. Figure 5 represents the systemic procedure of activated sludge for the treatment of wastewater.

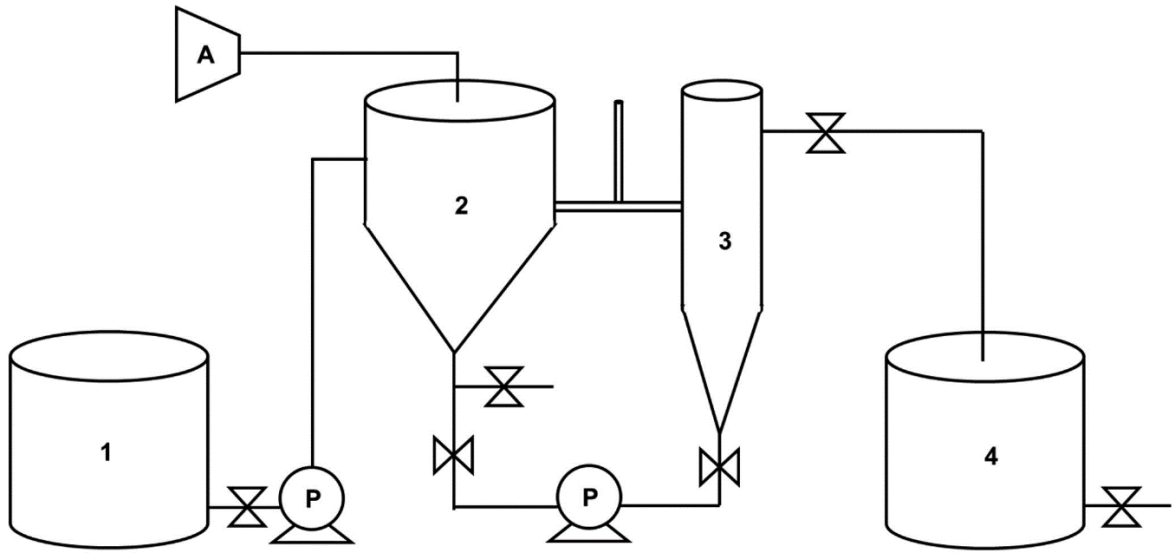

Figure 5: Activated Sludge process used for treatment of wastewater. 1, 2, 3 and 4 represents feed, aeration, settling and storage tanks respectively. A is the air compressor and P is for peristaltic pumps (Magalhães, E. R. et al. 2021).

However, with the introduction of high recalcitrant toxic components in wastewater, the process becomes inefficient for the separation of oily wastewater. This was evidenced by the work of ((Mazumder and Mukherjee 2011) who used coagulation and activated sludge method for the treatment of automobile service wastewater and the activated sludge yielded 18-65% oil and grease removal efficiency.

2.2.7 API Separators

API separators are commonly used for the separation of O/W emulsion due to its low cost, technique simplicity, maintenance low cost, and high potency. The

mechanism behind this method is the use of specific gravity variations present in the medium that allows heavy materials to settle at the bottom and light components flow at the top. In the case of O/W emulsion, it is expected that oil content will float at the top leaving the water content to settle at the bottom as seen in Figure 6. It has been reported that separation by gravity can reduce oil or suspended solids in oily wastewater to about 60% (Varjani et al. 2020). Though the energy consumption for this method is very minimal and maintenance of the instrument is low, there is production of sludges that might arise when using real O/W from industries that will create a secondary pollution. Furthermore, this method will not be suitable for O/W emotions of lower concentration with droplet size below 20 µm. This can be seen in the research of (Krebs, Schroën and Boom 2012) with study of enhanced gravity separation kinetics of O/W emulsion where a reduction in droplet size for O/W emulsion resulted in a reduction in separation efficiency.

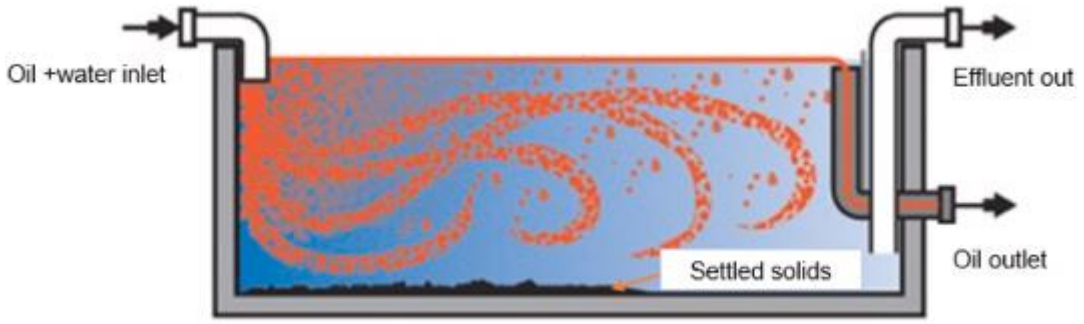

Figure 6: Schematics of API oil-water separator. *(Amakiri et al. 2022)*.

2.2.8 Skimmers

This involves the use of mechanical devices in the recovery of oil and O/W emulsions from the surface of the sea, especially during oil spills (Abidli et al. 2020). This method does not require to change the physical and chemical properties of the oil or O/W emulsions. All skimmers based methods use one of the following processes in oil recovery

- Suction recovery: which includes vortex, weir, and Dynamic inclined plane (DIP)
- Adhesion recovery: skimmers using this process are belt, drum, disc, rope, mope, and brush skimmers.

All these conventional methods are encountered with various shortcomings such as flux ineffectiveness, high capital, and operational costs, and sometimes get contaminated again. Additionally, when it comes to small droplets of O/W emulsions in the region of microns, conventional technologies become inefficient and cannot remove smaller emulsions (Rashad et al. 2021). Also, the separation percentage of oil from water has not achieved 99% for conventional methods (Chakrabarty, Ghoshal and Purkait 2010). Based on this, permeate water from the treatment of conventional methods must undergo further treatments to achieve regulatory limits before discharge or reuse. Membrane separation has recently drawn attention as the most research technology for the separation of oily wastewater due to its separation efficiency especially in micrometre scale. Membrane technologies are recognized worldwide as oily wastewater separation technology because it is cost effectiveness, simple to operate and high energy efficiency. This technology is employed in this research for the separation of O/W emulsion.

2.3 Membrane Technology

Membranes have been used for variety of applications in various areas of human lives, which includes separation processes, catalytic processes, biomaterial production and its use in for the creation of analytical devices in the laboratories (Schuller et al. 2020). The application of membrane technology is present in all sectors of industry ranging from pharmaceuticals, mines, or food industries (Agboola 2019; Motuzas et al. 2018; Dhineshkumar and Ramasamy 2017). (Magalhães, H. et al. 2018a) defined membranes as a semipermeable and selective barrier, that can separate phases limiting, totally or partially, the passage of one or more constituent contained in a solution. Membrane filtration as a definition that is the separation method of particulate matter with the use of a permeable barrier i.e., the membrane in a continuous liquid flow (Urošević and Trivunac 2020). During this membrane filtration process, there is an accumulation of the particulate matter on the surface of the membrane and the permeate which is the filtrate is received at the opposite side of the membrane. Retentates which are particulate matters from the feed that does not permeate through the pores of the membrane is recirculated back to the feed to go through the membrane filtration process again to squeeze out as much permeate as possible. Asides the normal membrane filtration, there is the crossflow filtration which allows the parallel or tangential movement of the feed stream to the surface of the membrane (Girard and Fukumoto 2000). Crossflow filtration process reduces membrane fouling due to the shear acting on the membrane during the retentate flow across it (Zsirai et al. 2016). Permeate flux is the quantity of permeate in this case water produced at the opposite side of membrane filtration during separation per unit of time over the membrane filtrate area (Pal 2015). The driving force and the permeate flux through the membrane is proportional. In this case, transmembrane pressure gradient is the driving force for micro and ultra-filtration. The applied transmembrane pressure and the membrane permeability determines the permeate flux (Mulder and Mulder 1996). Two factors are responsible for the separation process in membranes which includes: concentration gradient occurring between two phases of a semi-permeable membrane and pressure in membrane, which happens in micro, ultra, nano filtrations and reverse osmosis processes ((Timoteo Júnior 2007). Based on these two factors, membrane becomes a

formidable technology in separation and has gained an increase in research interest for the separation of O/W emulsions.

2.3.1 Classification of membrane

Membranes are commonly classified based on conventional methods than range from membrane materials, preparations methods, cross-section, membrane shape (Bardhan and Subbiah 2022). In the case of membrane materials, classification is grouped based on the material for production of the membranes like organic polymers or inorganic materials (Li, C. et al. 2020). Two varied materials are used for the development of membranes, and they include organics, which are mostly used for polymeric membranes; inorganic which are used for producing ceramic membranes. The cross-section classification methods include symmetric, asymmetric, or multi-layered membranes. The preparation method of classification involves both physical – stretching and track etching, and chemical – sol-gel and phase inversion processes etc methods. Membrane shape classification methods includes hollow or tubular and flat sheet membranes. In this subsection focus is placed on the material type methods of classification as other classification methods will be discussed in later sections.

2.3.1.1 Polymeric Membranes

Polymeric membranes were the first to be introduced in the early 1960s for the separation of O/W emulsions (Hubadillah et al. 2019). Polymeric membranes have gained several recognitions in industries for filtration and separation with membrane. This arises from the fact that polymeric membranes can withstands high volumes water separation, economic strength, lower carbon footprint and easy application (Schuller et al. 2020). Presently, polymeric membrane from various kind of materials has been commercialized all over the world. Some commonly used polymeric membranes includes polytetrafluoroethylene (PTFE), polypropylene (PP), polyethylene (PE), and polyvinylidene fluoride (PVDF) and a widely used for different separation processes. Asides been the mostly studied and used membranes for water purification and separation (Liu, Z. et al. 2017) and ((Tul Muntha, Kausar and Siddiq 2017), polymeric membranes contain some drawbacks of not being able to withstand increase in temperature and serious chemical situation (Jamalludin et al. 2016); hence the increase in focus on ceramic membranes. Despite these disadvantages several polymerics

membranes have been used for the study of water and wastewater purification processed as reviewed by ((Bardhan and Subbiah 2022). For instance, the reported study of (Shaikhiev et al. 2019) used two modified polymeric membranes polyether sulfone and polyacrylonitrile to intensity separation efficiency of O/W emulsion. (Guan et al. 2020) reported the use of aliphatic Poly ketone as a polymer matrix for the separation of O/W emulsion. The polymeric membrane was reported to show promising results in the separation efficiency of O/W emulsion.

2.3.1.2 Ceramic membrane

Ceramic membrane is classified as inorganic membrane and the description is illustrated as a permselective barrier that has two different separation and permeability factors used as indicators for performance of the membranes (Li, K. 2007). Usually, ceramic membranes are classified into two major classifications – Porous and Dense ceramic membrane. Porous ceramic membranes are ruled by factors such as porosity, pore size and the thickness of the membrane. Whereas dense membrane is governed by principles with complex permeation and separation. Both classifications of ceramic membrane application and separation depends on the pore size of the membrane ((Hubadillah et al. 2019)

Ceramic membranes are also called Composite Membranes because they are made up of several layers of one or more different ceramic material. Ceramic membranes are composed or produced from metal oxides like alumina, zirconia, titania, mullite, silica and some other oxides and are usually sintered at elevated temperatures in a three-layered structure. This structure is composed of a support inner layer which is referred to as the macro porous layer, the intermediate layer, and the top layer, which is usually densely packed, where separation takes place (Abdullayev et al. 2019). Ceramic membranes are classified into two groups namely Porous ceramic membrane and dense ceramic membrane.

The ceramic membrane is made with asymmetric layers of aluminium oxides composites. As mentioned previously, the ceramic membrane is composed of three layers illustrated in Figure 7; the layers are made of the active or microporous layer also called the dense layer with the smallest pore size that is responsible for separation processes and has a thickness range between 5 – 10 µm with a porosity of 30 to 50%. The second layer is the intermediate layer that

has approximate porosity of 40% with medium pore size and thickness range from 30 -40 µm. The intermediate layers act as a support and protection for the microporous layer. The macroporous layer is the third layer which is responsible for mechanical strength to the entire ceramic membrane. Its pore size and thickness ranges from 1.5 – 2 mm with a porosity percentage of 40 – 45 (Usman, J. et al. 2021).

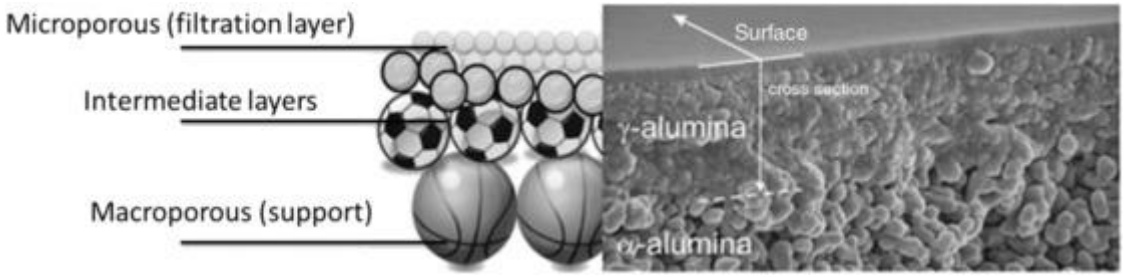

Figure 7: Ceramic membrane structural illustration. *(Zhang, Sui et al. 2014).*

Comparisons are ongoing between polymeric membranes and ceramic membranes about the advantages one has over the other. It has been reported by several authors (Phan et al. 2016; Hendren, Brant and Wiesner 2009) that ceramic membranes have more advantages in chemical, mechanical, and thermal stability, longer shelf life, high membrane flux and formidable corrosive resistance. Based on this, ceramic membrane is receiving recent attention in separation processes for water purification. Although surface modification will be required if used for hydrophobic processes as ceramic membranes are known to be hydrophilic in nature due to the presence of hydroxyl group ((Krajewski et al. 2006).

2.3.1.3 Symmetric Membrane & Asymmetric or Multi-Layered Membrane

Symmetric membranes also termed Isotropic Membrane are well known for their interconnecting pore, rigid and void structure that contains pore sized distribution between 0.01 – 10 µm (Baker 2012). This makes the pore size distribution the primary separation factor that influences separation process of symmetric membranes as well as the hydrodynamic conditions of the liquid phase (Abdullah et al. 2018). Any physical or chemical methods of membrane preparation can be used to achieve the production of symmetric membranes. Figure 8 represents the schematic of symmetric and asymmetric membrane.

Asymmetric membranes also termed Anisotropic reflect a whole change in porosity and porosity with a layered structures across the entire membrane.

Typically, asymmetric membrane is made up of thin surfaces outer layer placed on a thick microporous support layer (Baker 2012). The thin outer surface layer acts as the selective separation layer. This multi-layered membrane usually generates higher flux due to the different pore sized in the layers (Abdullah et al. 2018). There is always a change in porosity and pore size all through the cross section of the membrane. Usually, phase inversion is normally used to prepare asymmetric membranes.

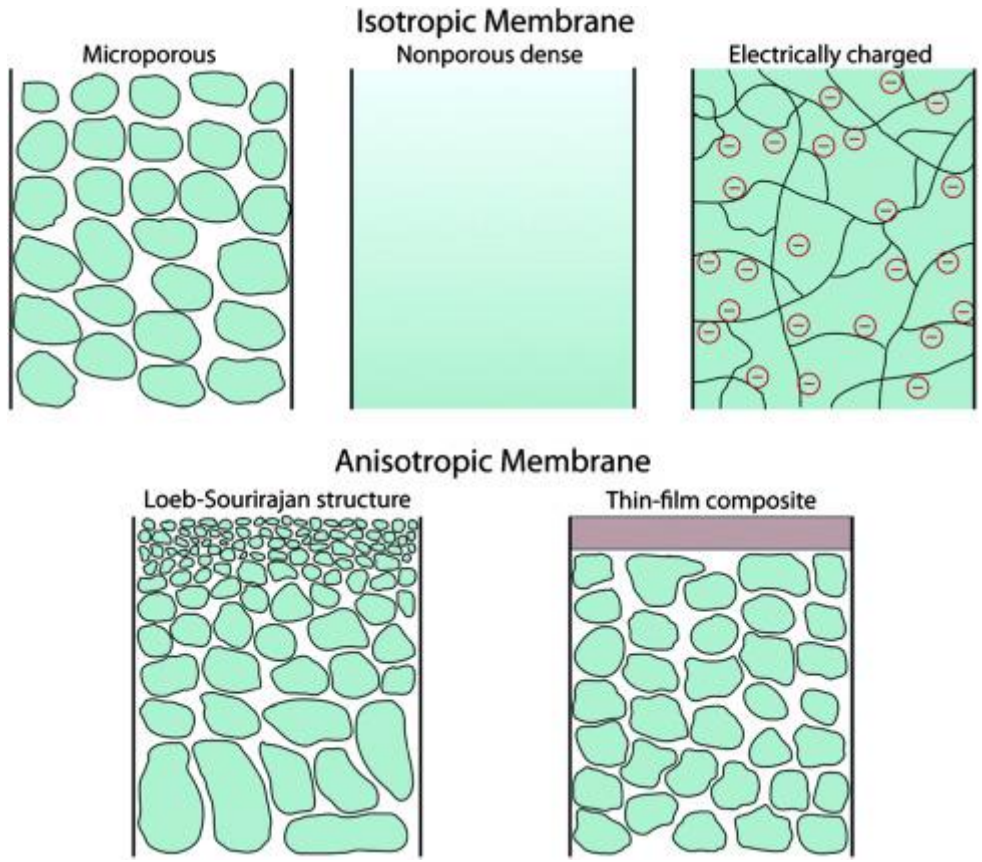

Figure 8: Schematic diagram of pore sizes and Porosity of Symmetric and Asymmetric Membrane. ***(Abdullah et al. 2018)****.*

2.3.1.4 Tubular and Flat sheet Membrane

In relation to flow of feed liquid and permeate, membrane configuration can be described as the geometry of membrane and how it is positioned in space. All membrane configurations are divided into two major membrane geometry named – Planar (where the flat sheet membrane falls) and Cylindrical (where the tubular or hollow fibre membrane falls) (Berk 2018). The membranes configurations that are found in the planar geometry square or circular that can also be arranged in a stack vertically or horizontally. Alternatively, the hollow fibre or tubular membrane has a wide range of diameter (50 -3000 μm). Fibres

are made by forming a microporous structure with a dense selective surface layer. As clearly elaborated in Figure 10, usually, the dead-end flow direction is inside out where the tubes contain the retentate flow and at the end shell the permeate is collected as seen in Figure 9. Crossflow filtration can be used with tangential flow that runs across the membrane surface. A backwash can be achieved with a reverse flow to clean and unclog the membrane pores.

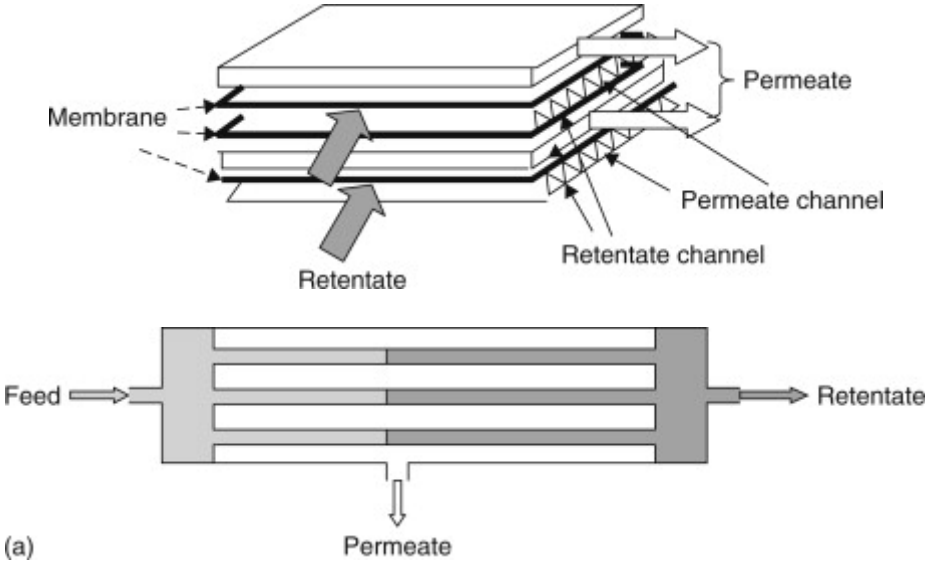

Figure 9: Schematic diagram of a Flat sheet and tubular membrane. *(Berk 2018)*.

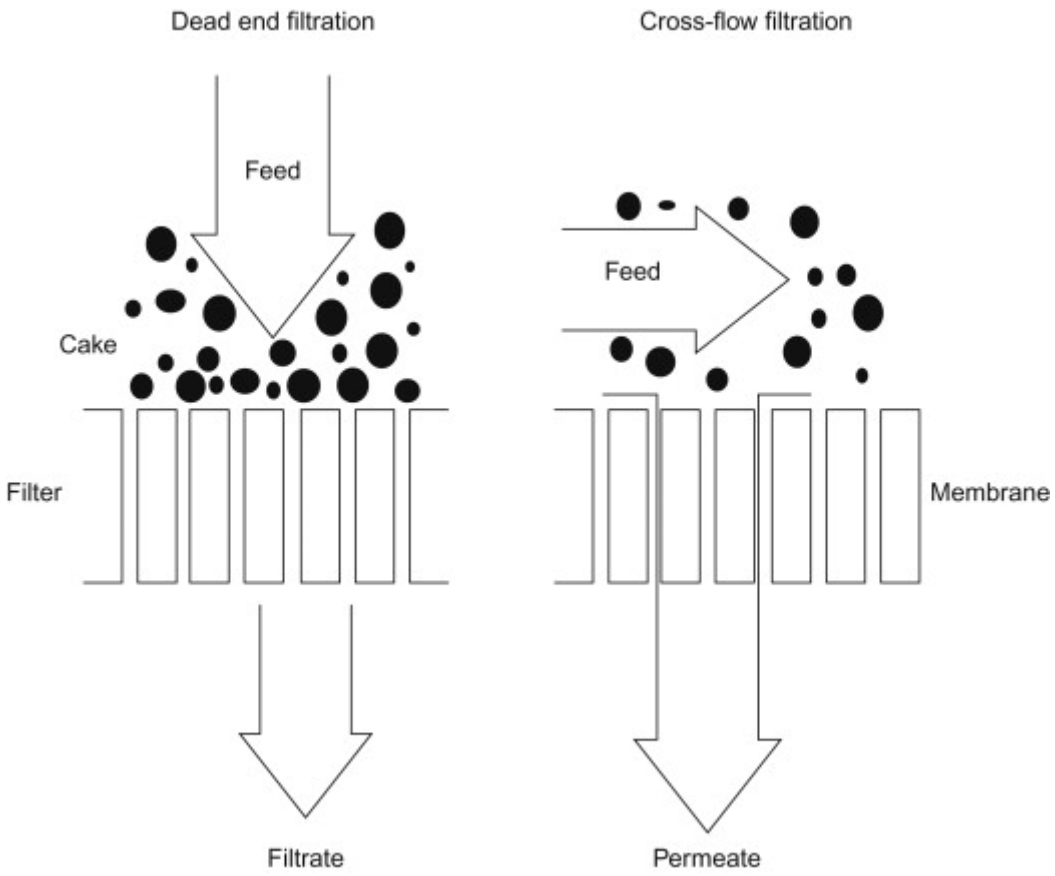

Figure 10: Schematic diagram of a dead and crossflow filtration mechanism through a membrane. *(Bhave 2014).*

2.3.2 Membrane types and materials

Membranes used in water purification can separate a wide range of contaminants or pollution starting from big colloids, algae, microorganisms with distinctive characteristics in size or dimensions from micrometres to picometers (Geise et al. 2010). Figure 11 represents the many sizes of different solutions that are commonly filtered using membrane filtration. Membrane types are distinguished based on their pore sizes into four groups. These groups are called Microfiltration (MF), Ultrafiltration (UF) and Nanofiltration (NF) and reverse osmosis (RO).

MF is a separation process that uses microporous permeable materials as a barrier for separation. When made with metal oxides as ceramic membrane is, MF exhibits the advantages of ceramic membranes (Magalhães, H. et al. 2018b). The pores of MFs are in the order of 1 μm and can be used to remove large colloids and other microorganisms (Miller et al. 2017).

UF is also a separation process like MF and deliver liquids mixtures into separate phases. The major difference is that UF have smaller pore sizes which becomes advantageous for certain separations (Alem, Sarpoolaky and Keshmiri 2009). The smaller pores of UFs are used to separate macromolecules, proteins, and smaller colloids from a solution (Miller et al. 2017). The separation mechanisms used in both MF and UF is size exclusion; where solutes larger than the membrane pore size are rejected and cannot permeate the membrane barrier and solutes or solvents smaller than the pore size of the membrane can flow through the membrane barrier (Baker 2012).

NF is a new separation process that is produced by the impregnation of nanoparticles on the surface of a membrane (Blumenschein et al. 2016). NF is gaining attention in water purification process due to their low energy consumption and acceptance of monovalent ions and rejection of divalent ions (Mohammad et al. 2015). NF membranes have been designed with characteristic small pores and the transport mechanism employed uses a combination of convection, diffusion, and electrostatic models (Hilal et al. 2004).

RO membranes are non-porous and highly dense that focuses on the removal of salt from water hence used for the desalination of sea and brackish water (Miller et al. 2017). The flow mechanism of RO membrane employs solution diffusion mechanism and rejects both monovalent and multivalent ions (Wijmans and Baker 1995; Lonsdale, Merten and Riley 1965).

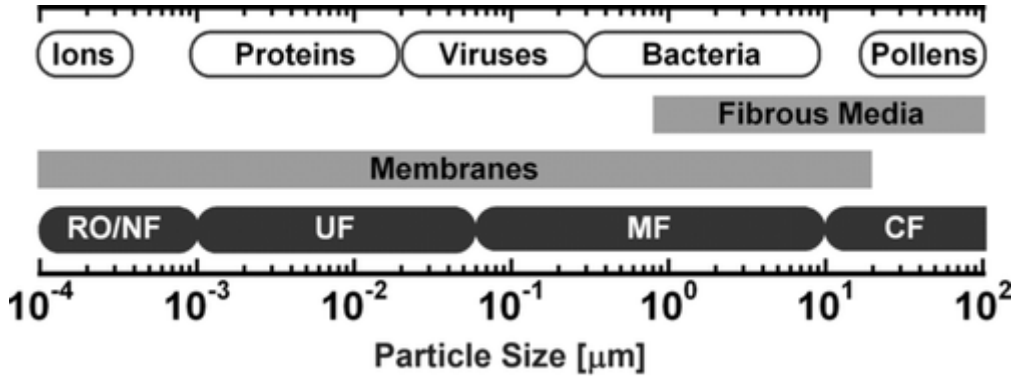

Figure 11: Relative sizes of various solute commonly rejected by membrane filtration. *(Miller et al. 2017).*

2.3.3 Types of ceramic membrane modification

Ceramic membranes are made up of metal oxides and they are produced at elevated temperatures by sintering. By production, they are made to be hydrophilic because of the hydroxyl (-OH) groups present in them. The density of the -OH groups, however, declines post elevated temperature calcination during production, making it less hydrophilic as should be (Chang et al. 2010a). In the last decades, so many applications generated interest in the modification of ceramic membranes for the improvement of separation efficiency, process development and reduction of fouling processes. The major drawback of membrane separation processes is fouling; based on this, surface modification of ceramic membrane will be a useful technique in the reduction of fouling by disallowing interactions between unwanted feed particles and the surface of the membrane (Liu, L. et al. 2019). Additionally, this surface membrane modification can boost selectivity of membrane for specific separation objectives (Padaki et al. 2015). Hydrophilic ceramic membrane can be achieved by appropriate choice of material for roughness and surface texture. This hydrophilic membrane can be prepared by attaching hydrophilic materials such as Silica Oxide, Titanium Oxide, magnesium oxide etc. on to the surface of a ceramic membrane. This aids in the improvement of affinity and the response of the membrane for the desired separation application, in this case of hydrophilic ceramic membrane, it will achieve excellent oil repellent. Ceramic membrane gives room for flexible surface modification to suit the analysis required. This surface modification can be fabricated on the top layer of the membrane using the technique required. There are four commonly used techniques for the surface modification of ceramic membrane, and they include chemical vapor deposition (CVD), Immersion, Sol-gel, and Lipid solution direct grafting (Usman, J. et al. 2021).

2.3.3.1 Dip-Coating

The dip-coating techniques has the advantage of easy operations and flexibility is one of the frequently used methods for ceramic membrane modification (Xia et al. 2000). This technique can be used to coat suspensions of powder in sub micrometres (Bonekamp 1996). By means of capillary forces, a dry substrate (membrane support) is dipped into a solution or powder suspension and subsequently withdrawn to allow the absorption of a layer on membrane

support. A controlled calcination is introduced once the substrate is dried due to interaction with the atmosphere (Barati, Husein and Azaiez 2021). Usually, coating thickness is within the range of 100 nm – 100 μm in the process of dip - coating. (Yang, Yulong et al. 2021) used dip-coating technique for surface modification of one-step Attapulgite (ATP) based nanotube ceramic membrane that resulted in high porosity of 61.9% and pore size of 20.2 nm as presented in Figure 12 below.

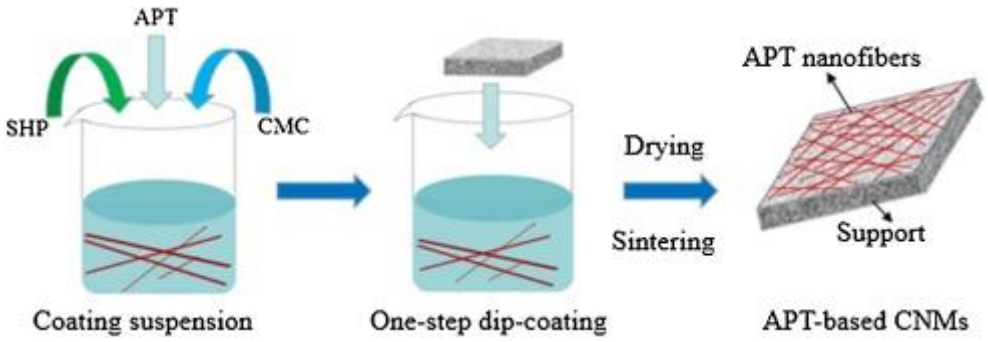

Figure 12: Schematic of dip-coating modification of nanofiber ceramic membrane. *(Yang, Yulong et al. 2021).*

2.3.3.2 Sol-gel

Sol-gel method is the most used for modification of ceramic membrane and is works by making a porous thin top layer with moderate porosity on diverse types of substrates and have been widely used for different industrial applications (Nair et al. 1997). Figure 13 represents a schematic process of the sol gel method on ceramic membrane. Two types of sol-gel techniques are known, and they are – Polymerization of Molecules Units (PMU) and Destabilization of Colloidal Solutions (DCS). The process of PMU occurs by the hydrolysis and polycondensation of alkoxides and subsequent ageing and drying of modified ceramic membrane in room temperature. The use of peptization of inorganic salts or hydrous metal oxides is the process deployed by DCS with an electrolyte and then gel solution are obtained as the colloidal solutions are destabilized (Amin et al. 2016). Using dip coating method, the precursor sol can be layered on the membrane support forming a top layer or made into a desired shaped by casting into a suitable container to produce a membrane (Guizard, Christian 1996). Preparation of the membrane should be done in a dust free area to avoid pinhole defects formation on membrane. At the sol stage particles might aggregate in the DCS, hence, PMU method is considered most suitable for NF ceramic membrane preparation (Cai et al. 2015). Narrowing membrane pore size

is the aim of the sol gel method of ceramic membrane modification thereby lowering fouling on the surface. (Bayat et al. 2016) used sol gel method to prepare γ-alumina UF membrane with a pore size of 20.3 nm to separate oil from oily wastewater and achieved permeate flux of 112.7 L/m^{2}H with % oil rejection of 84 at 5 bar pressure.

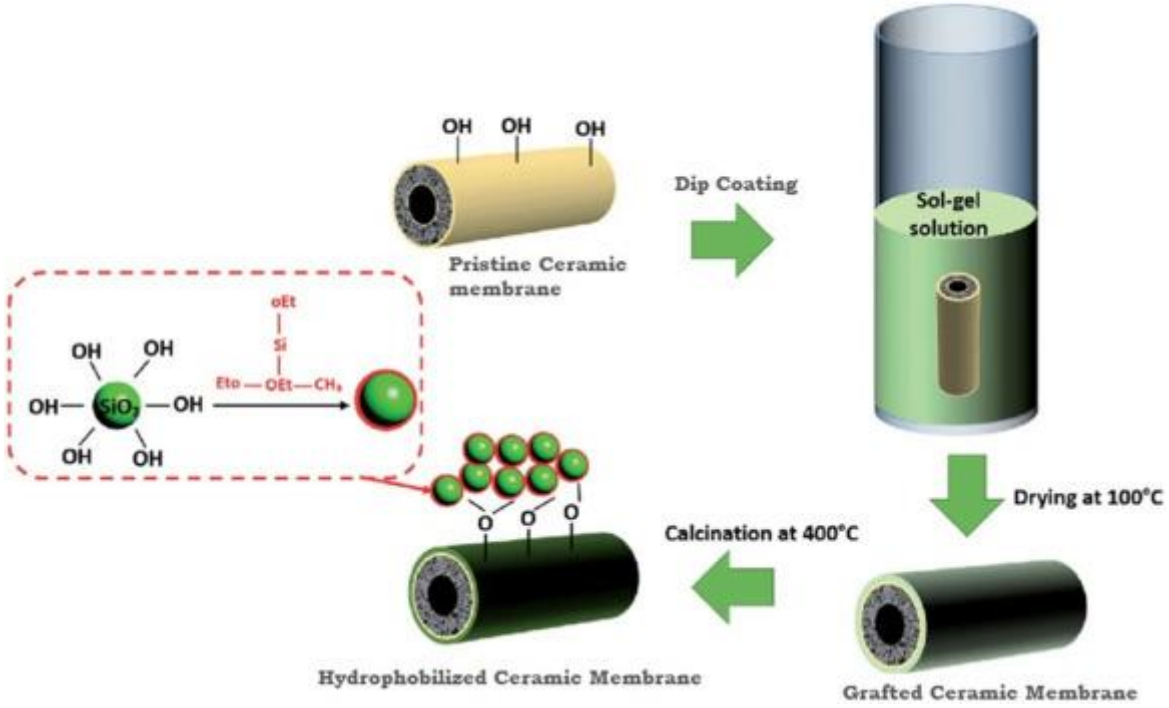

Figure 13: Sol-gel grafting process of the ceramic membrane. *(Feng et al. 2004).*

2.3.3.3 Surface Grafting

The combination of polymer chains is used to achieve surface grafting method of membrane modification when the polymer chain is bonded on a solid surface during a chemical reaction creating a covalent bond between the polymer chain and membrane surface (Rezakazemi et al. 2018; Faibish and Cohen 2001b). This type of modification gives a long-lasting chemical stability. Polymers like poly(vinylpyrrolidone) ((Faibish and Cohen 2001a), fluoroalkyl silanes (FAS) (Krajewski et al. 2006), and polyethylene oxide (PEO) (Atallah et al. 2019) are used as membrane precursors. Pre-treatment of membrane surfaces by chemicals, plasma, UV-irradiation, or enzymes is employed before initiation of membrane grafting (Nady et al. 2011). In the grafting process, depending on the polymer used, the membrane surface can be changed from hydrophilic to hydrophobic and vice versa. This grafting method is also useful for the reduction of fouling in membrane technologies for oily wastewater treatment. (Su et al.

2012) while preparing a superhydrophobic and super oleophilic membrane used the sol-gel method and subsequently used the surface grafting method to achieve a 161.2^0 water contact angle and 0^0 oil contact angle.

2.3.3.4 Blending or Doping

Inorganic nano-sized particles are blended or doped into the matrix of a membrane which is used as another form of surface modification in membrane technology (Monash, P. and Pugazhenthi 2011a; Zhang, Qi, Fan and Xu 2009). Physical mixing is employed in this method to mix membrane precursors with nanoparticles. The mixture is subsequently sintered via solid-state reactions at optimized temperatures. There has been a wide usage of the method for both organic and inorganic composite membranes with various types of inorganic materials like silicon dioxide, zeolites, titanium dioxide and carbon nanotubes have been used to produce Nanofiltration/reverse osmosis membranes in combination with organic polymers (Chen, M., Heijman and Rietveld 2021). (Liu, R. et al. 2018) has used nanoparticles of SiO_2 for doping alumina matrix and this resulted in an increase in hydrophilicity that later increased flux of water and oil by 20.5% and 6% respectively.

2.3.3.5 Hydrothermal Method

The usage of hydrothermal technique for coating of membranes has been applied to the fabrication of inorganic materials and zeolites (Yang, Guijun and Park 2019; Huang, A. and Yang 2007). Typically, a hydrothermal reaction heats up a mixture of precursors at temperatures between 80 – 230^0C in an autoclave for several hours even up to days (Yeo et al. 2013). There is then an immersion of membrane into the solution of mixed precursors to obtain membrane modification and subsequently the entire autoclave is moved into an oven for the hydrothermal process to take place. The modified membrane is calcined after been washed and dried. There are several merits associated with this method such as low cost, high yield, and an easy set up (Senapati and Maiti 2020). Based on these merits, several interests have been generated in research to use this method for membrane modification. (Suresh et al. 2016) reported this technique for the modification of TiO_2 and y-Al_2O_3 ceramic membrane that yielded not just a high flux during oil in water separation but high % oil rejection as well due to the increase in hydrophilicity of the membrane.

2.3.3.6 Chemical Vapour Deposition (CVD)

In CVD temperatures rising between 400 – 1000^{0}C are used to deposit a thin film of gas phase precursors that is generated by reaction on the porous substrates (Mavukkandy et al. 2020). The vapour from the solvent reacts with the surface of the ceramic membrane via hydrogen or covalent bond. The entire CVD process takes place in a sealed container like Teflon and heated in an oven at the boiling point of the solvent creating a modified ceramic membrane (Ahmad, N. A. et al. 2015). This optimizes the pore size and structure of the membrane to improve selectivity. In this technique of membrane modification, repeated coating is not required hence makes it preferred to dip coating or sol-gel techniques (Khatib and Oyama 2013). CVD creates thin films on the surfaces of ceramic membranes. A small volume of solvent is heated up to vaporization stage in CVD. Recently in CVD for ceramic membrane modification the target has been to achieve tailoring of membrane pore size for use in gas separation applications, catalyst membrane reactors and fuel cells. Though CVD has been reported in the use of water separation technology for the preparation of high-performance ceramic membranes ((Chen, M. et al. 2020; Zhang, Feng et al. 2017; Chen, X. et al. 2012).

2.3.3.7 Atomic Layer Deposition

Atomic scale thin films of metals polymers, oxides and many other materials are used is atomic layer deposition method for the modification of membranes. During the ALD process, the pulsation of two precursors is alternated and strictly separated from each other by a purge step in the gas phase. Therefore, one monolayer is formed in each cycle during this procedure and the repetition of this procedure can tune the thickness of the deposited layer (Grigoras, Airaksinen and Franssila 2009; George, Yoon and Dameron 2009). This method is opposite chemical vapour deposition (CVD) method in which precursors are simultaneously exposed to substrate to allow the reaction in the free space chamber, ALD has the following merits that is favourable for the functions and modification of porous materials. Firstly, the two precursors in ALD process can access very small pores and be absorbed on pore walls and react with pre-existing precursor formation because the precursors are vapourised (Jiang et al. 2007). Furthermore, ALD reaction takes place in the subsurface for polymeric

substrates and on substrate surface such as pore walls and creating thin films in each cycle that gives uniformity and conformality instead of thick particulates (Kucheyev et al. 2008). Lastly, a variety of substrates such as polymer (Kemell et al. 2008), ceramics (Qin et al. 2008), inert carbon materials (Qin et al. 2010) or even biomolecules (Lee et al. 2009) can be modified by ALD films giving a specific task function surface and modified structure. Figure 14 below displays the schematic diagram of ALD process. Recent research has been reported of the usage of ALD for the modification of membrane such as the report of ((Liang et al. 2010) for the modification of nano porous polymer membrane.

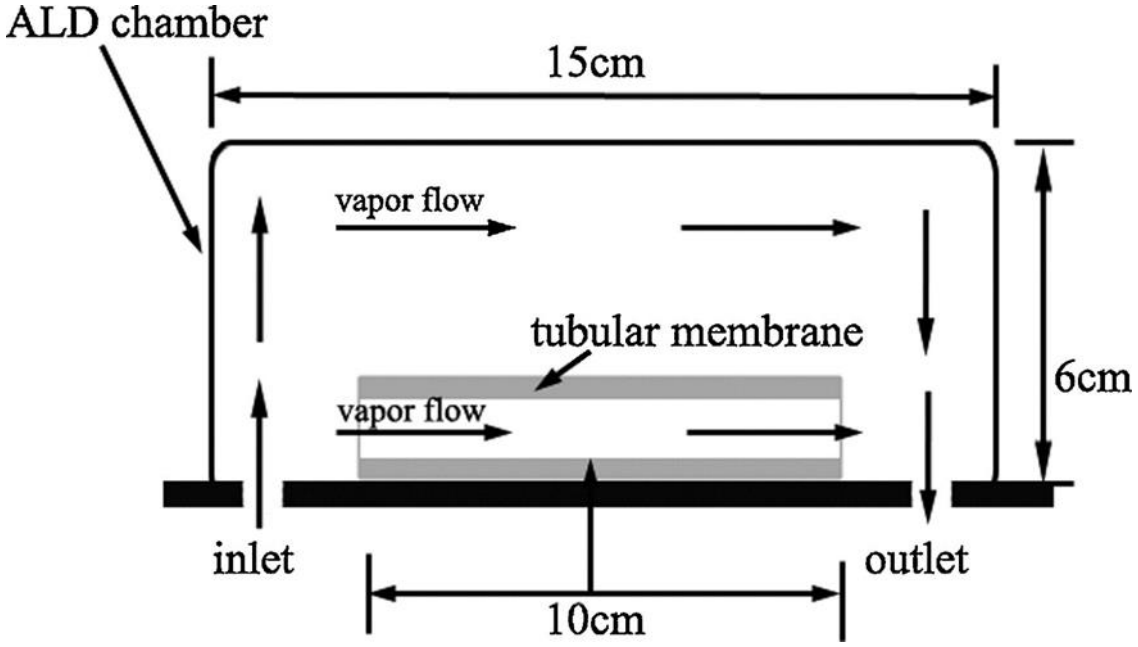

Figure 14: Schematic diagram of ALD chamber containing a tubular ceramic membrane. ***(Li, F. et al. 2012)***.

2.3.4 Common-type ceramic membranes

The determination of membrane performance and function is based on the criticality of the material and fabrication process. There is no random selection involved in the selectivity of ceramic membrane material in water and wastewater treatment. This is usually determined by some critical physical and chemical factors which include, hydrophilicity, chemical and thermal stability, porosity, and pore size (microstructure), mechanical strength and other necessary factors good for water treatment like the cost effectiveness of the entire material and process (He et al. 2019). Five major materials have been commonly used for the fabrication of ceramic membrane for water and

wastewater treatment and they are silica, alumina, zirconia, titania, and zeolite. Table 2 below compares the advantages and disadvantages of these five common materials. This section gives a critical overview of the features of these five materials considering their membrane performance, applications and limitations, and material features.

Table 2: Comparison of the merit and demerit amongst five ceramic membrane materials.

Material	Hydrophilicity	Microstructure	Chemical & thermal resistance	Mechanical strength	Other features	Reference
Silica	Third highest hydrophilicity	NF and RO	Fourth chemical and thermal resistance	Not for substrate	-	(Zheng et al. 2018; Ma, Kanezashi and Tsuru 2010)
Alumina	Lowest hydrophilicity	MF, UF & NF	3rd chemical & 2nd thermal resistance	Used as substrate (high strength)	-	(Wang, Z. et al. 2016; Hofs et al. 2011; Zhu, J., Fan and Xu 2011)
zirconia	Highest hydrophilicity	MF, UF & NF	2nd chemical & 1st thermal resistance	Used as substrate (high thermal fracture toughness		(Kayvani Fard et al. 2018; Da et al. 2016; Zhu, Y. et al. 2014)
Titania	4th hydrophilicity	UF & NF	1st chemical & 3rd thermal resistance	Occasional use as substrate (intermediate mechanical strength)	Photocatalytic oxidation	(Zhang, Xiwang et al. 2009; Van Gestel et

						al. 2002)
Zeolite	2nd hydrophilicity	MF, UF, & RO	Smallest chemical & thermal resistance	Not used as substrate	Pore structure of sub-nano zeolitic pores & inter-crystal micropores	(Basumatary et al. 2017; Kazemimoghadam 2010; Cui et al. 2008)

2.3.4.1 Silica Membrane

Several researchers have reported the development of silica (SiO_2) membrane for water and wastewater treatment (Zheng et al. 2018; Wang, F. et al. 2017; Elma et al. 2013a; Ma, Kanezashi and Tsuru 2010). Silica membrane pore sizes are controlled within the range for water molecule and hydrated salt ions which falls between the pore sizes of 3-5Å, so this enables silica membrane to purify water molecules (Kayvani Fard et al. 2018). One demerit of silica membrane is the necessity to enhance the hydro-stability due to its high affinity for water that makes the structure unstable when contacting water (Elma et al. 2013a). Metal doping, hybrid Organo silica and carbonized templating have been applied as approaches to change the surface properties of silica, to improve the hydro-stability of the membrane. On the contrast, (Elma et al. 2013b) increased the hydro-stability of silica membrane by using the sol-gel modification method to lower the silanol species concentration and this resulted in an increase in membrane performance desalination compared to other silica-based membrane.

Mitigation of organic substances from membrane fouling is particularly important to enhance proper membrane performance. (Wang, F. et al. 2017) tried to realize this purpose by the adoption of a silica sol-gel process to modify alumina membranes. As a result of this, anti-fouling behaviour was enhanced in the prepared silica membranes by the display of higher flux levels compared to only alumina membranes.

2.3.4.2 Alumina Membranes

One of the most common materials used in the fabrication of ceramic membrane is Alumina (Al_2O_3). Alumina has about four existing phases which includes α γ η and θ and the most thermodynamically stable phase is the α-alumina phase. The most used alumina phases used in water and wastewater treatment are the α and γ-alumina phases (Zou et al. 2019). The interesting thing about alumina substrate is that it can act as the active layer, intermediate layer, or the substrate support layer. This is achieved due to its attributes of chemical, thermal stability, and mechanical properties strength properties. This has enhanced the commercialization of alumina ceramic membrane in various shapes, pore sizes and module configuration from different suppliers (Hsieh, Bhave and Fleming 1988). Alumina membranes have been applied and reported in detail in various UF, NF, MF and RO wastewater treatments (Zou et al. 2019; Wang, Z. et al. 2016; Zhu, J., Fan and Xu 2011; Guillon, Weiler and Rödel 2007; Ecsedi, Lazău and Păcurariu 2007).

Pinhole defects and any defect free fabricated alumina ceramic membrane is the achievement goal as this is vital for performance efficiency in the treatment of water and wastewater (Mottern et al. 2008). Sintering, sol-gel and dip coating fabrication process are the common methods used. Modified dip coating method have been employed for the preparation of pinhole free MF alumina ceramic membrane for water purification (Zhu, J., Fan and Xu 2011). The modified MF alumina ceramic membrane is different from the common dip coating method because it assists capillary flow effect due to the application of a tangential flow of suspension against the substrate (Guillon, Weiler and Rödel 2007). This modified MF alumina ceramic membrane achieves a high pure water flux than a repeated coating and sintering process employed initially prior to using the modified method (Zhu, J., Fan and Xu 2011).

Alumina ceramic membrane has been widely researched and reported in literature. (Zou et al. 2019) reported the use of alumina UF ceramic membrane for the treatment or separation of dye in wastewater. As stated in the literature, the control of appropriate doping content of alumina nanoparticles and boehmite sols, bilayer α-alumina ceramic membranes were prepared. The modified UF α-alumina ceramic membrane exhibited good filtration performance with a molecular weight cut off about 10 kDa and water permeance of 70 L/m^2.H. Bar.

there was also a high percentage rejection of the dye of about 99% off the treated wastewater.

High flux performance is still a challenge for preparation of NF of α-alumina ceramic membrane. To meet up with industrial standard of high flux performance, water permeance of minimum 6 L/m2.H.bar for alumina ceramic membrane (Sadeghian, Zamani and Ashrafizadeh 2010; Chowdhury et al. 2003). γ-Al_2O_3/α-Al_2O_3 hollow fibre NF ceramic membrane was prepared by (Wang, Z. et al. 2016) with different molecular weight cut off (MWCO) using the sol-gel, dip coating and sintering method. The prepared NF alumina ceramic membrane met the industrial requirement with pore size of 1.61 nm and a pure water permeance of 17.4 L/m2.h.bar. The NF alumina ceramic membrane exceled solvent resistance and thermal and chemical stability.

2.3.4.3 Zirconia Membrane

Just like alumina (Al_2O_3) membrane, zirconia (ZrO_2) ceramic membrane is popular in the application of water and wastewater treatment. A monoclinic crystal structure is observed for zirconia at room temperature, which later changes into a tetragonal cubic phase at higher temperatures. This popular transformation toughening mechanism of the stabilized zirconia enhances the structure toughening (Kayvani Fard et al. 2018). There is an outstanding feature of zirconia which is – highest hydrophilicity and largest thermal stability (Da et al. 2016; Zhu, Y. et al. 2014) compared to the five evaluated ceramic membrane discussed in this section. It is well known that high hydrophilicity leads to low fouling and high flux in water treatment and liquid phase application under harsh conditions is improved with the use of high stability membranes (Hofs et al. 2011). Floods of literature about the use of zirconia membranes as top active layer in MF, UF and NF has been reported due to their stated merits (Da et al. 2016; Aust et al. 2006; Faibish and Cohen 2001b).

Treatment of wastewater is one of the most important applications of zirconia ceramic membrane. In terms of high flux, oil rejection and fouling decline, zirconia ceramic membrane displayed better performance efficiency compared to alumina ceramic membrane in O/W emulsion separation (Guizard, C., Rambault and Cot 1994). Tubular MF zirconia membranes on alumina support was prepared by (Yang, Chao et al. 1998) via suspension route to separate steelworks O/W emulsion discharge. A high permeance of about 400 L/m2.h/bar

and 500 L/m2.H/bar was achieved for zirconia's symmetric and asymmetric membrane support, respectively. there was an out performance of percentage oil rejection from zirconia ceramic membrane compared to alumina ceramic membrane with less fouling and a more stable flux.

High salinity wastewater treatment by zirconia membrane has been applied as well. Environmental protection also focuses on the recovery of water desalination. NF zirconia ceramic membrane was developed by (Da et al. 2016) for the desalination of wastewater treatment. NF zirconia ceramic membrane presented a double flux compared to the NF polymeric membrane that had similar molecular weight cut off (MWCO). This was achieved because the organic NF polymeric membrane had a higher contact angle and hydrophobicity (Zhu, Y. et al. 2014).

2.3.4.4 Titania Membrane

Tatania (TiO_2) is made up of three minerals which are rutile, anatase and brookite. The chemical resistance of titania membrane is best compared to the five membranes researched in this section (Hofs et al. 2011). Tatania membrane hold a peculiar function of mineralizing organic compounds under UV irradiation and as such they offer simultaneous photocatalytic oxidation and filtration processes. In addition to their photocatalytic features, titania ceramic membranes have been applied in the active layer, support and intermediate layer for the preparation of MF, UF, and NF membrane in water and wastewater treatment (Ahmad, R. et al. 2018; Manjumol et al. 2016; Ebrahimi et al. 2010; Zhang, Xiwang et al. 2009).

There is multi-functional water and wastewater treatment capabilities present in titania ceramic membrane due to its exceptional photocatalytic attribute. With the use of a membrane modification procedure of hydrothermal synthesis, hot press and filtration the development of UF titania nanowire membrane with layer hierarchical structure was achieved and used for the treatment of water (Zhang, Xiwang et al. 2009). The prepared UF nanowire titania membrane had several advantages present in it such as antibacterial, anti-fouling, and high permeability. Alumina and other ceramic membrane do not have the merit of antibacterial feature and alumina specifically lacks the photocatalytic capability.

Due to the high chemical stability of titania ceramic membrane, it can be used in the treatment of water regarding corrosive media (Hofs et al. 2011). The development of porous NF titania membrane has been prepared that displayed high retentions for organic molecules with lower MWCO that was less than 200 and titania could also be used in NF of solutions with various pH (Van Gestel et al. 2002). Titania ceramic membrane still presents some challenges which includes low surface area and anatase structure instability at higher temperatures (Jung et al. 2008).

2.3.4.5 Zeolite Membrane

Cations in group I and II along with hydrated and crystalline aluminosilicates make up the zeolite membrane. The determination of characteristics such as surface charge and wettability depend on the ratio of Si to Al in the preparation of zeolite membrane (Kayvani Fard et al. 2018). Two types of pore structures are contained in zeolite membrane, and they include inter-crystal micropores with various size distribution and uniform sub-nanometre zeolite pores (Kazemimoghadam 2010). As seen in Figure 15 which displays the schematic diagram and SEM of zeolite membrane, water passes through the inter and intra particle pores. Furthermore, the mitigation of fouling in zeolite membrane can be achieved by the high hydrophilicity present. Zeolite membrane is also applied in desalination processes using MF, UF, NF, and pervaporation (Basumatary et al. 2017).

Using in situ hydrothermal synthesis, NaA MF zeolite ceramic membrane was prepared on alumina substrate and used for the investigation of water separation and oil recovery (Cui et al. 2008). As seen in Figure 16, with an increase in time, there is a growth observed in the cubical shape of NaA crystal. 99% oil rejection was generated from the membrane along with 85 L/m^2.H in flux at 50kPa transmembrane pressure. In addition, fouling resistance was increased in the MF zeolite ceramic membrane in comparison to the alumina membrane.

Desalination of complex mixture potential has been displayed by zeolite ceramic membranes. For instance, a high rejection rate of reverse osmosis of concentrated solutions with different cations was observed while using zeolite membrane. (Kazemimoghadam 2010). However, there is still a challenge notice with zeolite membranes especially in the preparation procedures. This involves

preparing a defect free zeolite membrane that has a certain level of thickness (Kayvani Fard et al. 2018). Therefore, the performance of zeolite membrane in water and wastewater treatment must be improved regarding process innovation and optimization during the preparation or modification.

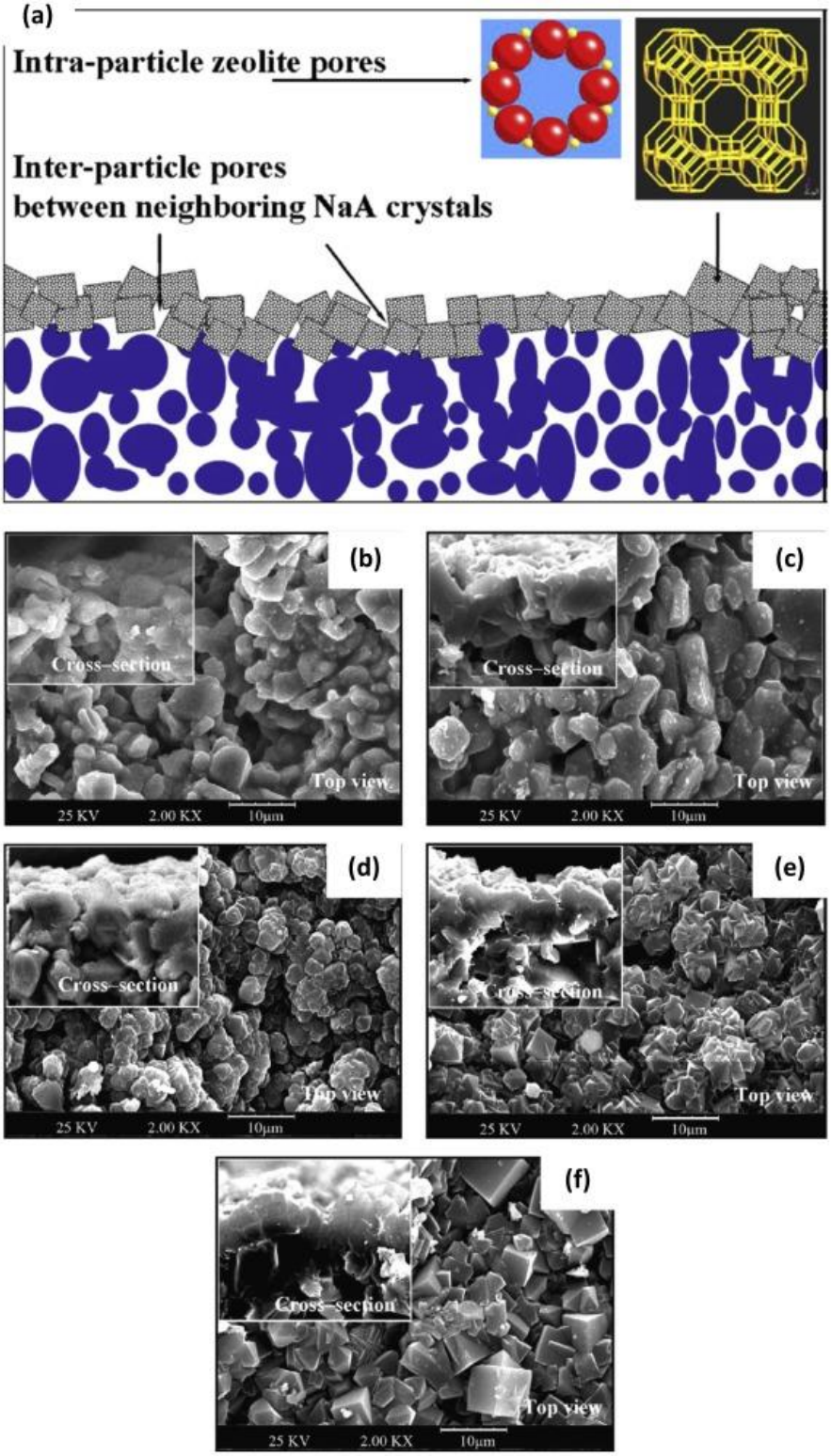

Figure 15: Zeolite membranes(a) schematic diagram showing different transport pathways and SEM images (b) alumina support and zeolite layer after in-situ hydrothermal synthesis (O'hare 2001) (c) 2h (d) 4h (e) 10h and (f) 18h. Reproduced with permission from (Cui et al. 2008).

2.4 Common Metals Oxides used for modification of membranes for water and wastewater Treatment

There are three common nanoparticles metal oxides that have been used for the modification of membrane in membrane technology for various separation activities in water and wastewater treatment, and these include TiO_2 nanoparticle metal oxide, ZnO nanoparticles metal oxide, and Iron Oxide nanoparticles metal oxide.

2.4.1 TiO_2 Nanoparticles Metal Oxide

The first usage of TiO_2 metal oxide for the treatment of water was observed when TiO_2 semiconductor electrode was used in the electrochemical photolysis of water during a photocatalytic degradation study by (Fujishima and Honda 1972). This became an emerging technology for the treatment of water and wastewater ever since. Based on this, photocatalytic degradation of contaminants in water and wastewater have been successfully applied in recent years. TiO_2 have found itself amongst the most common photocatalytic metal oxides and has also been the most extensively studied. This is because of its high photocatalytic activity, photostability, chemical and biological stability and reasonable price (Guesh et al. 2016; Rawal et al. 2013; Imamura et al. 2013). Furthermore, TiO_2 has an excellent Physico-chemical characteristic noticed in photogeneration reactions and because of its excellent hydrophilic attribute it has dragged attention in surface modification. Photo-induced surface hydroxyl groups and light-induced surface vacancies might be the reason behind TiO_2 hydrophilic properties (Gao et al. 2022; Banerjee, Dionysiou and Pillai 2015). Also, TiO_2 rough nanostructure might also contribute to the influence of its hydrophilic nature on modified ceramic membrane.

Due to these attributes present in TiO_2 metal oxides, it has been used on the modification of other substrates like ceramic, polymeric membrane technology and foam for change of surface structure or wettability to enhance the treatment or separation efficiency of O/W emulsion (Yang, Yang et al. 2022; Zhang,

Luhong et al. 2020; Suresh and Pugazhenthi 2017; Suresh and Pugazhenthi 2016). TiO_2 has also been used alongside other inorganic compounds for the effect flux enhancement and antifouling of membrane during separation of O/W emulsion.

Nowadays, there is a flood of reports on the different preparation methods engaged in the modification of TiO_2 ranging from the use of Sol-gel, dip coating etc. (Goei and Lim 2014) used the sol-gel method of membrane modification to prepare asymmetric TiO_2 hybrid photocatalytic membrane and this resulted in super hydrophilic ceramic membrane. (Hosseini et al. 2011) fabricated and characterized ceramic membrane with TiO_2 using the chemical vapour deposition method and this resulted in a high roughness surface which enhances hydrophilicity. (Ismail et al. 2020) the use of hydrothermal method for the synthesis if TiO_2 nano flower deposited on bauxite hollow fibre membrane to boost photocatalysis. This hydrothermal synthesis resulted in effective uniform distribution of morphological structure of the membrane surface. All these methodological syntheses of TiO_2 indicates the vast approach that can be employed in the modification of substrates using TiO_2 metal oxides.

2.4.2 ZnO Nanoparticles metal Oxide

Asides TiO2 nanoparticles metal oxides, ZnO is the second metal oxides wide used in the treatment and separation of water and wastewater efficiently. This is due to their good photocatalytic properties and oxidation abilities and direct wider band range in the near UV spectrum (Janotti and Van de Walle 2009). ZnO has be reported as eco-friendly due to the compatibility of microorganisms in their presence and this gives them the suitability to be used for the treatment of water and wastewater (Schmidt-Mende and MacManus-Driscoll 2007). ZnO has been used for photocatalytic analysis as they also contain similar photocatalytic features as TiO2. Nevertheless, the distinct advantage of ZnO nanoparticles over TiO2 is the ability to absorb wide range of solar spectra and quanta of light compared to other counterpart semiconductors. Also, ZnO nanoparticles has the merit of being cost effective (Behnajady, Modirshahla and Hamzavi 2006).

These attributes of ZnO being eco-friendly, cost effective and photocatalytic enhanced the interest of ZnO metal oxides in the modification on other substrates like ceramic, polymer, and nanowire for the treatment of O/W

emulsion or produced water. ZnO has also been reported in hybrid combination for surface wettability in conjunction with other compounds like graphene oxide (Kazemi et al. 2021). ZnO has been reported to have even more advantages properties asides from be antimicrobial and cost effective, such as, anti-corrosive, thermal and mechanical strength, low toxicity, and high active surface (Mahlangu et al. 2017; Alhoshan et al. 2013). Moreso, ZnO nanoparticles are naturally hydrophilic (OH-), giving the ability to easily absorb hydroxyl group leaving behind hydrophilic surfaces which enhance water and wastewater separation.

This vast number of advantageous properties have resulted in the use of ZnO for surface modifications specific to the task at hand and especially the task of separation of O/W emulsion. Many researchers have reported the use of ZnO in ceramic membrane modifications for O/W emulsion. An increase in water flux was observed when ZnO was used in the surface modification of PVC ultrafiltration membrane (Rabiee et al. 2015). This increase in flux was due to the modification of membrane structure that created an increase in porosity. The addition of various contents of ZnO nanoparticles gave an increase in hydrophilicity in polymeric PVDF microfiltration membrane as reported by (Hong and He 2012). There was an increase in mean roughness, pure water permeability, and enhanced hydrophilicity as illustrated in the research of ((Alsalhy et al. 2018) with the addition of difference concentrations of ZnO on PVC membrane modification process. Also, (Chung et al. 2017) reported the speed up of membrane formation process by the acceleration of solvent and antiplatelet exchange rate due to water loving groups of nano composite membrane; hence pore formation process can occur more rapidly. From this result, Porosity of pure polysulfone membrane increased to 86% from 75% by the mere addition of ZnO; and this further increase with the hybrid addition of ZnO-GO to 90%.

2.4.3 Iron Oxides Nanoparticles

In recent years, there has been a growing interest in the use of iron oxides nanoparticles due to their effective treatment of heavy metal from a simple approach and their availability. There are three distinct types of iron nanoparticles nano adsorbents presently used which includes, magnetic magnetite (Fe_3O_4), magnetic magemhite (y-Fe_3O_4), and nonmagnetic hematite

(α Fe_2O_4) (Lu, H. et al. 2016). Usually, the challenge associated with nano sorbent material use for water treatment is their recovery after separation from contaminated water. Magnetic magnetite and magnetic magemhite however, have shown easy recovery and separation from water purification process with the help of a magnetic field application. This has led to the recent usage of these two absorbent materials in water treatment processes from heavy metal contamination. Based on this attribute, magnetic magnetite (Fe_3O_4) has been reported in use for separation of O/W emulsion as a surface modification on ceramic membrane (Aboulella et al. 2022). The absorbent Fe_3O_4 have also been used alongside other metal oxide for the surface modification of ceramic membrane for separation and treatment of wastewater (Salhi et al. 2022). To avoid interference from other metal ions and metal oxides and to increase separation efficiency as well, there is usually an introduction of ligands and polymers in the modification process of iron oxides. Examples of some ligands and polymers used to function tune iron oxides includes ethylenediamine tetraacetic acid (EDTA), L-glutathione (GSH) and copolymers of acrylic acid and crotonic acid respectively ((Ge et al. 2012; Warner et al. 2010). Some iron oxide has been reported for the use of surface modification of ceramic membrane for the treatment and separation of O/W emulsion. (Barati, Husein and Azaiez 2022) reported the use of in situ doping iron oxide nanoparticles on ceramic membrane for the enhancement of anti-fouling features and removal of organic matters from wastewater. (Xu et al. 2022) reported the use of magnetic Fe_3O_4 grains for the enhancement of O/W emulsion separation performance and solar-assisted recyclability of graphene oxide. This resulted in excellent separation of O/W emulsion. (Moatmed et al. 2019) prepared a highly efficient and reusable superhydrophobic /super oleophilic polystyrene Fe_3O_4 nanofiber membrane for the highly efficient separation of O/W emulsion. This nanofiber membrane resulted in an excellent separation efficiency of 98% and high flux of 5000 L/m^2.H. and a reusability of over 50 cycles. (Elmobarak and Almomani 2021) applied Fe_3O_4 magnetite nanoparticles grafted in SiO_2 ceramic membrane for oil recovery from O/W emulsion. This resulted in the recovery of oil from O/W emulsion for over 9 cycles with an excellent oil recovery percentage of 93 - 94.5% and the Fe_3O_4 was easily recovered from the separation process using a magnetic field.

All these usages and applications are factual indications that metal oxides are effective in the separation of O/W emulsion. This is due to the versatile modification methods that can be used for ceramic membrane surface modification with metal oxides. Also, most of the reports mentioned the excellent oil rejection percentages, high surface roughness and enhanced hydrophilicity, all which underpins the excellent attributes of metal oxides for the surface wettability of ceramic membrane for O/W separation. This study reports the use of MgO surface modification on ceramic membrane for the separation of O/W emulsion.

2.5 Factors Affecting Ceramic Membrane Industrial Application

Ceramic membrane is considered as an excellent choice in the separation of O/W emulsions and may be launched industrially for this purpose with the rate of research attention given to it. The advantages of ceramic membrane which includes, but not limited to mechanical, chemical, and thermal strength, as well as high flux ability draws attention to its usage in O/W emulsion separation. With the expansion of ceramic membrane into nanofiltration that is produced with the impregnation of nanoparticle in ceramic membrane, gives a new surface modification that can reduce fouling of ceramic membrane in O/W emulsion separation. Fouling of membrane and low flux happens to be the greatest drawback of ceramic membranes for industrial use as reported by researchers (Chang et al. 2014c). A combination of nanoparticles and ceramic membrane surface modification might just be the way out to reduce fouling and increase flux in O/W emulsion separation. Nanoparticles are particles that have a dimension ranging from 1-100 nm (Gwak, Kim and Hong 2020). Hydrophilic functionalized nanoparticles modified ceramic membrane cannot only increase surface area for high flux, but also hindering membrane fouling in O/W emulsion separation. Some commonly used nanoparticles for ceramic membrane modification include Nano scale Zirconium dioxide (ZrO_2) (Zhou, Jian-er et al. 2010), Titanium dioxide/Aluminium oxide (TiO_2/Al_2O_3) (Yi et al. 2011), Aluminium Oxide (Al_2O_3) (Maguire-Boyle and Barron 2011), and Silicon dioxide (SiO_2) (Meng et al. 2013) for the separation of O/W emulsion. Several reports have been recorded concerning the combination with good and interesting outcomes as seen in Table 3 below.

Table 3: Comparison of nanoparticles of contact angles, % rejection and time for separation of O/W emulsion.

Comparison of nanoparticles performance on O/W emulsion separation				
authors	nanoparticles	Contact angle (^{0})	%rejection/flux	Time (min)
(Chang et al. 2014c)	Nano-TiO_2	8^0	-	100
(De Guzman et al. 2021)	Polydopamine (PDA)	54.60^0	96	100
(Liu, C. et al. 2021)	Carbon nanotubes Polyacrylic acid (CNTs-PAA)	3^0	98	100

This research targets the use of ceramic membrane with a suitable nanoparticles surface modification for the separation of O/W emulsion to impact the possibility of industrial use. Microfiltration ceramic membrane will be used over Ultrafiltration due to it porous surface that increases flux (Yi et al. 2013). Although microfiltration suffers from easy fouling of the membrane. Hence, nanoparticle surface modification will help tackle this issue by enhancing hydrophilic character of the surface of the ceramic membrane (Li, L. et al. 2009).

2.6 Characterization Instruments and how they work

This section describes the analytical instruments used in this research for the quantitative and qualitative measurements analysis. Analytical instruments were required to conduct several experiments such as during the characterization of prepared O/W emulsion, characterization of modified and unmodified ceramic membrane, and the quantitative measurement of percentage oil rejection after crossflow filtration analysis. The instruments discussed in this section includes Zetasizer Nano ZS instrument from Malvern Instrument Inc, Theta Lite Optical

Tensiometer, Scanning Electron Microscope (SEM) and Energy Dispersive X-ray Analysis, Quantachrome Analyser, and UV-Visible Spectrophotometer. These instruments are used for the characterization of O/W emulsion, measurement of contact angle for hydrophilicity test, measurement of morphology and element composition of ceramic membranes, measurement of pore size of the ceramic membrane, and determination of percentage oil rejection respectively in this research.

2.6.1 Zetasizer Nano ZS instrument

This sub section is designed to look in details the principles and applications behind the use of Zetasizer nano ZS for the determination of oil droplet size and size distribution in synthesized O/W emulsion. This is necessary because this instrument was employed in this research to determine the oil droplet size and size distribution of Soybean O/W emulsion.

2.6.1.1 Principles

The zetasizer nano series instrument is designed for the characterization of colloid, nanoparticles, and macromolecules. This instrument incorporates a Non-invasive backscatter (NIBS) optics. For size measurements, the zetasizer instrument is incorporated with Dynamic light Scattering (DLS) which is the ideal system for measurement of sizes in colloids, nanoparticles, and macromolecules without sample preparation or agitation. Based on the measured size of the particle, the molecular weight of the particle can then be measured.

The principles of DLS involves a constant random thermal motion termed as "Brownian motion" of fine particles and molecules diffuse at a speed related to the size of the molecule. Based on this principle, it is expected that smaller particles would diffuse faster than larger particles. Temperature is a major factor that controls the diffusion of these molecules; hence precise temperature control is necessary to give an accurate size measurement (Series—Performance and Simplicity).

The diffusion rate of the particles is measured by the speckle pattern from a laser that illuminates the particles. A sensitive avalanche photodiode detector (APD) is used to measure the scattering intensity when the particles fluctuate with time. A change in the intensity of the instrument can be analysed with a digital auto correlator that operates by generating a correlation function. The

particle size and the size distribution are analysed by this curve from the auto correlation (Series—Performance and Simplicity).

The zetasizer nano series is designed to provide optimized components at every stage while measurement is ongoing beginning from the laser to the temperature control and finally to the optical design and detection. This is necessary to produce high-quality data. In this research, the Zetasizer nano ZS was used, and it is equipped alongside other nano series with a NIBS. This NIBS aids in the illumination of a larger particle size quantity and produce 100 times sensitivity better than conventional optics due to efficient fibre detection system. A more stable signal is achieved by the measurement of a larger particle size quantity, leaving less room for fluctuations. The zetasizer is an instrument that has the capacity for the measurement of three features of molecules or particles in a liquid medium. These three characteristics are parameter usually used in analysis such as particle size, zeta potential and molecular weight of any liquid medium.

2.6.1.2 Application of Zetasizer nano ZS for droplet size in O/W emulsion

Many studies have reported the use of Zetasizer nano series for the measurement of synthesized O/W emulsion to determine the particle size and size distribution especially the nano size emulsions. (Ramisetty, Pandit and Gogate 2014) reported the use of zetasizer nano ZS for the determination of droplet size of O/W emulsion the study of a novel approach to produce O/W emulsion using cavitation reactor. (Loi, Eyres and Birch 2019) in the study of physical properties and stability effect of mono and diglycerides of a protein stabilized O/W emulsion, used Zetasizer nano ZS to measure the droplet size and zeta potential of the synthesized O/W emulsion. The instrument generated not just the droplet size but the size distribution in percentage of the different droplet size present in the synthesized O/W emulsion. Several studies (Nagasawa et al. 2020; Shi et al. 2019a; Wang, J., Wang and Geng 2018; Chen, H. et al. 2015; Milić et al. 2014) have reported the use of Zetasizer nano ZS for the determination of droplet size and size distribution of synthesized O/W emulsion for the separation of O/W emulsion with ceramic membrane. In this present work, Zetasizer nano ZS has been used for the determination of synthesized soybean O/W emulsion for droplet size and size distribution which has been detailed in the methodological section of the report.

2.6.2 Theta Lite Optical Tensiometer

This subsection takes a closer look at the theory and fundamentals, instrumentation, and application of Theta Lite Tensiometer in ceramic membrane and separation of O/W emulsion.

2.6.2.1 Theory and Fundamentals

From applied and fundamental point of view, wettability area of interest has received tremendous attention. A lot of industrial sectors uses this wettability topic in distinct roles such as lubrication, printing, liquid coating, oil recovery and spray quenching. The study of wettability normally involves measuring primary data of contact angles which state the degree of wetting with the contact of a solid and liquid. Int the measurement of wettability, results with $<90^0$ relates to wettability, in contrast, results $>90^0$ gives a low wettability value (Yuan and Lee 2013). A critical look at a flat horizontal surface where a liquid is dropped (Figure 16). The intersect angle of a liquid-solid interface and a liquid-vapor interface is defined as the contact angle ((Lafuma and Quéré 2003). From Figure 16, when there is a spreading of the liquid on the flat solid surface, this gives a smaller contact angle. One the other hand, there is a larger contact angle observed when the liquid droplet forms a bead on the flat solid surface. More specifically, a wetting surface is favourable if the contact angle is less than 90^0 allowing the liquid to spread widely on the solid surface; in contrast an unfavourable wetting surface inhibits liquid spreading making the fluid droplet form a bead indicating that the surface is greater than 90^0. For instance, at angle 0^0 is an indication that the liquid droplet placed on a flat surface has undergone complete wetting. This is synonymous with that surface been a hydrophilic surface. Flat surfaces greater with liquid droplets greater 150^0 are termed hydrophobic indicating almost no contact between the liquid droplet and the solid surface (Lafuma and Quéré 2003). contact angles can also be applied to liquid-liquid interface and not limited to liquid-vapour interface on solid alone.

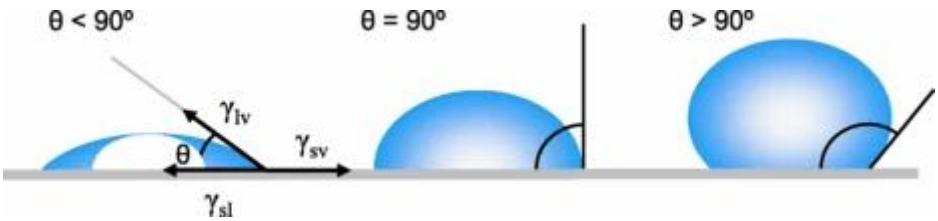

Figure 16: Illustration of contact angles formed by sessile liquid drops on a smooth homogeneous solid surface. ***(Yuan and Lee 2013)***.

Using a specific liquid-solid system, Young's equation applied three thermodynamic parameters γ_{lv}, γ_{sv}, and γ_{sl} to determine a unique single contact angle θ_Y. from Thomas Young's work (Young 1805), mechanical equilibrium of the droplet under the action of the three interfacial tension defines the contact angle of a liquid droplet on an ideal solid surface.

Equation 2

$$\gamma_{lv} Cos\ \theta_\gamma = \gamma_{sv} - \gamma_{sl}$$

where the parameters involved γ_{lv}, γ_{sv}, and γ_{sl} are represented as the liquid-vapour, solid-vapour, and solid-liquid interfacial tensions respectively, and θ_γ represents the contact angle.

2.6.2.2 Instrumentation

Direct measurement of the tangent angle at the point where the three phases contact is the most widely used technique for measuring contact angle using sessile drop profile. In this study, the Theta Lite Optical Tensiometer which is a compact computer-controlled video-based instrument was used for the measurement of contact angle. This instrument is designed for the measurement of contact angles, but it also measures the surface free energy. Furthermore, this instrument also uses pendant drop method and contact angle meniscus method to measure the surfaces and interfacial tension. A USB3 digital camera that can capture a maximum of 2680 frames per second (fps) is configured in the Theta Lite along with a LED light sources and an adjustable sample stage that can move both vertically and horizontally. Figure 17 below give a pictorial diagram of the Theta Lite Optical Tensiometer instrument.

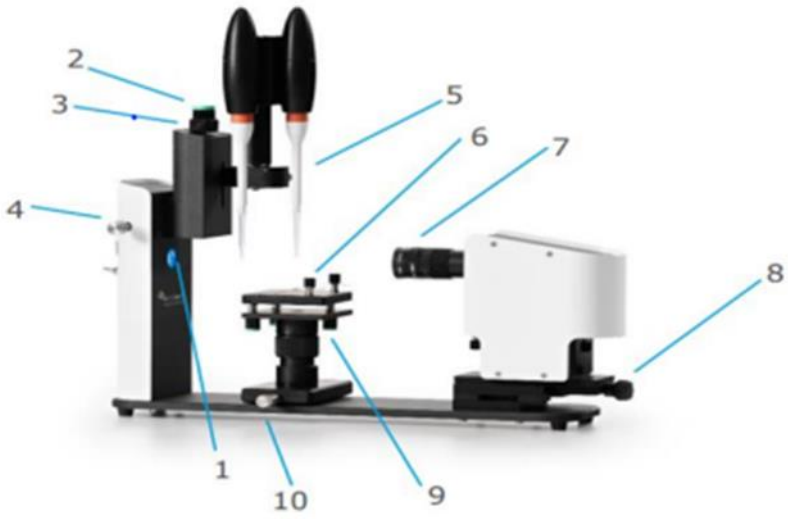

Figure 17: Image of OneAttension Theta Lite Optical Tensiometer -adapted from Biolin Scientific Manual. (1-LED light source, 2-syringe height adjustment, 3-manual dispenser adjustment, 4-syringe compartment adjustment, 5-syringe, 6-sample stage with sample attachment clips, 7-camera optics, 8-camera linear movement) (Scientific 2018).

2.6.2.3 Application in Ceramic membrane and O/W emulsion separation

Several researchers have used the contact angle measurement in the determination of hydrophilicity or hydrophobicity on ceramic membrane surface for separation of O/W emulsion. (Chang et al. 2014c) used the contact angle meter to measure the contact angle of microfiltration ceramic membrane that was modified by nano-TiO_2 coating using the sessile drop method for the separation of O/W emulsion. (de Melo et al. 2022) also reported the use of contact angle measurement with sessile drop method for the determination of hydrophilic on modified ceramic membrane for the separation of O/W emulsion. Similarly, the measurement of contact angle was conducted for the determination of hydrophilicity on anti-fouling zwitterion-functionalized ceramic membrane for the separation of O/W emulsion using contact angle meter (Luan et al. 2022). Also, (Gao et al. 2022) in the study super-hydrophilic/ underwater super-oleophobic performance of ceramic membrane, coated the membrane with TiO_2, used the contact angle measure for the determination of hydrophilicity of the modified and unmodified ceramic membrane. These usages of contact angle meters for the measurement of contact angle especially with the sessile drop method is an indication that using this technique for the measurement of hydrophilic or hydrophobicity is a norm particularly in the analysis involving separation of O/W emulsion.

2.6.3 SEM and EDXA

This section describes the theory and applications of SEM and EDX analysis for the evaluation of ceramic membrane for O/W emulsion treatment. This is necessary because this technique was utilized in this research for the morphological evaluation and elemental composition determination of unmodified and modified ceramic membrane.

2.6.3.1 Background theory

Energy Dispersive X-ray (EDX) analysis is widely normally used together with Scanning Electron Microscope (SEM) is a widely used technique or detector system which generates higher information about a sample than the mere use of SEM alone. SEM is designed to illustrate the properties of surface topography while a tandem of both SEM and EDX has been designed to elucidate the chemical composition present in a sample (Idris and El-Zahhar 2019). With the use of EDX alone, information regarding the chemical composition of a sample and detection of every elemental composition present in the sample, including their concentration and distribution is generated.

Two detectors which are used as signals to offer information about a sample is attached to SEM which includes backscatter detector and variable pressure detector. The backscatter detector produces images that share information about difference in atomic number of a sample using contrast images. The variable pressure is responsible for the topographic information about the sample (Davies et al. 2022). A tandem instrument of SEM and EDX detector creates X-rays that can also be used to provide information containing the chemical composition of the sample. For further understanding of how this X-ray works in SEM and EDX, the holistic look at an atom having a unique number of electrons is necessary. Every atom has a unique number of electrons that are sustained in specific energy levels in the atom that have different discrete energies.

In, EDX analysis an electron beam targets and hits an electron in the inner energy level shell of an atom, kicking out an electron from that shell as illustrated in Figure 18, leaving behind an electron vacancy or hole that is positively charged. The displacement of this electron creates an attraction for another electron from a higher energy shell level to fill up that hole. As the electron in the higher energy level moves into the vacancy in the inner and

lower energy level, this creates and energy difference which is released in the form of an X-ray. This x-ray generated from electron movement between two energy level differences is specific to that element and transition. The x-ray at that time is receive by a detector that conducts the measurement of the signal and uses software to interpret the result. By so doing, elements in a sample are identified using X-rays in EDX.

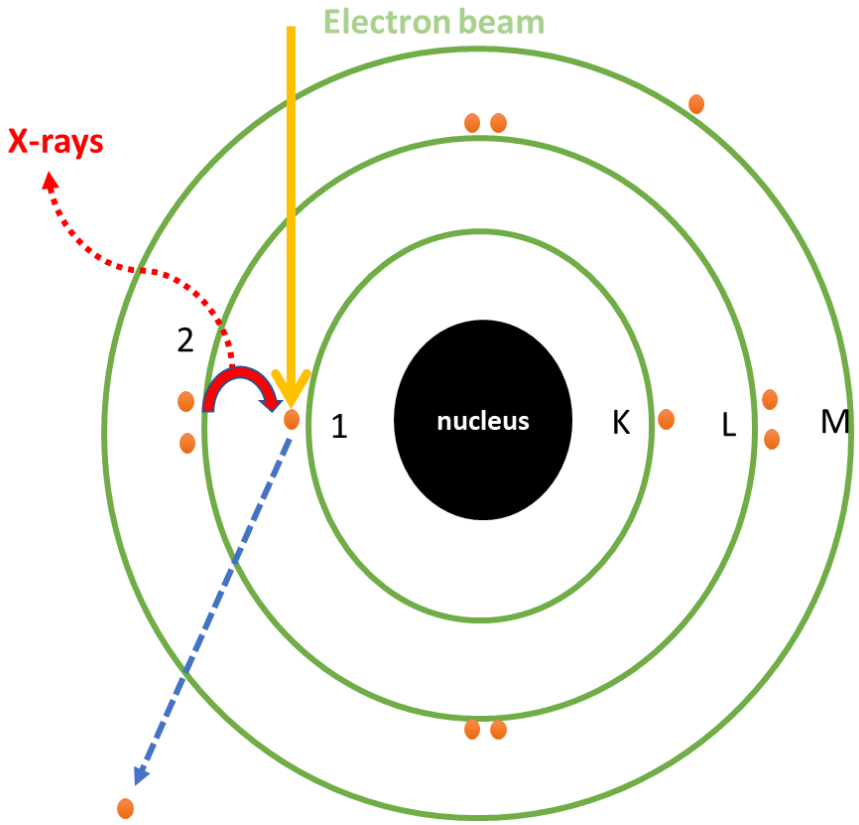

Figure 18: X-rays generated using SEM and EDX.

Furthermore, quantitative, and qualitative analysis can use of SEM tandem EDX that gives results to the composition of elements present in a sample and the concentration in percentage of the elements. Sample preparation stage is not necessary while using these instruments as the method is a non-destructive one i.e., there is no damage done to the sample during analysis.

2.6.3.2 Application of SEM and EDX in ceramic membrane for O/W emulsion separation

SEM and EDX analysis have been widely used in characterization of ceramic membrane for the separation of O/W emulsion by various researchers. This has been employed for the morphology and detection of chemical composition of some modified and support ceramic membrane with various coatings and surfaces. (Vinoth Kumar, Monash and Pugazhenthi 2016) engaged the use of

SEM and EDX analysis for the characterization of tubular ceramic membrane in the study for the treatment of O/W emulsion. (Aboulella et al. 2022) also utilized the SEM and EDX analysis instrument for the characterization of Fe_3O_4-Ag modified ceramic membrane for the treatment of produced water. The EDX analysis detector was able to detect the presence of Ag which was not present in the unmodified ceramic membrane spectrum. This technique was also utilized in various articles involving the characterization of support and modified ceramic membrane for morphology and elemental composition (Suresh and Katara 2021; Suresh and Pugazhenthi 2017; Suresh and Pugazhenthi 2016; Banerjee, Dionysiou and Pillai 2015). The results from these researchers gave not only the morphology and elemental composition results but also the concentrations of these elemental compositions present in the ceramic samples. In this research work, SEM and EDX analysis was employed to determine the morphology and elemental composition of unmodified Al_2O_3 ceramic membrane in comparison with modified MgO ceramic membrane. This was to determine any change after modification of the ceramic membrane to also see the presence of Mg element on the modified ceramic membrane.

2.6.4 Autosorb Analyzer

This sub-section was to take a deeper look at the background, instrumentation, and application of Autosorb analyser, which was employed in this research for the purposes of characterization in particular, the pore size and pore size distribution of unmodified and MgO modified ceramic membrane.

2.6.4.1 Background

Autosorb iQ MP physisorption analyser is an instrument that determines the pore size distribution, pore volume, active area, and specific surface area of microporous and mesoporous solids. Pore size distribution as small as 0.35 nm and specific surface areas that are less than 0.01 m^2/g can be measured using this instrument.

Degassing of the sample is the first stage of the physisorption analysis. The parameters used to measure degassing in this instrument includes heating rates and hold times after which the measurement is automatically conducted iQ

software. The degassing process is the sample preparation process that eliminates and gas present in the sample to give a quality data during analysis.

The adsorption of gas vapour and gas atoms and molecules onto a solid surface by the formation of weak attractive forces which is measured usually at cryogenic temperatures is described as physisorption or physical adsorption. Quantification of a solid surface area, the pore size and the volume distribution are also termed physisorption.

Pressures changes in the sample cell of the sensitivity of physisorption analysis is the dependent factor that defines the sorbed amounts. The sorbed amount increases with a decrease in free space or void which is known as the volume around the sample in a sample cell. Invariable, this means that a higher or increased void volume around the sample give an unabsorbed gas molecule. This is also temperature dependent as the cold free space around the sample in a cell will give higher unabsorbed molecules than a warm void space around the same sample in the sample cell. To avoid this, the area around the sample sell accessing the cryogenic coolant is controlled accurately to allow immersion of as little as possible, the sample cell as displayed in Figure 19 below.

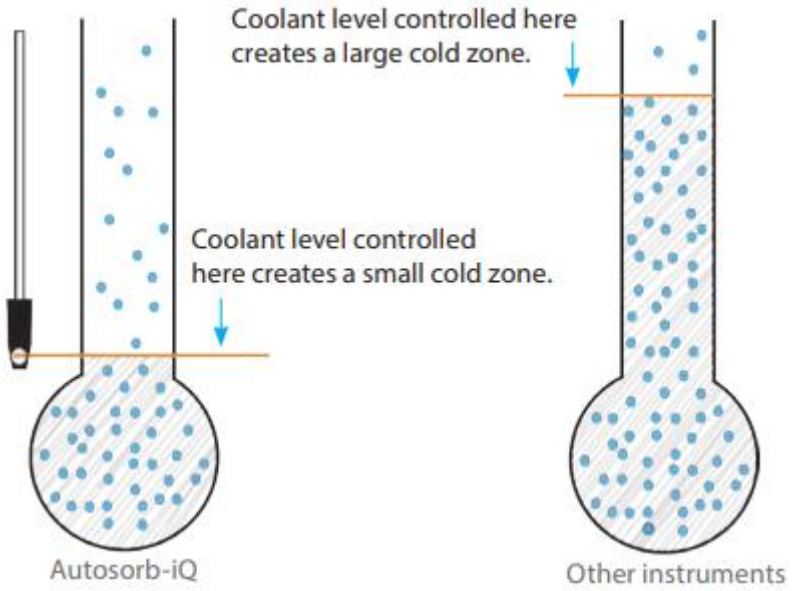

Figure 19: Control of cryogenic coolant and sample cell interaction to increase absorbed molecules. (Quantachrome instruments 2013).

The sensitivity of the Autosorb iQ analizer is very remarkable in the determination of Brunauer-Emmet-Teller (BET) surface area. The usage of

nitrogen at liquid nitrogen temperature or argon at liquid argon temperature as well can be used to determine surface area of 0.01 m^2/g and above in the MP and XR models of autosorb analyser. But the use of krypton at a liquid nitrogen temperature can even measure lower surfaces areas even down to 0.0005 m^2/g because of the addition of a sensitive material. The autosorb is associated with a software call the ASiQwin that can automatically present results from BET plot and computes the result based on constant, intercept, slope, and correlation coefficient of the best fit of least squares. There is a Micropore BET Assistant function in the software that can help to determine the appropriate linear BET range based on a published criteria for a microporous material.

2.6.4.2 Instrumentation

The Autosorb iQ Analyser pictorial diagram is shown in Figure 32 in chapter three of this report. The instrument contains two sides which includes the degassing unit as pointed out in the picture and the analysis unit. The analysis unit comprises of a transparent blue door that houses the physisorption station. This blue section is for temperature control of the analysis unit and for safety purposes. There is a sensor in between the sample cells that measures the absorbed molecules. There are also the sample cells that contain the samples. A dewar is attached at the base that contains the cryogenic coolant in this case liquid nitrogen sitting on a dewar support arm. The level sensor gives signal to the dewar drive to help maintain a constant and reduced cold zone. This is to allow for warmer area around the sample cell to increase sorbed molecules. Figure 20 displays the schematic diagram of the analysis unit for Autosorb analyser.

2.6.4.3 Application of Autosorb analyser on characterization of ceramic membrane

Several researchers have reported the use of Autosorb analyser for the nitrogen adsorption / desorption analysis on ceramic membrane for the separation of O/W analysis. (Monash, P. and Pugazhenthi 2011b) reported the use of nitrogen adsorption/desorption for characterization of pore size and pore size distribution of fabricated ceramic membrane support for separation of oil droplets. (Zhou, Jian Er et al. 2015) also used this instrument for the nitrogen adsorption desorption characterization of pore size of modified ceramic membrane for its application in O/W emulsion separation. Several other authors have also reported the use of nitrogen adsorption/desorption for similar purposes (Aloulou

et al. 2021; Medina-Llamas et al. 2020; Barbosa et al. 2020). In this research, the use of Autosorb analyser was for characterization analysis in the determination of pore size and pore size distribution of unmodified and modified MgO ceramic membrane and results were reported.

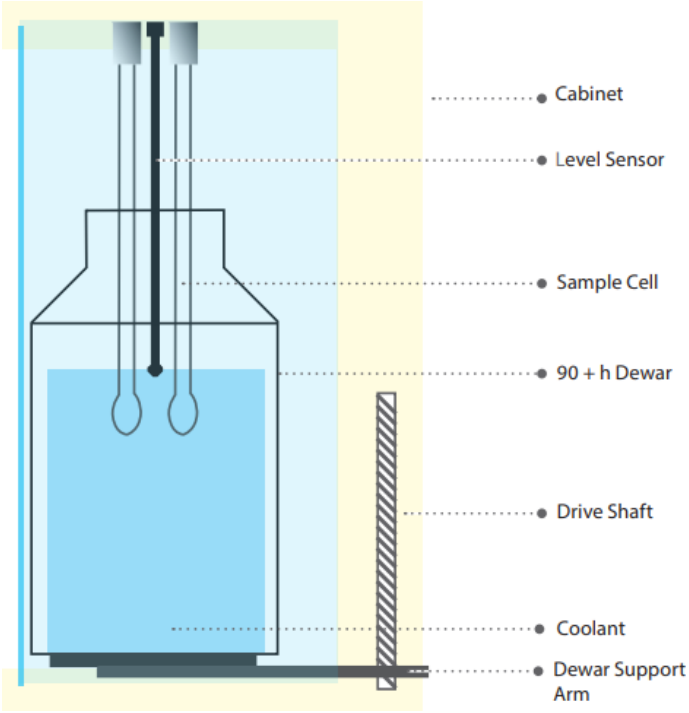

Figure 20: Schematic diagram of the analysis unit of Autosorb Analyser. (Quantachrome instruments 2013)

2.6.5 Ultraviolet and Visible Spectrophotometry

This sub-section was introduced to focus on the theory, instrumentation, and application of Ultraviolet to Visible spectrophotometer as this instrument was used in the determination of percentage oil rejection during cross flow filtration and separation of O/W emulsion.

2.6.5.1 General Theory

Ultraviolet to visible light region on the electromagnetic spectrum usually ranges between 185 nm to 760 nm. However, modern spectrophotometer comes with a wide range of ultraviolet to visible light which falls within the range of 185 nm to 2100 nm, and this is due to the recent advancement in technology (Kaur, Singh and Singh 2021). The knowledge of an absorbed light wavelength of an analyte that is present in each sample is discovered by the preparation of known concentrations of standards whose absorption spectrum is determined using a

UV/Vis spectrophotometer. The usual operation of a spectrophotometric method involves the provision of an electromagnetic radiation by the instrument from the measurement of absorption or transmittance from an analyte. The energy from an electromagnetic radiation transferred across a unit area per unit time is known as radiation power. This radiation power becomes reduced with the passage through an analyte in a sample. The proportion of analyte concentration determines the decrease in radiation power. This means that, an increase in concentration of the analyte present in the sample as well as the distance the radiation travels through the analyte called the cell path length, determines an increase in the absorbed electromagnetic radiation (Kaur, Singh and Singh 2021).

Quantitative analysis application: during the travel of radiation through the sample cell, the radiation beam that arrives at the photon detector after passing through the analyte declines. The concentration of the analyte in the sample is measured using the declining power of the radiation through a fixed path length cell containing the sample. The fact that different substances can absorb at different wavelengths, the instrument uses these differences to control the incident electromagnetic radiation (Kafle 2020). A monochromator which is attached to most UV/Vis spectrophotometer is used to filter the undesired wavelength that might be present thereby controlling wavelength passage as demonstrated in Figure 21 below. Other controlling wavelength tools are radiative filters or the usage of light sources emitting narrower wavelength band radiations.

Qualitative Analysis Application: furthermore, the chemical composition of a substance dictates the wavelength the wavelength radiation absorbance of that substance (Kafle 2020). Hence spectrophotometry capitalizes on this uniqueness for use in qualitative analysis. The analyte is present in the sample that is placed in the cell, and the wavelength from the incident radiation peculiar to that analyte is scanned through the sample allowing the absorption or transmittance measurement. The result which of the transmittance or absorption is plotted as a function of wavelength or energy of the incident radiation. The maximum absorbance peak of that wavelength is observed and used for the identification of the analyte present in the sample.

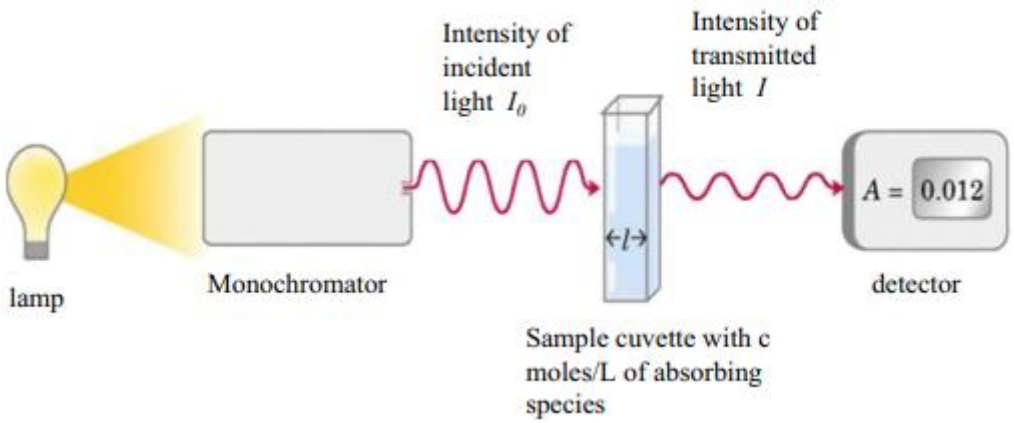

Figure 21: Schematic for the UV/Vis spectrophotometer absorbance measurement of a given sample. *(Kafle 2020)*.

2.6.5.2 Instrumentation

Within the electromagnetic radiation range, standard samples of known concentrations are used for calibrations on the instruments. Figure 22 displays a type of UV/Visible spectrophotometer which has been employed in research, academia, and industrial quality assurance. This instrument can measure transmittance, absorbance, and extinction coefficient of wavelengths between 190 nm to 1100 nm which falls in the ultraviolet to the near infrared (IR) region on the electromagnetic spectrum. UV/Vis spectrophotometer instruments are commercially available for use as a stand-alone instrument or coupled with PC-controlled instrument. The stand-alone instrument is comprised of a switch on/off button, wavelength selector, zero transmission adjustment knob, sample chamber, measurement mode (absorbance or transmittance) and measurement type (a broad or single wavelength range).

Figure 22: Ultraviolet / Visible Spectrophotometer.

2.6.5.3 Application in ceramic membrane for O/W emulsion separation

Several studies in O/W emulsion separation have used the UV/Vis spectrophotometer for the determination of percentage oil rejection using ceramic membrane. First, (Zhou, Hui et al. 2022) reported the use of UV/Vis spectrophotometer for the % oil rejection in the research for the Porous Al_2O_3 ceramics with directional gradient pore structure modified by cobweb bridged WO_3 nanowires. (Zhang, Lei et al. 2019) also reported the use of Ultraviolet/Visible spectrophotometer in the research with fouling- and solvent-resistant aliphatic polyketone membrane for high-flux filtration of difficult oil-in-water micro- and nano emulsions. This is a known method for the measurement of percentage rejection for the separation of O/W emulsion. This instrument was used in this research for the %oil rejection measurement of O/W emulsion separated via unmodified and MgO modified ceramic membrane which gave interested results that was reported in later sections.

In summary of the literature, the research in O/W emulsion informed my decision in preparation of synthesised O/W emulsion for this research. A thorough research on the conventional methods previously used for separation of O/W emulsion aided the discovery of use of ceramic membrane for this

research. A critical study of membrane technology led to the decision of modifying Al_2O_3 ceramic membrane to nana scale for the separation of O/W emulsion. Concise research on the existing metal oxides previously used for modifying ceramic membrane shined the beam on the use of MgO for the modification of Al_2O_3 ceramic membrane in this research. Indeed, an in-depth study on previous instruments used for the characterization of ceramic membrane was demonstrated in this research. Generally, the entire literature review informed and forms the bedrock for the success of the study.

Chapter three

3.0 Methodology

This chapter describes the eight main subsections used in this methodology to achieve the objectives of the study. The first subsection outlines the materials and equipment used in this research and what grade and where they were sourced from. The second subsection involves the preparation or synthesis of the synthetic Oil-in-water emulsion. During preparation, consideration is placed on droplet size and concentrations of the O/W emulsion. Moreso, focus is also placed on the type of surfactant that can enable proper mixing of the O/W to create an emulsion.

The third subsection involves the use of three different metal chlorides (Manganese chloride, Magnesium chloride, and Chromium chloride) to synthesize metal oxides on the surface of the ceramic membrane to determine the most hydrophilic oxide. This is to achieve best metal oxide for modification of ceramic membrane based on hydrophilicity and separation efficiency. Subsection four describes how the most hydrophilic metal oxide which was Magnesium Oxide dispersedly impregnated on whole Al_2O_3 ceramic membrane for the modification of the ceramic membrane to increase separation efficiency of synthetic O/W emulsion. The highly dispersive magnesium oxide ceramic membrane was obtained by using dip-coating methods which have all been reported to give an effective yield in membrane modification.

The subsection five lays out how the Al_2O_3 and the newly modified MgO ceramic membranes are characterized by four parameters (Porosity, hydrophilicity (contact angle), morphology and pore size) to note the differences in both membranes and confirm the successful modification of MgO on Al_2O_3 ceramic membrane. Subsection six discusses the membrane reactor unit that houses the ceramic membrane. It evaluates every component that makes up the membrane reactor and how each component functions with respect to this research. The subsection also explains the mechanism behind the ceramic membrane support and the modified MgO ceramic membrane.

Subsection seven elaborates on the methodology and procedures employed for the determination of permeates flux and percentage oil rejection using modified and unmodified ceramic membrane. It starts with the equipment and apparatus used for crossflow filtration process down to the health and safety precautions

undertaken during laboratory experimental work. The subsection further underpins the experimental procedures utilized to determine the permeate flux considering the pure water flux, flowrate, temperature, and concentration parameters. This chapter also explains the process used to generate percentage oil rejection and recovery ration results. Subsection eight describes how Oil rejection was measured both physically and chemically with appearance and use of ultraviolet-visible spectrophotometer. This measurement was performed on both unmodified and modified ceramic membrane cross filtration process to decipher the rate of oil rejection by the membranes.

3.1 Material

This sub section comprises of material or reagents and instrumentations/equipment used for the entire methodology of this research.

3.1.1 Materials/ Reagents

Soybean oil, 250 mL each of Span 80 non-ionic surfactant and Tween 20, all supplied by Merck Life Science, UK. Deionised Water by Purelab Flex, Elga. Manganese Chloride ($MnCl_2$) powder and chunks, ≥99% trace metals basis 50g, Magnesium Chloride (MgCl2) powder, <200 µm 100g, Chromium Chloride ($CrCl_3.6H_2O$) purum p.a., ≥98.0% (RT) 100 g and 2 L of Ethanol (absolute alcohol) anhydrous >99.5% all supplied by Merck Life Science UK. 6000nm pore size 7 channeled α-alumina support which consists of 77% alumina and 23% TiO_2 and has a permeable length of 32.8 cm and an internal and external diameter of 7 and 10 mm respectively, supplied by Ceramiques Techniques et Industrielles (CTI), France.

3.1.2 Instrumentation and Equipment

1. 1.5 L home food blender by George company
2. Zetasizer Nano ZS instrument from Malvern Instrument Inc.
3. Electric oven by Carbolite
4. pH meter by Checker
5. Weighing Balance by Sartorius
6. One Attension Theta Lite Optical Tensiometer by Biolin Scientific

3.2 Synthesis of O/W Emulsion

For the synthesis of oil-in-water emulsion, soybean oil purchased from Sigma Life Science was used. The hydrophilic and lipophilic balance (HLB) must be identified for better emulsion performance. To narrow down the appropriate emulsifying surfactant for the preparation of a stable soybean oil, the Croda's HLB system was used (Schmidts et al. 2012). Each lipophilic ingredient used in an O/W emulsion has an individual required HLB. The required HLB for an oil is the HLB value of the surfactant that will provide the lowest interfacial tension between oil phase and water phase. The "required HLB for O/W emulsion of a variety of ingredients" table was used to identify the soybean oil to be 6 as it belongs to the vegetable oil family which has their required HLB with 5 – 7 as precalculated by Croda's HLB system. A blend of surfactants (Span 80surfactant 250 ml and Tween 20 surfactant 500 ml) 87%:13% respectively was used to prepared surfactant blend required to arrive at the HLB factor of 6 needed to achieve soybean oil-in-water emulsion. With the aid of their individual HLB (span 80 -4.3 and Tween 20 – 16.7) gave a close HLB of 5.9 to the desired required HLB of 6 to achieve a stable emulsion with soybean oil. Figure 23 shows the process of preparing O/W stable emulsion. Having blended the surfactant, to prepare the O/W emulsion, the ratio of 1:10 of surfactant to soybean oil was applied to prepare a mixture according to the method and ratio reported in literature by (Judd 2010) in the preparation of O/W emulsion using North sea crude oil and Sodium dodecyl Sulfate surfactant. Three concentrations (100 mg/L, 250 mg/L and 500 mg/L of O/W emulsion were prepared by measuring 0.1 g, 0.25 g and 0.5 g of the mixture surfactant and soybean oil on an analytical balance and distilled water was added to make up the mark of 1L. subsequently, the mixture was placed on a magnetic stirrer and allowed to stir for 2 mins at 4 rpm. The O/W emulsion now formed was further transferred to a food blender for homogenous mixture for 1 minute which produced a hazy and whitish colour. The average droplet size of the O/W emulsion was measured using a Zetasizer Nano ZS instrument from Malvern Instrument Inc. (Figure 24).

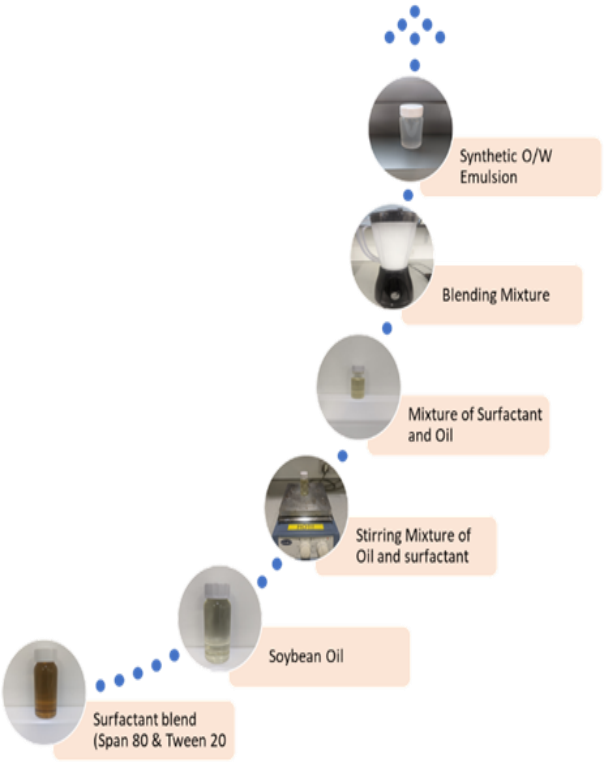

Figure 23: O/W stable emulsion synthesis process.

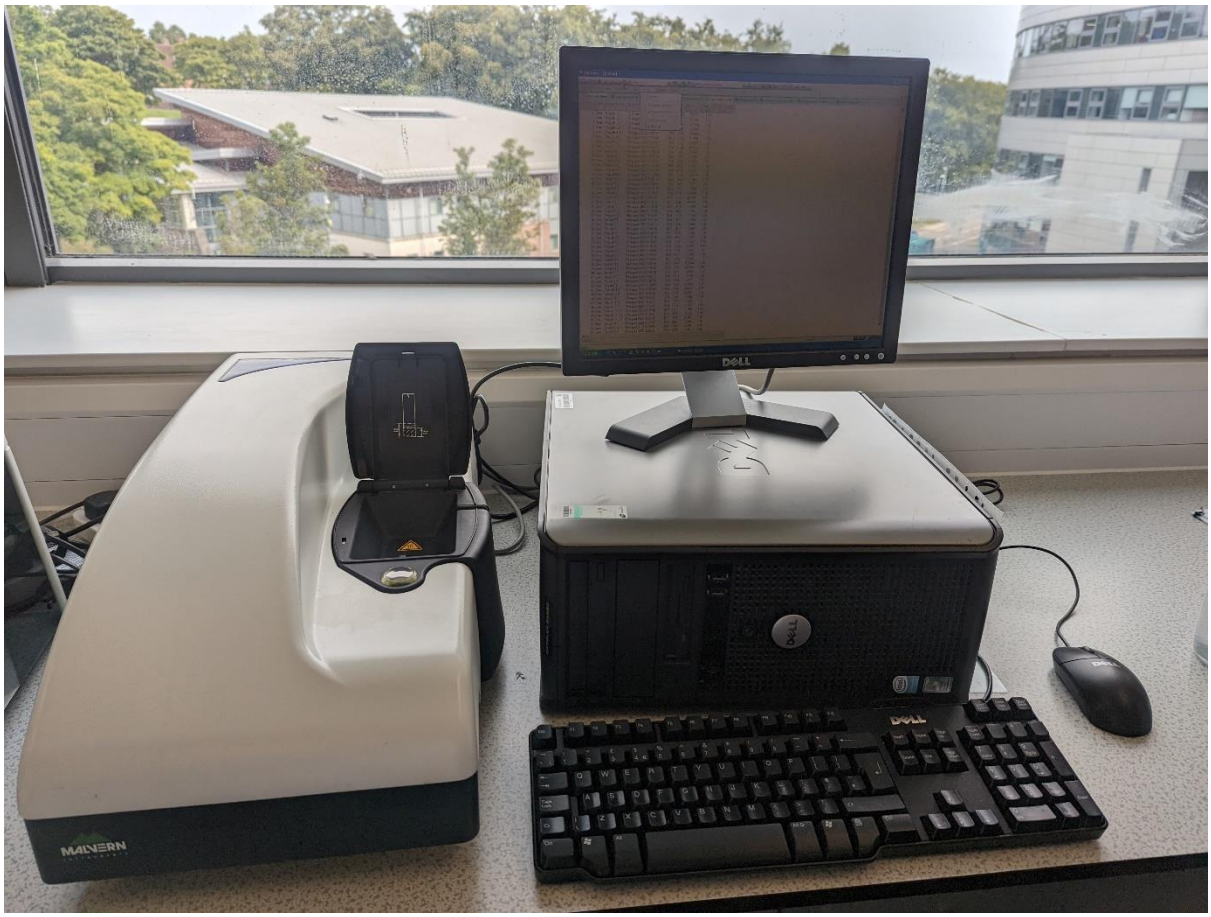

Figure 24: Zetasizer Nano ZS instrument from Malvern Instrument Inc. for Oil droplet size distribution measurement.

3.3 Testing Metal Oxides for Ceramic Membrane Modification

Three different metal oxides were examined for the modification of ceramic membranes for O/W emulsion separation. These metal oxides include Manganese Oxide (MnO_2), Magnesium Oxide (MgO) in powdered form 100 g was purchased from Merck in plastic containers with CAS number 7786-30-3 and Chromium Oxide (Cr_2O_3). Three witness samples of the three different metal oxides were broken from a 7 channelled fresh support Al_2O_3 ceramic membrane for surface modification. Manganese Chloride ($MnCl_2$) 99% trace metal basis 50g was supplied by Merck in plastic containers with CAS number 7773-01-5, Magnesium Chloride ($MgCl_2$) Magnesium Chloride in powdered form 100g was purchased from Merck in plastic containers with CAS number 7786-30-3, and Chromium Chloride ($CrCl_3$) 98% (RT) 100 g was supplied by Merck in plastic containers with CAS number 10060-12-5. Figure 25 represents the flowchart diagram of the step-by-step Al_2O_3 ceramic membrane witness samples modification. 0.48g of each powdered metal chloride was weighed into a vial and 10ml of absolute alcohol (99.5% 2 litres were purchased from Merck with CAS number 64-17-5) was measured with a cylinder and poured into three vials containing the three different metal chloride and shaken thoroughly to allow for complete dissolution. Witness samples of the ceramic membrane were placed in each vial containing the metal chloride solution for 36 hours at room temperature for the solution to saturate and modify the Al_2O_3 microfiltration fresh ceramic membrane witness samples. The Al_2O_3 ceramic membrane witness samples were first placed in the oven at temperature 110^0C for 12 hours to dry out any moisture before saturation in the metal chloride solutions. The three saturated witness samples of Al_2O_3 ceramic membrane were brought out of the metal chloride solutions and washed three time in absolute alcohol after which they were again immediately place in the oven to dry at 60^0C temperature for four hours. The Al_2O_3 ceramic membrane witness samples were brought out of the oven and bathed with hot steam for 6 hours after being plane above hot boiling water in hydrolysis process to oxidize the metals and reduce the chloride. At the end of the oxidation/reduction process, the modified Al_2O_3 ceramic membrane witness samples were calcined at 600^0C at a heating rate of 5^0C/min

for 2 hours. The hot modified Al_2O_3 ceramic membranes witness samples were allowed to cool down and then taken for contact angle measurement using One Attension Theta Lite Optical Tensiometer.

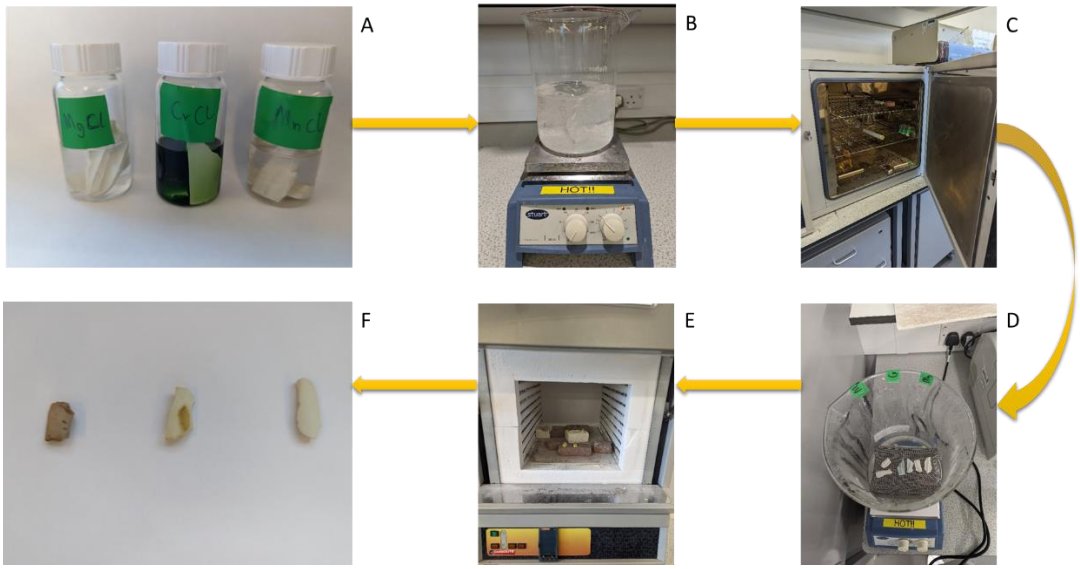

Figure 25: Flowchart diagram of Al2O3 ceramic membrane modification witness samples. A-sample saturation in metal chloride solution, B-washing samples in absolute alcohol, C-drying samples in oven, D-hydrolysis for oxidation of metal oxides on samples, E-calcining samples, F-Modified Al_2O_3 ceramic membrane witness samples to MnO_2, CrO_2 and MgO respectively.

3.3.1 Contact Angle (Hydrophilicity) measurements in Modified Al_2O_3 Ceramic Membrane Witness Samples.

Using One Attension Theta Lite Optical Tensiometer (Figure 26) contact angle measurement instrument, contact angle experiments were conducted by dropping model liquids in this case deionized water and soybean oil onto the ceramic membrane witness samples surface. Sessile drop method was used to test the ceramic membrane's wettability. Deionized water and soybean oil separately were used to measure static contact angles of MgO, MnO_2, and MgO_2 modified as well as unmodified ceramic membrane witness samples. The droplet size of deionized water from syringe of the instrument used for this analysis on all ceramic membrane with pore size 6000 nm was 5 µL. The contact angles [^{0}] formed by a single drop of 5 µL distilled water were seen and recorded using a software programme of "One Attension Theta Lite Optical Tensiometer" on the computer connected to the apparatus. For all ceramic membranes witness samples, the recipes were set to the same time of 5 seconds (5s) at the same frames-per-second (FPS) rate (100 FPS). The software determined the angles

that were formed between the baseline and the deionized water droplet's right and left contact points with the solid surface. The software computes the average angle value between the right and left points. The final average contact angle was obtained after averaging all the mean data over various time intervals.

Figure 26: Image of OneAttension Theta Lite Optical Tensiometer - adapted from Biolin Scientific Manual. (a – camera area, b - syringe in syringe holder for sample liquid phase injection, c – sample stage for any solid sample placement).

3.4 MgO Modification on Fresh Al_2O_3 Ceramic Membrane Support

Having concluded that MgO modification on ceramic membrane witness samples was more hydrophilic than the MnO and CrO_2 modifications, MgO was used to modify fresh Al_2O_3 ceramic membrane support for the separation of O/W emulsions. A similar procedure from section 3.2 was used for the modification process. As illustrated in Figure 27, from the method also reported in (Zhou, Jian-er et al. 2010), fresh support ceramic membrane was oven dried at 110^0C for 12 hours and then $MgCl_2$ powder was measured (24 g) into a beaker and 500 ml absolute alcohol was added to the beaker to form $MgCl_2$ solution. The mixture

was allowed to dissolve with the help of a magnetic stirrer (Figure 28 A) and fresh tubular ceramic membrane support (Figure 28 B) sealed on both ends (to inhibit solution getting into the channels of the membrane) was immersed into the solution alongside a witness sample. The membrane and witness sample were allowed in the solution to saturate for 36 hours producing a modified ceramic membrane precursor (Figure 28 C). The modified membrane and witness sample precursor were brought out of the solution and washed with absolute alcohol three times to aid drying. The membrane and witness sample precursors were immediately transferred to the oven for drying at 60^0C for 24 hours (Figure 29 A) and subsequently exposed to hot steam from boiling water for 6 hours to oxidize the $MgCl_2$ to MgO (Figure 29 B and equation 3). Finally, the MgO modified ceramic membrane and witness samples were calcined at 600^0C for 2 hours at a heating rate of 5^0C/Min (Figure 29 C). The newly prepared MgO-modified ceramic membrane is characterized for morphology, Pore size, porosity and hydrophilicity using SEM/EDAX, Nitrogen Adsorption & desorption Analysis (BET), Archimedes Principle, and One Attention Theta Lite Optical Tensiometer.

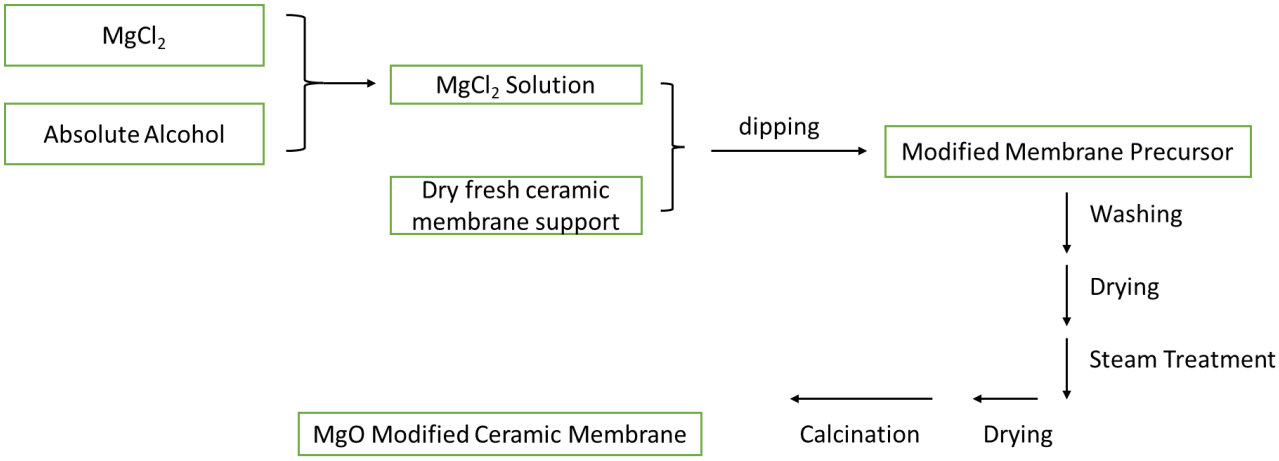

Figure 27: Flow chart of the preparation procedure of Al2O3 Ceramic Membrane by MgO modification.

Figure 28: A-MgCl2 solution, B-fresh support ceramic membrane, C- Ceramic membrane and witness sample in MgCl2 solution.

Equation 3

$$MgCl_2 + 9H_2O = MgO + 2HCl + 8H_2O$$

Figure 29: A-MgCl2 solution, B-fresh support ceramic membrane, C- Ceramic membrane and witness sample in MgCl2 solution.

3.5 Characterization

This sub-section reports on the step-by-step characterization methods used to analyse Al_2O_3 unmodified and MgO-modified ceramic membrane. These methods include contact angle measurements for hydrophilicity testing, Porosity measurement, morphology, and pore size measurements.

3.5.1 Contact Angle Measurement

As discussed in sub-section 3.3 the procedure for preparation of MgO-modified ceramic membrane witness sample was used in the same method to prepare a full MgO-modified tubular ceramic membrane for this study. Most importantly, the procedure, instruments and recipes used in that sub-section was also employed for the measurement of contact angle for hydrophilicity test in the newly MgO-modified tubular ceramic membrane. The results were reported and used to compare the unmodified Al_2O_3 ceramic membrane.

3.5.2 Porosity

To determine the porosity (ε) of the porous modified and unmodified ceramic membrane the famous Archimedes Principle was used as reported in (Monash, Purushothaman and Pugazhenthi 2011). Equation 4 below (Gohari et al. 2015) was used to calculate the porosity ε (%) of MgO-modified and Al_2O_3 unmodified ceramic membrane with the procedure as follows. Firstly, both modified and unmodified were dried in the oven at 110^0C for 6 hours to evaporate any moisture content present in the ceramic membrane. The ceramic membranes were allowed to cool to room temperature and then measured on an analytical balance to obtain the dry weight (W_d) Subsequently, both ceramic membranes were immersed in deionized water separately to saturation point for 24 hours. This was done to achieve the wet weight (W_w) of the membranes. The membranes were brought out of the deionized water after 24 hours and excess dripping water was quickly wiped with absorbent tissue and the membranes were weighed on analytical balance in turns to obtain the W_w and recorded. To achieve the membrane volume (V), the saturated membrane was placed into a known amount of deionized water able to exceed the length of the membrane in a graduated measuring cylinder. This procedure displaced the known volume of deionized water from the initial gradient on the measuring cylinder to a higher gradient. This volume difference between the initial gradient on the cylinder to a

higher gradient becomes the membrane volume (V) and $d_w$represents density of water. Equation 4 was then applied to calculate the ε (%).

Equation 4

$$\varepsilon\,(\%) = \left(\frac{W_w - W_d}{d_w \times V}\right) \times 100$$

3.5.3 Morphology (SEM/ EDXA)

The Scanning Electron Microscope (SEM) can be used to characterize the morphology of the cross section and surface of a sample. High resolution images are obtained of a sample by means of electron beams from SEM being focussed across the sample surface. The SEM can detect any surface irregularities, surface smoothness, cracks, size or shape, defeat, and segregation effects by examination of analysis. The SEM can also be used for the measurement of thickness of surface modifications or coatings on a sample (Smart et al. 2013; Usman, M. R.).

Figure 30: Zeiss EVO LS10 Variable Pressure (VP) and Back Scatter Detector (BSD) Scanning Electron Microscope (SEM).

The characterization of the morphology for unmodified and modified tubular ceramic membrane conducted using Zeiss EVO LS10 Variable Pressure (VP) and Back Scatter Detector (BSD) system with Scanning Electron Microscope (SEM). This SEM was also equipped with Energy Dispersive X-Ray Analyser (EDXA) that is used to quantify and identify element present in a sample for elemental composition analysis. Figure 30 highlights a pictorial image of the SEM instrument. The fragments from witness samples of the fresh support Al_2O_3 and

modified MgO ceramic membranes were placed on a stainless-steel disc stub and help on position on the stub with the aid of an adhesive (Figure 31). The adhesive does not only provide a steady grip of the membrane fragment to the stub but also aid in the provision of electrical continuity. The stub holding the samples were loaded onto the sample carousel of the SEM. The samples analysis was operated under vacuum and did not require any sputtering. The SEM photographs of the cross section and outer surface areas of the samples were obtained at three different magnifications. SEM and EDXA images from both VP and BSD for outer surface and cross section of modified MgO and unmodified Al_2O_3 will be analysed and compared.

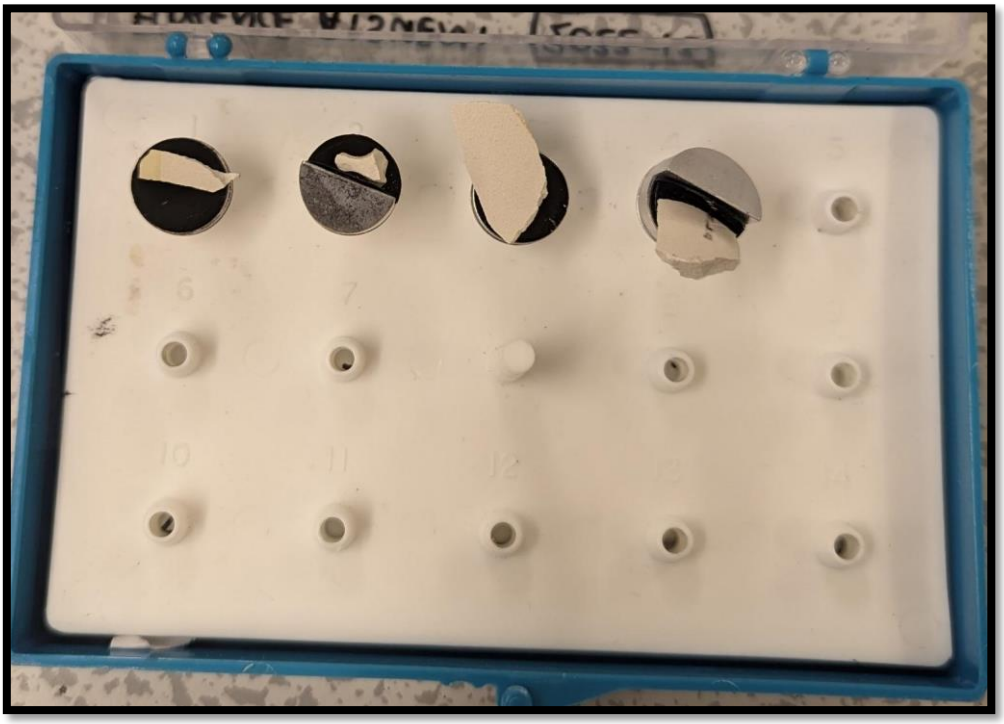

Figure 31: Unmodified and Modified ceramic membrane witness sample on stainless steel disc stub.

3.5.4 Nitrogen Adsorption Desorption Analysis

Nitrogen absorption and desorption is a common analytic method used in the characterization of porous materials. It is used in the determination of pore size distribution, specific surface area and pore diameter in porous membrane (Smart et al. 2013). Quantachrome®AsiQwin™ nitrogen adsorption desorption analyzer is the instrument used for the determination of the Barret, Joyner and Halenda (BJH) and the Brunauer, Emmett and Teller (BET) results. The calculation for pore size distribution and average pore size is analyzed by the BJH method, while the calculation for specific surface area is analyzed by BET by the measurement of how much gas is absorbed per gram of a sample (Othman, Mukhtar and Ahmad 2004). The quantitative measurement of the pore volume with a representative range of pore radii is described as the pore size distribution measurement. Usually, pore volume is plotted against pore radius in a graph representation (Usman, M. R.). Results for pore size, pore diameter and specific surface area of unmodified and modified MgO ceramic membrane were analyzed by BJH and BET, respectively.

Two stages are involved in the analysis using nitrogen adsorption desorption analyzer. This involves the degassing stage and the main analysis stage. Samples are usually in the treated to be powdered to coarse before usage in Quantachrome analyzer. A mortar and pestle were used to ground unmodified and MgO modified samples to a coarse form during sample pre-treatment. Washed and dried in the oven sample cells have been weighed initially, noting the weight of the empty cells. The empty cells weight is subsequently zeroed, and samples are placed in the cells and weighed. The samples' weights usually fall between 0.1 to 1 g depending on the nature of the sample. The unmodified ceramic membrane weighed 1 g while the MgO-modified samples weighed 0.1 g.

3.4.4.1 Degassing Stage

Degassing is a necessary step in the procedure while using Quantachrome analyzer to remove moisture content present in the samples. In this procedure, sample cells containing samples to the degassing station on the Quantachrome analyzer instrument as seen in Figure 32 using the work instruction procedure in the manual. The degassing process took about 4-5 hours at 338K temperature with Helium and Nitrogen gases.

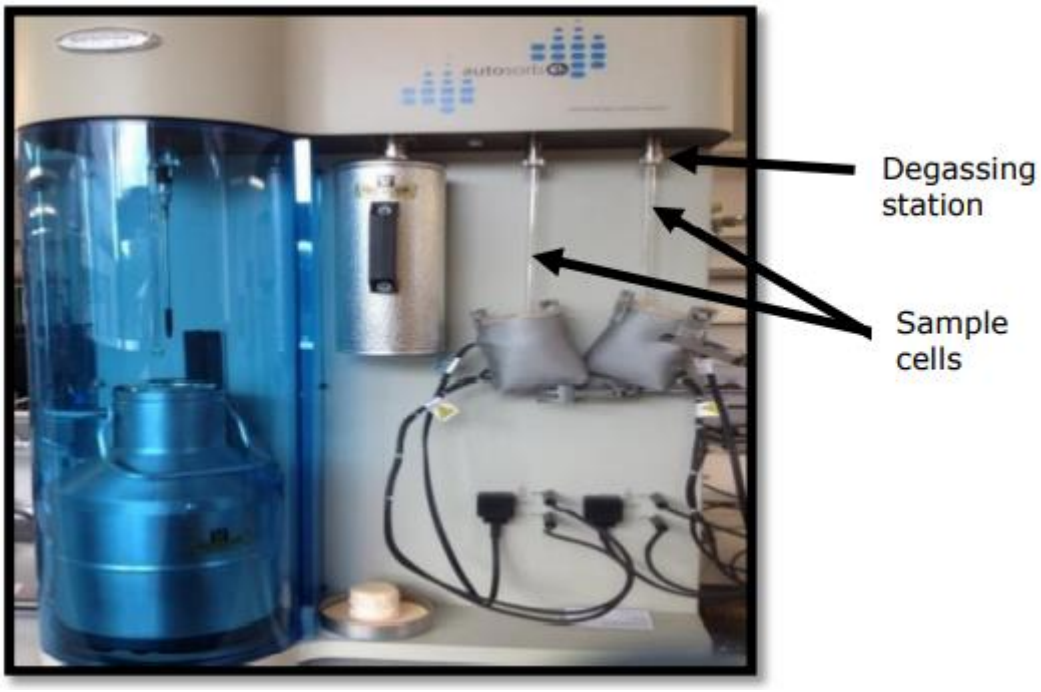

Figure 32: Pictorial representation of samples undergoing degassing using Quantachrome Analyzer.

3.4.4.2 Analysis Stage

Upon the degassing process's conclusion, the sample cells are transferred to the analysis stage on the instrument with liquid nitrogen during analysis. Once the analysis stage is initiated based on the work instruction, the liquid nitrogen contained in a dewar is lifted to allow immersion of the cells containing the sample in the liquid nitrogen. The analysis is carried out at 77K. Figure 33 displays samples analyzed in the analysis stage.

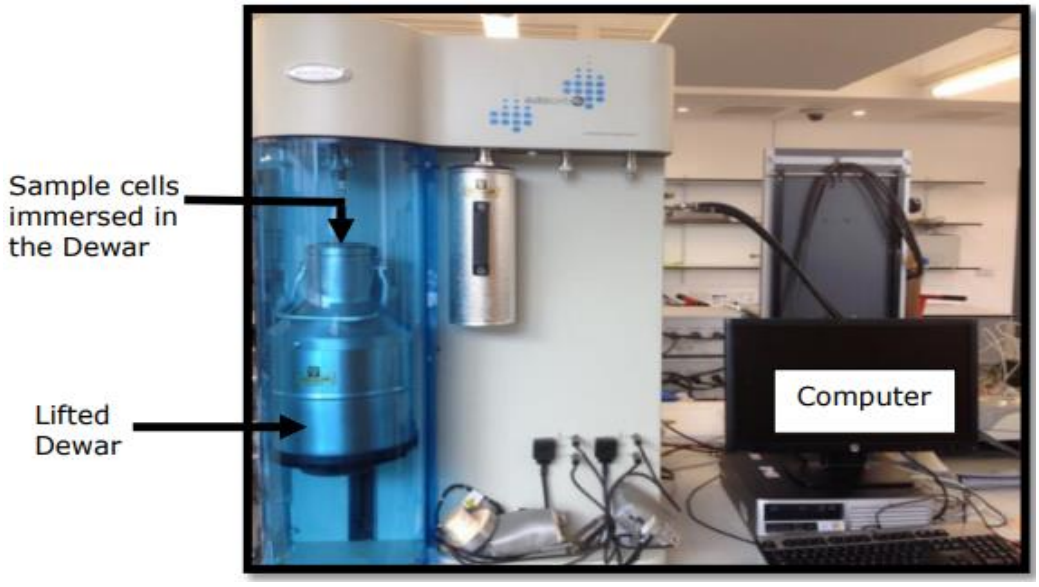

Figure 33: Ongoing analysis stage process using Quantachrome Analyzer.

3.6 Reactor Design

(Gobina 2006) in a patent, the apparatus and method for separating gases which are reactors that are also used in this study to the installation of crossflow nanofiltration of O/W emulsion separation rig. Figure 34 shows a pictorial representation of the reactor or holder used to house the Al_2O_3 unmodified and MgO-modified ceramic membranes for separation of O/W emulsion. These reactors can be made in varied sizes and are made from stainless steel material. The structure of the reactor is cylindrical with a hollow inner centre for placing ceramic membrane and are accompanied by caps made also from stainless steel, for both ends to close the inside of the reactor. The reactors are normally welded and tested at pressures up to 50 bar and inspected for leak test by accredited industries. The reactors are made up of three major sections: the feed; the retentate and the permeate sections. Heating test of the reactor can get up to heights of 450^0C with the notice or damage of any structural deformation of the shell material.

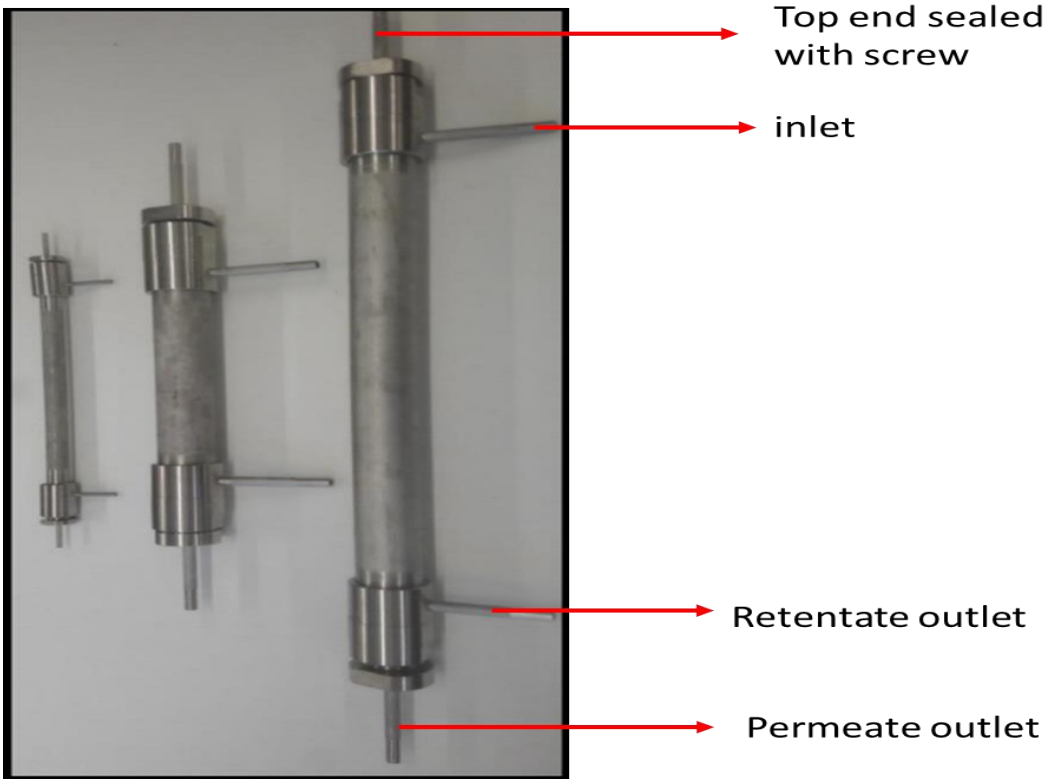

Figure 34: Stainless-steel reactors.

The separation rig itself consists of the ceramic membrane (modified/ unmodified), the stainless steel where the ceramic membrane is housed, and the

caps closing the entrance and exit of the hollow stainless-steel reactor. The ceramic membrane is gently place into the hollow space of the stainless-steel reactor and sealed with graphite seals on both ends to prevent water leakages during analysis. Figure 35 displays the coupling of ceramic membrane in the hollow stainless-steel reactor with graphite seals and caps for closing the reactors. During analysis, the ceramic membrane is expected to act as a semi-permeable barrier for the separation of O/W emulsion i.e., rejection of oil phase and allowance of water phase. This is a vital aspect of determining the separation mechanism of O/W emulsion through these ceramic membranes.

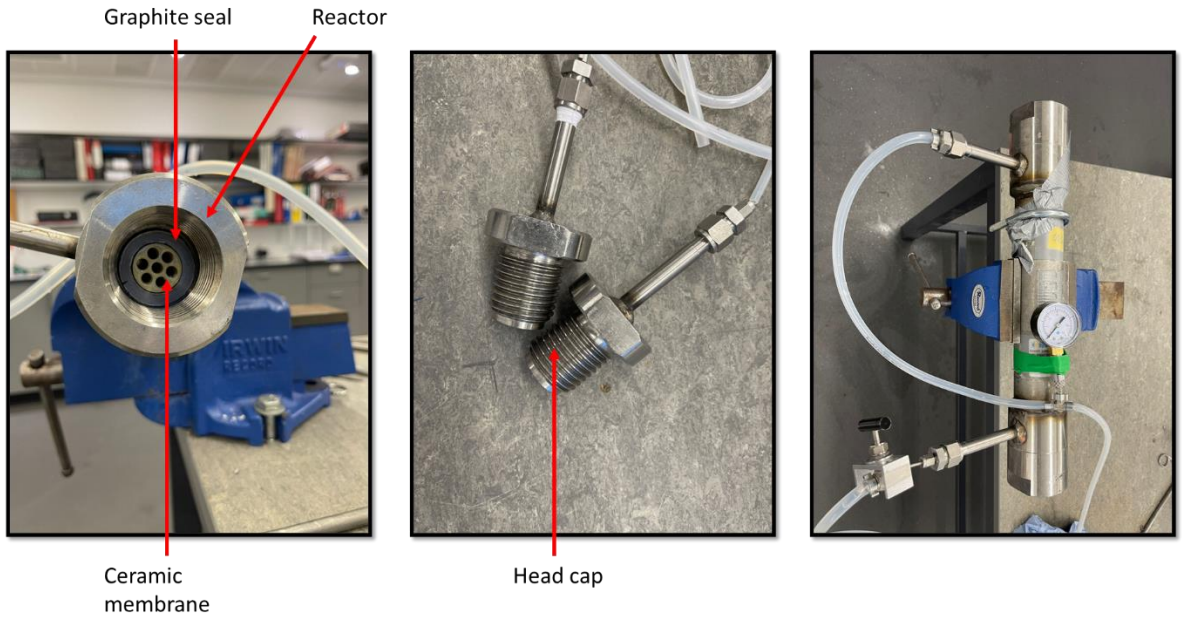

Figure 35: Coupled Ceramic membrane in reactor with graphite seal and head cap.

Once the ceramic membrane is properly sealed in the reactor and caps covered, a leak test is conducted. Tubing is attached to the entrance of the reactor from the peristaltic pump. The peristaltic pump is used to pump O/W emulsion or in the case of leak test, pure water from the feed tank at varying pressures and flowrates. So, the tubing is connected from the feed tank via the peristaltic pump to the entrance of the reactor where and o ring is used to seal the tubing to the reactor. A pressure gauge is attached to the entry tubing to measure the pressure of fluid going into the reactor. Another tubing is attached to the permeate exit of the reactor with the help of an o ring. The permeate tubing empties permeated fluid into a calibrated beaker placed on a scale to measure the permeate volume or flux per unit time. A third tubing is also attached to the retentate section of the reactor with the help of an o ring. The retentate received

rejected fluid from the semi permeable ceramic membrane and recycles fluid back into the fluid tank for further analysis. The top of the reactor is sealed with a screw to discourage the leak of any fluid passing through the reactor during analysis. Figure 36 displays a pictorial representation of the entire rig and Figure 37 shows the flow diagram used in the separation of O/W emulsion process starting from the feed tant to the reactor and even to the permeate on the scale and retentate flowing back to the feed.

Figure 36: Rig for O/W emulsion crossflow nanofiltration.

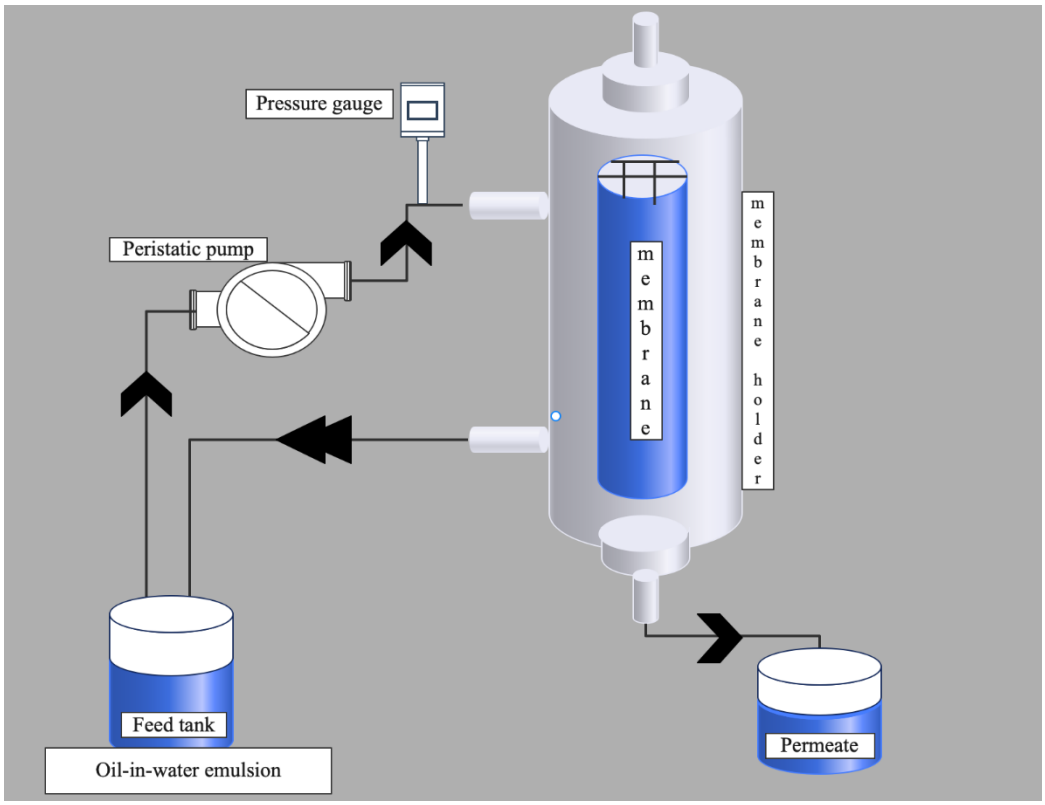

Figure 37: Process flow diagram of the rig set up

3.6.1 Ceramic membrane support design

Ceramiques Techniques et Industrielles (CTI SA) France was tasked with the production and design of a porous tubular ceramic membrane. A porous design was requested to allow room for coating or dispersion of ceramic membrane modification giving a hydrophilic surface that aids the aim of this study. A tubular design was preferred over a flat sheet as this can fit suitably into the reactor present in the laboratory for the research purposes. The tubular membrane was designed with 7 channels that also aid in filtration purposes. The tubular ceramic membrane fits well in the reactor with the aid of a graphite seal in such a way that it forces the reactants in this case O/W emulsion to encounter the surface of the membrane. This reaction allows liquid pass through the pores of the membrane and rejected solutes flows over the surface of the membrane and out of the reactor via the retentate exit. Also, the tubular shape of the ceramic membrane support gives room for expanded surface area compared to the flat sheet membrane which is advantageous in mass transfer.

3.6.2 MgO Ceramic Membrane and Process Design

Figure 38 describes the design and layers of the hydrophilic nano sized MgO-modified tubular ceramic membrane for the utilization in O/W emulsion separation process. As previously mentioned in section 2, porous ceramic membranes usually consist of three layers before modification. This includes the macropores which acts as the support layer, the mesopores as the intermediate layer aiding the support layer and finally the micropores as the outer layer where separation takes place. MgO was chosen as the molecule for surface modification of ceramic membrane support due to its hydrophilic nature. The hydrophilicity of MgO was ascertained after comparing it with other metal oxides using contact angle measurements.

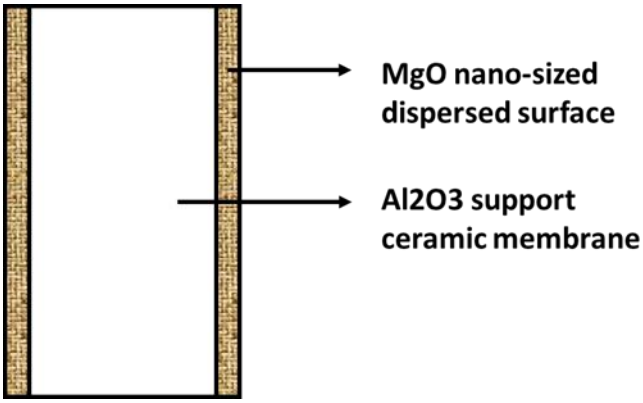

Figure 38: Cross-sectional view MgO dispersed tubular ceramic membrane modification.

Enormous quantities (16 litres) of O/W emulsion synthesized by the mixture of soybean oil, surfactant blend of Tween 20 and Span 80, and deionized water are fed at the entrance of the reactor inlet from the feed tank via a tubing to the modified ceramic membrane in the reactor. Upon contact with the hydrophilic surface of the modified ceramic membrane, there arises the formation of a water layer developing from the affinity of water molecules to the membrane surface creating a separation between the oily and water phase in the O/W emulsion. Most water molecules permeate through the pores of the membrane into the channels and are filtered out as permeated volume. This process creates a cleaner and less oily permeate compared to the concentrations of oil in the feed. Although some oily molecules might be found in the permeated volume, this might occur from the peristaltic pump pressure and capillary pressure of the O/W emulsion flow. The oily phase remains suspended as a thin layer stream above the waterbed layer and flushed down with the aid of pressure and capillary flow down the length of the membrane surface and exits with some water through the retentate which feeds back into the feed tank as a continuous flow. This process is described in Figure 39 below.

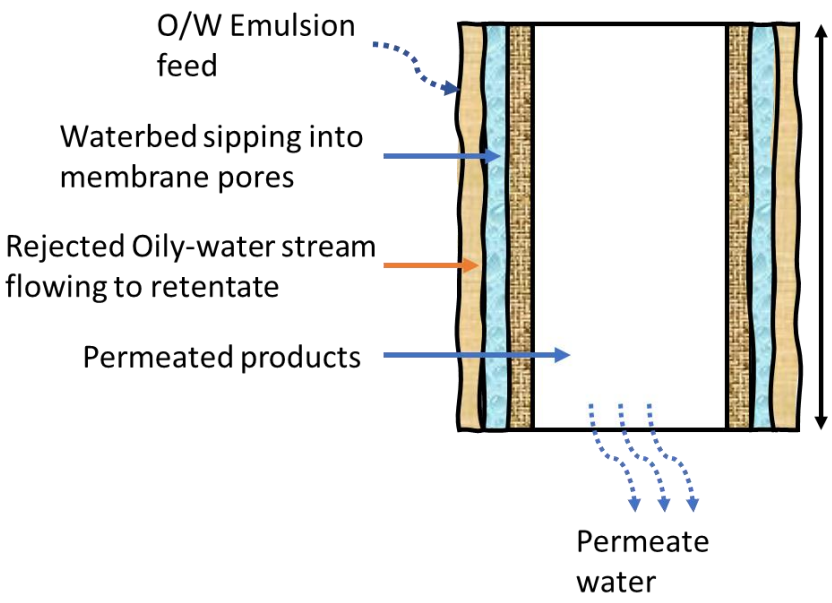

Figure 39: Cross-sectional description of O/W emulsion separation across modified MgO surface tubular ceramic membrane.

3.7 Cross flow Nanofiltration Rig for O/W Emulsion Separation

This sub section involves the measurement of the flux of O/W emulsion through the MgO modified tubular ceramic membrane and comparing it with the unmodified.

3.7.1 Equipment and Apparatus

A hollow stainless-steel reactor including its head cap was used for housing ceramic membrane and held vertically on a rig panel with the help of a clamp. Tubing size 27 mm was used for connecting reactor openings (entrance and exits) to other apparatus of the entire rig. Both MgO modified and Al_2O_3 unmodified tubular ceramic membrane were used in the reactor as separating material O/W emulsion. Peristaltic pump was also used to pump the O/W emulsion or pure water to the reactor; and it was also used to adjust the flowrate of the fluids. A 20 litres ultrasonic bath was used as the feed tank containing pure water or O/W emulsion at separate times; it was also used to heat up the feed tank for temperature flux measurement. A pressure gauge was used to measure the pressure of fluids flowing into the reactor per unit time. A 5000 mL gradient beaker was used as a receiver of the permeate volume exiting the ceramic membrane permeate. This beaker was placed on a scale that is used to confirm the volume of the permeate per unit time in kilograms. All these apparatuses are represented in Appendix I.

3.7.2 Health and Safety

During the experimental process all, personal protective equipment was worn for safety purposes and details of the PPE are found in Appendix III. The analysis was carried out in the fume hood and beside the sink in the laboratory to withstand any spillage that may occur. Safe handling and storage of every chemical used was adhered to as listed in appendix III.

3.7.3 Experimental Procedure

A separation test rig comprising of all the apparatus mentioned above was assembled as shown in a schematic diagram in Figure 40 below. Based on the aim of this experiment which is determine the flux of O/W emulsion through the ceramic membrane, the experimental procedure is divided into 5 sections. These

sections include Flux based on Flowrate, Flux based on Temperature and Pure water flux and modified versus unmodified ceramic membrane recyclability Flux.

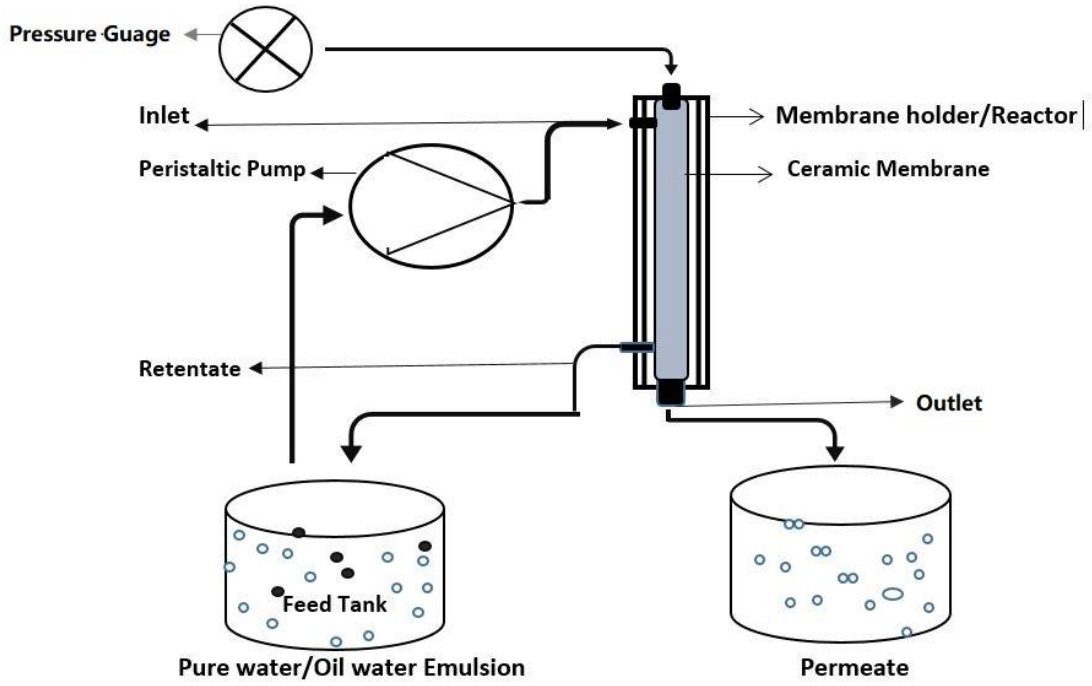

Figure 40: Schematic diagram of Separation rig *(Suresh and Pugazhenthi 2017).*

3.7.3.1 Flux based on Flowrate

Flux of O/W emulsion permeation was determined using a continuous crossflow in-house separation rig set-up apparatus. Flux was measured both on Al_2O_3 unmodified and MgO-modified tubular ceramic membranes which was inserted into the reactor prior to analysis. Two flowrates 25 L/Hr and 50 L/Hr were used and set on the peristaltic pump to investigate the flux on both membranes. First, 20 litres of O/W emulsion was poured into the ultrasonic tank acting as the feed tank was pumped by the peristaltic pump at 25 L/Hr flowrate via the inlet tubing. The O/W emulsion gained access through the entrance of the reactor and encountered the surface of the Al_2O_3 unmodified ceramic membrane. The top position of the reactor entrance and the crossflow set of the rig allowed the fluid run along the length of the ceramic membrane surface where separation takes place. Oily phases are expected to flow in a stream down the retentate as the ceramic membrane poses as a semi-permeable barrier for the oily molecules. The retentate fluid exits the reactor via a tubing the leads the stream back to

the feed tank for continuous flow separation. Permeated water phase flows through the pores of the membrane and into the channels where the water exits at the bottom via a permeate tubing into a beaker placed on scale. The O/W emulsion was allowed to run for 30 minutes to stabilize the flowrate and pressure in the separation rig before measurement was recorded. The entire cycle of process is allowed to run for 30 minutes during which measurements of the permeate volume is recorded every 5 minutes to ascertain any change or decline in volume. Based on the aim of this experiment, the O/W emulsion permeate flux $J_w\ (L/m2\ h)$ via the unmodified ceramic membrane was established by dividing the water permeate $Q_p\ (L)$ by the ceramic membrane permeate area $A\ (m^2)$ and the filtration time $t\ (h)$ as seen in Equation 5 below. Q_p was directed measured from the permeate volume every 5 min with the permeate volume measurement on the scale and in the beaker. *A* was achieved with the Equation 2 below for the ceramic membrane and t was from a change in time by an increment of 5 mins converted to hours. This entire process was repeated for the MgO-modified tubular ceramic membrane and the results of the fluxes from both modified and unmodified will be compared. The raw recorded data of the different parameters can be seen in Appendix V.

Equation 5

$$J_w = \frac{Q_p}{A \times t}$$

3.7.3.2 Area of Tubular Ceramic membrane

Equation 6 and 7 below is used to calculate the area A of the tubular ceramic membrane. Figure 41 below demonstrate the measure used to calculate the *A* of the ceramic membrane. The height - h (32.8 cm) was measured with the help of a meter rule and the diameter - D (2.59 cm) was measured with the help of a vernier calliper as seen in appendix II. The diameter measurement was used to calculate the just one radius (the outer radius) instead of r^2 because only the lateral surface area of the ceramic membrane interacted with O/W emulsion in the reactor.

Ceramic Surface Area = Lateral Surface Area of the Ceramic Membrane is:

Equation 6

$$2\pi rh$$

Where r =Ceramic membrane outer radius, h = Ceramic membrane height, and π = 3.14.

Equation 7

$$r = D/2$$

Therefore,

$$A = 2 \times 3.14 \times 1.30cm \times 32.8cm$$

$$A = 267.8cm^2$$

$$A = 0.027m^2$$

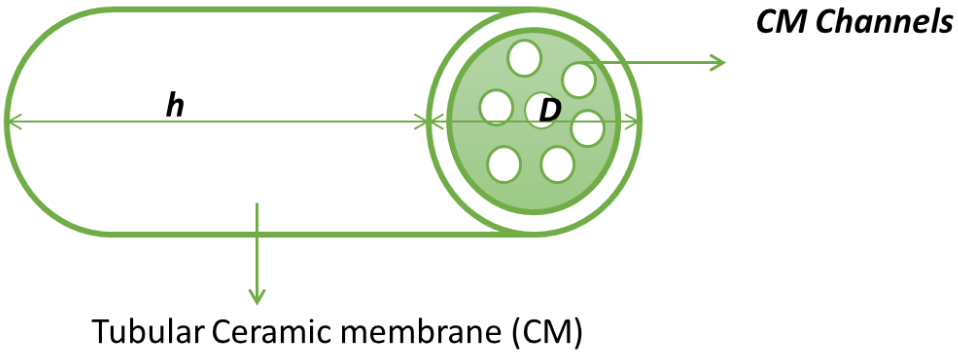

Figure 41: Schematic diagram of area A of Ceramic Membrane.

3.7.3.3 Flux based on Temperature

Similar procedure reported in the sub section 3.7.3.1 above was used to determine the flux of O/W emulsion with the effect of temperature via unmodified and modified tubular ceramic membrane. The temperatures used to determine these temperature-based fluxes are room temperature (20^0C) and 50^0C. The only additional step used in this section that differs from sub section 3.7.3.1 above is the heating of the O/W emulsion in the ultrasonic bath prior to analysis. The temperature of the bath was set for 20 and 50^0C as calibrated on the ultrasonic bath and these temperatures were further confirmed with the use of a thermometer. Subsequently, every step in sub section 3.7.3.1 was affected.

3.7.3.4 Pure Water Flux (PWF)

Before the measurement of O/W emulsion flux with both flowrate and temperature via the unmodified and modified ceramic membranes, pure water flux was measured. PWF on unmodified ceramic membrane was first investigated using the separation rig to ascertain a steady-state flux flow through the rig and for subsequent comparison of PWF with modified ceramic membrane. The pure water flux procedure involves the same steps used in sub section 3.7.3.1. The difference is the use of deionized water instead of O/W emulsion. Also, the PWF was done in triplicate and used to calculate for any system or instrumental errors that may develop.

3.7.3.5 Flux recovery

The determination of the flux recovery is aimed at establishing the reusability of both unmodified and modified ceramic membranes after the passage or separation of O/W emulsions in the separation rig. The procedure involves washing the tubular ceramic membrane with deionized water at 50 L/H flowrate, allowing it to run through the rig to a dead-end waste for both permeate and retentate exits for 30 minutes to remove as much O/W emulsion as possible. PWF was then redetermined to achieve flux recovery ratio (R_{FR}) using Equation 8 below.

Equation 8

$$R_{FR}\ (\%) = \left(\frac{J_{w'}}{J_w}\right) \times 100$$

Where $J_{w'}$ is the PWF after treatment or separation of O/W emulsion; J_w is the PWF before separation or treatment of O/W emulsion via ceramic membrane.

3.8 Oil Rejection

Oil rejection was measured both physically and chemically with appearance and use of ultraviolet-visible spectrophotometer. This measurement was performed on both unmodified and modified ceramic membrane cross filtration process to decipher the rate of oil rejection by the membranes.

3.8.1 Physical Analysis

Firstly, appearance was measured by compared permeate flux from cross filtration against the O/W emulsion in the feed to note any difference. This was performed by collecting O/W emulsion feeds in glass vials prior to experiments and later collecting permeate flux after 30 minutes run of every O/W concentration (100, 250 and 500 mg/L) in another glass vial. The before and after were compared to note any difference in appearance. This was conducted for both flowrates (25 and 50 L/H), in all concentrations for both unmodified and modified ceramic membrane.

3.8.2 Chemical Analysis

For chemical analysis, Ultraviolet-Visible (UV-Vis) spectrophotometer was used for quantitative measurement of permeate flux after 30 minutes run for all concentrations of O/W emulsion on both Al_2O_3 unmodified and MgO-modified ceramic membrane. First, O/W emulsion standards of known concentrations were prepared from soybean oil, deionized water, and surfactants blends (Tween 20 and span 80) using the parameters in Table 4 below. Deionized water and the surfactant blend were used to prepare the blank for UV-Vis analysis. Prior to analysing the O/W emulsion standards, a mixture of deionized water and soybean oil was made (9:1) to run through the UV-Vis spectrophotometer at broad band wavelength of 200-800 nm to determine the optimum wavelength for soybean oil absorbance. The highest peak was noted at 248 nm wavelength, and this was used throughout the analysis for any UV-Vis experiments requiring soybean oil. Following the work instructions, the UV-Vis spectrophotometer was operated to achieve the absorbance of the various known prepared standards of O/W emulsion. These absorbances were plotted on excel to get a calibration curve against the known concentration standards of O/W emulsion. Subsequently, the unknown permeate flux concentrations from the crossflow filtration of the two different flowrates was measured using the UV-Vis

spectrophotometer to ascertain the absorbance. The absorbances obtained from the unknown permeate flux concentrations were used to interpolate their concentrations from the straight-line calibration curve obtained from the known standards O/W emulsion using the straight-line calibration curve Equation 9 below. Figure 42 displays the calibration graph of 100 mg/l feed with data from Table 4. Other concentrations (250 and 500 mg/l) calibration graphs are represented in Appendix V. This was aimed at deciphering any concentrations of oil after cross filtration through the unmodified and modified ceramic membrane present in the permeate flux.

Table 4: Parameters for O/W emulsion standard preparation for various concentrations and their absorbance

	M1 (mg/l)	V1 (ml)	M2 (mg/l)	V2 (ml)	Unmodified Absorbance	Wavelength (nm)	Modified Absorbance
100mg/l							
Std. 1	100	1	10	10	0.029	248	0.034
Std. 2	100	2	20	10	0.076	248	0.052
Std. 3	100	3	30	10	0.119	248	0.075
Std. 4	100	4	40	10	0.154	248	0.096
Std. 5	100	5	50	10	0.190	248	0.117
Std. 6	100	6	60	10	0.228	248	0.131
Std. 7	100	7	70	10	0.272	248	0.145
250mg/l							
Std. 1	250	1	25	10	0.182	248	0.044
Std. 2	250	2	50	10	0.292	248	0.059
Std. 3	250	3	75	10	0.386	248	0.089
Std. 4	250	4	100	10	0.477	248	0.108
Std. 5	250	5	125	10	0.561	248	0.129
Std. 6	250	6	150	10	0.637	248	0.144
Std. 7	250	7	175	10	0.703	248	0.163
500mg/l							
Std. 1	500	1	50	10	0.279	248	0.182
Std. 2	500	2	100	10	0.424	248	0.300
Std. 3	500	3	150	10	0.623	248	0.396
Std. 4	500	4	200	10	0.784	248	0.497
Std. 5	500	5	250	10	0.955	248	0.571
Std. 6	500	6	300	10	1.067	248	0.657
Std. 7	500	7	350	10		248	0.703

Equation 9

$$Y = mx + c$$

Where Y is the absorbance of unknown on the standard calibration curve on y axis, *m* is the slope and *c* are the intercept, *x* is the unknown concentration to be calculated.

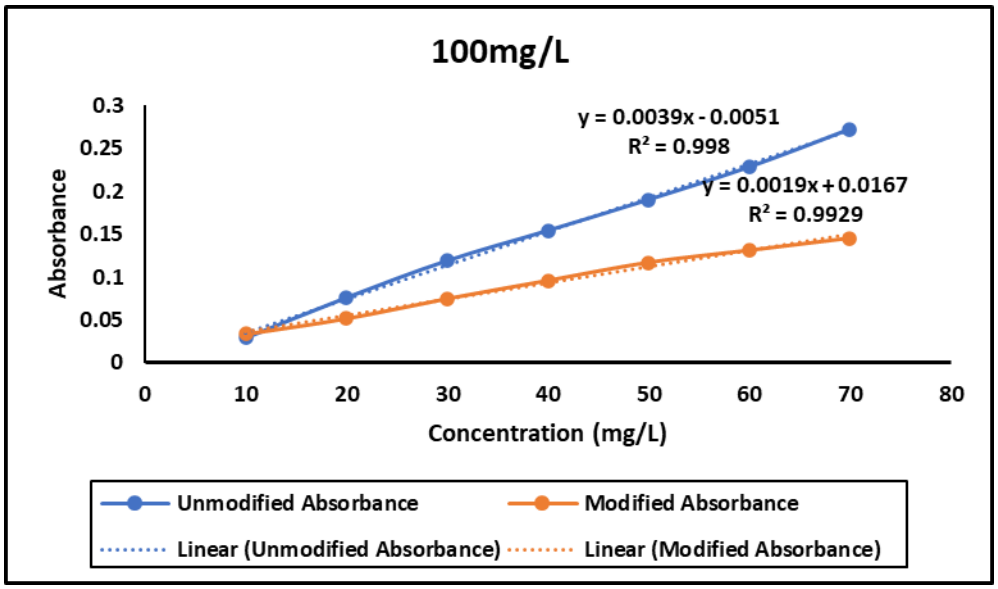

Figure 42: Calibration curve of 100mg/l feed concentration for unmodified and modified ceramic membrane.

Chapter 4

4.0 Results and Discussions

This section reports and discusses the results acquired from characterization of unmodified and modified membrane. This chapter also records and explains results from analysis of O/W emulsion preparation results, permeate flux results from all parameters which includes pure water flux, flux based on flowrate, flux based on temperature, and flux recovery ratio of both unmodified and modified ceramic membrane. The chapter further reports results from physical and chemical analysis of percentage oil rejection for both modified and unmodified ceramic membrane, considering all the parameters such as flowrate, temperature, and concentration.

4.1 Synthesis of O/W Emulsion

Three concentrations (100, 250, and 500 mg/l) of O/W emulsions were synthesized using soybean oil and surfactants Span 20 and Tween 80 similar to reported literature (Chang et al. 2014c; Fang et al. 2013; Judd 2010) of synthesized O/W emulsion. The result was to create a stable emulsion with oil particle size in the micro range below 10 µm to determine separation of smaller oil droplets but large enough not to penetrate the pores of the ceramic membrane causing pore blocking and foul the membrane. This micrometre limit was decided because convention methods lacked the separation efficiency to clean oil droplets below that size (Chakrabarty, Ghoshal and Purkait 2010). After preparation of the O/W emulsion, the characteristic of the emulsion which includes pH, Viscosity, and Oil particle size were measured using a pH meter, Viscometer, and a Zetasizer respectively. Table 5 shows the results of the entire characteristics of the three consecrations of O/W emulsion. Figures 43 to Figure 45 represents the Oil particle size of the three O/W emulsion concentrations which were measured in triplicate.

As evident in Figure 43, the oil particle size for 100mg/L O/W emulsion fall between 50 – 500 nm distribution. The intensity is higher towards the 800 nm compared to below 100 nm hence the average particle size distribution figure. This is like the result displayed in the chart of Figure 44 for 250 mg/l O/W emulsion in terms of average oil particle size distribution. Nevertheless, the range of oil particle size falls between 100 – 1000 nm and not below 100 nm. Also, the intensity though still higher in the 800 nm regions but much intensity is

observed in the 100 nm regions than that of Figure 43. Figure 45 has three distinct oil particle size intensities running from the 100s to 1000s and to 6000s nanometres, though the 6000 nm peak intensity is less. Most intensities lie between 100s and 1000 nm for the 500 mg/l O/W emulsion equally hence the average oil particle size figure.

Synthesis of all three concentrations of O/W emulsions produced an almost uniform oil particle size distribution with similar average and intensity. Most importantly the oil particle distribution size for the three concentrations falls below the limit of 10 µm aim as seen in Figure 43 to Figure 45. The average oil particle size distribution (461.7 nm) for 500 mg/L was smaller than that of 250 and 100 (813.3 and 629.2 nm) respectively and this might from human error or instrumental errors during production so consistency and quality control during synthesis is key. The average oil droplet size of all concentrations falls in the 100 s which is like the studies of Lu(Lu, D. et al. 2016; Gohari et al. 2015) that synthesized O/W emulsions below 1000 mg/l in their work with flat sheet polysulfone (PSF) Hydous Aluminium Oxide (HAO) and Iron oxide dynamic ceramic membrane respectively for the separation of O/W emulsion. Their O/W emulsion synthesis produced average oil droplet size of 369.5 nm and 386.8 nm, respectively.

Table 5: Characteristics of O/W Emulsion

Concentrations (mg/l)	**ph**	**Viscosity (Pa.s)**	**Average oil partcile size (nm)**
100	6.78	0.8271	629.2
250	6.35	0.8523	813.3
500	6.15	0.8872	461.7

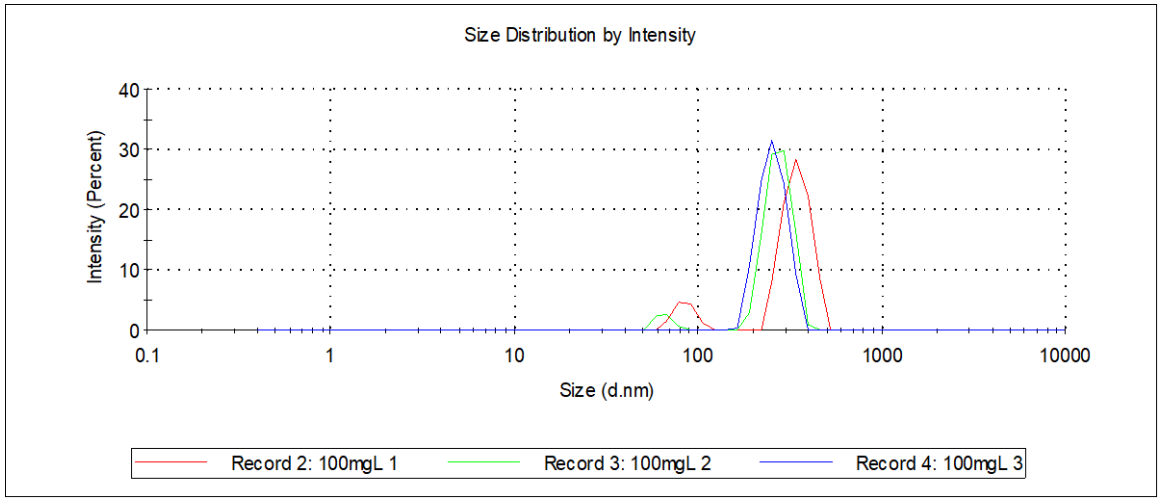

Figure 43: Oil particle size distribution of 100mg/l O/W emulsion.

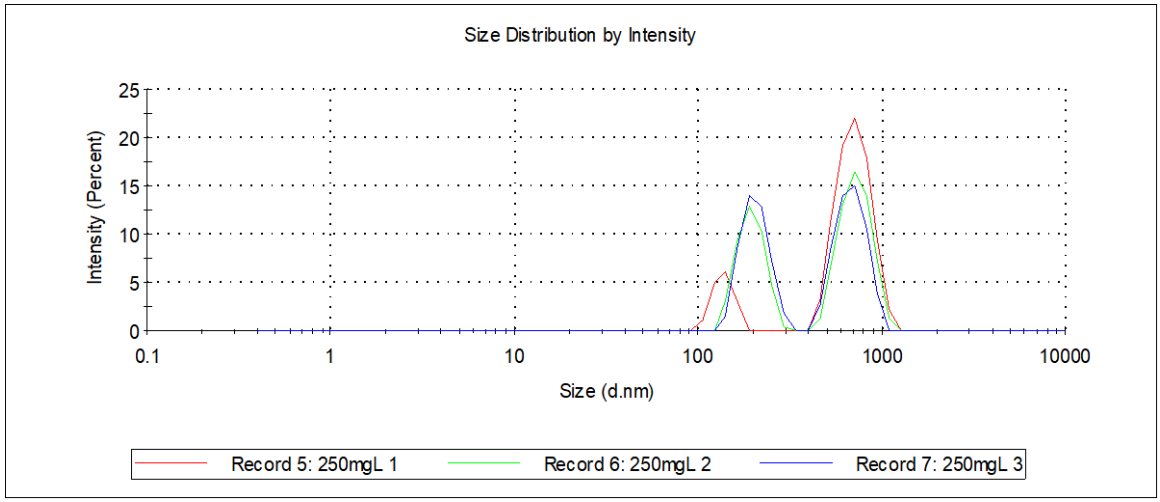

Figure 44: Oil particle size distribution of 250mg/l O/W emulsion.

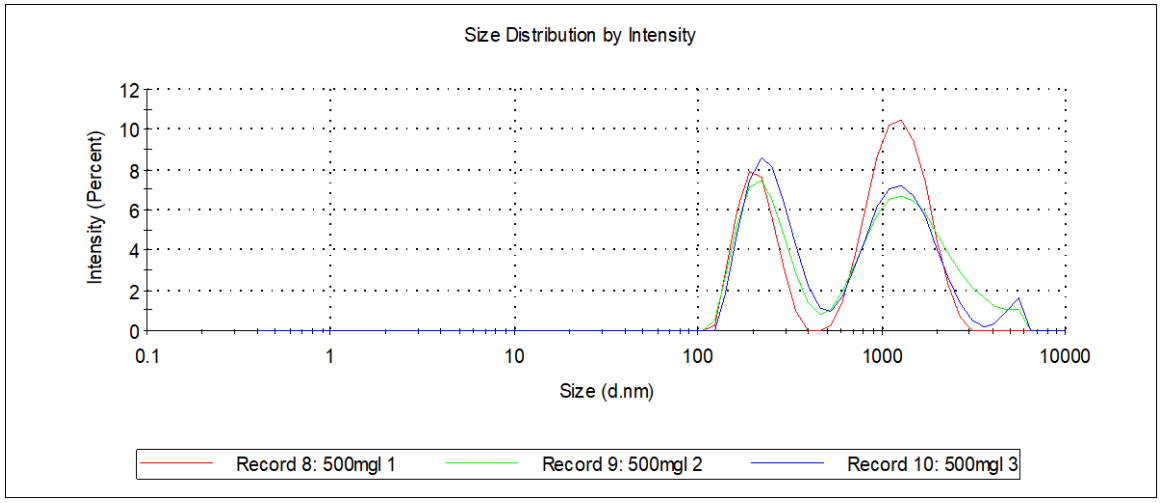

Figure 45: Oil particle size distribution of 500mg/l O/W emulsion.

4.2 Metal Oxides for Ceramic Membrane Modification

Three metal chlorides ($MgCl_2$, $MnCl_2$ and $CrCl_3$) were used to form a solution with absolute alcohol separately for the modification of Al_2O_3 microfiltration ceramic membrane witness sample using dip coating. The aim was to synthesize a more hydrophilic membrane compared to the fresh support Al_2O_3 ceramic membrane suitable for the separation of O/W emulsion below 500mg/L with droplet sizes <10 µm. These modified now MgO, MnO_2 and CrO_2 coated Al_2O_3 ceramic membrane witness samples (Figure 46) were examined for best hydrophilicity for contact angle measurements using One Attension Theta Lite Optical Tensiometer. The solvents used for testing these modified witness samples were deionized water and soybean oil (pure). The hydrophilicity (contact angle testing) was performed on both modified and unmodified Al_2O_3 ceramic membrane witness samples.

Figure 46: From left to right – MnO, CrO2, and MgO modified ceramic membrane witness samples.

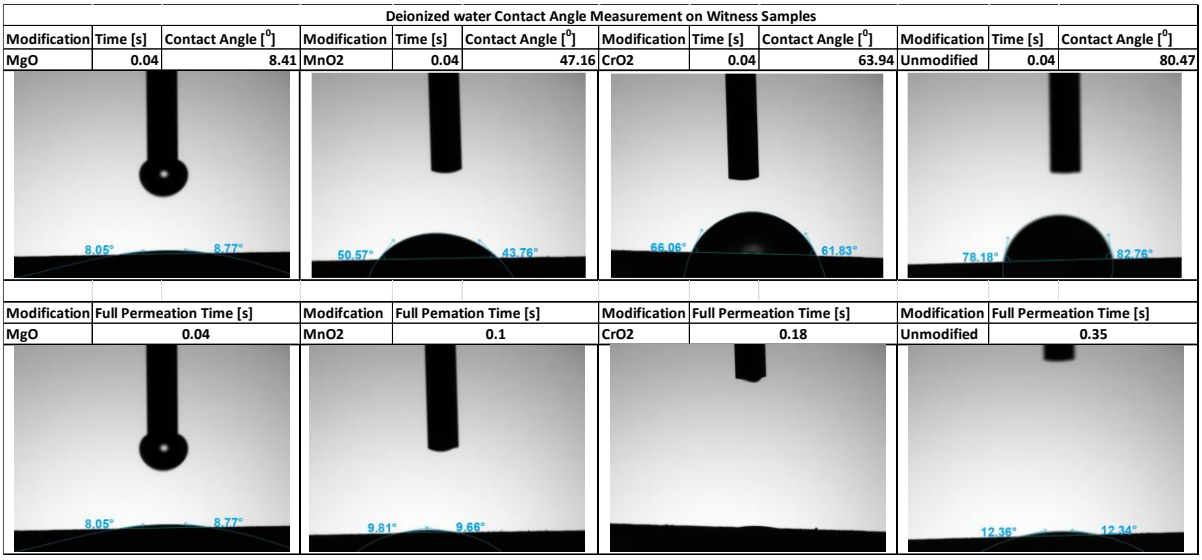

Figure 47: Water droplet Contact angle of MgO, MnO2, CrO2 modified and Unmodified Al2O3 fresh support Ceramic membrane witness samples.

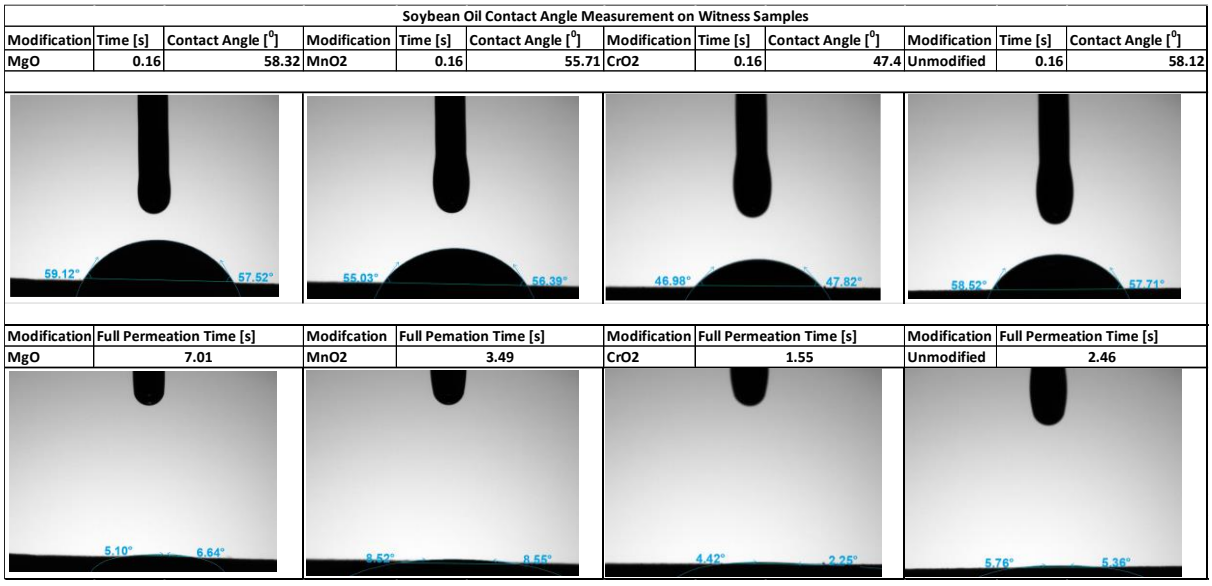

Figure 48: Oil droplet Contact angle of MgO, MnO2, CrO2 modified and unmodified Al2O3 fresh support Ceramic membrane witness samples.

Figure 47 shows the shape of the water droplet Contact angle of MgO, MnO_2, CrO_2 modified and Al_2O_3 unmodified fresh support ceramic membrane witness samples. As is evident the most hydrophilic modified ceramic membrane witness sample is the MgO with mean contact angle of 8.41 [^{0}] compared to the Al_2O_3 unmodified fresh support ceramic membrane with contact angle of 80.47 [^{0}] at the same water droplet time of 0.04s droplet size of 5 µL. This was quickly noticed from Figure 47 because it the less semi-circle shape of MgO-modified ceramic membrane contact angle on the solid surface, indicating dispersiveness of the droplet which invariably means hydrophilicity. The hydrophilicity of MgO-

modified ceramic membrane is also evident in the comparison with contact angles of modified MnO and CrO_2 modified ceramic membranes whose mean contact angles are 47.16 and 63.94 [^{0}] respectively all at the same water droplet size and time of 0.04 s. The hydrophilicity hierarchy of the metal oxides modified ceramic membrane is from higher to lower in this order of MgO>MnO>CrO_2.

The greater hydrophilicity is found in MgO which gives a rougher surface compared to other MnO and CrO_2 ceramic membrane surface modification as seen in Figure 47. (Chang et al. 2010a) in the study of Al_2O_3 surface membrane modification implied that an increase in membrane surface roughness decreases contact angle which indicates an increase in hydrophilicity of the membrane. In that case, surface modification of MgO ceramic membrane witness sample (Figure 47) shows more roughness in comparison with surface modification of MnO and CrO_2 ceramic membrane witness samples. This roughness on MgO might arises from it been a naturally occurrent solid mineral characteristic. This might be the reason for the decrease in contact angle measurement of MgO.

Another possibility might be the molecular weight of the metal oxides modified on the surface of the ceramic membrane witness samples. CrO_2 has a molecular weight of 83.9949 g/mol, MnO with a molecular weight of 70.9374 g/mol while MgO has a molecular weight of 40.3044 g/mol. Hence the descend in contact angle measurement like so 63.94>47.16>8.41 [^{0}] which implies that CrO_2>MnO>MgO, respectively. A major factor to elucidate the hydrophilic nature of the MgO modified ceramic membrane witness sample is the permeation duration of water droplet through the membrane. From Figure 47 full permeation time for MgO is 0.04 s as against 0.1 s and 0.18 s for MnO and CrO_2 witness samples, respectively. The modification of fresh support ceramic membrane with metal oxides improves the wettability of the membrane surface thereby increasing hydrophilicity as reflected in the study of ((Zhou, Jian-er et al. 2010) with Zirconia Oxide (ZrO_2) and (Chang et al. 2010a) with Hydrous Aluminium Oxide (HAO).

To confirm the hydrophilicity of the modified MgO, MnO, CrO_2 ceramic membrane and Al_2O_3 unmodified ceramic membrane, deionized water was replaced with soybean oil for contact angle measurement on these witness samples using the same One attension Theta Lite Optical Tensiometer. Figure 48

depicts the Oil droplet Contact angle of MgO, MnO_2, CrO_2 modified and unmodified Al_2O_3 fresh support Ceramic membrane witness samples. As can be seen from the picture, MgO had the highest mean contact angle measurement of 58.32 [^{0}] for oleophobicity which invariably means it is more hydrophilic, compared to MnO and CrO_2 which had lower mean contact angle measurements of 55.71 and 47.4 [^{0}] for oleophobicity. The oil droplet size and oil droplet time for oleophobic measurement on MgO, MnO and CrO_2 were all the same at 5 µL and 0.16 s respectively. The oleophobic hierarchy from highest to lowest is like so MgO>MnO>CrO_2.

Another fact to mention is the duration it takes for the oil to fully permeate the modified ceramic membranes. In this case, the longer the time, the higher the oleophobic molecule. From Figure 48, MgO had the longest permeation time of 7.01 s for soybean oil to permeate the modified ceramic membrane witness sample, hence, the most oleophobic molecule compared to MnO and CrO_2 with permeation time as 3.49 and 1.55 s, respectively. This further study confirms the hydrophilicity of MgO-modified ceramic membrane witness sample, hence, was used in the modification of the whole ceramic membrane for separation of lower concentrations of O/W emulsion.

4.3 Characterization

This sub sections reports and discuss the results from characterization analysis of modified and unmodified ceramic membrane. These results were gotten from the contact angle measurement, porosity testing, morphology analysis, and size determination of both modified and unmodified ceramic membrane.

4.3.1 Contact Angle Measurement

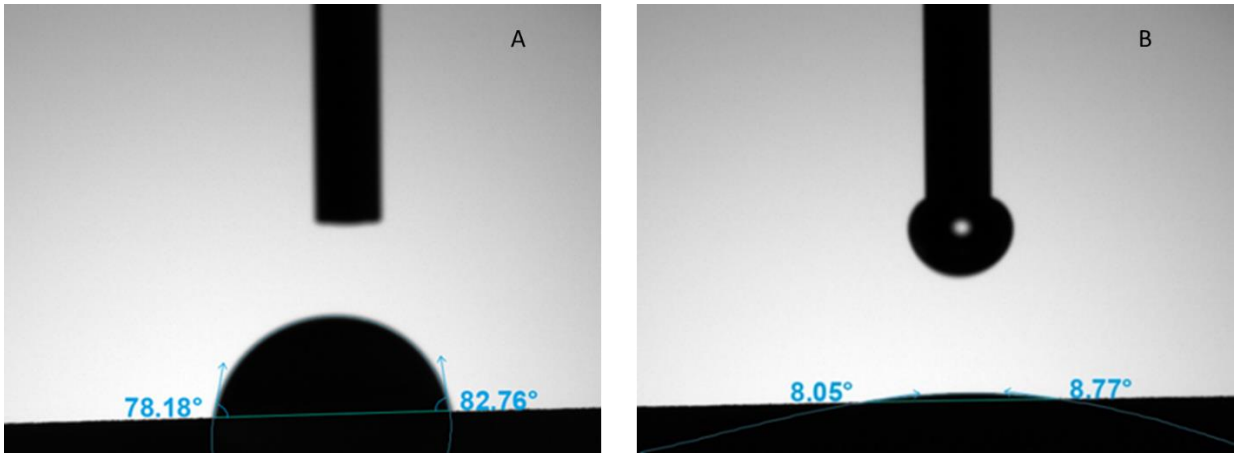

Figure 49: Contact angle of unmodified (A) and modified (B) ceramic membrane.

The degree of wetting of a surface is characterized by the contact angle. A perfectly wet surface is represented by 0° contact angle measurement while a perfectly non wetting surface is denoted by 180° contact angle. A water droplet will quickly spread out on the surface of a hydrophilic material give a contact angle of zero or something close to zero. On the contrary, there will be less spreading of water droplet observed with a hydrophobic surface. For water droplets a 90° contact angle is observed for solid surfaces less hydrophilic. In literature, contact angles below 90° has been reported as hydrophilic surfaces (Chinnam et al. 2015). The use of contact angle measurement has been reported by different researchers used for measuring activities in different industrial sectors in areas such as oil recovery, liquid coating, boiling and condensation, lubrication, and spray quenching. From the contact angle measurement in this study, modified MgO ceramic membrane gave an average of 8° as presented in Figure 49 which has a massive difference in reduction compared to that of the unmodified Al_2O_3 ceramic membrane with an average contact angle measurement of 80°. Based on this factor, the hydrophilic modified

MgO ceramic membrane helps in the repellent of oil molecules from being absorbed onto the surface of the membrane hence increase % rejection of oil helping the separation efficiency of the membrane. This result is like that observed and reported by (Suresh and Pugazhenthi 2017) who modified ceramic membrane with TiO_2 molecules and compared the modified membrane with that of ceramic membrane support. The result gave a modified ceramic membrane contact angle of 14.57° compared to that of the ceramic membrane support of 77.07°. This result was also like the result gotten and reported during the pilot study of this research where just the contact angle of an initial unmodified 6000nm ceramic membrane was measured and gave a measurement of 68° (Aisueni et al. 2022).

4.3.2 Porosity

Equation 3 in sub section 3.6.3 also written below was used to calculate the porosity of MgO-modified and Al_2O_3 unmodified ceramic membrane. Where, $W_w$and W_d represents the wet and dry weight of the membranes, respectively. d_w and V represents the density of water and the volume of the membranes, respectively.

For the unmodified Al_2O_3 tubular ceramic membrane the calculation of ε is as follows:

$$\varepsilon\ (\%) = \left(\frac{W_w - W_d}{d_w \times V}\right) \times 100$$

$$\varepsilon\ (\%) = \frac{309.1 - 269.0}{1 \times 140} \times 100$$

$$\varepsilon\ (\%) = \frac{40.1}{140} \times 100$$

$$\varepsilon\ (\%) = 0.29 \times 100$$

$$\varepsilon\ (\%) = 29$$

For the MgO modified tubular ceramic membrane the calculation of ε is as follows:

$$\varepsilon\ (\%) = \left(\frac{W_w - W_d}{d_w \times V}\right) \times 100$$

$$\varepsilon\ (\%) = \frac{315.7 - 274.1}{1\ \times 146} \times 100$$

$$\varepsilon\ (\%) = \frac{41.6}{146} \times 100$$

$$\varepsilon\ (\%) = 0.28\ \times 100$$

$$\varepsilon\ (\%) = 28$$

As is seen in Figure 50 and in the porosity calculations above, the MgO modified tubular ceramic membrane is less porous with a porosity average of 28.1% ±0.1 (SE) compared to the unmodified Al_2O_3 support tubular ceramic membrane with a porosity average of 29.2% ±0.2 (SE). This might be due to the nano molecules of MgO coating or dispersed on the surface or in the pores of the support membrane thereby, narrowing the pores and decreasing the porosity. These results of porosity are also like the outcome reported by (Suresh and Pugazhenthi 2017) in the study of metal ion coating of different concentrations of TiO_2 on support membranes. There was also a decrease in the coated membrane compared to the support membrane.

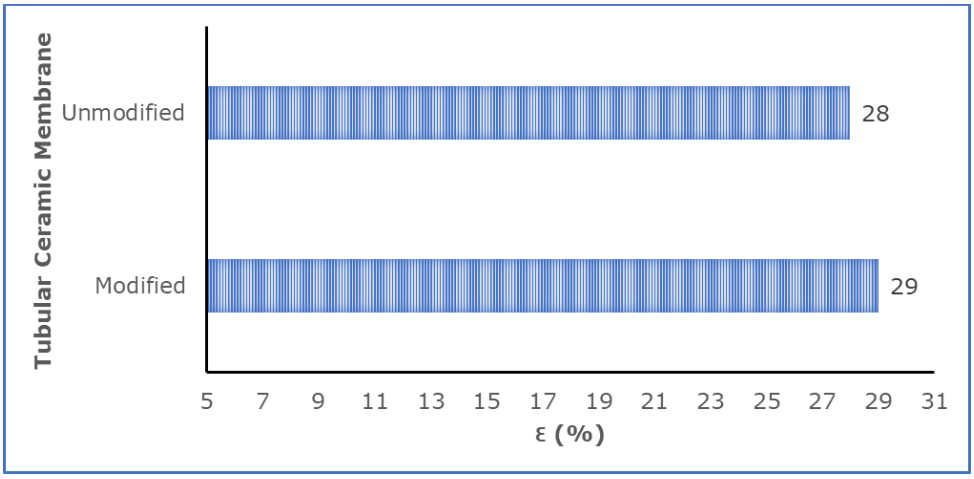

Figure 50: Porosity of Modified and unmodified Tubular Ceramic Membrane.

4.3.3 SEM/EDXA

Figure 51 to Figure 54 shows the SEM images of Unmodified Al_2O_3 and MgO-modified tubular ceramic membranes with both variable pressure and back scatter detector measurements 20000X magnifications. The EDXA spectrum to confirm the SEM results are also represented in Figures 55 to 58. The surface morphologies of Al_2O_3 unmodified and MgO-modified ceramic membranes have major similarities and fewer differences as can be seen from the images. The similarities are noticed in their asymmetric structures where microporous, mesoporous, and microporous structures seen in both Al_2O_3 unmodified and MgO-modified images. However, there is an increase in nano-sized structures present on the MgO-modified ceramic membrane which was not noticed in the unmodified membrane as seen in Figures 51 and 52. The MgO nano-sized deposition does not appear as clusters on the surface of the membrane but looks dispersed all over the surface.

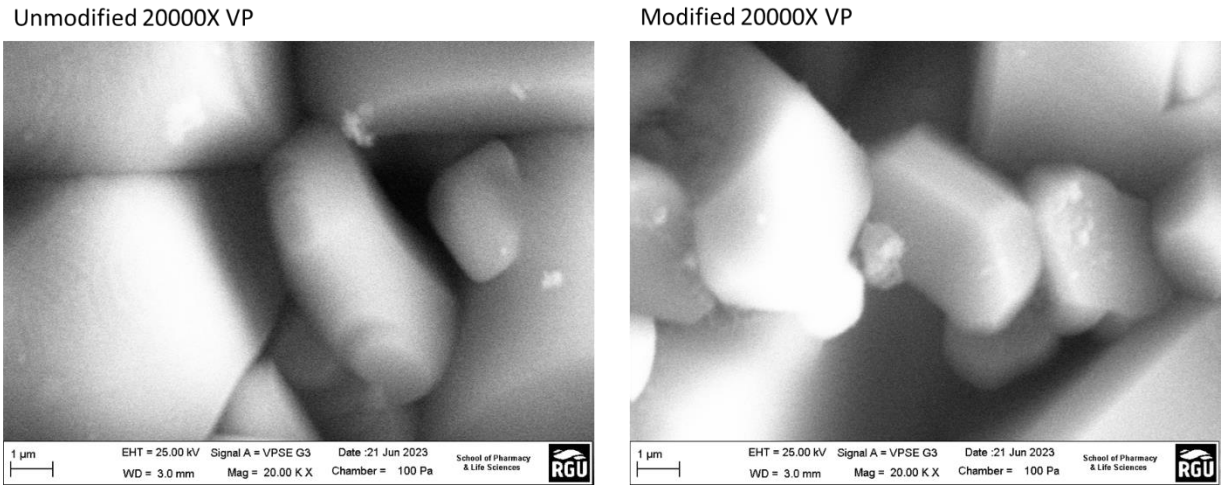

Figure 51: SEM images of Unmodified Al2O3 and Modified MgO Ceramic Membranes with Variable Pressure detector 1000X.

Unmodified 20000X BSD

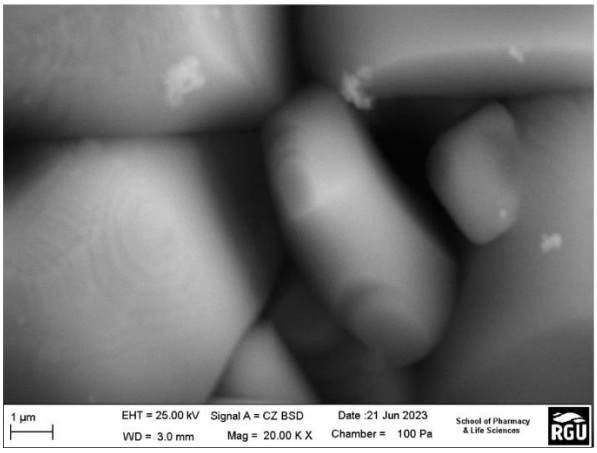

Modified 20000X BSD

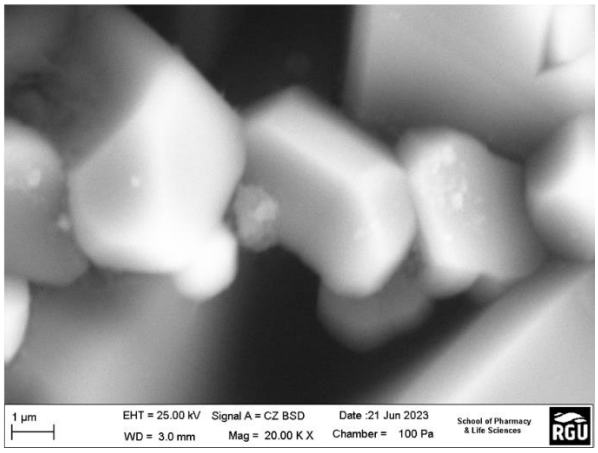

Figure 52: SEM images of Unmodified Al2O3 and Modified MgO Ceramic Membranes with Back Scatter detector 1000X.

Unmodified 20000X VP

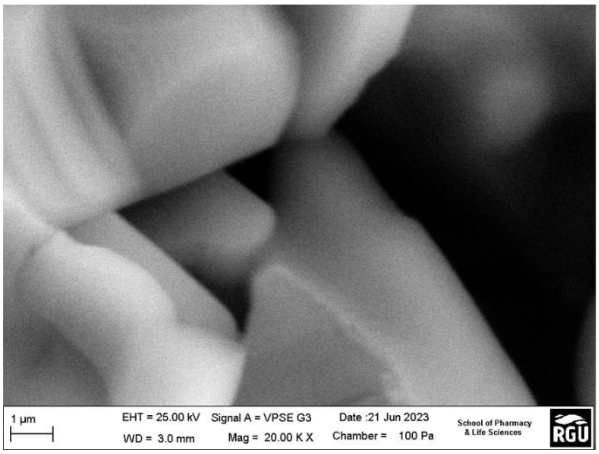

Modified 20000X VP

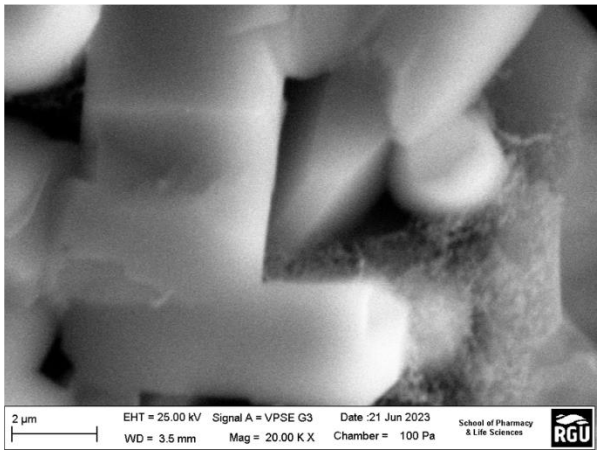

Figure 53: SEM images of Unmodified Al2O3 and Modified MgO Ceramic Membranes with Variable pressure detector 500X.

Unmodified 20000X BSD

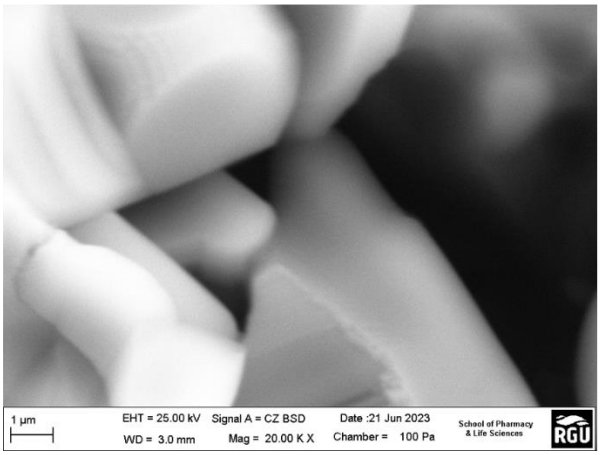

Modified 20000X BSD

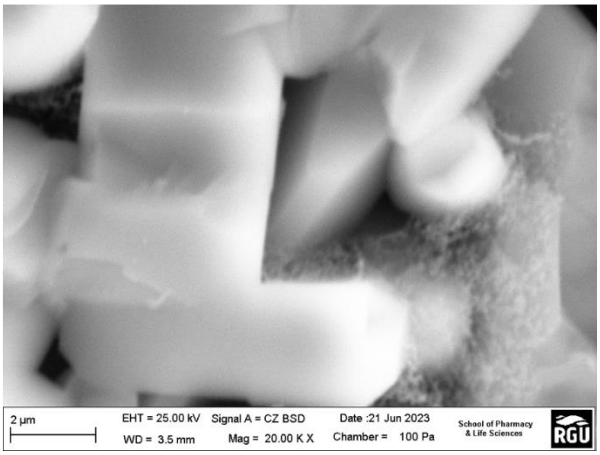

Figure 54: SEM images of Unmodified Al2O3 and Modified MgO Ceramic Membranes with Back Scatter detector 500X.

Figures 53 and 54 represents the SEM for both Al_2O_3 unmodified and MgO-modified ceramic membrane with variable pressure and backscatter detector, respectively. From these images, it is observed that the MgO-modified ceramic membrane shows more dense nano particles in the pores of the membrane. This is an indication that the MgO particles dispersed onto the surface of the pores of the ceramic membrane. This MgO nanoparticle structures are not observes in the cross section of the Al_2O_3 unmodified ceramic membrane. The dispersion of the MgO nanoparticles on the surface and in between the pores of the ceramic membrane is very ideal to further increase hydrophilicity of the membrane. It is noticed from the SEM images that the concentration of the MgO particles does give a roughness proportionality to the existing ceramic membrane particles. This roughness of the membrane has been reported ((Zhang, Dawei et al. 2018; Liu, R. et al. 2018; Chang et al. 2010b) to increase flux and %oil rejection is O/W emulsion separation.

Figure 55 to 58 is a representation of the surface and cross sections EDXA analysis on Al_2O_3 unmodified and MgO-modified ceramic membrane to confirm the elemental presence of MgO after modification on tubular ceramic membrane. The first unlabelled peak in the EDXA spectra is termed triggered noise peak, which usually appears in all EDXA spectrum. As is visualized in Figure 55 (the surface of the Al_2O_3 unmodified ceramic membrane), there is the presence of Aluminium (Al) and Oxygen (O) elements which forms the basis of the unmodified ceramic membrane. Other elements like Titanium (Ti), Vanandium (V), Zirconium (Zr) and Cabon (C) are sometime used to fabricate the membrane or arise from other interference during membrane production processes. Figure 56 (the surface of the MgO-modified ceramic membrane) illustrates the presence of Magnesium (Mg) in addition to the existing elements present on the Al_2O_3 unmodified ceramic membrane. This indicates that the modification process impregnating MgO into the surface and pores of Al_2O_3 unmodified ceramic membrane was a success. Figure 57 represents the cross section of Al_2O_3 unmodified ceramic membrane. This spectrum shows Aluminium and Oxygen elements as well as other elements found in the surface of the Al_2O_3 unmodified ceramic membrane in Figure 55. Figure 58 is a representation of the cross section of MgO-modified ceramic membrane. This similarly displays the minute presence of Magnesium (Mg) as seen in Figure 56 which is expected to

be a shorter peak as it is in nano size compared to other micro and microporous materials present in the membrane. This is an indication that the modification with MgO particles dispersed into the pores of the ceramic membrane.

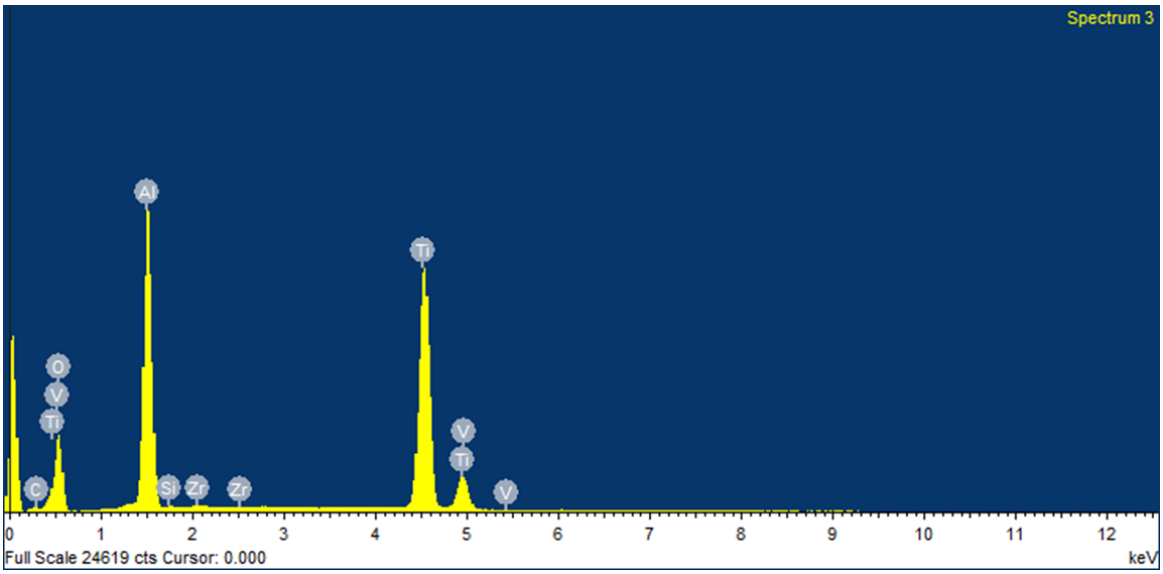

Figure 55: Surface of EDAX images for Al_2O_3 unmodified tubular ceramic membrane

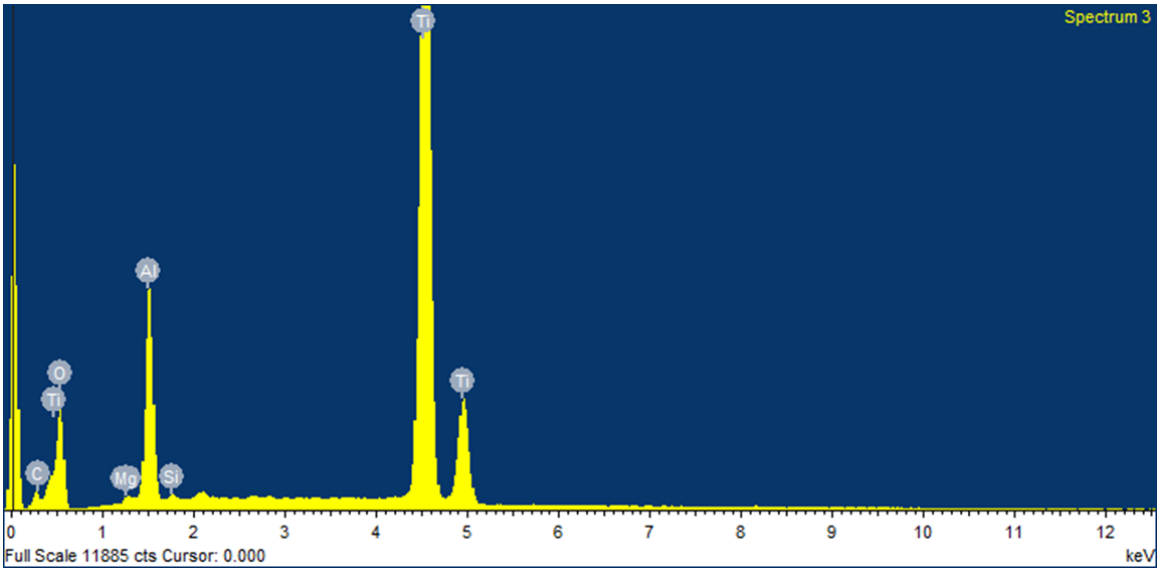

Figure 56: Surface of EDAX spectrum for MgO-modified tubular ceramic membrane.

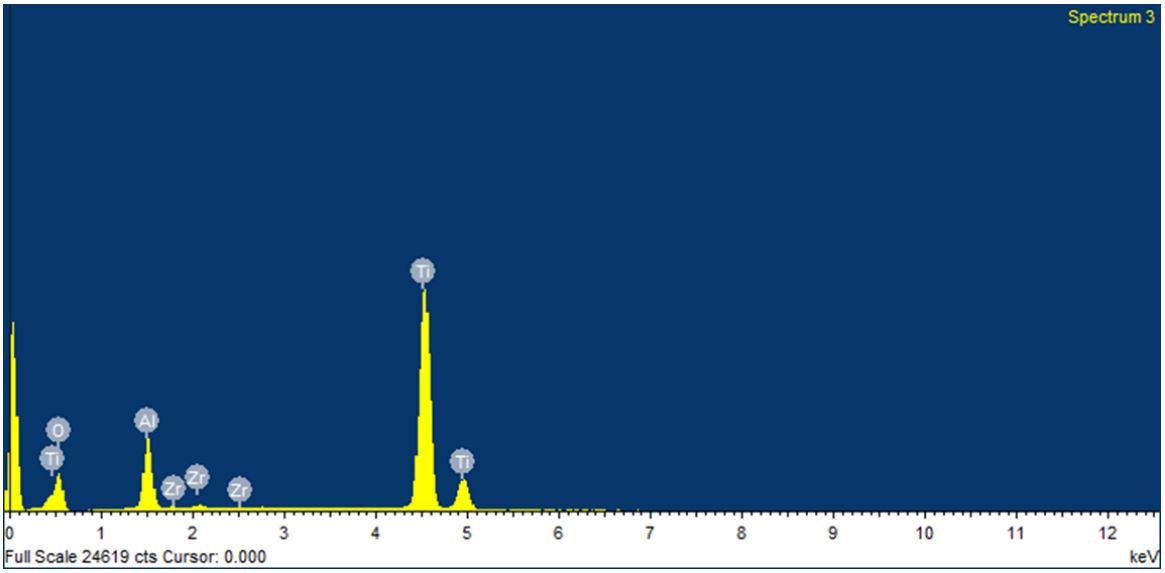

Figure 57: Cross section of EDAX images for Al_2O_3 unmodified tubular ceramic membrane

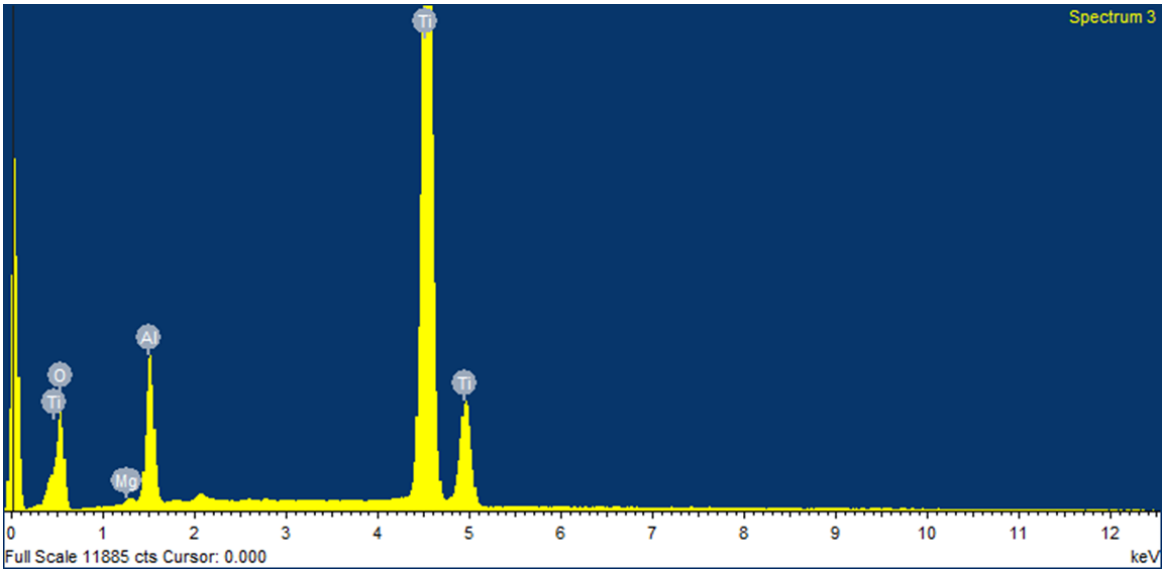

Figure 58: Cross section of EDAX spectrum for MgO-modified tubular ceramic membrane

4.3.4 BET Liquid Nitrogen Analysis

The liquid nitrogen adsorption and desorption isotherms for the unmodified and modified MgO ceramic membranes were used to determine the pore size analysis carried out at -15^{0}C (-77K) temperature. Figure 59 represents the physisorption isotherm of the unmodified ceramic membranes. In the linear isotherm of the physisorption, absorbed volumes are plotted against pressure (P/Po) where P signifies the applied pressure and Po represents the saturated pressure. The Barrett, Emmett, and Teller (BET) has been used to generate t-plot from the physisorption linear isotherms used for the calculation of surface areas of unmodified and modified ceramic membranes. The generation of pore size distribution, diameter and volume were calculated with the Barrett, Joyner and Halenda (BJH) model in both unmodified and modified ceramic membranes.

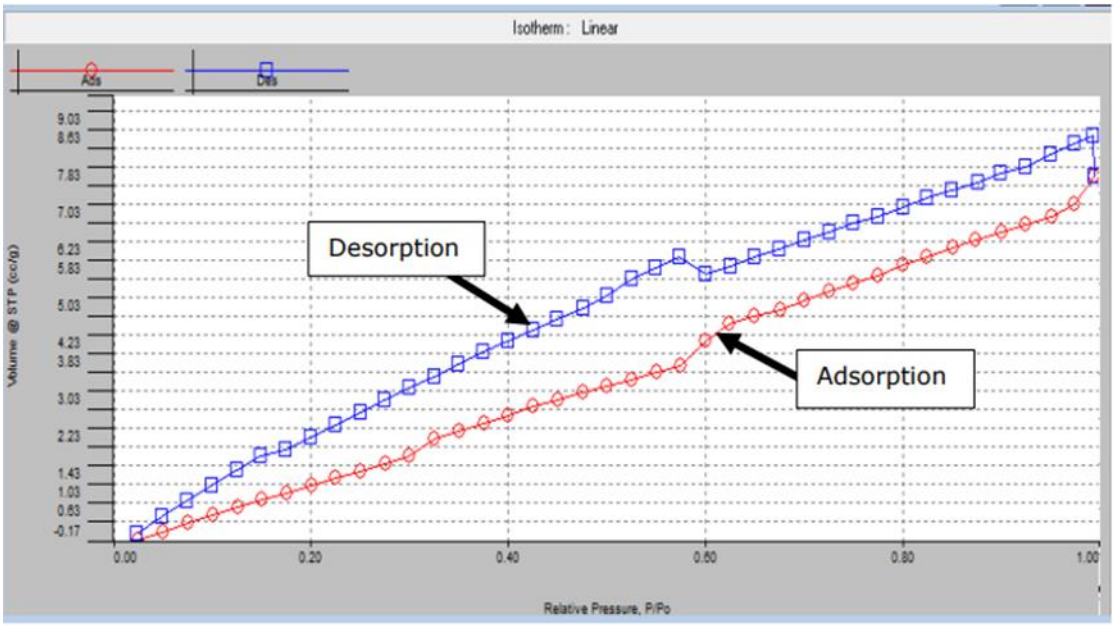

Figure 59: Physisorption isotherm of unmodified ceramic membrane.

Figure 60 displays the t-plot of Al_2O_3 unmodified ceramic membrane, while table 6 shows the BJH results from the pore diameter and volume; the graphical representation of the Al_2O_3 unmodified ceramic membrane result is displayed in Figure 61. The results characterizing the porosity of Al_2O_3 unmodified and MgO-modified ceramic membrane, i.e., the specific pore size, volume and diameter are illustrated in Table 7.

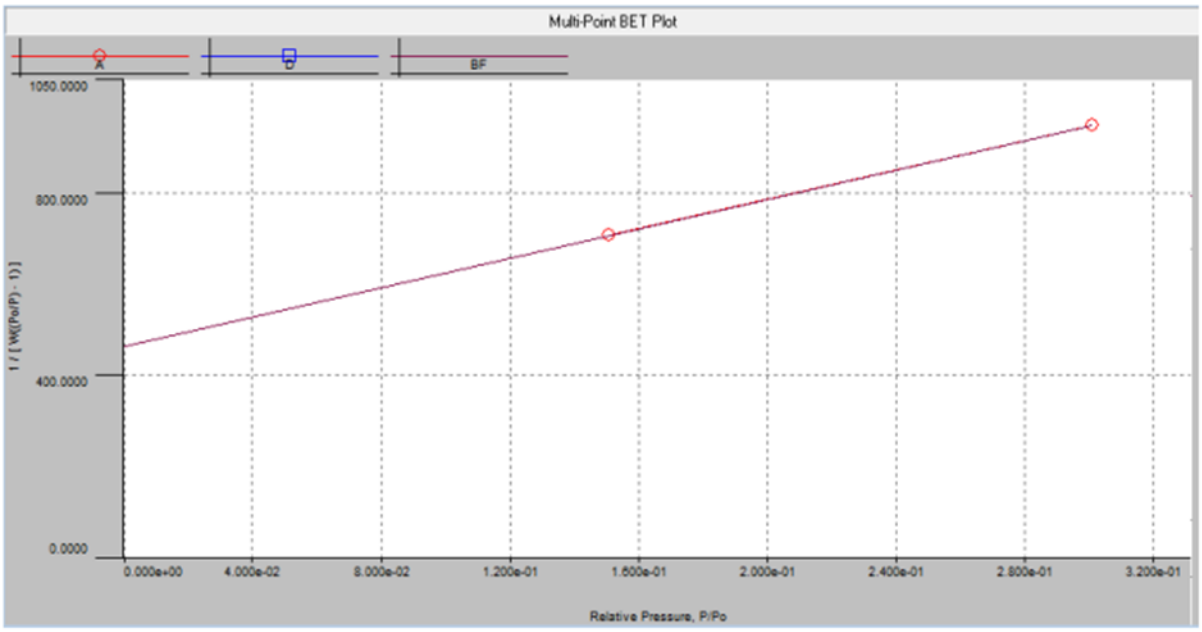

Figure 60: T-plot for unmodified ceramic membrane.

Table 6: Recipes obtained from the BJH method in unmodified ceramic membrane.

Sample Weight:	0.1 g	**Instrument:**	Autosorb iQ Station 1		
Outgas Time:	0.0 hrs	**Outgas Temp.:**	0 °C		
Analysis gas:	Nitrogen	**Non-ideality:**	6.58e-05 1/Torr	**CellType:**	9mm w/o rod
Analysis Time:	5:03 hr:min	**Bath temp.:**	77.35 K		
Analysis Mode:	Standard			**VoidVol Remeasure:**	off
VoidVol. Mode:	He Measure	**Cold Zone V:**	8.60405 cc	**Warm Zone V:**	14.1088 cc
		Data Reduction Parameters			
	Thermal Transpiration: on	**Eff. mol. diameter (D):**	3.54 Å	**Eff. cell stem diam. (d):**	4.0000 mm
t-Method	**Calc. method:** de Boer				
BJH/DH method	**Moving pt. avg.:** off	**Ignoring P-tags below 0.35 P/Po**			
Adsorbate	**Nitrogen**	**Temperature**	77.350K		
	Molec. Wt.: 28.013	**Cross Section:**	16.200 Å²	**Liquid Density:**	0.806 g/cc
		BJH desorption summary			
		Surface Area =	8.243 m²/g		
		Pore Volume =	0.012 cc/g		
		Pore Diameter Dv(d) =	4.176 nm		

From the Liquid nitrogen adsorption and desorption analysis, the results from the MgO-modified ceramic membrane indicate a high specific surface area in comparison with that of the unmodified ceramic membrane. This attribute of increased surface area gives room increased water absorption tendences that can improve permeate flux volume in the pore structure of MgO-modified ceramic membrane which is advantageous. This high specific surface area in modified ceramic membrane can be attributed to the nano-sized modification of MgO on the membrane's surface.

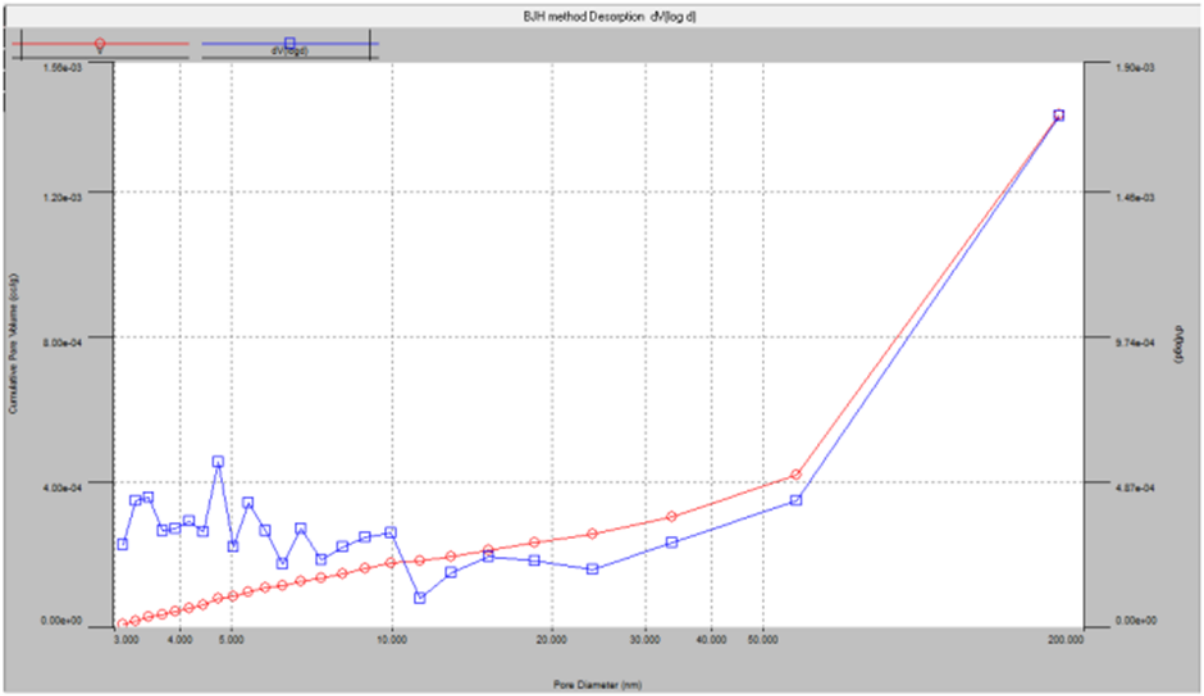

Figure 61: BJH graph displaying the pore size distribution and pore diameter for unmodified ceramic membrane.

Table 7: Results showing parameters obtained from unmodified and MgO modified ceramic membrane.

Parameters	*Al_2O_3 Unmodified ceramic membrane*	*MgO Modified ceramic membrane*
Specific surface area S_{BET}, m^2/g	1.676	10.680
Pore Volume Vp, cc/g	0.012	0.009
Pore diameter NJH, nm	4.176	3.139

In the analysis of pore diameter using BJH, there was an observed reduction in pore diameters of MgO-modified ceramic membrane in comparison to unmodified ceramic membrane. This arises from the modification of the ceramic membrane with MgO reducing the pore diameter as noted in the SEM results from morphology analysis. This reduction in pore diameters can cause a reduction in porosity of permeated flux volume.

4.4 Crossflow filtration

This sub section focuses on report and discussion of the results generated from the crossflow filtration analysis, considering the various parameters which includes pure water flux, O/W emulsion Flux based on flow rate, O/W emulsion flux based on temperature and finally flux recovery ratio for both modified and unmodified ceramic membrane.

4.4.1 Pure water Flux

Deionized water was run through separation rig to determine the flux for both Al_2O_3 unmodified and MgO-modified ceramic membrane housed in the rig alternatively. This was aimed at using the PWF result as a reference for O/W emulsion fluxes and as a measure for flux recovery ratio. The PWF analysis was carried out for both fluxes based on flowrate and temperature. Figure 62 represents the chart from the data (Appendix IV) of PWF based on flowrate for Al_2O_3 unmodified and MgO-modified ceramic membrane. It is evident from the chart that an increase in flowrate or pressure increases PWF linearly and this is because of driving force enhancement with an increase in pressure. The PWF did not decline with respect to time (30 minutes duration), and this was noticed in both MgO-modified and Al_2O_3 unmodified ceramic membrane.

Physical properties of the ceramic membrane which includes porosity, pore size and hydrophilicity of membrane surface (Kang et al. 2019) to the variations noticed in PWF between the MgO-modified and Al_2O_3 unmodified ceramic membrane. The PWF (7.78 $L/m^2.H$) from MgO-modified ceramic membrane is slightly more than PWF in Al_2O_3 unmodified ceramic membrane (7.68 $L/m^2.H$). This is noticed and similarly observed in both 25 L/H and 50 L/H flowrates. This might be due to the surface modification of MgO-modified ceramic membrane from less hydrophilic to more hydrophilic as measured by the contact angle (changing hydrophilicity Al_2O_3 unmodified ceramic membrane from 80.47^0 to MgO-modified ceramic membrane of 8.41^0). Other studies have reported such similarity results in PWF increase with respect to membrane surface modification (Suresh and Pugazhenthi 2017). The PWF from the higher flowrate (50 L/H) also gave comparable results of MgO-modified ceramic membrane flux (15.18 $L/m^2.H$) being higher than the Al_2O_3 unmodified ceramic membrane flux of 14.35 $L/m^2.H$.

In the work of ((Chang et al. 2014c) the modified nano-TiO_2 ceramic membrane revealed more PWF (400 L/m^2.H) than that of unmodified ceramic membrane (280 L/m^2.H). It is apparent that the modification of MgO nanoparticles on the fresh Al_2O_3 unmodified ceramic membrane does not reduce the flow of PWF however, an increase in surface hydrophilic character of the ceramic membrane is influential in getting higher PWF. This characteristic hydrophilic nature is the major contributing factor to an increase in PWF over that of Al_2O_3 unmodified ceramic membrane.

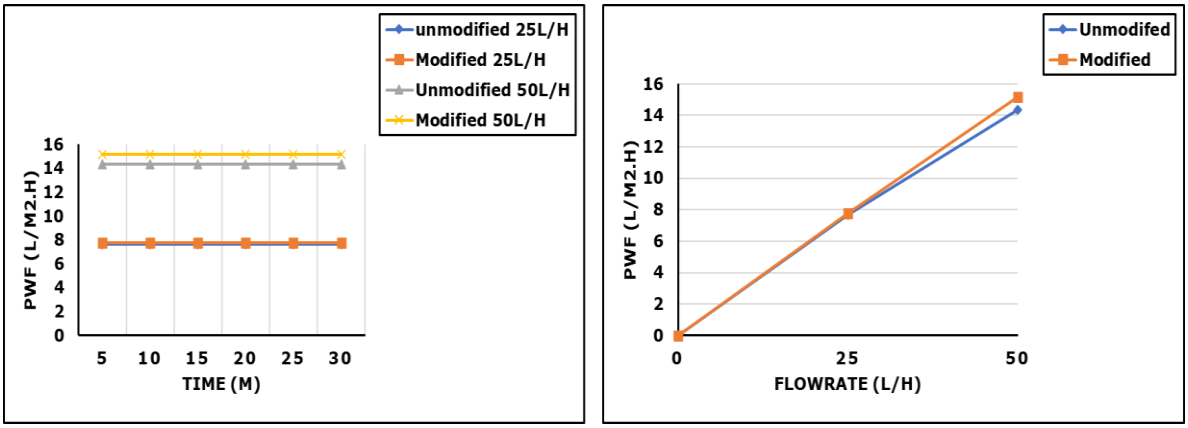

Figure 62: Chart of PWF based on flowrate from unmodified and modified tubular ceramic membrane.

Figure 63 represents the chart for illustrating temperature effect on PWF for MgO-modified and Al_2O_3 unmodified ceramic membranes with similar flowrates of 25 and 50 L/H. Two temperatures (20 and 50^{0}C) were used for the measurement of PWF. It is demonstrated from the chart below that an increase in temperature increases PWF as seen in the higher PWF differences from 7.67 to 7.77 L/m^2.H of Al_2O_3 unmodified ceramic membrane with an increase in temperature from 20-50^{0}C at 25 L/H flowrate. A similar increase of PWF from 14.45 to 15.55 L/m^2.H is also represented when there was a temperature increase from 20^o to 50^{o}C in the Al_2O_3 unmodified ceramic membrane with an increase in flowrate to 50 L/H. This is attributed to water molecular excitement from heat energy that causes water molecules to move more rapidly and results in an increase in water volume (Arya et al. 2018).

This is not the case for MgO-modified ceramic membrane. Temperature increase made no significant difference seeing that the PWF at 20^{0}C was already high at 7.776 L/m^2.H and an increase in temperature to 50^{0}C only made the PWF rise to 7.778 L/m2.H at 25 L/H flowrate. An increase in flowrate to 50 L/H, MgO-

modified PWF rose significantly from 15.45 to 16.35 L/m^2.H when temperature increased from 20° to 50°C which is unlike the lower flowrate (25 L/H) result. This might be due to two factors working simultaneously – higher flowrate and hydrophilicity in the MgO-modified ceramic membrane.

In summary, an increase in temperature from 20° to 50°C at 25 L/H flowrate, PWF rose significantly in only Al_2O_3 unmodified ceramic membrane but not in MgO-modified ceramic membrane, though there was still a slight unsignificantly rise. However, an increase in temperature from 20° to 50°C at 50 L/H flowrate, there was a significant rise in both Al_2O_3 unmodified and MgO-modified ceramic membrane. At this same 50 L/H flowrate, it is worth mentioning that MgO-modified ceramic membrane display an even higher PWF at both 20° and 50°C compared to Al_2O_3 unmodified ceramic membrane. This can be explained that Al_2O_3 unmodified ceramic mebrane only had the factor of increase in temperature, while MgO-modified ceramic membrane has two factors of temperature increase and hydrophilicity given its advantage of higher PWF. This is similar to the result reported in literature by (Milić et al. 2014) in the study of of ultratfiltration of O/W emulsion by uisng ceramic membrane. The report concluded that temperature difference increases PWF and even O/W emulsion flux though temperature as a parameter was evaluated as a statistical insignificant process compared to other parameters like trans membrane pressure, O/W emulsion concentrations and pH.

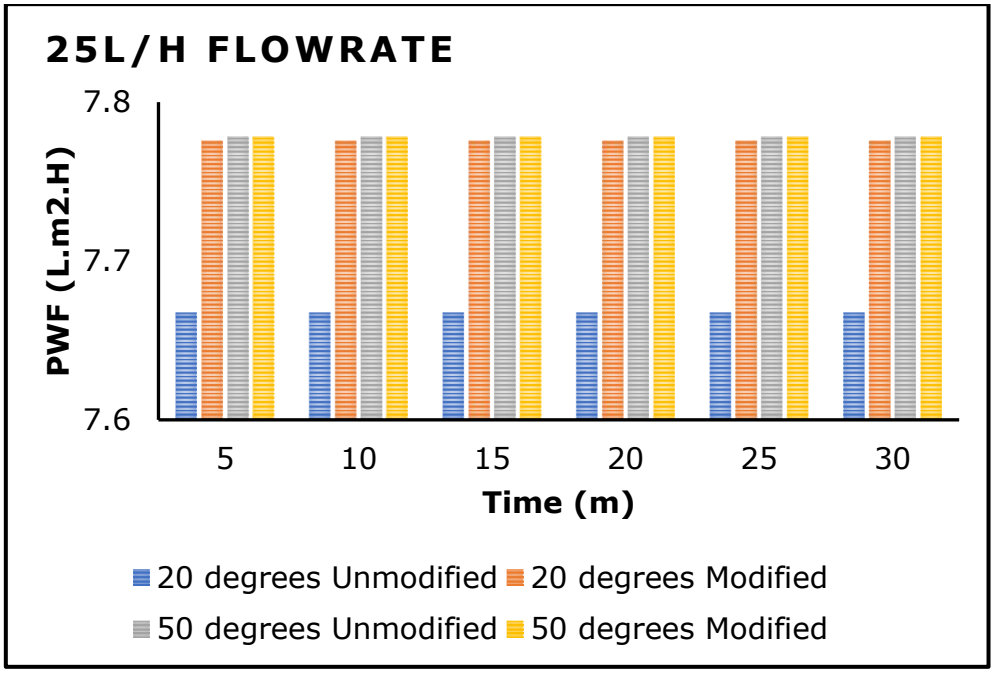

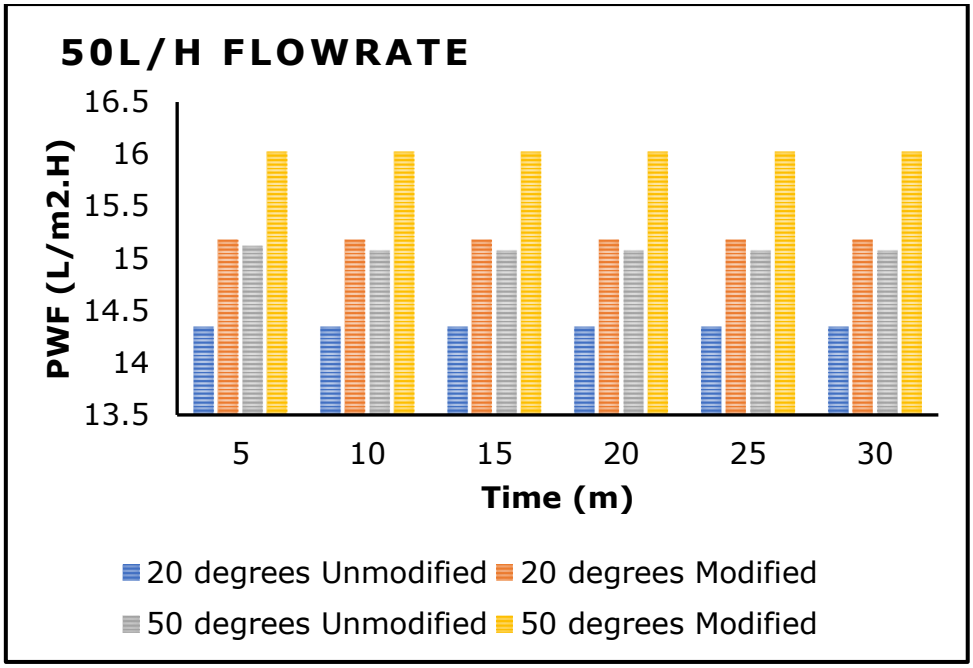

Figure 63: Chart for illustrating temperature effect on PWF for modified and unmodified ceramic membrane.

4.4.2 O/W emulsion Flux based on Flowrate

O/W emulsions with three different concentrations (100, 250 and 500 mg/l) was prepared used for the crossflow nanofiltration analysis. It is observed from Figures 43 to 45 that the droplet size of O/W emulsion falls with the ranges of 40-600 nm, 90-1100 nm, and 100-6000 nm for 100, 250 and 500 mg/l respectively. The average droplet size for the three concentrations were 629.2 nm, 813.3 nm, and 1461.7 nm; with viscosity of 0.8271, 0.8523, 0.8872, for 100 mg/l, 250 mg/l, and 500 mg/l, respectively. The separation efficiency of Al_2O_3 unmodified and MgO-modified tubular ceramic membranes was examined with the three different O/W emulsion at three concentrations at applied flowrates of 25 L/H and 50 L/H.

The variations of the permeate flux of Al_2O_3 unmodified and MgO-modified ceramic membrane over a 30-minute duration for the three concentrations and applied flowrates (20 L/H and 50 L/H) are displayed in Figure 64 and Figure 66, respectively. From Figure 64, the Al_2O_3 unmodified ceramic membrane maintained a steady permeate flux without decline throughout the 30-minute cross filtration duration at 25 L/H flowrate. This was observed and gave related results with respect to the three distinct O/W emulsion concentrations. The same steady flux throughout the 30-minute duration for all three O/W emulsion

concentrations was observed when the flowrate was increased to 50 L/H in Al_2O_3 unmodified ceramic membrane.

However, an observation at the flowrate difference in the charts revealed that with an increase in flowrate from 25 to 50 L/H comes an increase in permeate flux in Al_2O_3 unmodified ceramic membrane. This was the same when observed for all three O/W emulsion concentrations in both flowrates of 25 and 50 L/H as seen in Figure 65. The highest flowrates in Al_2O_3 unmodified ceramic membrane occurring in 100 mg/l O/W emulsion cross-filtration gave a permeate flux of 7.71 $L/m^2.H$ in 25 L/H flowrate and 15.24 $L/m^2.H$ in 50 L/H flowrate. The transport resistance which usually occurs because of concentration polarization and adsorption leading to permeate flux decline was not noticed over the 30 minutes period during cross filtration in Al_2O_3 unmodified ceramic membrane. This might be due to an earlier 30-minute cross filtration run across the unmodified ceramic membrane prior to measurement to allow for data stabilization. The lack of transport resistance and concentration polarization might also be due the bigger pore size of the Al_2O_3 ceramic membrane compared to the O/W emulsion concentration droplet sizes which is smaller with the highest being 6000 nm that is less frequent. Might also easily pass through the Al_2O_3 membrane without hindering permeate flux or causing any fouling.

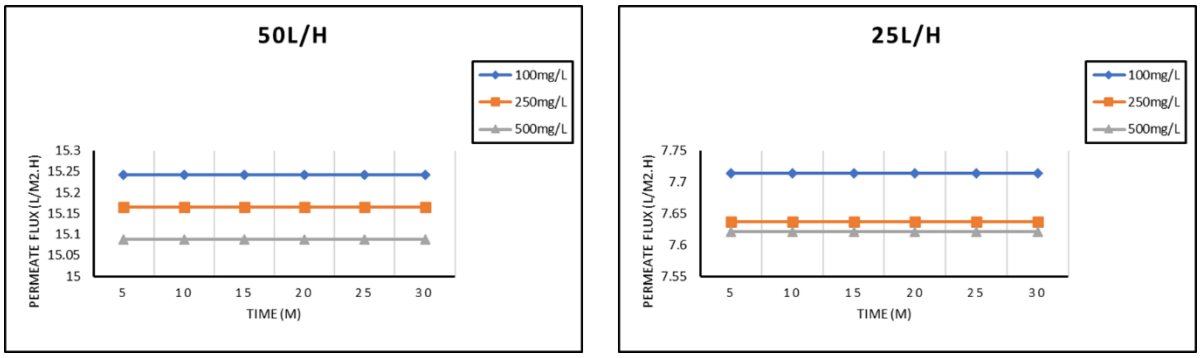

Figure 64: Permeate flux differences in 25 and 50 L/H flowrates for three O/W emulsion concentrations in Al_2O_3 unmodified ceramic membrane.

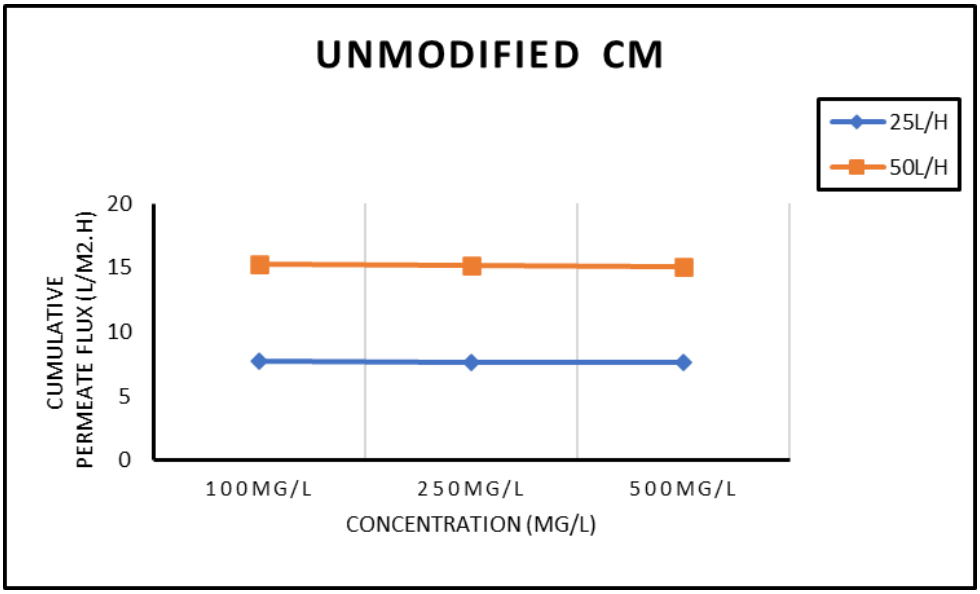

Figure 65:Cumulative permeate flux difference between 25 and 50 L/H flowrate of Al_2O_3 unmodified ceramic membrane.

From Figure 66, the MgO-modified ceramic membrane did not maintain a steady flux in the 100 mg/l O/W emulsion cross-filtration process. This was observed even after a 30-minute run was allowed for stability of measurement before data collection. 100 mg/l was an outlier because it consists of lower concentrations of O/W emulsion which was the first in contact with MgO-modified ceramic membrane hence there was no oil layer yet of the surface of the membrane. After concentration polarization, there was then an observation of flux decline in the 100 mg/l. However, Figure 66 also showed that after the 100 mg/l O/W emulsion concentration cross-filtration, subsequent cross-filtration of higher O/W concentration maintain a steady flux. This was observed even with an increase in flowrate to 50 L/H. All O/W emulsion concentration (100, 250 and 500 mg/l) cross-filtration in MgO-modified ceramic membrane maintained a steady flux after a 30-minute duration in both flowrates (25 and 50 L/H) except for the first 100 mg/l O/W concentration cross-filtration.

Further investigation of the permeate flux variations between the two flowrates (25 and 50 L/H) revealed that an increase in flow rate increases permeate flux in MgO-modified ceramic membrane. An increase in flowrate has an impact on concentration polarization and increases shear stress on the membrane surface that destabilizes the oil layer formation allowing water permeation. Hence, the permeate flux of 50 L/H is higher than that of 25 L/H. Figure 68 displays the cumulative difference in permeate flux between the 25 and 50 L/H flowrates in

MgO-modified ceramic membrane. Permeate flux is higher in 50 L/H as 15.09 $L/m^2.H$ compared to 25 L/H of 7.83 $L/m^2.H$.

The influence of difference flowrates on permeate flux is measured by analysing two cross flow flowrates of 25 L/H and 50 L/H as seen in Figures 64 to Figure 67. It is obvious that increasing flowrates leads to an increase in permeate flux. However, the permeate flux of Al_2O_3 unmodified ceramic membrane still stands higher than that of MgO-modified overall with an exception in 100 mg/l at 25 L/H flowrate. At 100 mg/l concentration at 25 L/H, the maximum permeate flux for both Al_2O_3 unmodified and MgO-modified ceramic membrane after 30 minutes cross filtration is 7.71 and 7.76 $L/m^2.H$, respectively, making MgO-modified permeate flux higher. This proves that initially modified MgO-modified ceramic membrane had a higher flux due to hydrophilic surface modification than Al_2O_3 unmodified ceramic membrane but with increasing concentrations and time, concentration polarization steps in, decreasing the permeate flux of modified membrane compared to unmodified membrane. This reduction in permeate flux for MgO-modified ceramic membrane is because of smaller pore size after surface modification that limits flux permeation. The highest permeate fluxes of 7.71 and 7.83 $L/m^2.H$ in lower flowrates (25 L/H) are seen in the 100 mg/L of the Al_2O_3 unmodified and MgO-modified, respectively. The highest permeate fluxes (15.24 and 15.09 $L/m^2.H$) for higher flowrates of 50 L/H are seen also at 100mg/l concentrations of both Al_2O_3 unmodified and modified MgO-ceramic membranes, respectively.

It was also noted from Figures 64 to 67 that permeate flux decreased from lower O/W emulsion concentrations to higher concentration like so 100>250>500 mg/l in both Al_2O_3 unmodified and MgO-modified ceramic membrane cross-filtration. This is because concentration polarization influences the permeability of water or fluid through the pores of the membrane. At higher concentrations (500 mg/l), the rate of flux decline is more which can be observed in the charts. This must have been due to high concentration of O/W emulsion having bigger oil droplets that might reduce the permeate flux by building a thin wall layer of oil on the surface of the membrane. This oil wall makes access to the surface of the membrane by water molecules harder. It is also noticed from Figure 65 and Figure 67 that most of the permeate flux of all three concentrations in both Al_2O_3 unmodified and MgO-modified ceramic membrane stays the same i.e., the flux

has plateaued and does not decline with further time except in 100 mg/l of MgO-modified ceramic membrane. This plateau trend may be since O/W emulsions of all concentrations was allowed to run through the MgO-modified and Al_2O_3 unmodified ceramic membrane for 30 minutes before the start of measurement. This time allowance was given to allow stability in result measurement. This is a good indication that after a period of 30 minutes, there will be no further flux decline with the use of MgO ceramic membrane especially in higher concentrations above 250 mg/l.

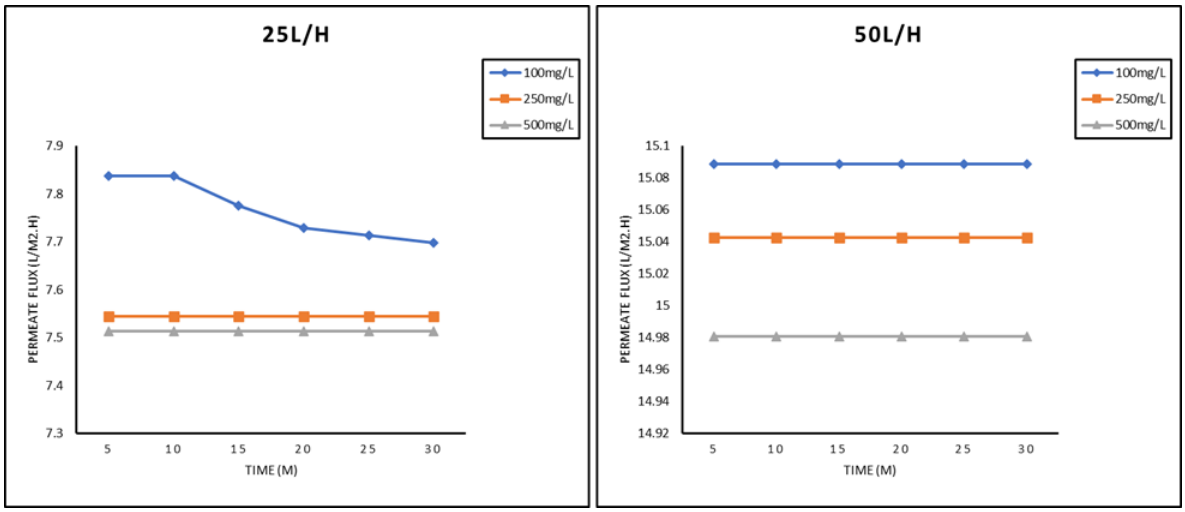

Figure 66: Permeate flux differences in 25 and 50 L/H flowrates for three O/W emulsion concentrations in MgO-modified ceramic membrane.

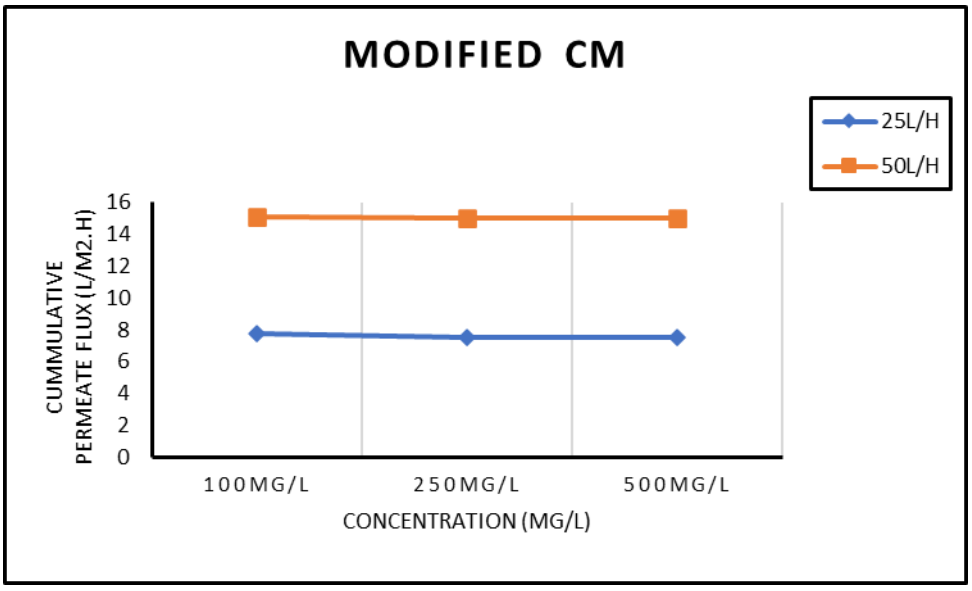

Figure 67: Variation of permeate flux of MgO modified ceramic membrane at three different concentrations and two flowrates.

4.4.3 O/W emulsion Flux based on Temperature

The separation efficiency of Al_2O_3 unmodified and MgO-modified ceramic membrane was also tested with 100, 250 and 500 mg/l concentrations of O/W emulsion at two applied temperatures of 20 and 50^0C at two flowrates of 25 and 50 L/H. As seen in Figure 68 and Figure 70, there were mostly no flux decline in the entire 30 minutes run time of permeate flux measurement for both 20 and 50°C in both Al_2O_3 unmodified and MgO-modified ceramic membranes. This outcome of permeate flux maintenance over time is due in part to the allowance of 30 minutes flow of O/W emulsions via the ceramic membranes before beginning permeate flux measurements. It is also partly due to concentration polarization of O/W emulsion reaching its optimum where it might not have a significant fouling effect on ceramic membrane surfaces anymore. There is however an exception of permeate flux in 20^0C temperature with 100mg/l O/W emulsion at 25 L/H flowrate where there was a noticed decline in flux for MgO-modified membrane. This arises because 100 mg/l concentration of O/W emulsion was the first to be run through the MgO-modified ceramic membrane and as such experienced a longer time before reaching concentration polarization to achieve plateau.

It is also noticed in Figure 69 and Figure 71 that an increase in temperature increases permeate flux. This is the case for both Al_2O_3 unmodified and MgO-modified ceramic membrane. The average permeate flux at 25 L/H flowrate for lower temperature 20^0C of 500 mg/l concentration in Al_2O_3 unmodified ceramic membrane is 7.64 L/m^2.H compared to the average flux of 500 mg/l concentration in Al_2O_3 unmodified ceramic membrane at 50^0C which is 7.76 L/m^2.H. This increased permeate flux based on temperature is also the case for other concentrations (100 mg/l and 250 mg/l) at 25 L/H and 50 L/H in Al_2O_3 unmodified ceramic membrane. For MgO-modified ceramic membrane, the average permeate flux at 25 L/H flowrate for lower temperature 20°C of 500 mg/l concentration is 7.51 L/m^2.H compared to the average of 500 mg/l concentration at 50°C which is 7.64 L/m^2.H. Similar results of an increase in permeate flux with increase in temperature is observed with other O/W emulsion concentrations (100 and 250 mg/l) for 25 and 50 L/H flowrates for MgO-modified ceramic membrane.

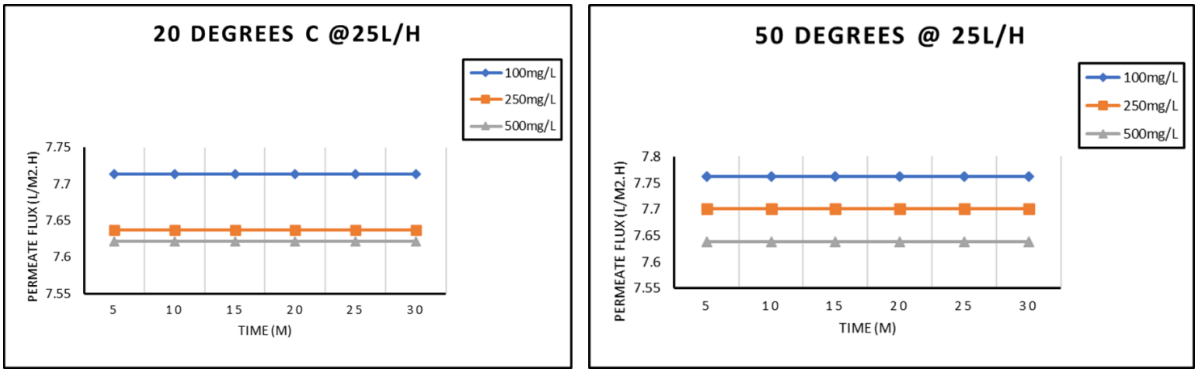

Figure 68: Permeate flux differences in 20º and 50ºC temperatures for three O/W emulsion concentrations in Al_2O_3 modified ceramic membrane.

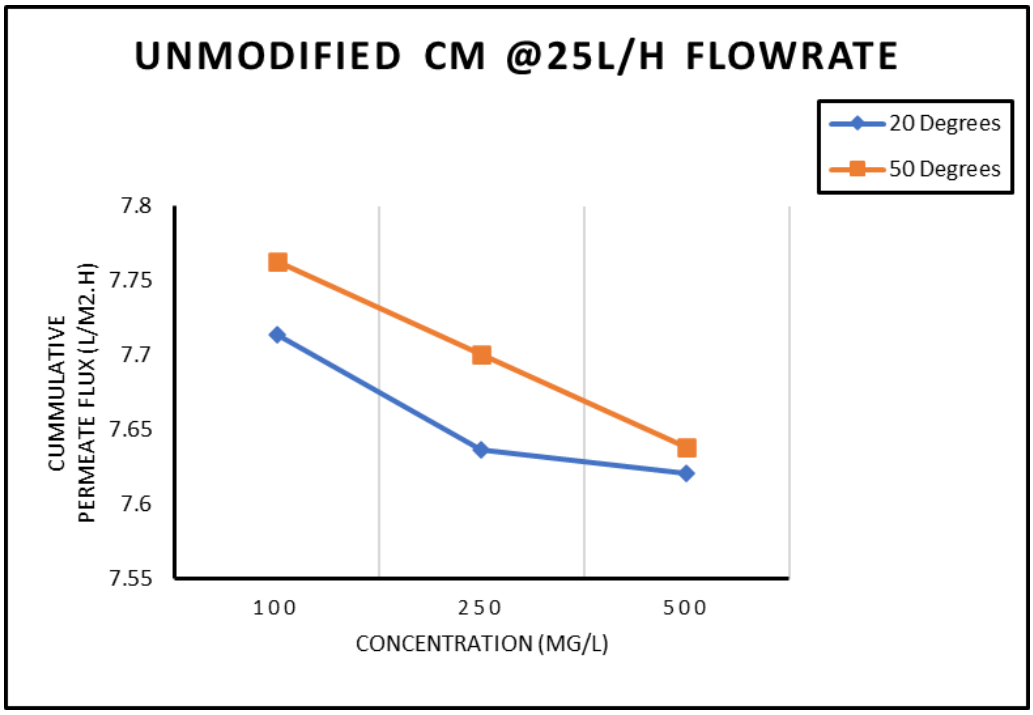

Figure 69: Variation of permeate flux of unmodified ceramic membrane at two temperatures and 25 L/H flowrates.

As displayed in Figure 68 to Figure 71, the permeate fluxes of Al_2O_3 unmodified is higher as 15.9 L/m2.H compared to MgO-modified ceramic membranes as 15.6 L/m2.H in higher temperature of 50^0C and higher flowrates (50 L/H) of 500 mg/L. This is mostly due to the pore size of the Al_2O_3 unmodified ceramic membrane being wider than the MgO-modified ceramic membrane. Hence an increase in temperature causes molecules to be highly active thereby increasing flow of liquid and a wider pore size results in higher permeate flux. This result is similar for both ceramic membranes of 500 mg/l O/W emulsion cross-filtration in all conditions which include – lower flowrate (25 L/H) and lower temperature (20ºC), lower flowrate (25 L/H) and higher temperature (50ºC), higher flowrate

(50 L/H) and lower temperature, higher flowrate, and higher temperature – even in the remaining O/W emulsion cross-filtration (100 and 250 mg/l).

It was also noted from Figures 68 to 71 that there is a decrease in permeate flux from lower O/W emulsion concentration to higher concentration like so 100>250>500 mg/l in both Al_2O_3 unmodified and MgO-modified ceramic membrane cross-filtration. This was the case in flux based on flowrate result. This is now like flux based on temperature result.

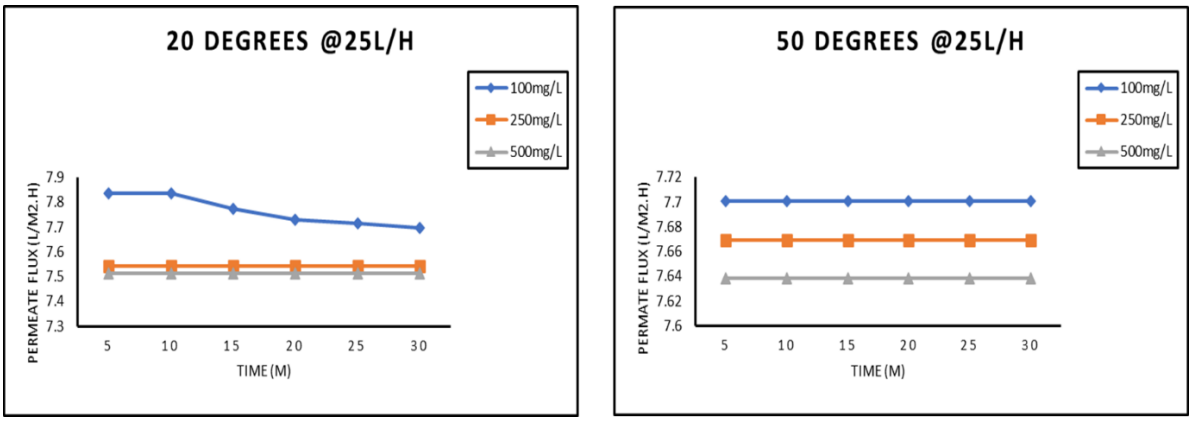

Figure 70 : Permeate flux differences in 20° and 50°C temperatures for three O/W emulsion concentrations in MgO-modified ceramic membrane.

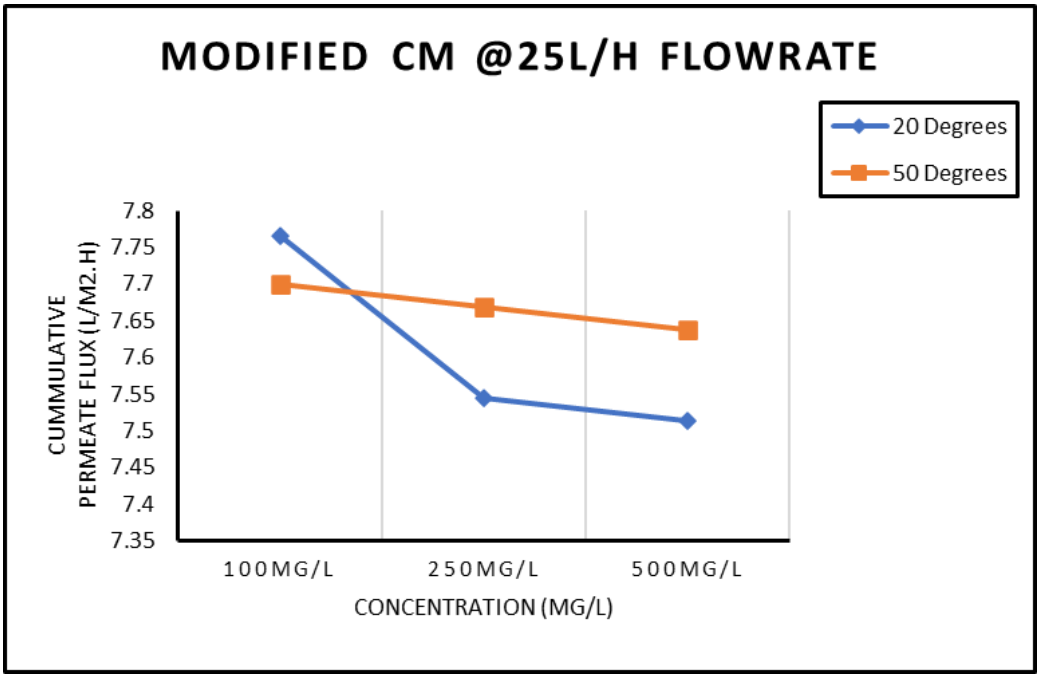

Figure 71: Variation of permeate flux of MgO modified ceramic membrane at two temperatures and 25 L/H flowrates.

4.4.4 Flux recovery

Flux recovery ratio was performed in both Al_2O_3 unmodified and MgO-modified ceramic membrane to determine the reusability of the ceramic membrane after O/W emulsion cross filtration by remeasuring pure water flux. Figure 72-74 illustrate the flux recovery calculated from Equation 4 in sub section 5.2.3.5. It is observed that PWF recovery ratio in Al_2O_3 unmodified ceramic membrane is higher than that of MgO-modified ceramic membrane. From Figure 74, the percentage flux recovery being 97.4 and 97% for higher and lower (50 and 25 L/H) versus 89.5 and 87.1% for higher and lower (50 and 25 L/H) for Al_2O_3 unmodified and MgO-modified ceramic membranes, respectively. This decline of flux recovery in MgO-modified ceramic membrane might be due to an increased oil concentration polarization arising from smaller pores after membrane modification. From Figures 72 and 73, it is also noted in both membranes that an increased flowrate (50 L/H) causes decline in flux recovery ratio. This is arising from pressure shear of O/W emulsion hitting the surfaces of both membranes and blocking the pores with the forceful entry of oil droplets causing higher fouling than in lower flowrates (25 L/H).

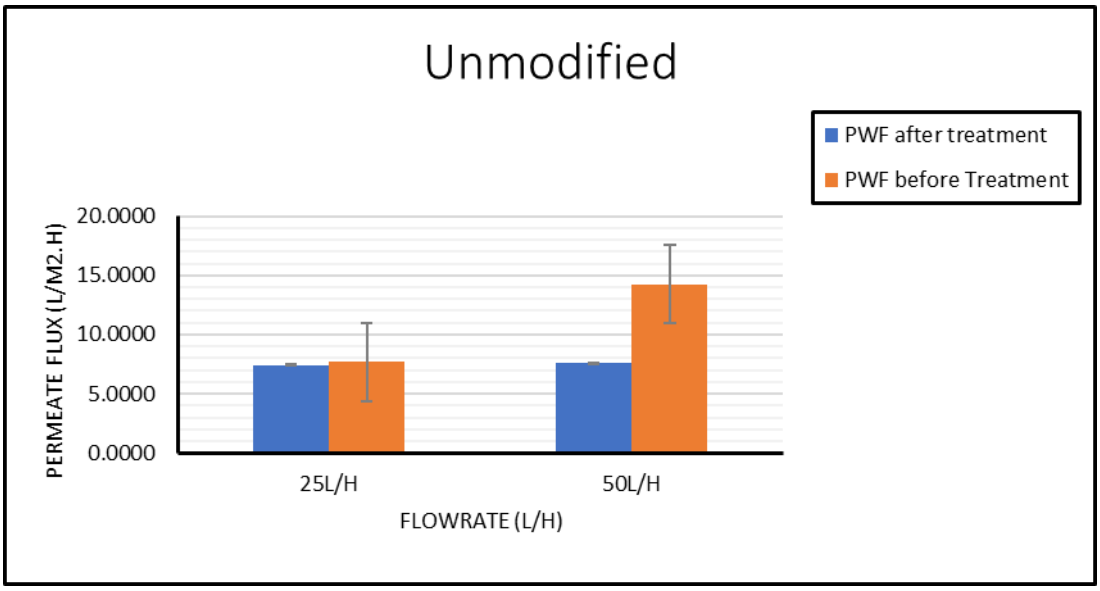

Figure 72 : Permeate flux difference between PWF and recovery ratio flux of 25 and 50L/H flowrates for Al_2O_3 unmodified ceramic membrane.

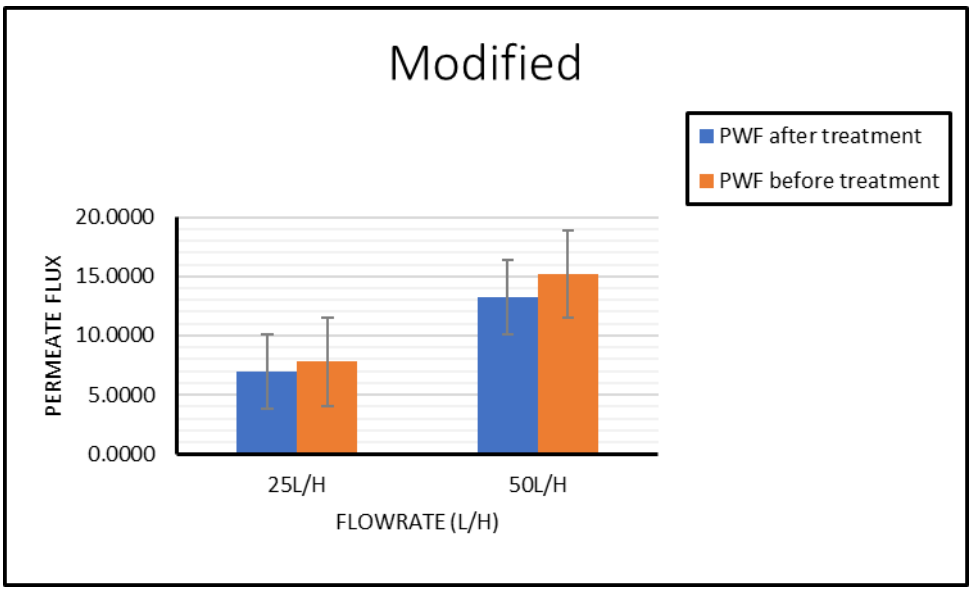

Figure 73: Permeate flux difference between PWF and recovery ratio flux of 25 and 50L/H flowrates for MgO-modified ceramic membrane.

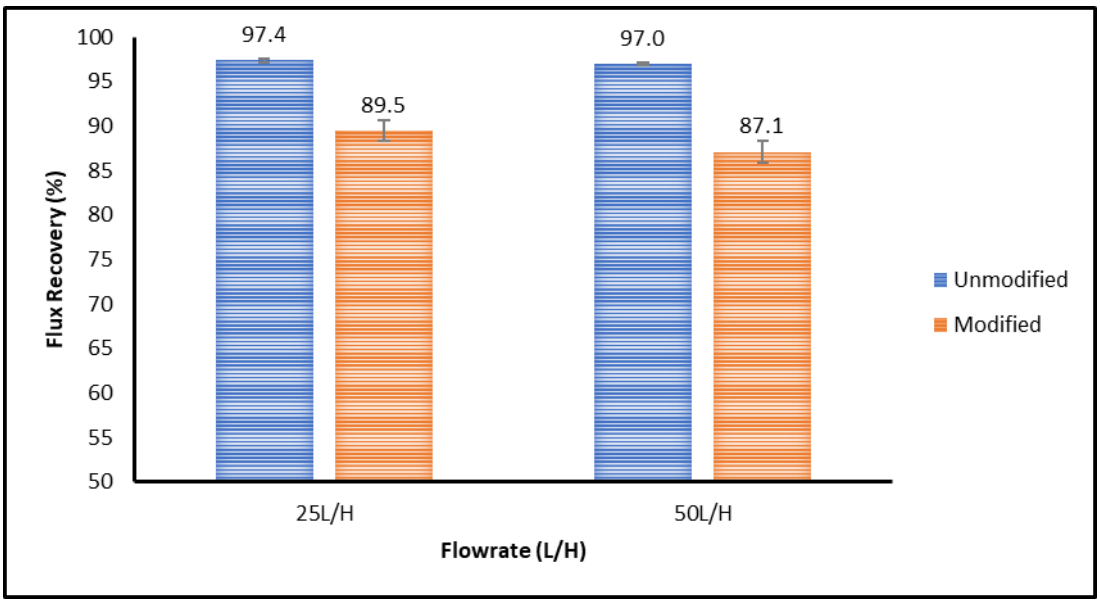

Figure 74: Recovery ratio of Al_2O_3 unmodified and MgO-modified ceramic membrane.

4.5 Oil Rejection

This sub section reports and discuss the physical and chemical analysis results from the experimental procedure for determining percentage oil rejection. This subsection considers the percentage oil rejection of all parameters measured including flowrate, temperature, and concentrations for both Al_2O_3 unmodified and MgO-modified ceramic membrane.

4.5.1 Physical Analysis

Figures 75 to 77 displays the physical appearance of difference concentrations (100, 250 and 500 mg/l) of O/W emulsion feed against the permeate flux through MgO-modified ceramic membrane. The difference in turbidity is obvious in both feed and permeate flux samples. After nanofiltration through MgO-modified ceramic membrane, the turbidity of O/W emulsion in the feed tank becomes more clearer at the permeate flux end. This is an indication of the oil rejection via MgO-modified ceramic membrane due to the surface hydrophilicity of the membrane.

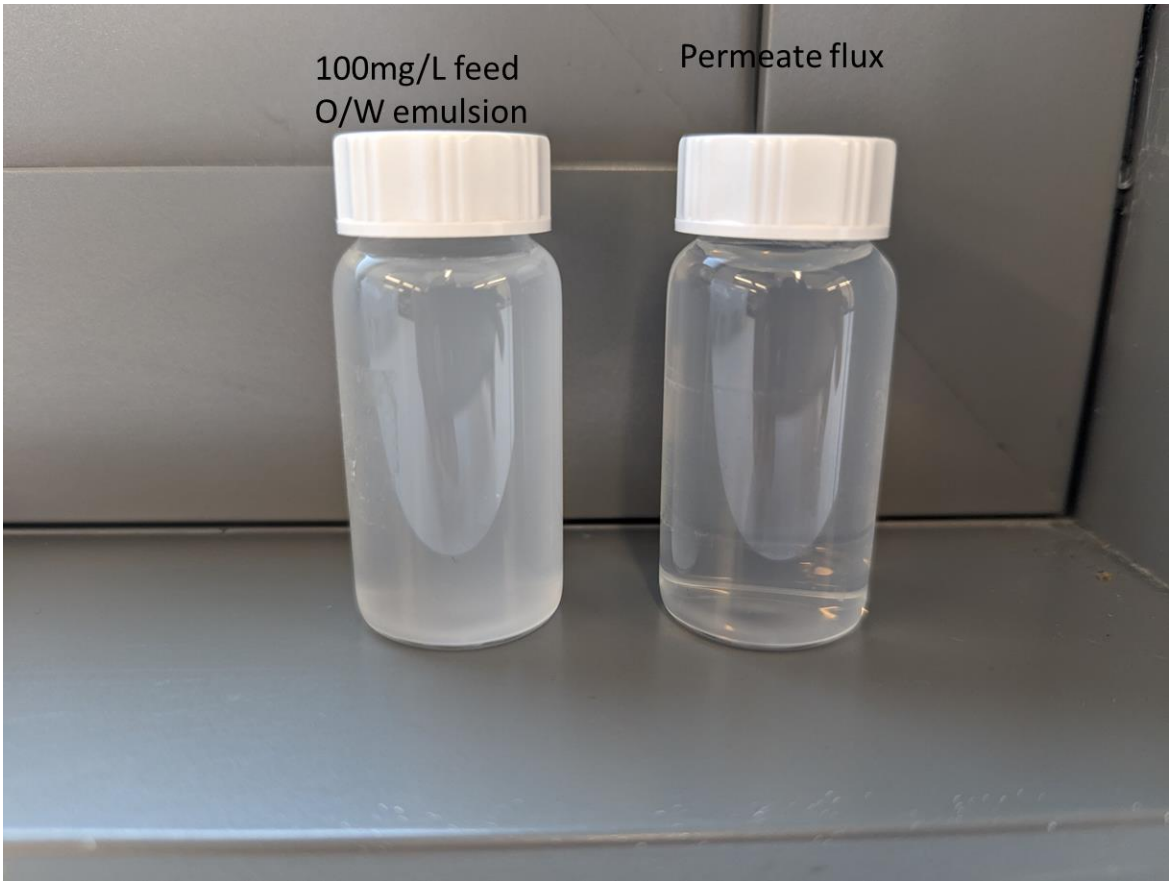

Figure 75: Appearance of O/W emulsion feeds versus Permeate flux for 100 mg/l concentration.

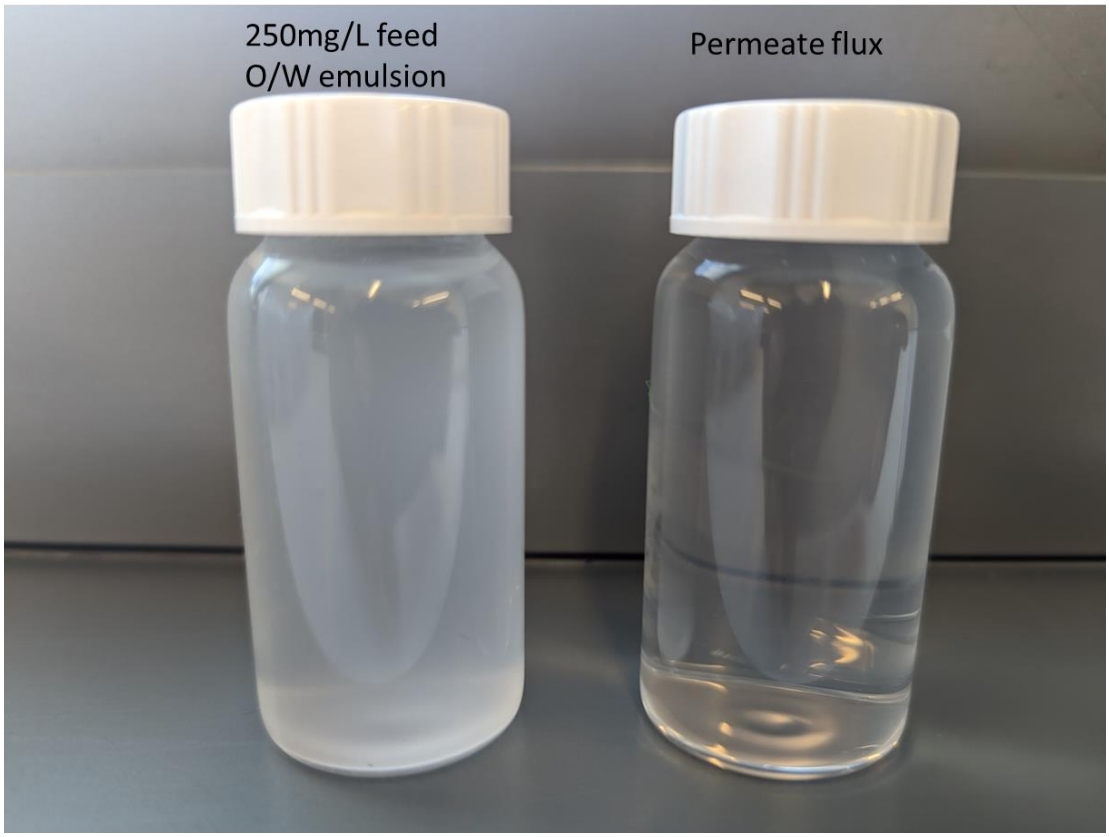

Figure 76: Appearance of O/W emulsion feeds versus Permeate flux for 250 mg/l concentration.

Figure 77: Appearance of O/W emulsion feeds versus Permeate flux for 500 mg/l concentration.

4.5.2 Chemical Analysis

A variation of percentage oil rejection arising from O/W cross-filtration separation through Al_2O_3 unmodified and MgO-modified ceramic is presented in Figure 78. These % oil rejection absorbance measurements were run in the spectrophotometer recorded in triplicates and averages to get the mean. From Figure 78, in Al_2O_3 unmodified ceramic membrane, % oil rejection at 25 L/H increase with increase in O/W emulsion concentration like so 100<250<500 mg/l. This low % oil rejection from 100 mg/l might come from the lower oil droplet sizes in 100 mg/l which can easily pass through the pores of Al_2O_3 unmodified ceramic membrane. However, as the O/W emulsion keeps increase to 250 and then 500 mg/l so does the oil droplet increase and becomes larger to squeeze through the pores of the Al_2O_3 ceramic membrane. This causes concentration polarization the surface of the membrane and thus, aiding % oil rejection. This is not the case however in MgO-modified ceramic membrane as there was no meaningful change in % oil rejection from the three different O/W emulsion concentrations. O/W emulsion concentrations had similar % oil rejection values, and this might be because of pore size and hydrophilicity. The MgO-modified ceramic membrane had smaller pore size and is more hydrophilic than Al_2O_3 unmodified ceramic membrane, hence was able to separation and repel oil molecules which was now in a larger droplet size compared to the membrane pore size regardless of the O/W emulsion concentrations.

From Figure 79, similarly, Al_2O_3 unmodified ceramic membrane at 50 L/H increases % oil rejection with increase in O/W emulsion concentration like the results seen in 25 L/H. The only difference is the % oil rejection further reduced in value. This can arise from shear pressure from increase in flowrate, that pushes oil droplets forcefully through the membrane pores and causing it the exit with permeate. MgO-modified ceramic membrane at 50 L/H flowrate increased with increase in O/W emulsion concentrations like so 100<250<500 mg/l which was not the case in 25 L/H above. This decrease in 100 mg/l might result from shear pressure push of smaller oil droplet through the smaller pores size as 100 mg/l has even smaller oil droplet size compared to 250 mg/l which also has smaller droplet size compared to 500 mg/l. Hence, the ascension in %oil rejection because 500mg/l oil droplet size would be even harder to push through tiny MgO-modified ceramic membrane pores compared to 100 mg/l oil

droplet size. It is worth noting that the % oil rejection for 50 L/H in MgO-modified ceramic membrane dropped compared to 25 L/H above.

From both Figures 78 and 79, the % oil rejection of Al_2O_3 unmodified ceramic membrane is lower marginally compared to MgO-modified ceramic membrane. MgO-modified ceramic membrane presents a higher %oil rejection with a maximum of 98.26%, 98.54 and 98.62 in the three O/W emulsion concentrations (100, 250 and 500 mg/l) respectively for 25 L/H flowrate. This is higher than the Al_2O_3 unmodified ceramic membrane with % oil rejection of 58.44, 67.96, and 69.96 in the three O/W emulsion concentration (100, 250, and 500 mg/l) respectively. This is due to the influence of higher hydrophilic surface of the MgO-modified ceramic membrane from MgO molecules which is not present in Al_2O_3 unmodified ceramic membrane. This aids in the repellent of oil droplets from the surface of the membrane ((Matindi et al. 2021; Gohari et al. 2015). Also, the impact of MgO modification reduced the porosity and pore size of the membrane making it difficult for oil droplets bigger than the pore size of the MgO-modified ceramic membrane to penetrate the permeate.

% oil rejections values from both Al_2O_3 unmodified and MgO-modified ceramic membranes of 50 L/H flowrates had related results as 25 L/H. This was observed in terms of MgO-modified having a higher % oil rejection than Al_2O_3 unmodified ceramic membranes in all three O/W emulsion concentrations. However, % oil rejections in 50 L/H for both Al_2O_3 unmodified and MgO-modified ceramic membranes was lower in value for all three O/W emulsion concentrations compared to 25 L/H. This arises from the fact that an increase in flowrate reduces oil concentration polarization thereby decreasing cake formation of oil on the surface of the ceramic membrane. Hence, resistance to the O/W emulsion permeate flow decreases. Also, surface shear stress increases with an increase in flowrate which also adds to the cake formation decrease. Based on these reasons, some oil droplets that was supposed to be resisted by ceramic membrane passes through the pores of the membrane and exits with permeate flux causing a decline in oil percentage rejection. Some literature has reported similar observations (Qiu et al. 2020; Suresh and Pugazhenthi 2017). Also, deformation of oil droplets occurs due to feed rush from higher flowrate that can easily pass through the pores of both Al_2O_3 unmodified and MgO-modified ceramic membrane.

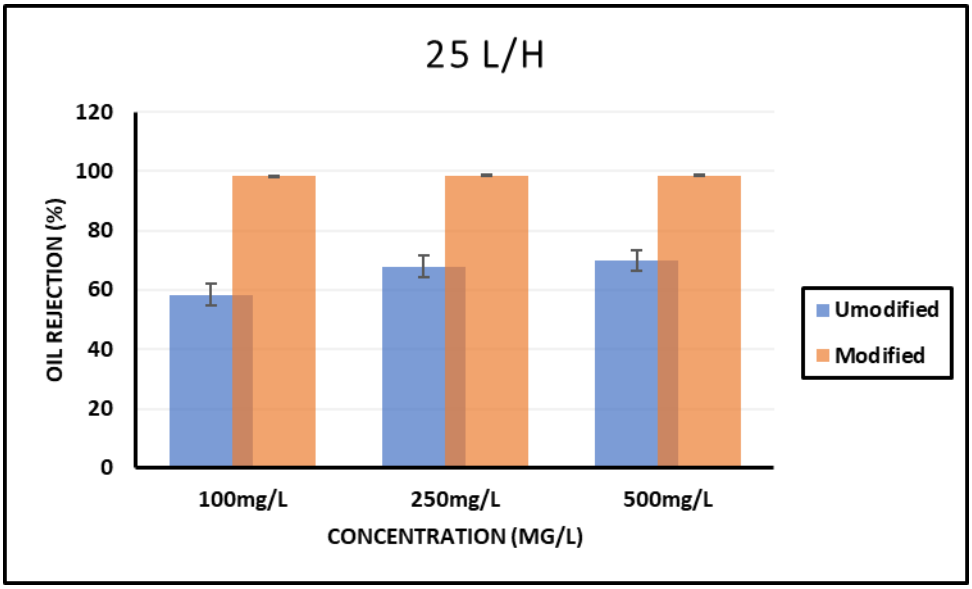

Figure 78: % Oil Rejection of Unmodified and MgO-modified ceramic membrane at 25 L/H flowrates.

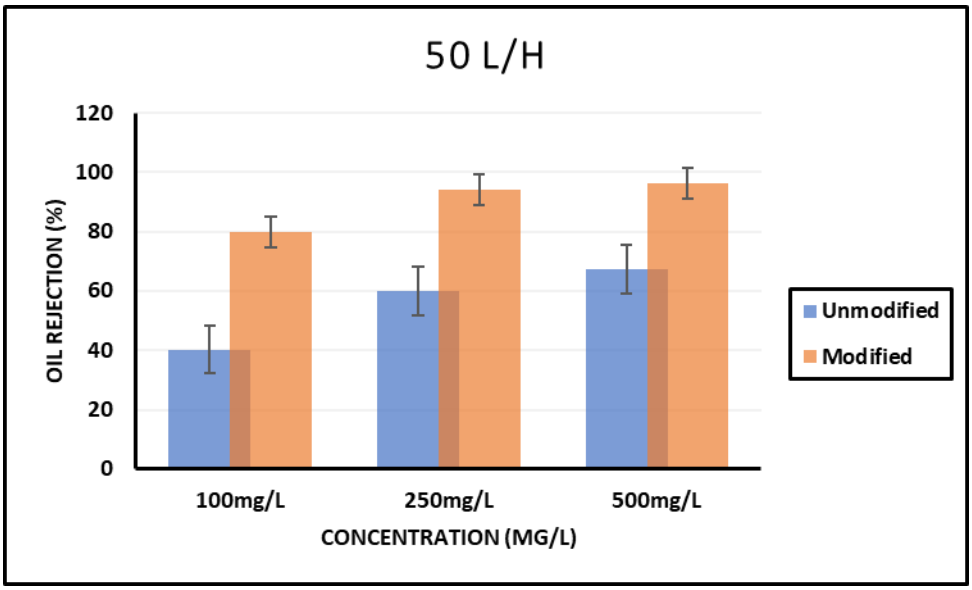

Figure 79: % Oil Rejection of Unmodified and MgO-modified ceramic membrane at 50 L/H flowrates.

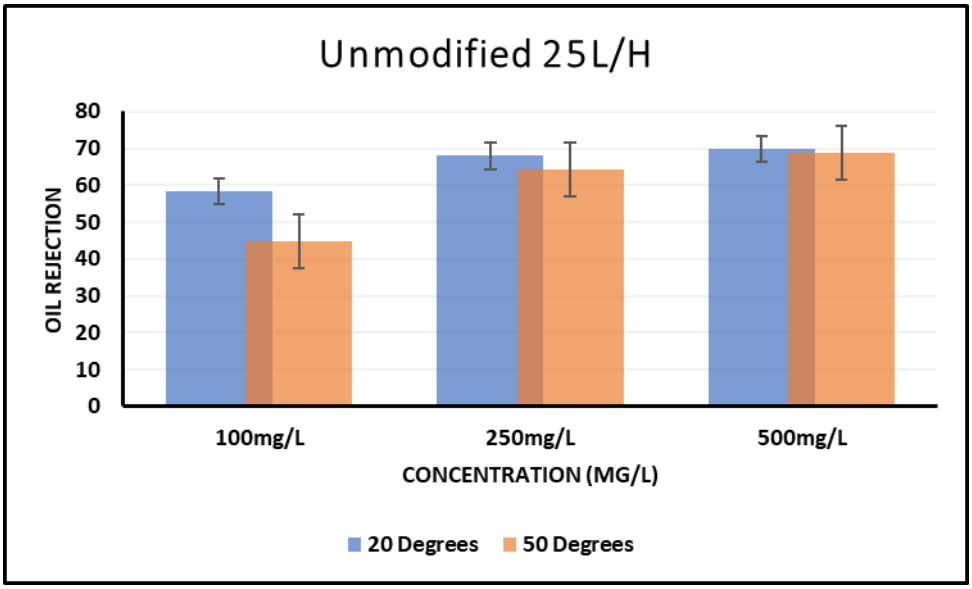

Figure 80: % Oil Rejection of Al_2O_3 Unmodified ceramic membrane at different temperatures.

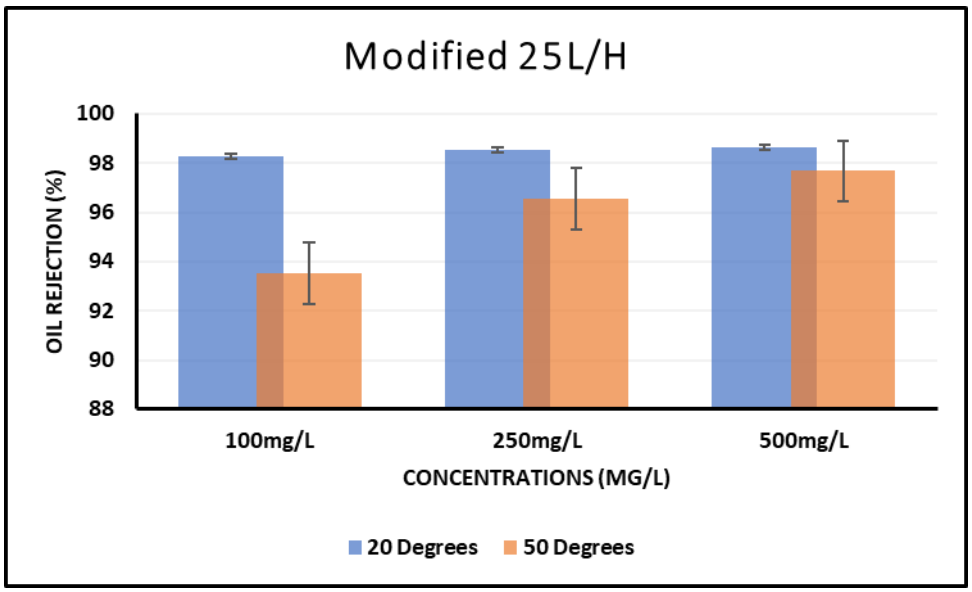

Figure 81: % Oil Rejection of MgO-Modified ceramic membrane at different temperatures.

From Figure 80, there is an increase in % oil rejection across O/W emulsion concentrations (100<250<500 mg/l) which is observed in both 20° (58.44, 67.96 and 69.96%) and 50°C (44.85, 64.31, 68.75%) in Al_2O_3 unmodified ceramic membrane @25 L/H. This smaller % oil rejection in 100 mg/l O/W emulsion concentration in both temperatures might again be due to oil droplet size. Ascension of oil droplet size from 100 to 500 mg/l causes an ascension of % oil rejection from 100 to 500mg/l. The higher the oil droplet size the higher the % oil rejection through the Al_2O_3 unmodified ceramic membrane. 50°C temperature rise reduces % oil rejection in Al_2O_3 unmodified ceramic membrane at 25 L/H. This is caused by an increase in temperature decreases oil rejection in

MgO-modified ceramic membrane as a higher temperature speeds up flow and decreases oil concentration polarization allowing oil molecules to easily pass through the MgO-modified ceramic membrane. Furthermore, the increase in temperature can denature or breakdown the shape of oil droplet size decreasing the oil droplet to a size that passes through the tiny nanopores of the MgO membrane. This result is the same with recorded observations with increase in flowrate at 50 L/H (Appendix IV). The 50°C had a smaller % oil rejection value compared to the 20°C across all O/W emulsion concentrations.

From Figure 81, similarly to Al_2O_3 results observed above, the MgO-modified ceramic membrane had an increase in % oil rejection across three O/W emulsion concentrations which was also observed in 20° and 50°C for both 25 and 50 L/H flowrates Appendix IV. Similar reason given in Al_2O_3 unmodified ceramic membrane is the case in the MgO-modified ceramic membrane. At 50°C temperature rise, there was also a reduction in % oil rejection which arose also based on the reason observed in Al_2O_3 unmodified ceramic membrane. However, all % rejections both at 20° and 50°C of 25 and 50 L/H across three O/W emulsion concentrations in MgO-modified ceramic membrane was higher than in Al_2O_3 unmodified ceramic membrane. The higher % oil rejection is because of MgO nanoparticles modification present on the membrane creating an affinity for water molecules compared to oil molecules thereby increasing % oil rejection in MgO-modified ceramic membrane.

Extensive literature review of lab studies was conducted to consolidate the results of %oil rejection of O/W emulsion separation using unmodified and modified ceramic membrane. Table 8 gives the summary of appropriate findings from research work in line with this study for % oil rejection data.

Table 8: Research findings in line with this study for % Oil Rejection.

Material	*Pore size 9 (nm)*	*Concentration (mg/L)*	*Oil Rejection (%)*	*Author*
TiO_2	19	900	95	(Matindi et al. 2021)
Carbon membrane	1000	120	97.8	(Song et al. 2006)
TiO_2	2000	300	95	(Chang et

				al. 2010a)
Kaolin	2850	125	98.4	(Nandi et al. 2010)
ZrO_2/α-Al_2O_3	1000	5500	94.3	(Yang, Chao et al. 1998)
α-Al_2O_3	2000	141	97.8	(Abadi et al. 2011)
TiO2 membrane	9000	200	99.56	(Suresh and Pugazhenthi 2017)
HAO nano-sized membrane	1700	1000	100	(Gohari et al. 2015)
Unmodified ceramic membrane	4179	500	69.96	This work
Modified MgO ceramic membrane	3139	500	98.62	This work

4.6 Results Summary

This sub-section presents a summary of the comparison results between Al_2O_3 unmodified and MgO-modified ceramic membranes as regards cross-filtration and % oil rejection generated from this research.

4.6.1 Cross-filtration and % Oil Rejection Results Summary

The PWF (7.78 L/m^2.H) from MgO-modified ceramic membrane is slightly more than PWF in Al_2O_3 unmodified ceramic membrane (7.68 L/m^2.H). This is noticed and similarly observed in both 25 L/H and 50 L/H flowrates. MgO-modified ceramic membrane display an even higher PWF at both 20^o and 50^{o}C compared to Al_2O_3 unmodified ceramic membrane.

An increase in flowrates leads to an increase in permeate flux. However, the permeate flux of Al_2O_3 unmodified ceramic membrane still stands higher than that of MgO-modified overall with an exception in 100 mg/L at 25 L/H flowrate. It is also noted that permeate flux decreased from lower O/W emulsion

concentrations to higher concentration like so 100>250>500 mg/l in both Al_2O_3 unmodified and MgO-modified ceramic membrane cross-filtration at both 25 and 50 L/H flowrates.

The permeate fluxes of Al_2O_3 unmodified is higher compared to MgO-modified ceramic membranes with an increase in temperature from 20°C to 50°C and higher flowrates (50 L/H) across all O/W emulsion concentration (100, 250 and 500 mg/L).

It is observed that PWF recovery ratio in Al_2O_3 unmodified ceramic membrane is higher than that of MgO-modified ceramic membrane. It is also noted in both membranes that an increased flowrate (50 L/H) causes decline in flux recovery ratio.

After nanofiltration through MgO-modified ceramic membrane, the turbidity of O/W emulsion in the feed tank becomes more clearer at the permeate flux end. The % oil rejection of Al_2O_3 unmodified ceramic membrane is lower marginally compared to MgO-modified ceramic membrane. MgO-modified ceramic membrane presents a higher % oil rejection in the three O/W emulsion concentrations for 25 and 50 L/H flowrate. All % rejections both at 20° and 50°C of 25 and 50 L/H across three O/W emulsion concentrations in MgO-modified ceramic membrane was higher than in Al_2O_3 unmodified ceramic membrane.

When comparing permeate fluxes and % oil rejections, from Figure 82, the higher the permeate flux, the lower the % oil rejection and the lower the permeate flux, the higher the % oil rejection. This is observed in both Al_2O_3 unmodified and MgO-modified ceramic membrane for 25 and 50 L/H flowrates (Figure 82). This result is like that reported in literature by (Gohari et al. 2015). This was the similar result when temperature parameters were measured (Figure 83) where permeate flux decreased with increase in concentrations (100>250>500 mg/l) for both lower and higher flowrates (25 and 50 L/H); then % oil rejection increased with increase in concentrations (100<250<500 mg/l) in both lower and higher flowrates. It is also worth noting from Figures 82 to 84 that the increase in oil rejection is higher in MgO-modified ceramic membrane than Al_2O_3 unmodified ceramic membrane. There is also a decline in flux for MgO-modified ceramic membrane than Al_2O_3 unmodified membrane especially with increasing concentration. Hence, it is obvious that the nanofiltration of O/W

emulsion with MgO-modified ceramic membrane offers lower permeate flux but higher % oil rejection.

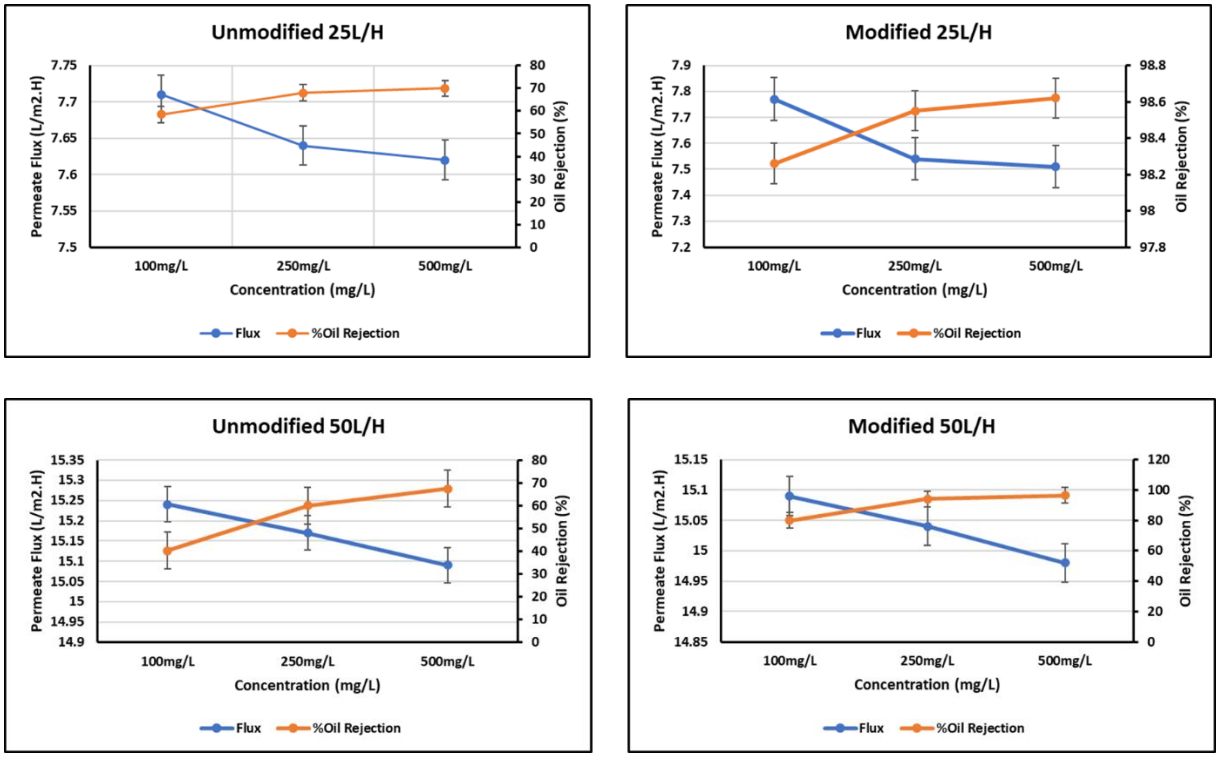

Figure 82: Permeate Flux vs Oil rejection in modified and unmodified ceramic membrane.

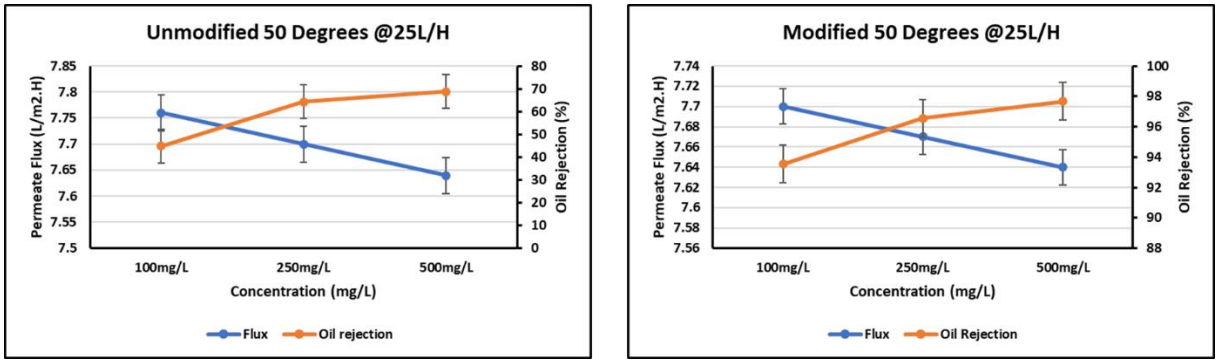

Figure 83: Permeate flux versus Oil rejection with temperature effect in unmodified and modified ceramic membrane.

Chapter Five

5.0 Conclusion and Recommendations

This chapter emphasis the conclusion drawn from the entire research based on the aim and objectives and results from the laboratory analysis. This chapter also suggests future recommendations as regards this research.

5.1 Conclusion

This research was conducted test and compare the separation efficiency of both modified and characterized metal oxide (MgO) nanoparticle ceramic membrane and Al_2O_3 unmodified tubular ceramic membrane for the separation of lower concentrations (<500 mg/l) and smaller oil droplets (<20 µm) of synthetic O/W emulsion to meet up stringent regulatory limits (30 mg/l).

Research finding clearly demonstrated that the MgO-modified ceramic membrane offers better oil rejection percentage which was found to be 98.26% in comparison with Al_2O_3 unmodified ceramic membrane which had % oil rejection of 58.44%. It was also observed from this study that and increase in O/W emulsion concentration (100>250>500 mg/l) increased % oil water rejection for MgO modified ceramic membrane. This was similar for Al_2O_3 ceramic membrane although with lesser % oil rejection.

Howbeit, the study also demonstrated that a higher permeate flux result was observed in Al_2O_3 ceramic membrane in comparison to MgO-modified ceramic membrane in all concentrations, temperatures and flowrates. However, the optimum flux for MgO modified ceramic membrane was found to be 7.83 $L/m^2.H$ at 25 L/H flowrate where MgO ceramic membrane demonstrated a higher flux compared to Al_2O_3 ceramic membrane flux (7.76 $L/m^2.H$).

The percentage oil rejection result was found to be 98.26% and 58.44% for MgO-modified and Al_2O_3 unmodified ceramic membrane, respectively. This was again the trend even with increased concentration, pressure, or temperature.

The recyclability of both MgO and Al_2O_3 ceramic membrane were analysed. The result from the flux recovery displays a higher flux recovery for Al_2O_3 unmodified ceramic membrane with 97.4% recovery compared to 89.5% recovery found in MgO-modified ceramic membrane.

Conclusively, MgO-modified Ceramic membrane O/W emulsion separation efficiency is higher than that of Al_2O_3 ceramic membrane and able to separation lower concentrations (<500 mg/l) or lower oil droplets (<20 um) >98% and meets up the OSPAR regulatory limit.

5.2 Recommendation for Future Work

This study has shown the ability for MgO modified ceramic membrane to separate oil from O/W emulsion beyond regulatory limits. This research can be categorized as a good pilot study for the understanding and development of a good system that is compact and serve the purpose of O/W emulsion separation to meet regulatory requirements in industrial environments.

To further make this process applicable soon for industrial purposes, the following can be improved upon:

1. It would be a great idea to test this MgO-modified ceramic membrane with the use of real representative sampled O/W emulsion from industrial sites.
2. Try other modification methods for the preparation of MgO-modified ceramic membrane to see the enhancement inn permeate flux.
3. Construction of the reactor rigs strictly for unmodified and modified membrane to give a simultaneous, uninterrupted measurement of parameters.
4. Use of other membrane sizes and shapes to evaluate the effectiveness of surface area in permeate flux and oil rejection.
5. Stability test of MgO-modified ceramic membrane to determine the duration or cycle of use before recovery, cleaning, or change.
6. Detailed research on the cost of production and operation of this method for industrial application.

References

ABADI, S.R.H. et al., 2011. Ceramic membrane performance in microfiltration of oily wastewater. *Desalination,* 265(1-3), pp. 222-228.

ABD AZIZ, M.H. et al., 2019. Pretreated aluminium dross waste as a source of inexpensive alumina-spinel composite ceramic hollow fibre membrane for pretreatment of oily saline produced water. *Ceramics International,* 45(2), pp. 2069-2078.

ABDALLA, M. et al., 2019. Impact of combined oil-in-water emulsions and particulate suspensions on ceramic membrane fouling and permeability recovery. *Separation and Purification Technology,* 212, pp. 215-222.

ABDULLAH, N., RAHMAN, M.A., OTHMAN, M.H.D., JAAFAR, J. and ISMAIL, A.F., 2018. Membranes and membrane processes: fundamentals. *Current Trends and Future Developments on (Bio-) Membranes.* Elsevier. pp. 45-70.

ABDULLAYEV, A. et al., 2019. Materials and applications for low-cost ceramic membranes. *Membranes,* 9(9), pp. 105.

ABIDLI, A. et al., 2020. Novel separator skimmer for oil spill cleanup and oily wastewater treatment: From conceptual system design to the first pilot-scale prototype development. *Environmental Technology & Innovation,* 18, pp. 100598.

ABOULELLA, A.M. et al., 2022. TiO2 ceramic membrane decorated with Fe3O4–Ag composite nanoparticles for produced water treatment. *Chemosphere,* 308, pp. 136470.

ACHEAMPONG, T. and KEMP, A.G., 2022. Health, safety and environmental (HSE) regulation and outcomes in the offshore oil and gas industry: Performance review of trends in the United Kingdom Continental Shelf. *Safety Science,* 148, pp. 105634.

AGBOOLA, O., 2019. The role of membrane technology in acid mine water treatment: A review. *Korean Journal of Chemical Engineering,* 36(9), pp. 1389-1400.

AHMAD, N.A. et al., 2015. Membranes with great hydrophobicity: a review on preparation and characterization. *Separation & Purification Reviews,* 44(2), pp. 109-134.

AHMAD, R. et al., 2018. Effect of polymer template on structure and membrane fouling of TiO2/Al2O3 composite membranes for wastewater treatment. *Journal of industrial and engineering chemistry,* 57, pp. 55-63.

AISUENI, F. et al., 2022. Effect of pore size and porosity on contact angle of ceramic membrane for oil-in-water emulsion separation.

ALEM, A., SARPOOLAKY, H. and KESHMIRI, M., 2009. Sol–gel preparation of titania multilayer membrane for photocatalytic applications. *Ceramics International,* 35(5), pp. 1837-1843.

ALHOSHAN, M. et al., 2013. Fabrication of polysulfone/ZnO membrane: influence of ZnO nanoparticles on membrane characteristics. *Advances in Polymer Technology,* 32(4),

ALOULOU, H. et al., 2021. Silane-grafted sand membrane for the treatment of oily wastewater via air gap membrane distillation: Study of the efficiency in comparison with microfiltration and ultrafiltration ceramic membranes. *Materials Chemistry and Physics,* 261, pp. 124186.

ALSALHY, Q.F. et al., 2018. A study of the effect of embedding ZnO-NPs on PVC membrane performance use in actual hospital wastewater treatment by membrane bioreactor. *Chemical Engineering and Processing-Process Intensification,* 130, pp. 262-274.

AMAKIRI, K.T. et al., 2022. Review of oilfield produced water treatment technologies. *Chemosphere,* , pp. 134064.

AMETA, S.C. and AMETA, R., 2018. *Advanced oxidation processes for wastewater treatment: Emerging green chemical technology.* Academic press.

AMIN, S.K. et al., 2016. An overview of production and development of ceramic membranes. *Int.J.Appl.Eng.Res,* 11(12), pp. 7708-7721.

ARYA, A. et al., 2018. Thermal performance analysis of a flat heat pipe working with carbon nanotube-water nanofluid for cooling of a high heat flux heater. *Heat and Mass Transfer,* 54, pp. 985-997.

ATALLAH, C. et al., 2019. Surface-modified multi-lumen tubular membranes for SAGD-produced water treatment. *Energy & Fuels,* 33(6), pp. 5766-5776.

AUST, U. et al., 2006. Development of microporous ceramic membranes in the system TiO2/ZrO2. *Journal of Membrane Science,* 281(1-2), pp. 463-471.

BAKER, R.W., 2012. *Membrane technology and applications.* John Wiley & Sons.

BANERJEE, S., DIONYSIOU, D.D. and PILLAI, S.C., 2015. Self-cleaning applications of TiO2 by photo-induced hydrophilicity and photocatalysis. *Applied Catalysis B: Environmental,* 176, pp. 396-428.

BARATI, N., HUSEIN, M.M. and AZAIEZ, J., 2021. Modifying ceramic membranes with in situ grown iron oxide nanoparticles and their use for oily water treatment. *Journal of Membrane Science,* 617, pp. 118641.

BARATI, N., HUSEIN, M.M. and AZAIEZ, J., 2022. Ceramic membranes with in situ doped iron oxide nanoparticles for enhancement of antifouling characteristics and organic removal. *Environmental Science: Water Research & Technology,* 8(12), pp. 2856-2872.

BARBOSA, T. et al., 2020. Synthesis and application of a composite NaA zeolite/gamma-alumina membrane for oil-water separation process. *Cerâmica,* 66, pp. 137-144.

BARDHAN, A. and SUBBIAH, S., 2022. Polymer-based microfiltration/ultrafiltration membranes. *Advancement in Polymer-Based Membranes for Water Remediation.* Elsevier. pp. 43-80.

BASUMATARY, A.K. et al., 2017. Removal of trivalent metal ions from aqueous solution via cross-flow ultrafiltration system using zeolite membranes. *Journal of Water Reuse and Desalination,* 7(1), pp. 66-76.

BAYAT, A. et al., 2016. Preparation and characterization of γ-alumina ceramic ultrafiltration membranes for pretreatment of oily wastewater. *Desalination and Water Treatment,* 57(51), pp. 24322-24332.

BEHNAJADY, M.A., MODIRSHAHLA, N. and HAMZAVI, R., 2006. Kinetic study on photocatalytic degradation of CI Acid Yellow 23 by ZnO photocatalyst. *Journal of hazardous materials,* 133(1-3), pp. 226-232.

BEHROOZI, A.H. and ATAABADI, M.R., 2020. Improvement in microfiltration process of oily wastewater; a comprehensive review over two decades. *Journal of Environmental Chemical Engineering,* , pp. 104981.

BENNETT, M.A. and WILLIAMS, R.A., 2004. Monitoring the operation of an oil/water separator using impedance tomography. *Minerals Engineering,* 17(5), pp. 605-614.

BERK, Z., 2018. *Food process engineering and technology.* Academic press.

BHAVE, R.R., 2014. Chapter 9 - Cross-Flow Filtration. In: H.C. VOGEL and C.M. TODARO, eds. *Fermentation and Biochemical Engineering Handbook (Third Edition).* Boston: William Andrew Publishing. pp. 149-180.

BLUMENSCHEIN, S. et al., 2016. Rejection modeling of ceramic membranes in organic solvent nanofiltration. *Journal of Membrane Science,* 510, pp. 191-200.

BONEKAMP, B.C., 1996. Preparation of asymmetric ceramic membrane supports by dip-coating. *Membrane Science and Technology.* Elsevier. pp. 141-225.

CAI, Y. et al., 2015. Modified colloidal sol–gel process for fabrication of titania nanofiltration membranes with organic additives. *Journal of Membrane Science,* 476, pp. 432-441.

CALCAGNILE, P. et al., 2012. Magnetically driven floating foams for the removal of oil contaminants from water. *ACS nano,* 6(6), pp. 5413-5419.

CHAKRABARTY, B., GHOSHAL, A.K. and PURKAIT, M.K., 2010. Cross-flow ultrafiltration of stable oil-in-water emulsion using polysulfone membranes. *Chemical Engineering Journal,* 165(2), pp. 447-456.

CHANG, Q. et al., 2014a. Application of ceramic microfiltration membrane modified by nano-TiO2 coating in separation of a stable oil-in-water emulsion. *Journal of Membrane Science,* 456, pp. 128-133.

CHANG, Q. et al., 2014b. Application of ceramic microfiltration membrane modified by nano-TiO2 coating in separation of a stable oil-in-water emulsion. *Journal of Membrane Science,* 456, pp. 128-133.

CHANG, Q. et al., 2014c. Application of ceramic microfiltration membrane modified by nano-TiO2 coating in separation of a stable oil-in-water emulsion. *Journal of Membrane Science,* 456, pp. 128-133.

CHANG, Q. et al., 2010a. Hydrophilic modification of Al2O3 microfiltration membrane with nano-sized γ-Al2O3 coating. *Desalination,* 262(1-3), pp. 110-114.

CHANG, Q. et al., 2010b. Hydrophilic modification of Al2O3 microfiltration membrane with nano-sized γ-Al2O3 coating. *Desalination,* 262(1-3), pp. 110-114.

CHEN, H. et al., 2015. Oil–water separation property of polymer-contained wastewater from polymer-flooding oilfields in Bohai Bay, China. *Environmental technology,* 36(11), pp. 1373-1380.

CHEN, M., HEIJMAN, S.G. and RIETVELD, L.C., 2021. State-of-the-art ceramic membranes for oily wastewater treatment: Modification and application. *Membranes,* 11(11), pp. 888.

CHEN, M. et al., 2020. Highly permeable silicon carbide-alumina ultrafiltration membranes for oil-in-water filtration produced with low-pressure chemical vapor deposition. *Separation and purification technology,* 253, pp. 117496.

CHEN, X. et al., 2012. Ceramic pore channels with inducted carbon nanotubes for removing oil from water. *ACS Applied Materials & Interfaces,* 4(4), pp. 1909-1918.

CHINNAM, J. et al., 2015. Measurements of the contact angle of nanofluids and development of a new correlation. *International Communications in Heat and Mass Transfer,* 62, pp. 1-12.

CHOWDHURY, S.R. et al., 2003. Pore size and surface chemistry effects on the transport of hydrophobic and hydrophilic solvents through mesoporous γ-alumina and silica MCM-48. *Journal of Membrane Science,* 225(1-2), pp. 177-186.

CHUNG, Y.T. et al., 2017. Development of polysulfone-nanohybrid membranes using ZnO-GO composite for enhanced antifouling and antibacterial control. *Desalination,* 402, pp. 123-132.

COMNINELLIS, C. et al., 2008. Advanced oxidation processes for water treatment: advances and trends for R&D. *Journal of Chemical Technology &*

Biotechnology: International Research in Process, Environmental & Clean Technology, 83(6), pp. 769-776.

CUI, J. et al., 2008. Preparation and application of zeolite/ceramic microfiltration membranes for treatment of oil contaminated water. *Journal of Membrane Science,* 325(1), pp. 420-426.

DA, X. et al., 2016. Preparation of zirconia nanofiltration membranes through an aqueous sol–gel process modified by glycerol for the treatment of wastewater with high salinity. *Journal of Membrane Science,* 504, pp. 29-39.

DAVIES, T.E. et al., 2022. Experimental methods in chemical engineering: Scanning electron microscopy and X-ray ultra-microscopy—SEM and XuM. *The Canadian Journal of Chemical Engineering,* 100(11), pp. 3145-3159.

DE GUZMAN, M.R. et al., 2021. Increased performance and antifouling of mixed-matrix membranes of cellulose acetate with hydrophilic nanoparticles of polydopamine-sulfobetaine methacrylate for oil-water separation. *Journal of Membrane Science,* 620, pp. 118881.

DE MELO, W. et al., 2022. Microfiltration of Oil-in-water Emulsion Using Modified Ceramic Membrane: Surface Properties, Membrane Resistance, Critical Flux, and Cake Behavior. *Materials research (São Carlos, São Paulo, Brazil); Mat.Res,* 25, pp. 1.

DENG, W. et al., 2019. Efficient oil/water separation by a durable underwater superoleophobic mesh membrane with TiO2 coating via biomineralization. *Separation and Purification Technology,* 222, pp. 35-44.

DHINESHKUMAR, V. and RAMASAMY, D., 2017. Review on membrane technology applications in food and dairy processing. *J.Appl.Biotechnol.Bioeng,* 3, pp. 399-407.

DULIC, Z. et al., 2010. Water quality in semi-intensive carp production system using three different feeds. *Bulg J Agric Sci,* 16(3), pp. 266-274.

EBRAHIMI, M. et al., 2010. Investigations on the use of different ceramic membranes for efficient oil-field produced water treatment. *Desalination,* 250(3), pp. 991-996.

ECSEDI, Z., LAZĂU, I. and PĂCURARIU, C., 2007. Synthesis of mesoporous alumina using polyvinyl alcohol template as porosity control additive. *Processing and Application of Ceramics,* 1(1-2), pp. 5-9.

ELMA, M. et al., 2013a. Performance and long term stability of mesoporous silica membranes for desalination. *Membranes,* 3(3), pp. 136-150.

ELMA, M. et al., 2013b. Performance and long term stability of mesoporous silica membranes for desalination. *Membranes,* 3(3), pp. 136-150.

ELMOBARAK, W.F. and ALMOMANI, F., 2021. Application of Fe3O4 magnetite nanoparticles grafted in silica (SiO2) for oil recovery from oil in water emulsions. *Chemosphere,* 265, pp. 129054.

ENGINEERING, A.C. et al., 1992. The treatment of oily water by coalescing. *Filtration & Separation,* 29(4), pp. 295-300.

FAIBISH, R.S. and COHEN, Y., 2001a. Fouling and rejection behavior of ceramic and polymer-modified ceramic membranes for ultrafiltration of oil-in-water emulsions and microemulsions. *Colloids and Surfaces A: Physicochemical and Engineering Aspects,* 191(1-2), pp. 27-40.

FAIBISH, R.S. and COHEN, Y., 2001b. Fouling-resistant ceramic-supported polymer membranes for ultrafiltration of oil-in-water microemulsions. *Journal of Membrane Science,* 185(2), pp. 129-143.

FAKHRU'L-RAZI, A., PENDASHTEH, A., ABDULLAH, L.C., BIAK, D.R.A., MADAENI, S.S. and ABIDIN, Z.Z., *Review of technologies for oil and gas produced water treatment.*

FANG, J. et al., 2013. Elaboration of new ceramic membrane from spherical fly ash for microfiltration of rigid particle suspension and oil-in-water emulsion. *Desalination,* 311, pp. 113-126.

FENG, L. et al., 2004. A super-hydrophobic and super-oleophilic coating mesh film for the separation of oil and water. *Angewandte Chemie,* 116(15), pp. 2046-2048.

FUJISHIMA, A. and HONDA, K., 1972. Electrochemical photolysis of water at a semiconductor electrode. *Nature,* 238(5358), pp. 37-38.

GAO, Y. et al., 2022. Enhancement of super-hydrophilic/underwater super-oleophobic performance of ceramic membrane with TiO2 nanowire array prepared via low temperature oxidation. *Ceramics International,* 48(7), pp. 9426-9433.

GE, F. et al., 2012. Effective removal of heavy metal ions Cd2 , Zn2 , Pb2 , Cu2 from aqueous solution by polymer-modified magnetic nanoparticles. *Journal of hazardous materials,* 211, pp. 366-372.

GEISE, G.M. et al., 2010. Water purification by membranes: the role of polymer science. *Journal of Polymer Science Part B: Polymer Physics,* 48(15), pp. 1685-1718.

GEORGE, S.M., YOON, B. and DAMERON, A.A., 2009. Surface chemistry for molecular layer deposition of organic and hybrid organic– inorganic polymers. *Accounts of Chemical Research,* 42(4), pp. 498-508.

GIRARD, B. and FUKUMOTO, L.R., 2000. Membrane processing of fruit juices and beverages: a review. *Critical Reviews in Food Science Nutrition,* 40(2), pp. 91-157.

GIRI, S. and QIU, Z., 2016. Understanding the relationship of land uses and water quality in Twenty First Century: A review. *Journal of environmental management,* 173, pp. 41-48.

GOBINA, E., 2006. No title. *Apparatus and method for separating gases,*

GOEI, R. and LIM, T., 2014. Asymmetric TiO2 hybrid photocatalytic ceramic membrane with porosity gradient: Effect of structure directing agent on the resulting membranes architecture and performances. *Ceramics International,* 40(5), pp. 6747-6757.

GOHARI, R.J. et al., 2015. A novel super-hydrophilic PSf/HAO nanocomposite ultrafiltration membrane for efficient separation of oil/water emulsion. *Separation and purification technology,* 150, pp. 13-20.

GRIGORAS, K., AIRAKSINEN, V. and FRANSSILA, S., 2009. Coating of nanoporous membranes: atomic layer deposition versus sputtering. *Journal of nanoscience and nanotechnology,* 9(6), pp. 3763-3770.

GUAN, K. et al., 2020. Controlling the formation of porous polyketone membranes via a cross-linkable alginate additive for oil-in-water emulsion separations. *Journal of Membrane Science,* 611, pp. 118362.

GUESH, K. et al., 2016. Enhanced photocatalytic activity of TiO2 supported on zeolites tested in real wastewaters from the textile industry of Ethiopia. *Microporous and Mesoporous Materials,* 225, pp. 88-97.

GUILLON, O., WEILER, L. and RÖDEL, J., 2007. Anisotropic microstructural development during the constrained sintering of dip-coated alumina thin films. *Journal of the American Ceramic Society,* 90(5), pp. 1394-1400.

GUIZARD, C., RAMBAULT, D. and COT, L., 1994. No title. *Deasphalting of a long residue using ultrafiltration inorganic membranes,*

GUIZARD, C., 1996. Sol-gel chemistry and its application to porous membrane processing. *Membrane Science and Technology.* Elsevier. pp. 227-258.

GUPTA, R.K. et al., 2017. Oil/water separation techniques: a review of recent progresses and future directions. *Journal of Materials Chemistry A,* 5(31), pp. 16025-16058.

GWAK, G., KIM, D.I. and HONG, S., 2020. Draw solutes for FO: Model, polymer hydrogels, and nanoparticles. *Current Trends and Future Developments on (Bio-) Membranes,* , pp. 37-56.

HE, Z. et al., 2019. Ceramic-based membranes for water and wastewater treatment. *Colloids and Surfaces A: Physicochemical and Engineering Aspects,* 578, pp. 123513.

HENDREN, Z.D., BRANT, J. and WIESNER, M.R., 2009. Surface modification of nanostructured ceramic membranes for direct contact membrane distillation. *Journal of Membrane Science,* 331(1-2), pp. 1-10.

HILAL, N. et al., 2004. A comprehensive review of nanofiltration membranes: Treatment, pretreatment, modelling, and atomic force microscopy. *Desalination,* 170(3), pp. 281-308.

HOFS, B. et al., 2011. Comparison of ceramic and polymeric membrane permeability and fouling using surface water. *Separation and Purification Technology,* 79(3), pp. 365-374.

HONG, J. and HE, Y., 2012. Effects of nano sized zinc oxide on the performance of PVDF microfiltration membranes. *Desalination,* 302, pp. 71-79.

HOSSEINI, A.A. et al., 2011. Fabrication and characterization of high performance ceramic membrane having nanometer pores. *Iranian Journal of Materials Science & Engineering,* 8(3),

HSIEH, H.P., BHAVE, R.R. and FLEMING, H.L., 1988. Microporous alumina membranes. *Journal of Membrane Science,* 39(3), pp. 221-241.

HUANG, A. and YANG, W., 2007. Hydrothermal synthesis of uniform and dense NaA zeolite membrane in the electric field. *Microporous and mesoporous materials,* 102(1-3), pp. 58-69.

HUANG, S., RAS, R.H. and TIAN, X., 2018. Antifouling membranes for oily wastewater treatment: Interplay between wetting and membrane fouling. *Current opinion in colloid & interface science,* 36, pp. 90-109.

HUBADILLAH, S.K. et al., 2019. Hydrophobic ceramic membrane for membrane distillation: A mini review on preparation, characterization, and applications. *Separation and Purification Technology,* 217, pp. 71-84.

IDRIS, A.M. and EL-ZAHHAR, A.A., 2019. Indicative properties measurements by SEM, SEM-EDX and XRD for initial homogeneity tests of new certified reference materials. *Microchemical journal,* 146, pp. 429-433.

IGUNNU, E.T. and CHEN, G.Z., 2014. Produced water treatment technologies. *International Journal of Low-Carbon Technologies,* 9(3), pp. 157-177.

IMAMURA, K. et al., 2013. Stoichiometric production of aminobenzenes and ketones by photocatalytic reduction of nitrobenzenes in secondary alcoholic suspension of titanium (IV) oxide under metal-free conditions. *Applied Catalysis B: Environmental,* 134, pp. 193-197.

ISHAK, N.F. et al., 2017. Recent progress in the hydrophilic modification of alumina membranes for protein separation and purification. *Ceramics International,* 43(1), pp. 915-925.

ISMAIL, N.J. et al., 2020. Hydrothermal synthesis of TiO2 nanoflower deposited on bauxite hollow fibre membrane for boosting photocatalysis of bisphenol A. *Journal of Water Process Engineering,* 37, pp. 101504.

JAMALLUDIN, M.R. et al., 2016. Antifouling polysulfone membranes blended with green SiO2 from rice husk ash (RHA) for humic acid separation. *Chemical Engineering Research and Design,* 114, pp. 268-279.

JANOTTI, A. and VAN DE WALLE, C.G., 2009. Fundamentals of zinc oxide as a semiconductor. *Reports on progress in physics,* 72(12), pp. 126501.

JIANG, Y. et al., 2007. Sub-10 nm thick microporous membranes made by plasma-defined atomic layer deposition of a bridged silsesquioxane precursor. *Journal of the American Chemical Society,* 129(50), pp. 15446-15447.

JUDD, S., 2010. *The MBR book: Principles and applications of membrane bioreactors for water and wastewater treatment.* Elsevier.

JUNG, Y. et al., 2008. Synthesis of alumina–titania solid solution by sol–gel method. *Journal of Physics and Chemistry of Solids,* 69(5-6), pp. 1464-1467.

KAFLE, B.P., 2020. Chapter 2 - Theory and instrumentation of absorption spectroscopy: UV–VIS spectrophotometry and colorimetry. In: B.P. KAFLE, ed. *Chemical Analysis and Material Characterization by Spectrophotometry.* Elsevier. pp. 17-38.

KANG, L. et al., 2019. A new architecture of super-hydrophilic β-SiAlON/graphene oxide ceramic membrane for enhanced anti-fouling and separation of water/oil emulsion. *Ceramics International,* 45(13), pp. 16717-16721.

KAUR, G., SINGH, H. and SINGH, J., 2021. Chapter 2 - UV-vis spectrophotometry for environmental and industrial analysis. In: INAMUDDIN, R. BODDULA and A.M. ASIRI, eds. *Green Sustainable Process for Chemical and Environmental Engineering and Science.* Elsevier. pp. 49-68.

KAYVANI FARD, A. et al., 2018. Inorganic membranes: Preparation and application for water treatment and desalination. *Materials,* 11(1), pp. 74.

KAZEMI, F. et al., 2021. Oil-in-water emulsion separation by PVC membranes embedded with GO-ZnO nanoparticles. *Journal of Environmental Chemical Engineering,* 9(1), pp. 104992.

KAZEMIMOGHADAM, M., 2010. New nanopore zeolite membranes for water treatment. *Desalination,* 251(1-3), pp. 176-180.

KEMELL, M. et al., 2008. Surface modification of thermoplastics by atomic layer deposition of Al2O3 and TiO2 thin films. *European Polymer Journal,* 44(11), pp. 3564-3570.

KHADER, E.H. et al., 2022. Removal of organic pollutants from produced water by batch adsorption treatment. *Clean Technologies and Environmental Policy,* 24(2), pp. 713-720.

KHAN, J.A. et al., 2019. Influence of alkali-surfactant-polymer flooding on the coalescence and sedimentation of oil/water emulsion in gravity separation. *Journal of Petroleum Science and Engineering,* 173, pp. 640-649.

KHATIB, S.J. and OYAMA, S.T., 2013. Silica membranes for hydrogen separation prepared by chemical vapor deposition (CVD). *Separation and Purification Technology,* 111, pp. 20-42.

KONG, J. and LI, K., 1999. Oil removal from oil-in-water emulsions using PVDF membranes. *Separation and purification technology,* 16(1), pp. 83-93.

KRAJEWSKI, S.R. et al., 2006. Application of fluoroalkylsilanes (FAS) grafted ceramic membranes in membrane distillation process of NaCl solutions. *Journal of Membrane Science,* 281(1-2), pp. 253-259.

KREBS, T., SCHROËN, C. and BOOM, R.M., 2012. Separation kinetics of an oil-in-water emulsion under enhanced gravity. *Chemical Engineering Science,* 71, pp. 118-125.

KRISTENSEN, P. et al., 2018. European waters assessment of status and pressures 2018. *EEA Report,* (7/2018),

KRIŽAN MILIĆ, J. et al., 2013. Recent developments in membrane treatment of spent cutting-oils: a review. *Industrial & Engineering Chemistry Research,* 52(23), pp. 7603-7616.

KUCHEYEV, S.O. et al., 2008. Mechanisms of atomic layer deposition on substrates with ultrahigh aspect ratios. *Langmuir,* 24(3), pp. 943-948.

KUNDU, P. and MISHRA, I.M., 2019. Treatment and reclamation of hydrocarbon-bearing oily wastewater as a hazardous pollutant by different processes and technologies: A state-of-the-art review. *Reviews in Chemical Engineering,* 35(1), pp. 73-108.

LAFUMA, A. and QUÉRÉ, D., 2003. Superhydrophobic states. *Nature materials,* 2(7), pp. 457-460.

LEE, S. et al., 2009. Greatly increased toughness of infiltrated spider silk. *Science,* 324(5926), pp. 488-492.

LI, C. et al., 2020. Ceramic nanocomposite membranes and membrane fouling: A review. *Water research,* 175, pp. 115674.

LI, F. et al., 2012. Modification of ceramic membranes for pore structure tailoring: The atomic layer deposition route. *Journal of Membrane Science,* 397, pp. 17-23.

LI, K., 2007. *Ceramic membranes for separation and reaction.* John Wiley & Sons.

LI, L. et al., 2009. Recovery of linseed oil dispersed within an oil-in-water emulsion using hydrophilic membrane by rotating disk filtration system. *Journal of Membrane Science,* 342(1-2), pp. 70-79.

LIANG, X. et al., 2010. Modification of nanoporous supported lyotropic liquid crystal polymer membranes by atomic layer deposition. *Journal of Membrane Science,* 349(1-2), pp. 1-5.

LIU, C. et al., 2021. Multifunctional CNTs-PAA/MIL101(Fe)@Pt Composite Membrane for High-throughput Oily Wastewater Remediation. *Journal of hazardous materials,* 403, pp. 123547.

LIU, L., LUO, X., DING, L. and LUO, S., 2019. 4 - Application of Nanotechnology in the Removal of Heavy Metal From Water. In: X. LUO and F. DENG, eds. *Nanomaterials for the Removal of Pollutants and Resource Reutilization.* Elsevier. pp. 83-147.

LIU, R. et al., 2018. Inorganic microfiltration membranes incorporated with hydrophilic silica nanoparticles for oil-in-water emulsion separation. *Journal of water process engineering,* 26, pp. 124-130.

LIU, W. et al., 2020. A novel smart coating with ammonia-induced switchable superwettability for oily wastewater treatment. *Journal of Environmental Chemical Engineering,* 8(5), pp. 104164.

LIU, Z. et al., 2017. A review on cleaning of nanofiltration and reverse osmosis membranes used for water treatment. *Desalination and Water Treatment,* 87, pp. 27-67.

LOI, C.C., EYRES, G.T. and BIRCH, E.J., 2019. Effect of mono-and diglycerides on physical properties and stability of a protein-stabilised oil-in-water emulsion. *Journal of Food Engineering,* 240, pp. 56-64.

LONSDALE, H.K., MERTEN, U. and RILEY, R.L., 1965. Transport properties of cellulose acetate osmotic membranes. *Journal of Applied Polymer Science,* 9(4), pp. 1341-1362.

LU, C., BAO, Y. and HUANG, J., 2021. Fouling in membrane filtration for juice processing. *Current Opinion in Food Science,* 42, pp. 76-85.

LU, D. et al., 2016. Hydrophilic Fe2O3 dynamic membrane mitigating fouling of support ceramic membrane in ultrafiltration of oil/water emulsion. *Separation and Purification Technology,* 165, pp. 1-9.

LU, D. et al., 2016. Influence of surface properties of filtration-layer metal oxide on ceramic membrane fouling during ultrafiltration of oil/water emulsion. *Environmental science & technology,* 50(9), pp. 4668-4674.

LU, H. et al., 2016. An overview of nanomaterials for water and wastewater treatment. *Advances in Materials Science and Engineering,* 2016

LUAN, W. et al., 2022. Effective construction of anti-fouling zwitterion-functionalized ceramic membranes for separation of oil-in-water emulsion based on PDA/PEI co-deposition. *Journal of Environmental Chemical Engineering,* 10(5), pp. 108396.

MA, Y., KANEZASHI, M. and TSURU, T., 2010. Preparation of organic/inorganic hybrid silica using methyltriethoxysilane and tetraethoxysilane as co-precursors. *Journal of Sol-Gel Science and Technology,* 53, pp. 93-99.

MADDELA, N.R. and TORRES, R.O.V., 2021. The presence of low fouling-causing bacteria can lead to decreased membrane fouling potentials of mixed cultures. *Journal of Environmental Chemical Engineering,* 9(2), pp. 105131.

MAGALHÃES, E.R. et al., 2021. Activated sludge treatment for promoting the reuse of a synthetic produced water in irrigation. *Journal of Environmental Science and Health, Part B,* 56(2), pp. 132-141.

MAGALHÃES, H., DE LIMA, A.G.B., DE FARIAS NETO, S.R., DE ALMEIDA, A.F., DE ANDRADE, T. and BRANDÃO, V., 2018a. Ceramic Membranes: Theory and Engineering Applications. *Transport Phenomena in Multiphase Systems.* Springer. pp. 111-137.

MAGALHÃES, H., DE LIMA, A.G.B., DE FARIAS NETO, S.R., DE ALMEIDA, A.F., DE ANDRADE, T. and BRANDÃO, V., 2018b. Ceramic Membranes: Theory and Engineering Applications. *Transport Phenomena in Multiphase Systems.* Springer. pp. 111-137.

MAGUIRE-BOYLE, S.J. and BARRON, A.R., 2011. A new functionalization strategy for oil/water separation membranes. *Journal of Membrane Science,* 382(1-2), pp. 107-115.

MAHLANGU, O.T. et al., 2017. Development of hydrophilic GO-ZnO/PES membranes for treatment of pharmaceutical wastewater. *Water Science and Technology,* 76(3), pp. 501-514.

MANJUMOL, K.A. et al., 2016. A novel approach to formulate high flux multifunctional ultrafiltration membranes from photocatalytic titania composite precursors on multi-channel tubular substrates. *RSC advances,* 6(63), pp. 58813-58822.

MATINDI, C.N. et al., 2021. Tailoring the morphology of polyethersulfone/sulfonated polysulfone ultrafiltration membranes for highly efficient separation of oil-in-water emulsions using TiO2 nanoparticles. *Journal of Membrane Science,* 620, pp. 118868.

MAVUKKANDY, M.O. et al., 2020. Thin film deposition techniques for polymeric membranes–A review. *Journal of Membrane Science,* 610, pp. 118258.

MAZUMDER, D. and MUKHERJEE, S., 2011. Treatment of automobile service station wastewater by coagulation and activated sludge process. *International Journal of Environmental Science and Development,* 2(1), pp. 64.

MEDINA-LLAMAS, M. et al., 2020. Continuous production of metal oxide nanoparticles via membrane emulsification–precipitation. *Industrial & Engineering Chemistry Research,* 59(19), pp. 9085-9094.

MENDONÇA, E.T. et al., 2017. Evaluation of produced water treatment using advanced oxidation processes and sodium ferrate (VI). *International Journal of Chemical and Molecular Engineering,* 11(2), pp. 135-140.

MENG, T. et al., 2013. Nano-structure construction of porous membranes by depositing nanoparticles for enhanced surface wettability. *Journal of Membrane Science,* 427, pp. 63-72.

MILIĆ, J.K. et al., 2014. Ultrafiltration of oil-in-water emulsion by using ceramic membrane: Taguchi experimental design approach. *Central European Journal of Chemistry,* 12, pp. 242-249.

MILLER, D.J. et al., 2017. Surface modification of water purification membranes. *Angewandte Chemie International Edition,* 56(17), pp. 4662-4711.

MOATMED, S.M. et al., 2019. Highly efficient and reusable superhydrophobic/superoleophilic polystyrene@ Fe3O4 nanofiber membrane for high-performance oil/water separation. *Journal of Environmental Chemical Engineering,* 7(6), pp. 103508.

MOHAMMAD, A.W. et al., 2015. Nanofiltration membranes review: Recent advances and future prospects. *Desalination,* 356, pp. 226-254.

MONASH, P. and PUGAZHENTHI, G., 2011a. Effect of TiO2 addition on the fabrication of ceramic membrane supports: A study on the separation of oil droplets and bovine serum albumin (BSA) from its solution. *Desalination,* 279(1-3), pp. 104-114.

MONASH, P. and PUGAZHENTHI, G., 2011b. Effect of TiO2 addition on the fabrication of ceramic membrane supports: A study on the separation of oil droplets and bovine serum albumin (BSA) from its solution. *Desalination,* 279(1-3), pp. 104-114.

MONASH, P. and PUGAZHENTHI, G., 2011. Development of ceramic supports derived from low-cost raw materials for membrane applications and its optimization based on sintering temperature. *International Journal of Applied Ceramic Technology,* 8(1), pp. 227-238.

MOTTERN, M.L. et al., 2008. Permeation porometry: Effect of probe diffusion in the condensate. *Journal of Membrane Science,* 313(1-2), pp. 2-8.

MOTUZAS, J. et al., 2018. Novel inorganic membrane for the percrystallization of mineral, food and pharmaceutical compounds. *Journal of Membrane Science,* 550, pp. 407-415.

MULDER, M. and MULDER, J., 1996. *Basic principles of membrane technology.* Springer science & business media.

NADY, N. et al., 2011. Modification methods for poly (arylsulfone) membranes: A mini-review focusing on surface modification. *Desalination,* 275(1-3), pp. 1-9.

NAGASAWA, H. et al., 2020. Filtration of surfactant-stabilized oil-in-water emulsions with porous ceramic membranes: Effects of membrane pore size and surface charge on fouling behavior. *Journal of Membrane Science,* 610, pp. 118210.

NAIR, B.N. et al., 1997. Sol-gel synthesis of molecular sieving silica membranes. *Journal of Membrane Science,* 135(2), pp. 237-243.

NANDI, B.K. et al., 2010. Treatment of oily wastewater using low cost ceramic membrane: Comparative assessment of pore blocking and artificial neural network models. *Chemical Engineering Research and Design,* 88(7), pp. 881-892.

NGUYEN, D.D. et al., 2012. Superhydrophobic and superoleophilic properties of graphene-based sponges fabricated using a facile dip coating method. *Energy & Environmental Science,* 5(7), pp. 7908-7912.

NICHOLAS, N., 2019. Benefits and Disadvantages of the Advanced Oxidation Process. *Genesis Water Technologies,*

O'HARE, D., 2001. Hydrothermal synthesis. *Encyclopedia of Materials: science and Technology,* , pp. 3989-3992.

OTHMAN, M.R., MUKHTAR, H. and AHMAD, A.L., 2004. Gas permeation characteristics across nano-porous inorganic membranes. *IIUM Engineering Journal,* 5(2),

PADAKI, M. et al., 2015. Membrane technology enhancement in oil–water separation. A review. *Desalination,* 357, pp. 197-207.

PAL, P., 2015. *Groundwater arsenic remediation: Treatment technology and scale UP.* Butterworth-Heinemann.

PHAN, H.V. et al., 2016. Biological performance and trace organic contaminant removal by a side-stream ceramic nanofiltration membrane bioreactor. *International Biodeterioration & Biodegradation,* 113, pp. 49-56.

QIN, Y. et al., 2010. Preparation and elastic properties of helical nanotubes obtained by atomic layer deposition with carbon nanocoils as templates. *small,* 6(8), pp. 910-914.

QIN, Y. et al., 2008. Rayleigh-instability-induced metal nanoparticle chains encapsulated in nanotubes produced by atomic layer deposition. *Nano letters,* 8(1), pp. 114-118.

QIU, Z. et al., 2020. Fabrication of dynamic zero-valent iron/MnO2 nanowire membrane for efficient and recyclable selenium separation. *Separation and Purification Technology,* 230, pp. 115847.

RABIEE, H. et al., 2015. Improvement in flux and antifouling properties of PVC ultrafiltration membranes by incorporation of zinc oxide (ZnO) nanoparticles. *Separation and purification technology,* 156, pp. 299-310.

RAMISETTY, K.A., PANDIT, A.B. and GOGATE, P.R., 2014. Novel approach of producing oil in water emulsion using hydrodynamic cavitation reactor. *Industrial & Engineering Chemistry Research,* 53(42), pp. 16508-16515.

RAN, J. et al., 2013. Experimental investigation and modeling of flotation column for treatment of oily wastewater. *International Journal of Mining Science and Technology,* 23(5), pp. 665-668.

RASHAD, M. et al., 2021. A novel monolithic mullite microfiltration membrane for oil-in-water emulsion separation. *Journal of Membrane Science,* 620, pp. 118857.

RAWAL, S.B. et al., 2013. Design of visible-light photocatalysts by coupling of narrow bandgap semiconductors and TiO 2: effect of their relative energy band positions on the photocatalytic efficiency. *Catalysis science & technology,* 3(7), pp. 1822-1830.

REZAKAZEMI, M. et al., 2018. Fouling-resistant membranes for water reuse. *Environmental Chemistry Letters,* 16(3), pp. 715-763.

SADEGHIAN, Z., ZAMANI, F. and ASHRAFIZADEH, S.N., 2010. Removal of oily hydrocarbon contaminants from wastewater by γ-alumina nanofiltration membranes. *Desalination and Water Treatment,* 20(1-3), pp. 80-85.

SADHUKHAN, J. et al., 2016. A critical review of integration analysis of microbial electrosynthesis (MES) systems with waste biorefineries for the production of biofuel and chemical from reuse of CO2. *Renewable and Sustainable Energy Reviews,* 56, pp. 116-132.

SAHA, L. and BAUDDH, K., 2021. Characteristics of mining spoiled and oil drilling sites and adverse impacts of these activities on the environment and human health. *Phytorestoration of Abandoned Mining and Oil Drilling Sites.* Elsevier. pp. 87-101.

SALHI, B. et al., 2022. High flux polyaniline-coated ceramic membrane for effective separation of emulsified oil-in-water. *Ceramics International,* 48(17), pp. 25246-25253.

SANTOS, T.M. et al., 2020. Synthesis of activated carbon from oleifera moringa for removal of oils and greases from the produced water. *Environmental Nanotechnology, Monitoring & Management,* 14, pp. 100357.

SCHMIDT-MENDE, L. and MACMANUS-DRISCOLL, J.L., 2007. ZnO–nanostructures, defects, and devices. *Materials today,* 10(5), pp. 40-48.

SCHMIDTS, T. et al., 2012. Required HLB determination of some pharmaceutical oils in submicron emulsions. *Journal of Dispersion Science and Technology,* 33(6), pp. 816-820.

SCHULLER, P. et al., 2020. A lab-on-a-chip system with an embedded porous membrane-based impedance biosensor array for nanoparticle risk assessment on placental Bewo trophoblast cells. *Sensors and Actuators B: Chemical,* 312, pp. 127946.

SCIENTIFIC, B., 2018. Contact Angle| Measurements| Biolin Scientific. *Contact Angle*| *Measurements*| *Biolin Scientific,*

SENAPATI, S. and MAITI, P., 2020. Emerging bio-applications of two-dimensional nanoheterostructure materials. *2D nanoscale heterostructured materials.* Elsevier. pp. 243-255.

SERIES—PERFORMANCE, M.Z.N. and SIMPLICITY, V., No title. *Malvern Instruments Ltd.2014,*

SHAIKHIEV, I. et al. , 2019. Modification of polymeric membranes with unipolar corona discharge to intensify the separation of oil-in-water emulsions. *IOP conference series: Materials science and engineering.* 2019. IOP Publishing, pp. 012031.

SHI, L. et al., 2019a. Ultrafiltration of oil-in-water emulsions using ceramic membrane: Roles played by stabilized surfactants. *Colloids and Surfaces A: Physicochemical and Engineering Aspects,* 583, pp. 123948.

SHI, L. et al., 2019b. Ultrafiltration of oil-in-water emulsions using ceramic membrane: Roles played by stabilized surfactants. *Colloids and Surfaces A: Physicochemical and Engineering Aspects,* 583, pp. 123948.

SMART, S., LIU, S., SERRA, J.M., DA COSTA, J.D., IULIANELLI, A. and BASILE, A., 2013. Porous ceramic membranes for membrane reactors. *Handbook of Membrane Reactors.* Elsevier. pp. 298-336.

SONG, C. et al., 2006. Preparation of coal-based microfiltration carbon membrane and application in oily wastewater treatment. *Separation and Purification Technology,* 51(1), pp. 80-84.

STEWART, M. and ARNOLD, K., 2011. *Produced water treatment field manual.* Gulf Professional Publishing.

SU, C. et al., 2012. Porous ceramic membrane with superhydrophobic and superoleophilic surface for reclaiming oil from oily water. *Applied Surface Science,* 258(7), pp. 2319-2323.

SUN, Y. et al., 2017. Characterization and coagulation behavior of polymeric aluminum ferric silicate for high-concentration oily wastewater treatment. *Chemical Engineering Research and Design,* 119, pp. 23-32.

SURESH, K. and KATARA, N., 2021. Design and development of circular ceramic membrane for wastewater treatment. *Materials Today: Proceedings,* 43, pp. 2176-2181.

SURESH, K. and PUGAZHENTHI, G., 2016. Development of ceramic membranes from low-cost clays for the separation of oilâ€"water emulsion. *Desalination and Water Treatment,* 57(5), pp. 1927-1939.

SURESH, K. and PUGAZHENTHI, G., 2017. Cross flow microfiltration of oil-water emulsions using clay based ceramic membrane support and TiO2 composite membrane. *Egyptian journal of petroleum,* 26(3), pp. 679-694.

SURESH, K. et al., 2016. Preparation and characterization of TiO 2 and γ-Al 2 O 3 composite membranes for the separation of oil-in-water emulsions. *RSC advances,* 6(6), pp. 4877-4888.

SYARIFAH NAZIRAH, W.I. et al., 2017. A review of oilfield wastewater treatment using membrane filtration over conventional technology Malaysian J. *Anal.Sci,* 21, pp. 643-658.

TEH, C.Y., WU, T.Y. and JUAN, J.C., 2014. Optimization of agro-industrial wastewater treatment using unmodified rice starch as a natural coagulant. *Industrial Crops and Products,* 56, pp. 17-26.

TIAN, M., LIAO, Y. and WANG, R., 2020. Engineering a superwetting thin film nanofibrous composite membrane with excellent antifouling and self-cleaning properties to separate surfactant-stabilized oil-in-water emulsions. *Journal of Membrane Science,* 596, pp. 117721.

TIMOTEO JÚNIOR, J.F., 2007. No title. *Anodização para obtenção de membranas cerâmicas,*

TONG, T. and ELIMELECH, M., 2016. The global rise of zero liquid discharge for wastewater management: drivers, technologies, and future directions. *Environmental science & technology,* 50(13), pp. 6846-6855.

TUL MUNTHA, S., KAUSAR, A. and SIDDIQ, M., 2017. Advances in polymeric nanofiltration membrane: A review. *Polymer-Plastics Technology and Engineering,* 56(8), pp. 841-856.

UROŠEVIĆ, T. and TRIVUNAC, K., 2020. Achievements in low-pressure membrane processes microfiltration (MF) and ultrafiltration (UF) for wastewater

and water treatment. *Current Trends and Future Developments on (Bio-) Membranes.* Elsevier. pp. 67-107.

USMAN, J. et al., 2021. An overview of superhydrophobic ceramic membrane surface modification for oil-water separation. *Journal of Materials Research and Technology,* 12, pp. 643-667.

USMAN, M.R., CHE 611 Advanced Chemical Reaction Engineering.

VAN GESTEL, T. et al., 2002. Alumina and titania multilayer membranes for nanofiltration: preparation, characterization and chemical stability. *Journal of Membrane Science,* 207(1), pp. 73-89.

VARJANI, S. et al., 2020. Treatment of wastewater from petroleum industry: current practices and perspectives. *Environmental Science and Pollution Research,* 27, pp. 27172-27180.

VINOTH KUMAR, R., MONASH, P. and PUGAZHENTHI, G., 2016. Treatment of oil-in-water emulsion using tubular ceramic membrane acquired from locally available low-cost inorganic precursors. *Desalination and Water Treatment,* 57(58), pp. 28056-28070.

WANG, D. et al., 2020. Techniques for treating slop oil in oil and gas industry: A short review. *Fuel,* 279, pp. 118482.

WANG, F. et al., 2017. Surface modification of alumina membranes via a sol-gel process for antifouling properties. *Materials Letters,* 191, pp. 200-202.

WANG, J., WANG, H. and GENG, G., 2018. Highly efficient oil-in-water emulsion and oil layer/water mixture separation based on durably superhydrophobic sponge prepared via a facile route. *Marine pollution bulletin,* 127, pp. 108-116.

WANG, Z. et al., 2016. Preparation, characterization and solvent resistance of γ-Al2O3/α-Al2O3 inorganic hollow fiber nanofiltration membrane. *Journal of Membrane Science,* 503, pp. 69-80.

WARNER, C.L. et al., 2010. High-Performance, Superparamagnetic, nanoparticle-based heavy metal sorbents for removal of contaminants from natural waters. *ChemSusChem,* 3(6), pp. 749-757.

WIJMANS, J.G. and BAKER, R.W., 1995. The solution-diffusion model: a review. *Journal of Membrane Science,* 107(1-2), pp. 1-21.

XIA, C. et al., 2000. Preparation of yttria stabilized zirconia membranes on porous substrates by a dip-coating process. *Solid State Ionics,* 133(3-4), pp. 287-294.

XU, Y. et al., 2022. Desert beetle-like microstructures bridged by magnetic Fe3O4 grains for enhancing oil-in-water emulsion separation performance and solar-assisted recyclability of graphene oxide. *Chemical Engineering Journal,* 427, pp. 130904.

YANG, C. et al., 1998. Preparation and application in oil–water separation of ZrO2/α-Al2O3 MF membrane. *Journal of Membrane Science,* 142(2), pp. 235-243.

YANG, G. and PARK, S., 2019. Conventional and microwave hydrothermal synthesis and application of functional materials: A review. *Materials,* 12(7), pp. 1177.

YANG, Y. et al., 2022. Potocatalytic antifouling membrane with dense nano-TiO2 coating for efficient oil-in-water emulsion separation and self-cleaning. *Journal of Membrane Science,* 645, pp. 120204.

YANG, Y. et al., 2021. One-step dip-coating method for preparation of ceramic nanofiber membrane with high permeability and low cost. *Journal of the European Ceramic Society,* 41(16), pp. 358-368.

YEO, Z.Y. et al., 2013. Synthesis and performance of microporous inorganic membranes for CO2 separation: a review. *Journal of Porous Materials,* 20(6), pp. 1457-1475.

YI, X.S. et al., 2011. The influence of important factors on ultrafiltration of oil/water emulsion using PVDF membrane modified by nano-sized TiO2/Al2O3. *Desalination,* 281, pp. 179-184.

YI, X.S. et al., 2013. Estimation of fouling stages in separation of oil/water emulsion using nano-particles Al2O3/TiO2 modified PVDF UF membranes. *Desalination,* 319, pp. 38-46.

YOUNG, T., 1805. Phjlo5. 1} ans. *Roy. soc.* 1805. , pp. 65-87.

YOUNKER, J.M. and WALSH, M.E., 2014. Bench-scale investigation of an integrated adsorption–coagulation–dissolved air flotation process for produced water treatment. *Journal of environmental chemical engineering,* 2(1), pp. 692-697.

YU, L., HAN, M. and HE, F., 2017. A review of treating oily wastewater. *Arabian journal of chemistry,* 10, pp. S1913-S1922.

YUAN, Y. and LEE, T.R., 2013. Contact angle and wetting properties. *Surface science techniques.* Springer. pp. 3-34.

ZENG, Y. et al., 2007. Feasibility investigation of oily wastewater treatment by combination of zinc and PAM in coagulation/flocculation. *Journal of hazardous materials,* 147(3), pp. 991-996.

ZHANG, D. et al., 2018. Superhydrophilicity and underwater superoleophobicity TiO2/Al2O3 composite membrane with ultra low oil adhesion for highly efficient oil-in-water emulsions separation. *Applied Surface Science,* 458, pp. 157-165.

ZHANG, F. et al., 2017. Porous superhydrophobic and superoleophilic surfaces prepared by template assisted chemical vapor deposition. *Surface and Coatings Technology,* 315, pp. 385-390.

ZHANG, L. et al., 2019. A comprehensively fouling- and solvent-resistant aliphatic polyketone membrane for high-flux filtration of difficult oil-in-water micro- and nanoemulsions. *Journal of Membrane Science,* 582, pp. 48-58.

ZHANG, L. et al., 2020. Superhydrophilic and underwater superoleophobic Ti foam with robust nanoarray structures of TiO2 for effective oil-in-water emulsion separation. *Separation and Purification Technology,* 252, pp. 117437.

ZHANG, Q., FAN, Y. and XU, N., 2009. Effect of the surface properties on filtration performance of Al2O3–TiO2 composite membrane. *Separation and Purification Technology,* 66(2), pp. 306-312.

ZHANG, S. et al., 2014. Sustainable water recovery from oily wastewater via forward osmosis-membrane distillation (FO-MD). *Water research,* 52, pp. 112-121.

ZHANG, X. et al., 2009. High-performance multifunctional TiO2 nanowire ultrafiltration membrane with a hierarchical layer structure for water treatment. *Advanced Functional Materials,* 19(23), pp. 3731-3736.

ZHAO, S. et al., 2017. Gas field produced/process water treatment using forward osmosis hollow fiber membrane: Membrane fouling and chemical cleaning. *Desalination,* 402, pp. 143-151.

ZHENG, F. et al., 2018. Preparation of bridged silica RO membranes from copolymerization of bis (triethoxysilyl) ethene/(hydroxymethyl) triethoxysilane. Effects of ethenylene-bridge enhancing water permeability. *Journal of Membrane Science,* 546, pp. 173-178.

ZHOU, H. et al., 2022. Porous Al2O3 ceramics with directional gradient pore structure modified by cobweb-bridged WO3 nanowires for oil/water emulsions separation. *Ceramics International,* 48(13), pp. 18753-18764.

ZHOU, J.E. et al. , 2015. Membrane modification of ceramic membrane and its application in separation of waste o/w emulsion. *Advanced materials research.* 2015. Trans Tech Publ, pp. 190-194.

ZHOU, J. et al., 2010. Separation of stable oil–water emulsion by the hydrophilic nano-sized ZrO2 modified Al2O3 microfiltration membrane. *Separation and Purification Technology,* 75(3), pp. 243-248.

ZHU, J., FAN, Y. and XU, N., 2011. Modified dip-coating method for preparation of pinhole-free ceramic membranes. *Journal of Membrane Science,* 367(1-2), pp. 14-20.

ZHU, Y. et al., 2014. Recent progress in developing advanced membranes for emulsified oil/water separation. *NPG Asia Materials,* 6(5), pp. e101.

ZOLFAGHARI, R. et al., 2016. Demulsification techniques of water-in-oil and oil-in-water emulsions in petroleum industry. *Separation and Purification Technology,* 170, pp. 377-407.

ZOU, D. et al., 2019. One step co-sintering process for low-cost fly ash based ceramic microfiltration membrane in oil-in-water emulsion treatment. *Separation and Purification Technology,* 210, pp. 511-520.

ZSIRAI, T. et al., 2016. Ceramic membrane filtration of produced water: Impact of membrane module. *Separation and Purification Technology,* 165, pp. 214-221.

Appendices

Appendix I – Experimental Apparatus

This subsection deals with instruments and apparatus utilized during the process of experiment.

1. Vernier calliper and tape rule: the vernier calliper was required for the inner and outer diameter measurement of the tubular ceramic membrane while the ruler was used to measure the length of the ceramic membrane. The pictures of these apparatus in use are displayed in figure 75.

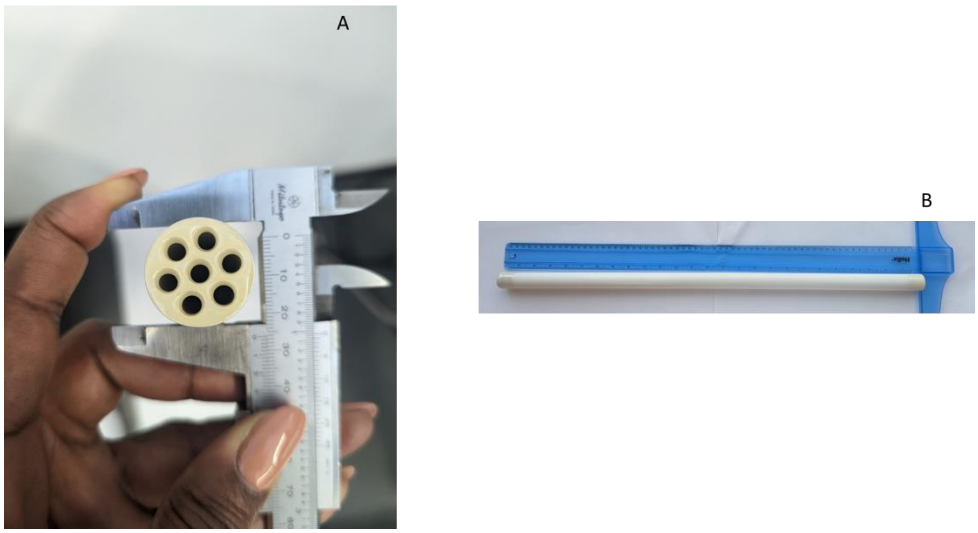

Figure 84: Picture of Vernier calliper (A), and tape rule (B).

2. Weighing balance: these was position at the exit of the reactor to measure the permeate flux during crossflow filtration process. The weighing balance was also used for measurement of ceramic membrane and reagents. The weighing balance image is shown in figure 76.

Figure 85: Picture of weighing scale.

3. Glassware: different glassware like beaker, measuring cylinder and conical flask were all required in this study. For instance, beaker was used to received permeate flux, measuring cylinder was used for the soaking and saturation of ceramic membrane in MgO solution, and conical flasks were used to prepare standard solutions for UV spectrophotometer tests. Images of glassware used are shown in figure 77.

Figure 86: Pictures of glassware: A – measuring cylinder, B- conical flasks, c- beakers.

4. Ultrasonic bath: this was used as a feed tant during cross filtration process to contain pure water or O/W emulsion. It was also used to heat up the liquid inside of it when temperature test was measured. Figure 78 displays the picture of the ultrasonic bath.

Figure 87: Pictures of glassware: A – measuring cylinder, B- conical flasks, c- beakers.

5. Oven: this equipment was used to dry ceramic membranes and glassware at different temperatures. Figure 79 represents the picture of the used oven.

Figure 88: Picture of oven.

6. Furnace: this equipment was used to calcine ceramic membrane after modification to assure the adhesion of the nanoparticles on and in the ceramic membrane. A picture of the furnace used in this research is shown in figure 80.

Figure 89: Picture of furnace.

7. Food Blender: this was used for the homogenization of the synthesized O/W emulsion and the image is shown in Figure 81 below.

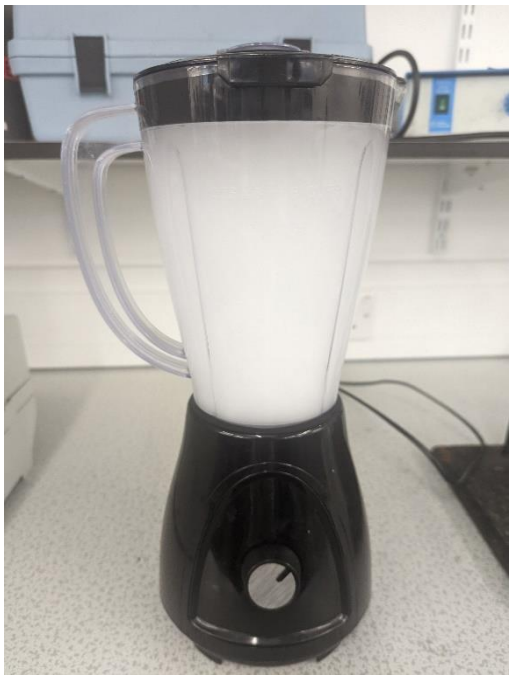

Figure 90: Picture of food blender.

Appendix II – Materials

The materials used in this research involves ceramic membrane support and chemicals or reagents used during the experimental procedure.

1. Ceramic membrane support: ceramic membrane support was purchased from suppliers and used for this research. These ceramic membrane support can be found in varied sizes and are tubular in shape. The are mostly made up of alumina (77%) and titania (23%). Figure 82 displays a representative of tubular ceramic membrane.

Figure 91: Picture of a tubular ceramic membrane.

2. Chemicals: Chemicals were purchased and used especially during membrane modification and O/W emulsion synthesis. These chemicals include:
   i. Manganese (II) Chloride 99% trace metal basis 50g was supplied by Merck in plastic containers with CAS number 7773-01-5. This was used during metal oxide modification of witness samples of ceramic membrane.
   ii. Chromium (III) chloride 98% (RT) 100g was supplied by Merck in plastic containers with CAS number 10060-12-5. This was also used during metal oxide coating of ceramic membrane witness samples.
   iii. Magnesium Chloride in powdered form 100g was purchased from Merck in plastic containers with CAS number 7786-30-3. They were used during modification of ceramic membrane witness samples.
   iv. Ethyl Alcohol pure anhydrous 99.5% 2 litres were purchased from Merck with CAS number 64-17-5. This was used to dissolve and prepare the metal salts solutions.
   v. Span 80 surfactant 250ml was purchased from Merck with CAS number 1338-43-8 for the synthesis of O/W emulsion.

vi. Tween 20 surfactant 500ml was purchased from Merck with CAS number 9005-64-5 and used also for the preparation of O/W emulsion.

vii. Soybean oil was already present in the reagent cabinet in N405 sealed and was used for the preparation of O/W emulsion.

3. Gases: Two gases were used in the research and was supplied by BOC, Aberdeen, United Kingdom. The individual regulators suitable for the gases were also purchased along with the gases although the second gas was in a liquid form and required a specialized container (dewar) for fetch and transfer which was made available.

   i. Hydrogen gas: 99.9% purity, was used during degassing on the Autosorb analyzer for pore size and pore distribution analysis.

   ii. Liquid Nitrogen: 99.9% purity, was used in the same pore size and pore size distribution analysis on Autosorb analiser for characterization processes of the ceramic membrane.

Appendix III – Health and Safety

Risk assessment s and COSHH assessments were carried out every year to keep up to date with the safety procedures necessary for carrying out all experimental work regarding the research in the laboratory. This was assessed and approved by the health and safety co-ordinator. Gas safety training and liquid nitrogen handling in the university was also undertaken to gain competency for using these materials. A sample of both Risk assessment and COSHH assessments are attached to the end of this report.

Appendix IV – Some results

Table 9: Raw data for Unmodified Ceramic Membrane Pure water Flux

Core size: 6000nm							
Water Type: Pure water							
Membrane Name: Unmodified CM							
Temp (20^0)	Flowrate	Pressure (bar)	Weight (kg)	Volume (l)	Area (m2)	Time (h)	Flux (L/m2.H)
20	25	0.10	2.480	2.484	0.027	0.083333	7.6674323
20	25	0.10	2.480	2.484	0.027	0.083333	7.6674323
20	25	0.10	2.480	2.484	0.027	0.083333	7.6674323
20	25	0.10	2.480	2.484	0.027	0.083333	7.6674323
20	25	0.10	2.480	2.484	0.027	0.083333	7.6674323
20	25	0.10	2.480	2.484	0.027	0.083333	7.6674323
20	50	0.30	4.640	4.648	0.027	0.083333	14.345518
20	50	0.30	4.640	4.648	0.027	0.083333	14.345518
20	50	0.30	4.640	4.648	0.027	0.083333	14.345518
20	50	0.30	4.640	4.648	0.027	0.083333	14.345518
20	50	0.30	4.640	4.648	0.027	0.083333	14.345518
20	50	0.30	4.640	4.648	0.027	0.083333	14.345518
50	25	0.10	2.490	2.520	0.027	0.083333	7.7783701
50	25	0.10	2.490	2.520	0.027	0.083333	7.7783701
50	25	0.10	2.490	2.520	0.027	0.083333	7.7783701
50	25	0.10	2.490	2.520	0.027	0.083333	7.7783701
50	25	0.10	2.490	2.520	0.027	0.083333	7.7783701
50	25	0.10	2.490	2.520	0.027	0.083333	7.7783701
50	50	0.30	4.840	4.899	0.027	0.083333	15.119402
50	50	0.30	4.825	4.884	0.027	0.083333	15.072544
50	50	0.30	4.825	4.884	0.027	0.083333	15.072544
50	50	0.30	4.825	4.884	0.027	0.083333	15.072544
50	50	0.30	4.825	4.884	0.027	0.083333	15.072544
50	50	0.30	4.825	4.884	0.027	0.083333	15.072544

Table 10: : Raw data for MgO-modified Ceramic Membrane Pure water Flux

Core size: 6000nm MgO							
Water Type: Pure water							
Membrane Name: Modified CM							
Temp (20^0	Flowrate	Pressure (bar)	Weight (kg)	Volume (l)	Area (m2)	Time (m)	Flux (L/m2. H)
20	25	0.20	2.515	2.519	0.027	0.083333	7.775642027
20	25	0.20	2.515	2.519	0.027	0.083333	7.775642027
20	25	0.20	2.515	2.519	0.027	0.083333	7.775642027
20	25	0.20	2.515	2.519	0.027	0.083333	7.775642027
20	25	0.20	2.515	2.519	0.027	0.083333	7.775642027
20	25	0.20	2.515	2.519	0.027	0.083333	7.775642027
20	50	0.50	4.910	4.918	0.027	0.083333	15.18027927
20	50	0.50	4.910	4.918	0.027	0.083333	15.18027927
20	50	0.50	4.910	4.918	0.027	0.083333	15.18027927
20	50	0.50	4.910	4.918	0.027	0.083333	15.18027927
20	50	0.50	4.910	4.918	0.027	0.083333	15.18027927
20	50	0.50	4.910	4.918	0.027	0.083333	15.18027927
50	25	0.10	2.490	2.520	0.027	0.083333	7.778370058
50	25	0.10	2.490	2.520	0.027	0.083333	7.778370058
50	25	0.10	2.490	2.520	0.027	0.083333	7.778370058
50	25	0.10	2.490	2.520	0.027	0.083333	7.778370058
50	25	0.10	2.490	2.520	0.027	0.083333	7.778370058
50	25	0.10	2.490	2.520	0.027	0.083333	7.778370058
50	50	0.70	5.130	5.192	0.027	0.083333	16.02531663
50	50	0.70	5.130	5.192	0.027	0.083333	16.02531663
50	50	0.70	5.130	5.192	0.027	0.083333	16.02531663
50	50	0.70	5.130	5.192	0.027	0.083333	16.02531663
50	50	0.70	5.130	5.192	0.027	0.083333	16.02531663
50	50	0.70	5.130	5.192	0.027	0.083333	16.02531663

Table 11: Raw data for Unmodified Ceramic Membrane 100 mg/L O/W Emulsion

Core size: 6000nm							
Water Type: 100mg/L O/W Emulsion							
Membrane Name: Unmodified Ceramic Membrane							
Temp (20^{0}C)	Flowrate	Pressure (bar)	Weight (kg)	Volume (l)	Area (m2)	Time (h)	Flux (L/m2.H)
20	25	0.60	2.505	2.509	0.027	0.083	7.713746061
20	25	0.60	2.505	2.509	0.027	0.083	7.713746061
20	25	0.60	2.505	2.509	0.027	0.083	7.713746061
20	25	0.60	2.505	2.509	0.027	0.083	7.713746061
20	25	0.60	2.505	2.509	0.027	0.083	7.713746061

20	25	0.60	2.505	2.509	0.027	0.083	7.713746061
20	50	1.00	4.950	4.958	0.027	0.083	15.24273174
20	50	1.00	4.950	4.958	0.027	0.083	15.24273174
20	50	1.00	4.950	4.958	0.027	0.083	15.24273174
20	50	1.00	4.950	4.958	0.027	0.083	15.24273174
20	50	1.00	4.950	4.958	0.027	0.083	15.24273174
20	50	1.00	4.950	4.958	0.027	0.083	15.24273174
50	25	0.30	2.495	2.525	0.027	0.083	7.762813318
50	25	0.30	2.495	2.525	0.027	0.083	7.762813318
50	25	0.30	2.495	2.525	0.027	0.083	7.762813318
50	25	0.30	2.495	2.525	0.027	0.083	7.762813318
50	25	0.30	2.495	2.525	0.027	0.083	7.762813318
50	25	0.30	2.495	2.525	0.027	0.083	7.762813318
50	50	0.80	5.180	5.243	0.027	0.083	16.11678276
50	50	0.80	5.180	5.243	0.027	0.083	16.11678276
50	50	0.80	5.180	5.243	0.027	0.083	16.11678276
50	50	0.80	5.180	5.243	0.027	0.083	16.11678276
50	50	0.80	5.180	5.243	0.027	0.083	16.11678276
50	50	0.80	5.180	5.243	0.027	0.083	16.11678276

Table 12: Raw data for Unmodified Ceramic Membrane 250 mg/L O/W Emulsion

Core size: 6000nm							
Water Type: 250mg/L O/W Emulsion							
Membrane Name: Unmodified Ceramic Membrane							
Temp (20^0C)	**Flowrate**	**Pressure (bar)**	**Weight (kg)**	**Volume (l)**	**Area (m2)**	**Time (h)**	**Flux (L/m2.H)**
20	25	0.60	2.480	2.484	0.027	0.083	7.6368
20	25	0.60	2.480	2.484	0.027	0.083	7.6368
20	25	0.60	2.480	2.484	0.027	0.083	7.6368
20	25	0.60	2.480	2.484	0.027	0.083	7.6368
20	25	0.60	2.480	2.484	0.027	0.083	7.6368
20	25	0.60	2.480	2.484	0.027	0.083	7.6368
20	50	1.00	4.925	4.933	0.027	0.083	15.1657
20	50	1.00	4.925	4.933	0.027	0.083	15.1657
20	50	1.00	4.925	4.933	0.027	0.083	15.1657

20	50	1.00	4.925	4.933	0.027	0.083	15.1657
20	50	1.00	4.925	4.933	0.027	0.083	15.1657
20	50	1.00	4.925	4.933	0.027	0.083	15.1657
50	25	0.45	2.475	2.505	0.027	0.083	7.7006
50	25	0.45	2.475	2.505	0.027	0.083	7.7006
50	25	0.45	2.475	2.505	0.027	0.083	7.7006
50	25	0.45	2.475	2.505	0.027	0.083	7.7006
50	25	0.45	2.475	2.505	0.027	0.083	7.7006
50	25	0.45	2.475	2.505	0.027	0.083	7.7006
50	50	1.00	5.165	5.228	0.027	0.083	16.0701
50	50	1.00	5.165	5.228	0.027	0.083	16.0701
50	50	1.00	5.165	5.228	0.027	0.083	16.0701
50	50	1.00	5.165	5.228	0.027	0.083	16.0701
50	50	1.00	5.165	5.228	0.027	0.083	16.0701
50	50	1.00	5.165	5.228	0.027	0.083	16.0701

Table 13: Raw data for Unmodified Ceramic Membrane 500 mg/L O/W Emulsion

Core size: 6000nm							
Water Type: 500mg/L O/W Emulsion							
Membrane Name: Unmodified Ceramic Membrane							
Temp (20^0C)	**Flowrate**	**Pressure (bar)**	**Weight (kg)**	**Volume (l)**	**Area (m2)**	**Time (h)**	**Flux (L/m2.H)**
20	25	0.60	2.475	2.479	0.027	0.083	7.621
20	25	0.60	2.475	2.479	0.027	0.083	7.621
20	25	0.60	2.475	2.479	0.027	0.083	7.621
20	25	0.60	2.475	2.479	0.027	0.083	7.621
20	25	0.60	2.475	2.479	0.027	0.083	7.621
20	25	0.60	2.475	2.479	0.027	0.083	7.621
20	50	1.00	4.900	4.908	0.027	0.083	15.089
20	50	1.00	4.900	4.908	0.027	0.083	15.089
20	50	1.00	4.900	4.908	0.027	0.083	15.089
20	50	1.00	4.900	4.908	0.027	0.083	15.089
20	50	1.00	4.900	4.908	0.027	0.083	15.089
20	50	1.00	4.900	4.908	0.027	0.083	15.089
50	25	0.50	2.455	2.485	0.027	0.083	7.638
50	25	0.50	2.455	2.485	0.027	0.083	7.638

50	25	0.50	2.455	2.485	0.027	0.083	7.638
50	25	0.50	2.455	2.485	0.027	0.083	7.638
50	25	0.50	2.455	2.485	0.027	0.083	7.638
50	25	0.50	2.455	2.485	0.027	0.083	7.638
50	50	1.10	5.140	5.202	0.027	0.083	15.992
50	50	1.10	5.140	5.202	0.027	0.083	15.992
50	50	1.10	5.140	5.202	0.027	0.083	15.992
50	50	1.10	5.140	5.202	0.027	0.083	15.992
50	50	1.10	5.140	5.202	0.027	0.083	15.992
50	50	1.10	5.140	5.202	0.027	0.083	15.992

Table 14: Raw data for MgO-modified Ceramic Membrane 100 mg/L O/W Emulsion

Core size: 6000nm							
Water Type: 100mg/L O/W Emulsion							
Membrane Name: Modified Ceramic Membrane							
Temp (20^0C)	**Flowrate**	**Pressure (bar)**	**Weight (kg)**	**Volume (l)**	**Area (m2)**	**Time (h)**	**Flux (L/m2.H)**
20	25	0.30	2.545	2.549	0.027	0.083	7.837
20	25	0.30	2.545	2.549	0.027	0.083	7.837
20	25	0.30	2.525	2.529	0.027	0.083	7.775
20	25	0.30	2.510	2.514	0.027	0.083	7.729
20	25	0.30	2.505	2.509	0.027	0.083	7.714
20	25	0.30	2.500	2.504	0.027	0.083	7.698
20	50	0.50	4.900	4.908	0.027	0.083	15.089
20	50	0.50	4.900	4.908	0.027	0.083	15.089
20	50	0.50	4.900	4.908	0.027	0.083	15.089
20	50	0.50	4.900	4.908	0.027	0.083	15.089
20	50	0.50	4.900	4.908	0.027	0.083	15.089
20	50	0.50	4.900	4.908	0.027	0.083	15.089
50	25	0.20	2.475	2.505	0.027	0.083	7.701
50	25	0.20	2.475	2.505	0.027	0.083	7.701
50	25	0.20	2.475	2.505	0.027	0.083	7.701
50	25	0.20	2.475	2.505	0.027	0.083	7.701
50	25	0.20	2.475	2.505	0.027	0.083	7.701
50	25	0.20	2.475	2.505	0.027	0.083	7.701
50	50	0.40	5.090	5.152	0.027	0.083	15.837

50	50	0.40	5.090	5.152	0.027	0.083	15.837
50	50	0.40	5.090	5.152	0.027	0.083	15.837
50	50	0.40	5.090	5.152	0.027	0.083	15.837
50	50	0.40	5.090	5.152	0.027	0.083	15.837
50	50	0.40	5.090	5.152	0.027	0.083	15.837

Table 15: Raw data for MgO-modified Ceramic Membrane 250 mg/L O/W Emulsion

Core size: 6000nm							
Water Type: 250mg/L O/W Emulsion							
Membrane Name: Modified Ceramic Membrane							
Temp (20^0C)	**Flowrate**	**Pressure (bar)**	**Weight (kg)**	**Volume (l)**	**Area (m2)**	**Time (h)**	**Flux (L/m2.H)**
20	25	0.30	2.450	2.454	0.027	0.083	7.544
20	25	0.30	2.450	2.454	0.027	0.083	7.544
20	25	0.30	2.450	2.454	0.027	0.083	7.544
20	25	0.30	2.450	2.454	0.027	0.083	7.544
20	25	0.30	2.450	2.454	0.027	0.083	7.544
20	25	0.30	2.450	2.454	0.027	0.083	7.544
20	50	0.70	4.885	4.893	0.027	0.083	15.043
20	50	0.70	4.885	4.893	0.027	0.083	15.043
20	50	0.70	4.885	4.893	0.027	0.083	15.043
20	50	0.70	4.885	4.893	0.027	0.083	15.043
20	50	0.70	4.885	4.893	0.027	0.083	15.043
20	50	0.70	4.885	4.893	0.027	0.083	15.043
50	25	0.20	2.465	2.495	0.027	0.083	7.669
50	25	0.20	2.465	2.495	0.027	0.083	7.669
50	25	0.20	2.465	2.495	0.027	0.083	7.669
50	25	0.20	2.465	2.495	0.027	0.083	7.669
50	25	0.20	2.465	2.495	0.027	0.083	7.669
50	25	0.20	2.465	2.495	0.027	0.083	7.669
50	50	0.40	5.055	5.116	0.027	0.083	15.728
50	50	0.40	5.055	5.116	0.027	0.083	15.728
50	50	0.40	5.055	5.116	0.027	0.083	15.728
50	50	0.40	5.055	5.116	0.027	0.083	15.728
50	50	0.40	5.055	5.116	0.027	0.083	15.728
50	50	0.40	5.055	5.116	0.027	0.083	15.728

Table 16: Raw data for MgO-modified Ceramic Membrane 250 mg/L O/W Emulsion

Core size: 6000nm							
Water Type: 500mg/L O/W Emulsion							
Membrane Name: Modified Ceramic Membrane							
Temp (20^0C)	**Flowrate**	**Pressure (bar)**	**Weight (kg)**	**Volume (l)**	**Area (m2)**	**Time (h)**	**Flux (L/m2.H)**
20	25	0.30	2.440	2.444	0.027	0.083	7.514
20	25	0.30	2.440	2.444	0.027	0.083	7.514
20	25	0.30	2.440	2.444	0.027	0.083	7.514
20	25	0.30	2.440	2.444	0.027	0.083	7.514
20	25	0.30	2.440	2.444	0.027	0.083	7.514
20	25	0.30	2.440	2.444	0.027	0.083	7.514
20	50	0.80	4.865	4.873	0.027	0.083	14.981
20	50	0.80	4.865	4.873	0.027	0.083	14.981
20	50	0.80	4.865	4.873	0.027	0.083	14.981
20	50	0.80	4.865	4.873	0.027	0.083	14.981
20	50	0.80	4.865	4.873	0.027	0.083	14.981
20	50	0.80	4.865	4.873	0.027	0.083	14.981
50	25	0.20	2.455	2.485	0.027	0.083	7.638
50	25	0.20	2.455	2.485	0.027	0.083	7.638
50	25	0.20	2.455	2.485	0.027	0.083	7.638
50	25	0.20	2.455	2.485	0.027	0.083	7.638
50	25	0.20	2.455	2.485	0.027	0.083	7.638
50	25	0.20	2.455	2.485	0.027	0.083	7.638
50	50	0.50	5.035	5.096	0.027	0.083	15.666
50	50	0.50	5.035	5.096	0.027	0.083	15.666
50	50	0.50	5.035	5.096	0.027	0.083	15.666
50	50	0.50	5.035	5.096	0.027	0.083	15.666
50	50	0.50	5.035	5.096	0.027	0.083	15.666
50	50	0.50	5.035	5.096	0.027	0.083	15.666

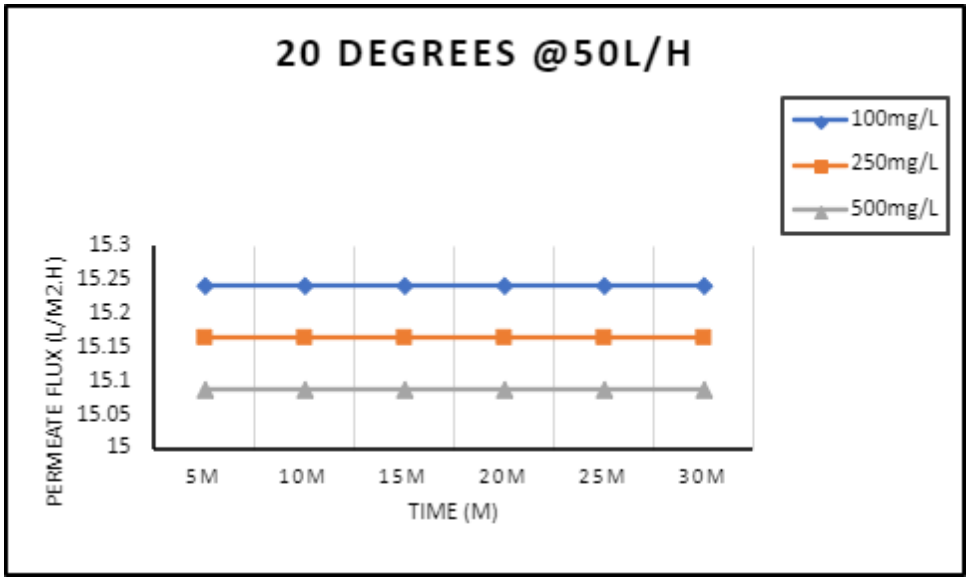

Figure 92: Permeate flux differences in 20°C temperatures for three O/W emulsion concentrations in Al_2O_3 modified ceramic membrane.

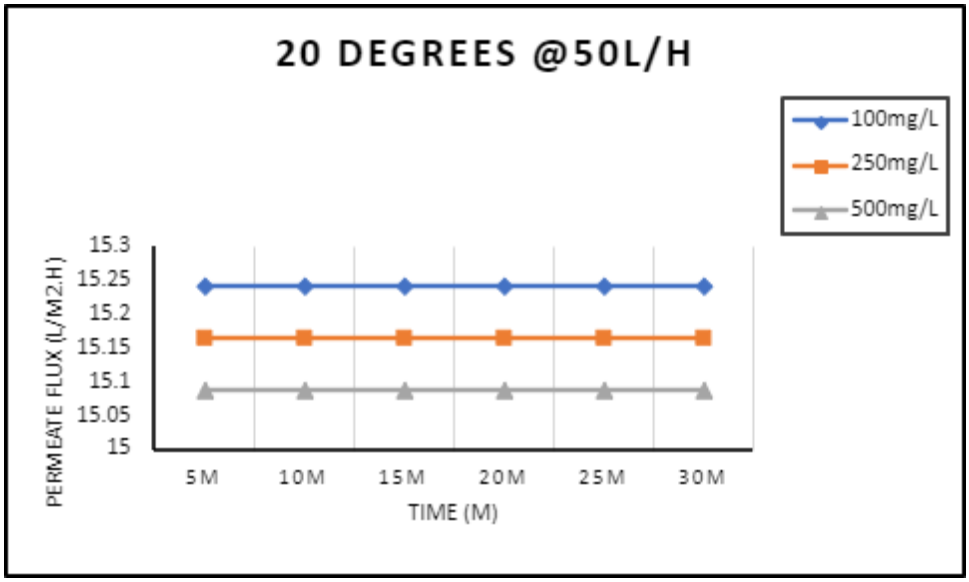

Figure 93: Permeate flux differences in 50°C temperatures for three O/W emulsion concentrations in Al_2O_3 modified ceramic membrane.

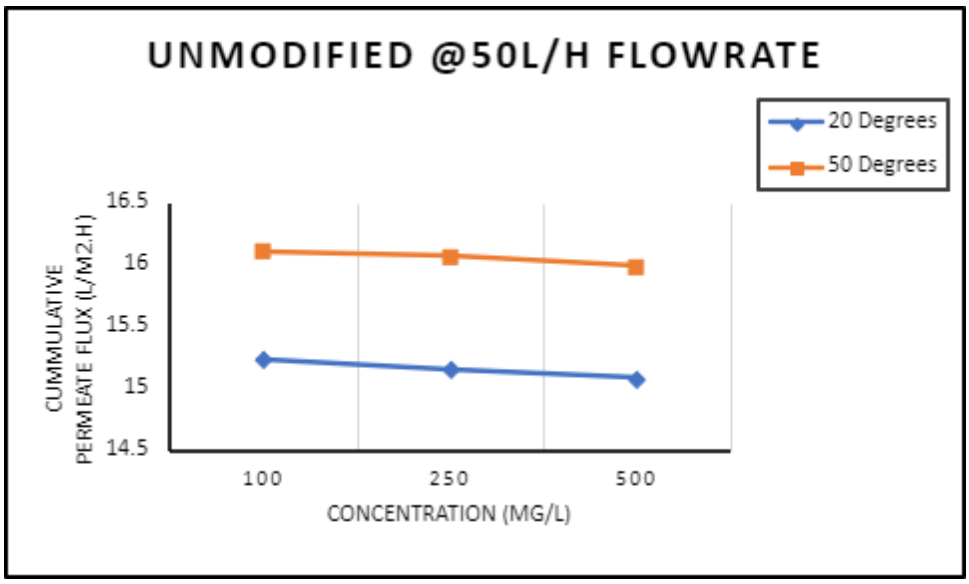

Figure 94: Variation of permeate flux of unmodified ceramic membrane at two temperatures and 50 L/H flowrates.

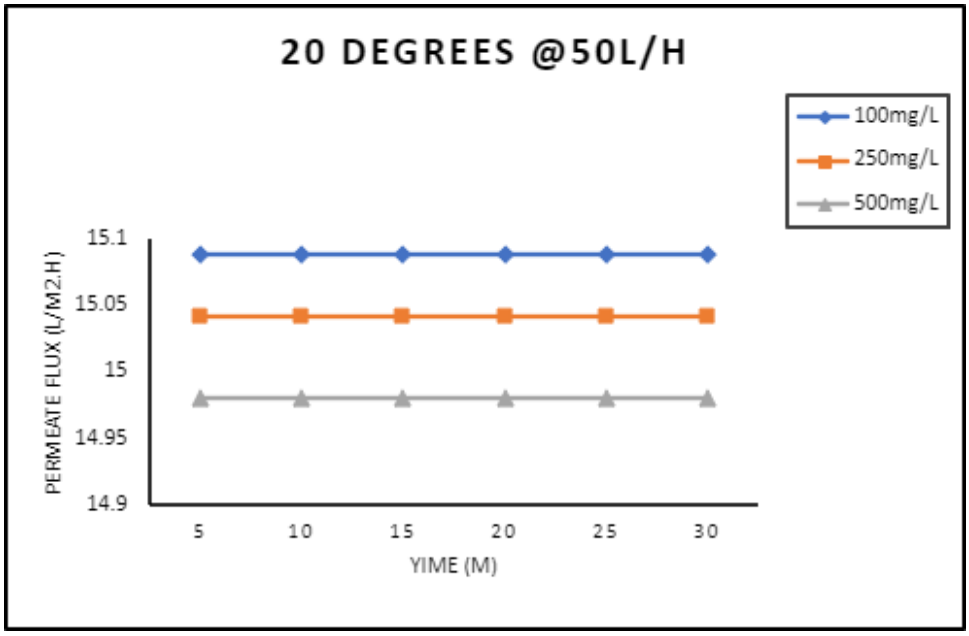

Figure 95: Permeate flux differences in 20°C temperatures for three O/W emulsion concentrations in MgO-modified ceramic membrane.

.

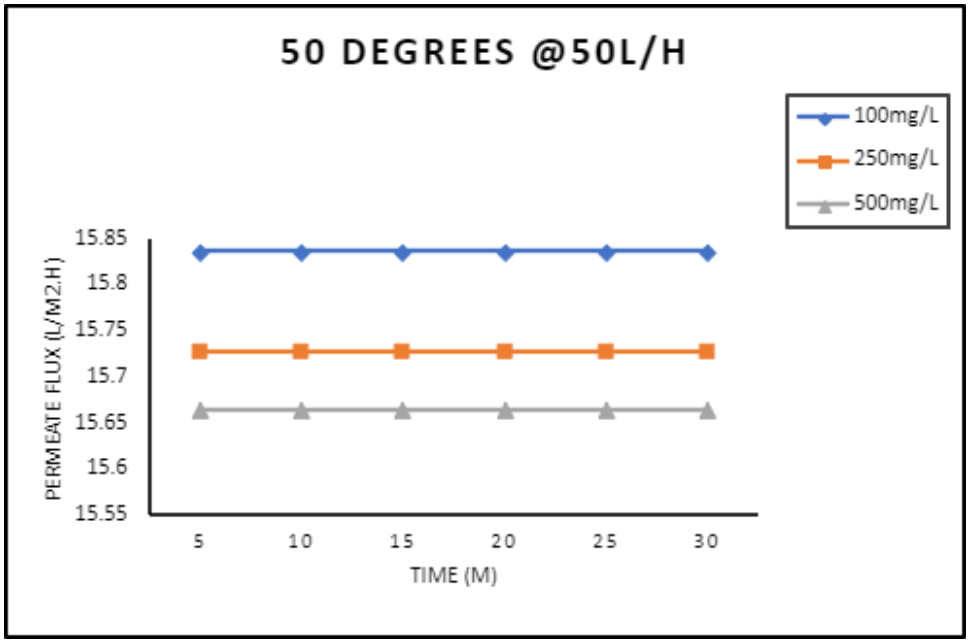

Permeate flux differences in 50°C temperatures for three O/W emulsion concentrations in MgO-modified ceramic membrane.

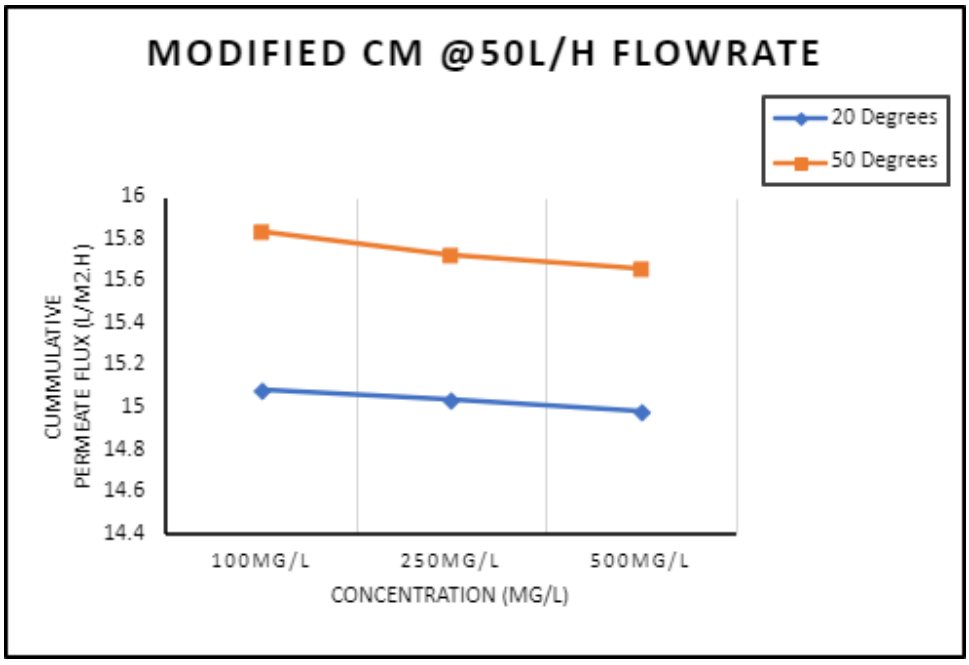

Figure 96: Variation of permeate flux of MgO-modified ceramic membrane at two temperatures and 50 L/H flowrates.

Table 17: Raw data for Unmodified Ceramic Membrane Flux Recovery ratio

Core size: 6000nm				
Water Type: Pure water after				
Membrane Name: Unmodified Ceramic Membrane				

Temp (20^0C)	Flowrate	Pressure (bar)	Weight (kg)	Volume (l)	Area (m2)	Time (h)	Flux (L/m2.H)
20	25	0.50	2.415	2.419	0.027	0.083	7.4366
20	25	0.50	2.415	2.419	0.027	0.083	7.4366
20	25	0.50	2.415	2.419	0.027	0.083	7.4366
20	25	0.50	2.415	2.419	0.027	0.083	7.4366
20	25	0.50	2.415	2.419	0.027	0.083	7.4366
20	25	0.50	2.415	2.419	0.027	0.083	7.4366
20	50	1.30	4.625	4.633	0.027	0.083	14.2419
20	50	1.30	4.625	4.633	0.027	0.083	14.2419
20	50	1.30	4.625	4.633	0.027	0.083	14.2419
20	50	1.30	4.625	4.633	0.027	0.083	14.2419
20	50	1.30	4.625	4.633	0.027	0.083	14.2419
20	50	1.30	4.625	4.633	0.027	0.083	14.2419
50	25	0.30	2.435	2.465	0.027	0.083	7.5761
50	25	0.30	2.435	2.465	0.027	0.083	7.5761
50	25	0.30	2.435	2.465	0.027	0.083	7.5761
50	25	0.30	2.435	2.465	0.027	0.083	7.5761
50	25	0.30	2.435	2.465	0.027	0.083	7.5761
50	25	0.30	2.435	2.465	0.027	0.083	7.5761
50	50	1.00	5.050	5.111	0.027	0.083	15.7123
50	50	1.00	5.050	5.111	0.027	0.083	15.7123
50	50	1.00	5.050	5.111	0.027	0.083	15.7123
50	50	1.00	5.050	5.111	0.027	0.083	15.7123
50	50	1.00	5.050	5.111	0.027	0.083	15.7123
50	50	1.00	5.050	5.111	0.027	0.083	15.7123

Table 18: Raw data for MgO-modified Ceramic Membrane Flux Recovery ratio

Membrane Name: Uncoated Ceramic Membrane							
Water Type: Pure water after							
Membrane Name: Modified Ceramic Membrane							
Temp (20^0C)	**Flowrate**	**Pressure (bar)**	**Weight (kg)**	**Volume (l)**	**Area (m2)**	**Time (h)**	**Flux (L/m2.H)**
20	25	0.10	2.260	2.264	0.027	0.083	6.9593
20	25	0.10	2.260	2.264	0.027	0.083	6.9593
20	25	0.10	2.260	2.264	0.027	0.083	6.9593

20	25	0.10	2.260	2.264	0.027	0.083	6.9593
20	25	0.10	2.260	2.264	0.027	0.083	6.9593
20	25	0.10	2.260	2.264	0.027	0.083	6.9593
20	50	0.50	4.295	4.302	0.027	0.083	13.2258
20	50	0.50	4.295	4.302	0.027	0.083	13.2258
20	50	0.50	4.295	4.302	0.027	0.083	13.2258
20	50	0.50	4.295	4.302	0.027	0.083	13.2258
20	50	0.50	4.295	4.302	0.027	0.083	13.2258
20	50	0.50	4.295	4.302	0.027	0.083	13.2258
50	25	0.10	2.255	2.282	0.027	0.083	7.0161
50	25	0.10	2.255	2.282	0.027	0.083	7.0161
50	25	0.10	2.255	2.282	0.027	0.083	7.0161
50	25	0.10	2.255	2.282	0.027	0.083	7.0161
50	25	0.10	2.255	2.282	0.027	0.083	7.0161
50	25	0.10	2.255	2.282	0.027	0.083	7.0161
50	50	0.30	4.620	4.676	0.027	0.083	14.3744
50	50	0.30	4.620	4.676	0.027	0.083	14.3744
50	50	0.30	4.620	4.676	0.027	0.083	14.3744
50	50	0.30	4.620	4.676	0.027	0.083	14.3744
50	50	0.30	4.620	4.676	0.027	0.083	14.3744
50	50	0.30	4.620	4.676	0.027	0.083	14.3744

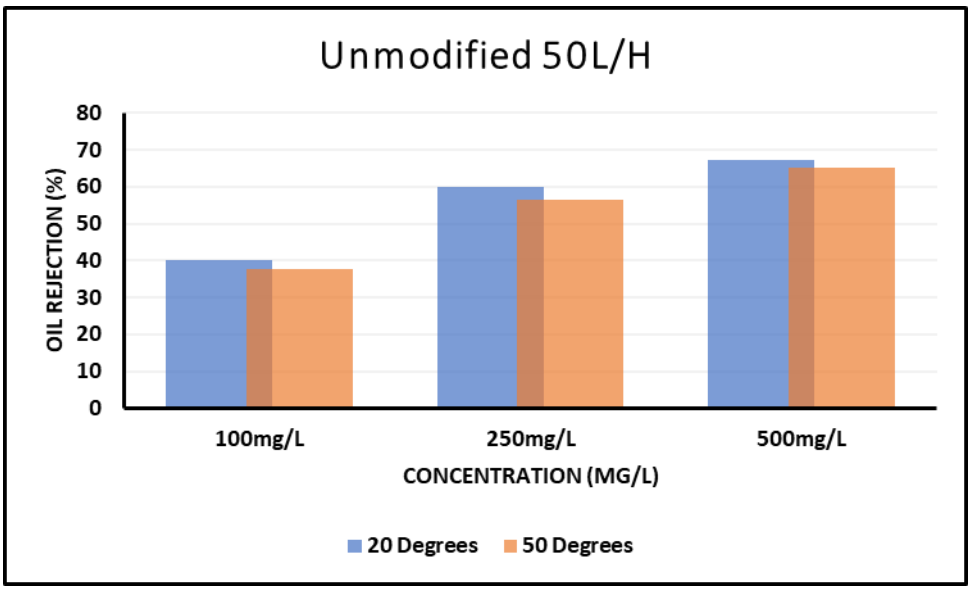

Figure 97: % Oil rejection of Unmodified ceramic membrane at 50 L/H for three O/W Emulsion concentrations

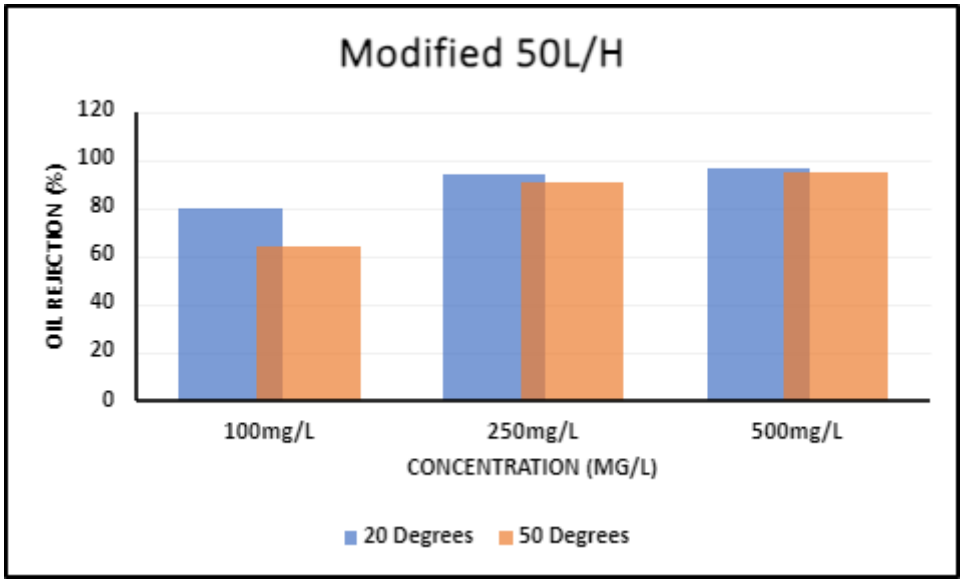

Figure 98: % Oil rejection of MgO-modified ceramic membrane at 50 L/H for three O/W Emulsion concentrations

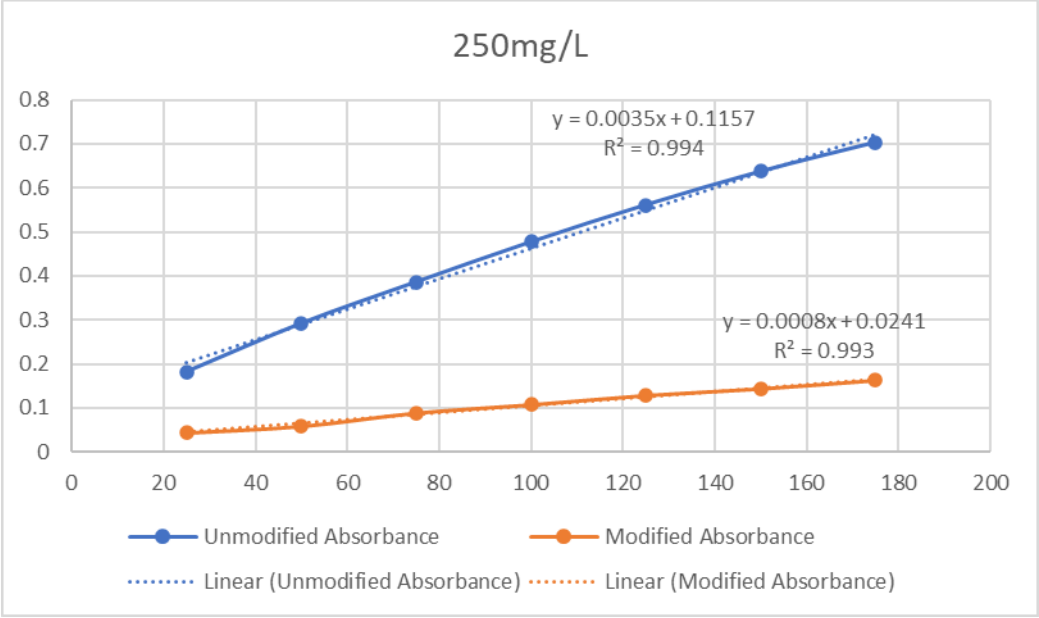

Figure 99: Calibration curve of 250mg/L feed concentration for unmodified and modified ceramic membrane.

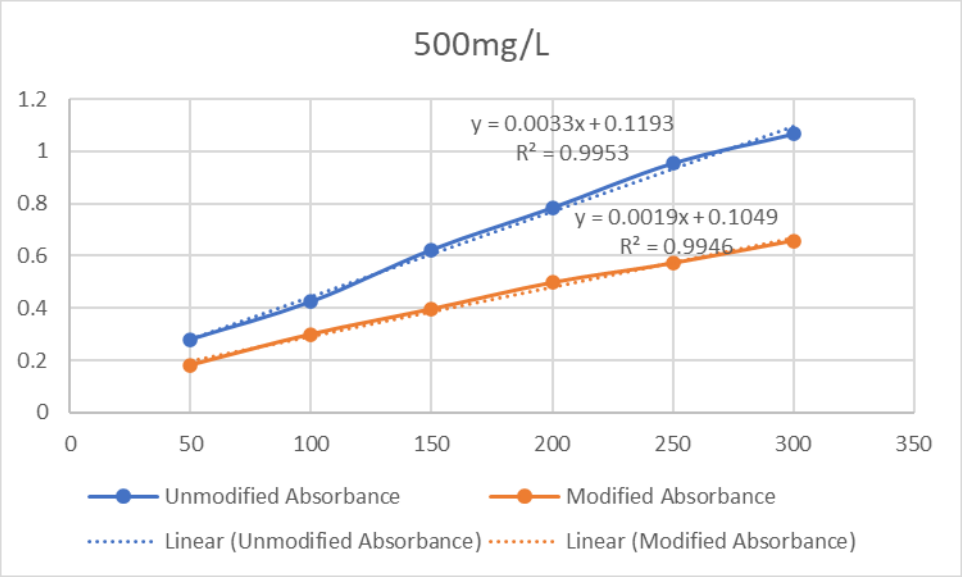

Figure 100: Calibration curve of 500mg/L feed concentration for unmodified and modified ceramic membrane.

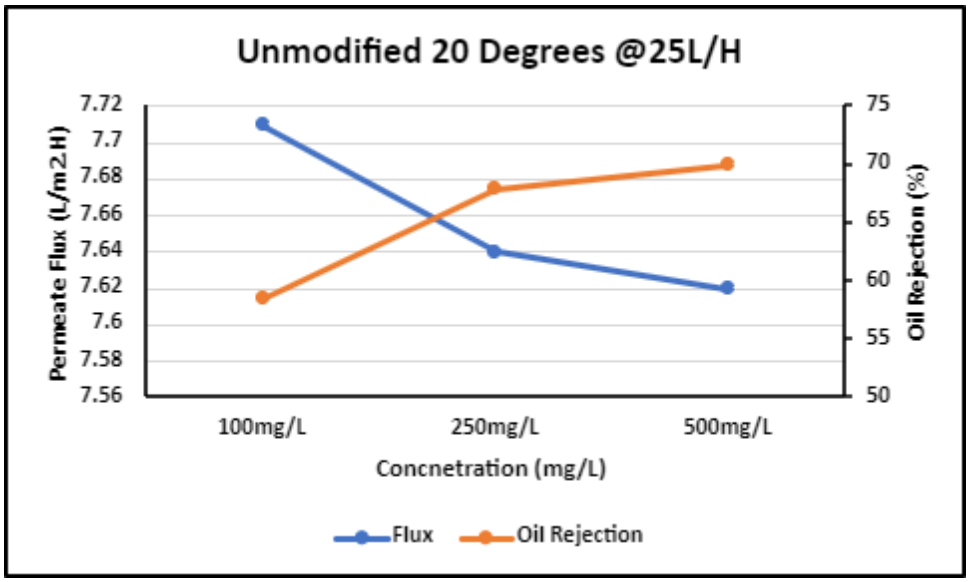

Figure 101: Permeate Flux vs Oil rejection in unmodified ceramic membrane for 20°C at 25 L/H

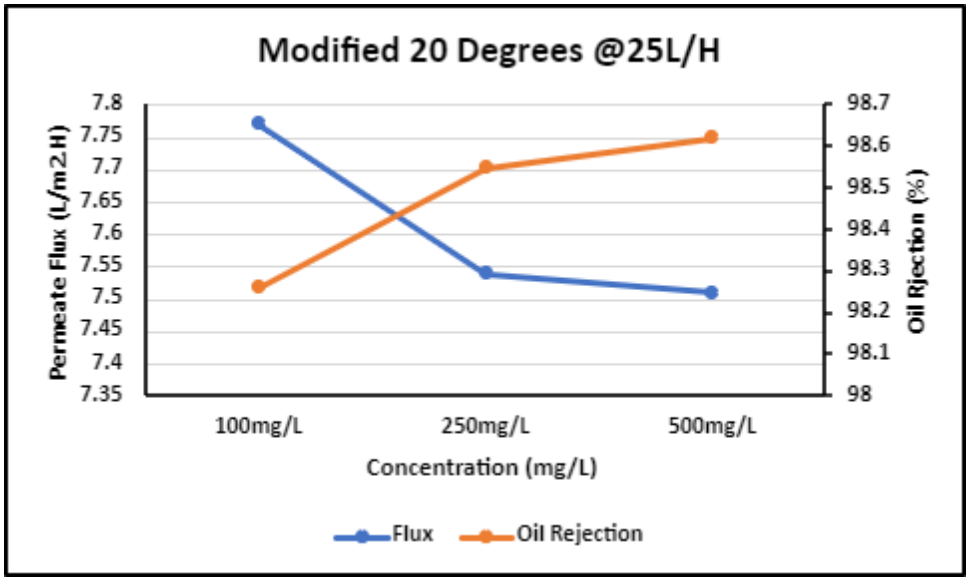

Figure 102: Permeate Flux vs Oil rejection in MgO-modified ceramic membrane for 20°C at 25 L/H

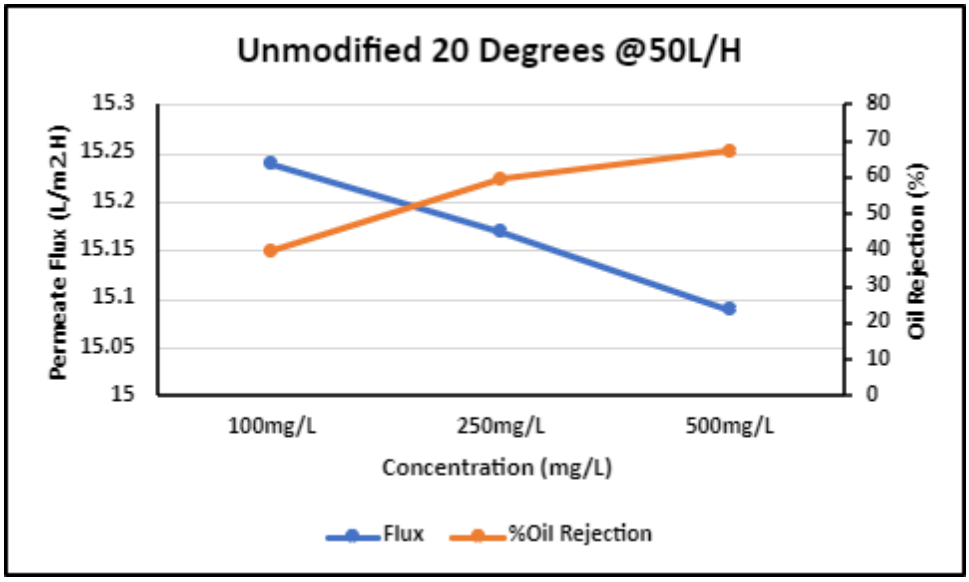

Figure 103: Permeate Flux vs Oil rejection in unmodified ceramic membrane for 20°C at 50 L/H

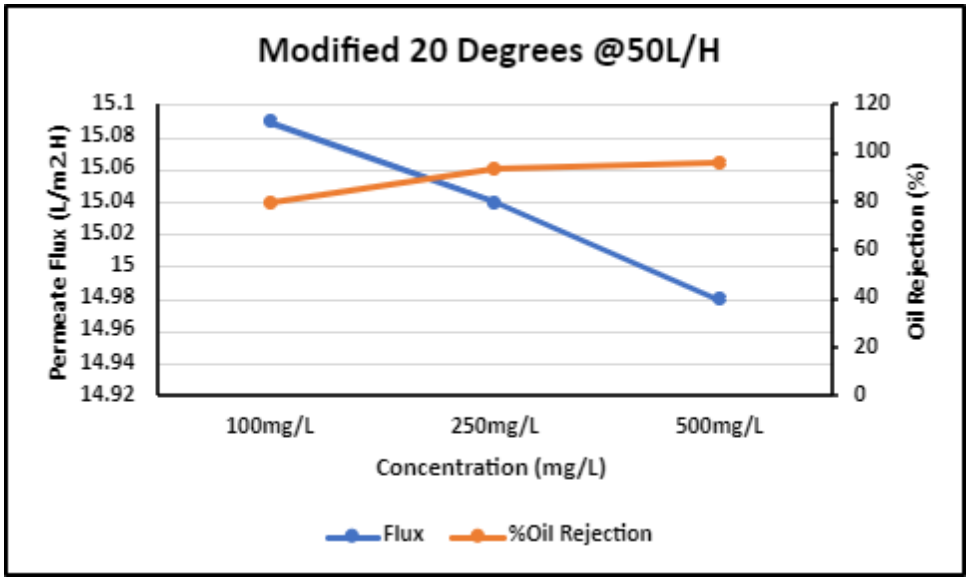

Figure 104: Permeate Flux vs Oil rejection in MgO-modified ceramic membrane for 20°C at 50 L/H

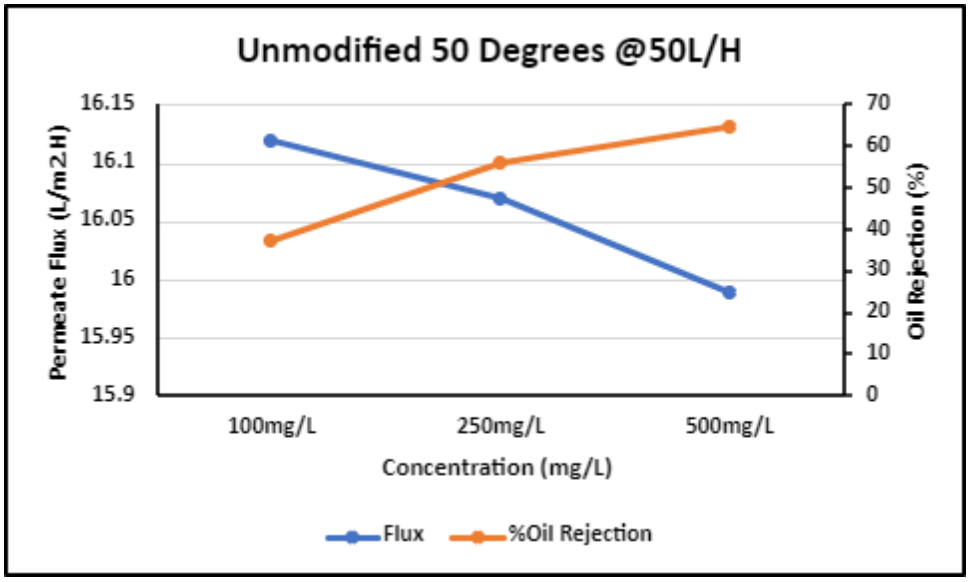

Figure 105: Permeate Flux vs Oil rejection in unmodified ceramic membrane for 50°C at 50 L/H

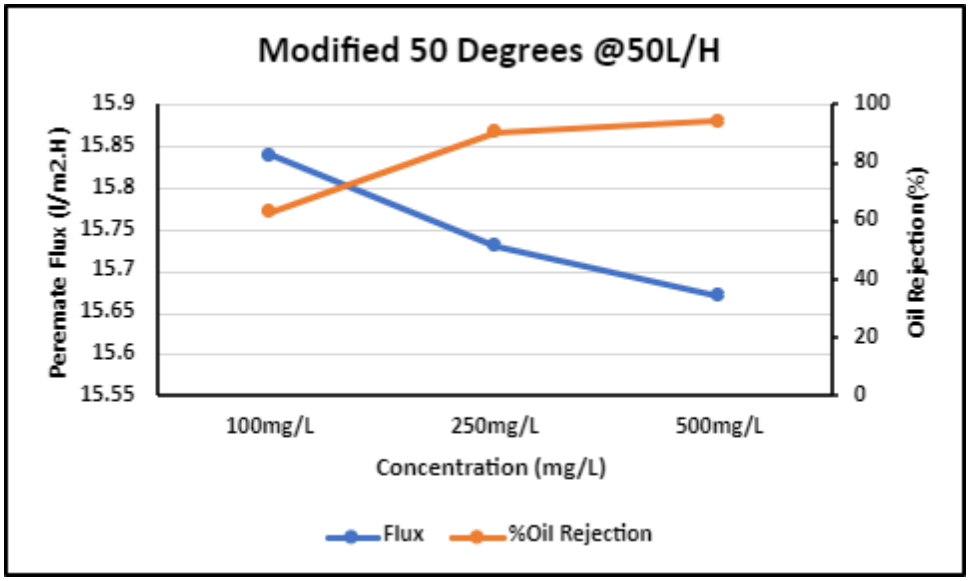

Figure 106: Permeate Flux vs Oil rejection in MgO-modified ceramic membrane for 20°C at 50 L/H.

Appendix V - Conference Papers and Articles

International Journal on Engineering, Science and Technology
Volume 4, Issue 1, 2022 ISSN: 2642-4088

Characterization and Hydrodynamic Evaluation of the Relationship between Permeability and Microstructure Parameters Ceramic Membranes for the Separation of Oil-in-water Emulsion

Florence Aisueni
Robert Gordon University, United Kingdom

Edward Gobina
Robert Gordon University, United Kingdom, e.gobina@rgu.ac.uk

Idris Hashim
Robert Gordon University, United Kingdom

Evans Ogoun
Robert Gordon University, United Kingdom

Abstract: Ceramic membranes for wastewater treatment are usually fine filters prepared by sintering of alumina, titania or zirconia powders at ultra-high temperatures and have an asymmetric cross-section using the same material or a combination of the three giving a base support and an active layer forming the membrane. The Carman–Kozeny (C–K) and Hagen–Poiseuille (H–P) transport equations have been used to predict water permeability of ceramic membranes and can be adapted to take account of the effects of microstructural parameters (porosity, and tortuosity) of ceramic membranes on pure water flux. The hydrodynamics of the membranes were evaluated by gas transport to obtain equivalent water permeability which was then used to obtain the porosity and tortuosity respectively. Gas permeability experiments showed good correspondence with the calculated water flux. Characterization of the membranes was carried out using scanning electron microscopy (SEM) imaging to determine the morphological aspects of the sample including shape and size of membranes while the electron diffraction with x-rays analysis (EDAX) was used to obtain information on the elemental composition.

Keywords: Membrane, Porosity, Tortuosity, Microstructure, Flux

Introduction

Oil refineries produced large quantity of oily wastewater which can also be termed as (O/W) emulsion with oil droplet of different sizes (oil in water or o water in oil emulsion). Offshore oil spillage produces huge amount of oily wastewater (Elanchezhiyan, Sivasurian, & Meenakshi, 2016). This O/W emulsion discharged into the environment directly will not only pollute the environment but reduce water resources especially drinking water. A way to address this problem is to separate oil from water and possibly reuse or recycle both components. Several promising methods have been reported so far by researchers for the separation of oil from O/W emulsions before discharge into the environment, which have their advantages and disadvantages (Wang, Wang, & Geng, 2018). Materials that can meet the challenging requirements of real-world applications are still in the process of development. Hence, there is a need for the advancement of a recyclable, cost -effective, environmentally friend, simple and efficient method that can separate big volumes of O/W emulsions into two phases with high flux and oil rejection rates. These several methods researched and reported for the separation of O/W emulsions are adsorption, electrocoagulation, flocculation, bioremediation, centrifugation, membrane etc (Shi et al., 2019).

These traditional methods are insufficient in the treatment of O/W emulsions due to the small size of oil droplets as well as lower concentrations of oil in water, because below 250mg/L separation is usually not possible (Huang et al., 2018). However, membrane technology has been recently most researched as a promising alternative for the separation of O/W emulsion. This may be because of merit features which includes an excellent combination of longer shelf life, better self-cleaning properties, mechanical, chemical, and thermal strength, survival in organic solvent, low cost, compact design, removal of secondary separation and superior separation factor (Suresh & Pugazhenthi, 2016).

Membranes are commonly classified into two main groups known as polymeric and ceramic membranes. This

AISUENI, F., ABUNUMAH, O., HASHIM, I., RAMALAN, M., OGOUN, E., PRABHU, R., GIWA, A. and GOBINA, E. 2022. Effect of pore size and porosity on contact angle of ceramic membrane for oil-in-water emulsion separation. In *Techconnect briefs 2022: papers from 2022 TechConnect world innovation conference and expo, 13-15 June 2022, Washington, USA*. Danville: TechConnect [online], pages 59-62. Available from: https://briefs.techconnect.org/wp-content/volumes/TCB2022/pdf/174.pdf

Effect of pore size and porosity on contact angle of ceramic membrane for oil-in-water emulsion separation.

AISUENI, F., ABUNUMAH, O., HASHIM, I., RAMALAN, M., OGOUN, E., PRABHU, R., GIWA, A. and GOBINA, E.

2022

Gas Diffusion, Transport Characteristics and Modelling in Porous Membrane Systems with Application for Polymer Electrolyte Membrane Fuel Cells

Florence Aisueni[1], Muktar Ramalan[1], Ofasa Abunumah[1], Priscilla Ogunlude[1], Ifeyinwa Orakwe[1], Evans Ogoun[1], Ayo Giwa[2], Habiba Shehu[1], Edward Gobina[1]*

e.gobina@rgu.ac.uk

[1] *Centre of Excellence for Process Integration and Membrane Technology (CPIMT), School of Engineering, Robert Gordon University, Garthdee Road, ABERDEEN, AB10 7GJ, UK, Tel: +441224262348*

[2] *McAlpha, Inc., 205 - 279 Midpark Way SE, Calgary, ALBERTA T2X 1M2, CANADA,*

Abstract: Fuel cells convert chemical energy in electrical energy and heat by consuming typically hydrogen and oxygen and producing water as the main by-product. This is achieved by reducing hydrogen at the anode (left hand side) and oxidising oxygen at the cathode (right hand side). The polymer electrolyte membrane fuel cell (PEMFC) gas diffusion layer (GDL) and the catalyst layer (CL) are crucial components mainly responsible for the distribution of gases, chemical reaction, and water transport in any PEMFC. The GDL consists of two main layers which are the macroporous substrate (MPS) and microporous layer (MPL). The MPS comes before the gas flow field and provides gas diffusion through a carbon-based paper or carbon cloth and collects the current. MPL is generally used to reduce the contact resistance between the CL and GDL. The most important parameters of porous membranes are derived from Fick's first law which relates the molar flux to membrane permeability. All possible gas transport mechanisms in porous membrane have been investigated in literature such as Hagen-Pouiselle, Knudsen, surface diffusion, capillary condensation, and molecular sieving.

Keywords: *Polymer Electrolyte, Fuel Cells, Membrane, Gas Diffusion Layer, Catalyst Layer, Knudsen Number, Mean Free Path.*

INTRODUCTION

Figure 1 (left) describes the conventional electrode design for PEMFCs. In the PEMFC the gas diffusion layer (GDL) and the catalyst layer (CL) are crucial components mainly responsible for the distribution of reactant gases, chemical reaction, and water transport in. The GDL consists of two main layers which are the macroporous substrate (MPS) and microporous layer (MPL). The MPS comes before the gas flow field (Figure 1-right) and provides gas diffusion through a carbon-based paper or carbon cloth and collects the current. The membrane electrode assembly (MEA) is located between two graphite bipolar plates (GBPs), which collect electric current and enable gas feeding and cooling of the system. At the anode, H_2 is oxidized in the CL, releasing electrons, and generating protons. The electrons flow to the cathode through an external circuit, where they recombine with the protons in the CL and the oxidant (oxygen) to produce water. Proton transfer from the anode CL to the cathode CL through the polymer membrane thus closes the electrical circuit. The overall reaction differs from hydrogen combustion because a fraction of the Gibbs free energy can be converted into electric energy. MPL is generally used to reduce the contact resistance between the CL and GDL. In ultra-micropores the permeance is low but increase as pore sizes increase and depends on the Knudsen number, K_n. If the mean-free path of a molecule is less than 0.01 times the pore radius, ordinary diffusion is the primary mode of mass transport. If the mean-free path is greater than

COMPARATTIVE EVALUATION OF OIL-IN-WATER EMULSION SEPARATION WITH ALUMINIUM OXIDE & ZINC OXIDE NANOPARTICLES CERAMIC MEMBRANE

[1] *Florence Aisueni,* [1] *Idris Hashim,* [1] *Evans Ogoun,* [1*] *Edward Gobina*
[1]Robert Gordon University, Centre for Process Integration & Membrane Technology), School of Engineering, Garthdee Road, Aberdeen AB10 7GJ
*Corresponding author e-mail: e.gobina@rgu.ac.uk

ABSTRACT

This research aims at comparing two nanoparticles (Aluminium oxide and zinc oxide) coated ceramic membrane with self-cleaning ability for the effectively separation of low concentration (<250mg/L) Oil-in-Water O/W Emulsion. Preliminary experimentals have been done to determine the morphology and pure water flux of unmodified commercial ceramic membrane using Scanning Electron Microscope(SEM) and in-house installed rig separator respectively. An uneven pore size with a densely packed image from SEM indicates an increase in flux. Steady pure water permeate flux shows possibility of anti-fouling in ceramic membrane.

Keywords: Oil-in-water emulsion, Nanoparticles, Ceramic membrane, Separation

INTRODUCTION

This research proposes the preparation and camparison of two nanoparticles coated ceramic membrane for real world industrial application to separate low concentrations of (O/W) emulsions before discharge into the environment. The mixture of oil with water from industrial activities creates an emulsion which is now termed as O/W emulsion (1) must beet regulatory limit (10mg/L) before discharge into the environment. Several chemical and physical methods have been successfully used for the separation of O/W emulsions; however, the trace amounts of oil (<250mg/L) remains unfiltered in the separated water (2) . Membrane technology has been used to separate low concentration of O/W emulsion yet this comes with a challenge of fouling in the membrane pores, hindering this technology from industrial use. Ceramic membranes were carefully chosen as a technique for review in separation of O/W emulsion due to their numerous advantage which include mechanical stability, chemical inertness, thermal stability, ability to be regenerated, high flux, and compactness in design (3). This study focuses on the modification and comparison of two nanoparticles coated ceramic membrane (Aluminium oxide and Zinc oxide) with self cleaning ability for the separation of <250mg/L O/W emulsion. The objectives includes:

- The assembling and installation of Rig (separator) for separation of O/W emulsion.
- Characterization and pure water flux separation is evaluated on unmodified commercial ceramic membrane to serve as a reference.
- Dip coating method is used for the modification of nanoparticles on ceramic membrane. Characterization of the modified ceramic membranes to determine pore size, porosity, contact angle, morphology using Quantachrome Analyzer, Mathematical model, ThetaLite Contact angle meter and Field Emission Scanning Electron Microscope respectively.
- Preparation and characterization of O/W emulsion parameters. Determination of flux, % oil rejection and anti-fouling in modified ceramic membrane is evaluated.
- Quantitative and qualitative analysis of permeate from modified ceramic membrane using UV-Visible Spectrophotometer is measured.

MATERIALS AND METHODS

The morphology unmodified commercial ceramic membrane was determined by of the membrane was determined by the use Zeiss EVO LS10 scanning electron Microscope (SEM). An in-house rig set was installed and used for the pure water flux evaluation of the unmodified commercial ceramic membrane. Both outcomes of the experiments serves as reference for the characterization and separation using modified nanoparticles ceramic membrane.

Characterization

Scanning electron microscopy (SEM) is used to characterize the surface of samples by identifying the morphology. The electron beam from SEM focuses on a sample and generates high resolution images of the sample. The SEM was used to examine support ceramic membrane to detect surface smoothness, cracks, structures, irregularities, and thickness. Support ceramic membrane samples were placed firmly on a stub and transferred to the sample carousel of the SEM for analysis. The SEM generated images of both outer and inner areas of the unmodified commercial ceramic membrane at 500X, 1000X and 3000X magnifications is represented in fig 1a.

Separation